Spatio-Temporal Presence of Micropollutants and their Metabolites in Lake Geneva and Susceptibility to Direct and Indirect Photodegradation Processes

THÈSE N^{O} 5677 (2013)

PRÉSENTÉE LE 8 MARS 2013

À LA FACULTÉ DE L'ENVIRONNEMENT NATUREL, ARCHITECTURAL ET CONSTRUIT

LABORATOIRE DE CHIMIE ENVIRONNEMENTALE

PROGRAMME DOCTORAL EN ENVIRONNEMENT

ÉCOLE POLYTECHNIQUE FÉDÉRALE DE LAUSANNE

POUR L'OBTENTION DU GRADE DE DOCTEUR ÈS SCIENCES

PAR

Florence BONVIN

acceptée sur proposition du jury:

Prof. D. A. Barry, président du jury
Prof. T. Kohn, directrice de thèse
Prof. J. Hollender, rapporteur
Prof. K. McNeill, rapporteur
Prof. T. Strathmann, rapporteur

ÉCOLE POLYTECHNIQUE
FÉDÉRALE DE LAUSANNE

Suisse
2013

Contemplating micropollutants from above...

Acknowledgements

First and foremost, I would like to thank my thesis supervisor and "scientific mom", **Tamar**. I am very grateful for her guidance and support and the confidence she showed in me and helped me gain throughout these four years. I thank her for providing a motivating working environment, for her constructive and critical reviews, her unbeatable availability, for all the conferences abroad and the entertaining anecdotes while eating my cookies. Thanks T.!!!

I also thank the president of the jury, Prof. **Andrew Barry**, and all the members of the jury: Prof. **Juliane Hollender**, Prof. **Kris McNeill** and Prof. **Timothy Strathmann** for accepting this task.

I would like to thank all the colleagues and friends who scientifically and socially made these four years fruitful and enjoyable: My very special thanks go to **Brian Pecson**, for his contagious good humor and positive vibes, all those laughs and midday jogs along the Venoge. I also thank **Barbara Morasch**, my "chem sis", who showed me the works in working with micropollutants and wastewater; **Hans Reiser**, "Hansli", for his help with the first sampling campaign, his fantastic integration skills, and our weekly Dütch Dunnschtig. **Thérèse**, **Loic** and **Michael** from the office next door, for intra-mural discussions, coffee breaks and great times. I also thank **Karine Maritz** for making all administrative work so easy. I would like to mention my special thanks to **Rebecca Rutler**, for her competence and effectiveness in the laboratory, and in the field, for her patience with our friend the SPE and all those early morning chats. I also thank **Julien**, the best master student and office mate ever, for his interesting questions, good humor and races to get the 4pm coke. Thanks to **Heather** for enduring my private defense talk so many times and motivating me before the big day! All past and present LCE group members: **Krista**, **Jessi**, **Corinne**, **Franziska**, **Shinobu**, **Qingxia** and **Andreas** are also acknowledged.

I am very grateful towards **Dominique Grandjean** and **Htet Kyi Wynn** who were always available for troubleshooting errors on lab instruments. I also thank **Philippe Arpagaus**, captain of "La Licorne" our faithful sampling boat. Thanks to **Johny Wuest** for helpful discussions and to **Benoit Crouzy** for his detailed mathematical input.

Acknowledgements

This thesis was part of an interdisciplinary project, PRODOC21. I would like to thank in particular **Nathalie Chèvre** for her efforts in organizing motivating summer and winter retreats in lovely places. Thanks also to all the PRODOC PhD students (**Ahn Dao, Elena, Janine, Nadine, Myriam, Jonas, Peter, Silwan, Sylvain** and **Vincent**) for stimulating discussions and sampling collaborations and to **Lucca Rossi** for his practical expertise and entertaining stories. In particular, I thank **Amir**, without whom the hydrodynamic-photolysis model would not have been possible and to Andrew Barry, for his motivation in the concept.

I am grateful to Kris McNeill for hosting me 6 months in his lab. During this stay, all the **McNeill lab group members** helped me find my way in the lab and in the (dark?) corridors of organic chemistry and to the rooftop for the apéros. In particular, I thank **Paul** and **Rachel** for their time and technical help with the instruments. Thanks also to PJ Alaimo for his contagious passion for chemistry and wine! Thanks to **Lilli** for afterwork sessions at Kafischnaps, and to **Anne** for showing me the cultural and alternative side of Zurich.

I would also like to thank my motivated running partners **Tim** and **Kevin** ("le Belge") for the frequent "brain aeration" sessions along the Venoge and for pulling me out of the office for beer at Sat. Thanks to **Annick**, **Val** et **"toute l'équipe..."** for fun evenings in Lausanne. I also thank **Arnaud, Claire, Virgile** and the others with whom I shared frequent adventures in the sun and snow of Valais.

I am cannot express how thankful I am towards **my parents**. Merci de m'avoir toujours permis et poussé à faire ce qui me plaît et d'en arriver ici! Merci pour votre support, votre patience (!) et votre aide tout au long de ces années et surtout ces derniers mois. Merci aussi à mes frères **Cricri** et **Gaby** qui rendent la vie familiale du week-end si pimentée.

Last, but not least: merci **HUGUES**! (et la troupe de moutons). Merci pour ton support inconditionnel, ton humour, pour les petits plats si bienvenus après une longue journée de travail, pour les discussions micropolluantesques en 3D, pour tes apports cartographiques à ma thèse, pour les virées en montagne, et tous les autres bons moments,...

Lausanne, le 19 Janvier 2013 Flo

Abstract

Invisible to the human eye, yet ubiquitous... The occurrence and the potential adverse effects of micropollutants in the environment are uncontested. Due to incomplete removal by conventional wastewater treatment technologies, the aquatic environment is contaminated with pharmaceuticals and other micropollutants (biocides, pesticides). This thesis discusses the occurrence and photolytic fate of micropollutants in the Vidy Bay of Lake Geneva, Switzerland and the resulting environmental risk.

The spatio-temporal variations in the concentrations of 39 micropollutants were investigated during a 10-month sampling campaign, at different locations around a wastewater outfall in Vidy Bay. A pronounced wastewater plume was observed from April to October, leading to locally elevated pharmaceutical concentrations compared to the surrounding water column. The plume depth followed the thermal lake stratification, which moved to lower depths over the course of the warm seasons. Pharmaceutical hotspots associated with the plume were detected as far as 1.5 km downstream of the wastewater outfall, but concentrations typically decreased with increasing distance from the source. A strong linear correlation between electrical conductivity and concentrations of wastewater-derived micropollutants was identified. This relation will allow future estimates of wastewater-derived micropollutant concentrations via simple conductivity measurements in the vicinity of the plume. On the other hand, from November to January, when uniform temperature prevailed throughout the water column, the plume surfaced or was not detected due to enhanced mixing of the water column. In contrast to pharmaceuticals, most pesticides showed homogeneous concentrations throughout the Vidy Bay during the whole study period, indicating that the effluent wastewater was not their dominant source.

To overcome the limitations of punctual sampling, a more complete picture of the distribution of wastewater-derived micropollutants in Vidy Bay was obtained by augmenting field measurements with a validated model, which incorporates the most important physical and chemical attenuation processes. Given the importance of photolysis in the fate of many organic pollutants, we proposed a model which combines the current hydrodynamics via 3D particle tracking, and the depth-dependent photodegradation of micropollutants. Moreover, the total ecotoxicological risk associated with the predicted concentrations of all micropollutants concentrations was determined.

Direct discharge of effluent wastewater into the Bay resulted in a limited zone, in which micropollutant concentrations were sufficiently high that commonly applied water quality

criteria were exceeded. The resulting ecotoxicoloigcal risk could mainly be attributed to only three among the 24 wastewater-derived compounds investigated, namely three antibiotics. As expected, photodegradation was an important removal mechanism for many compounds and thus, along with dilution, contributed to a reduction in the ecotoxicological risk over time and distance from the WW outfall especially for surface plumes in winter. In contrast, during thermal stratification, the importance of photodegradation processes in attenuating the plume extent is greatly reduced, due to light screening by the water column. Analysis of various scenarios showed that wind conditions and solar irradiation play an essential role in determining hydrodynamic currents and mixing processes, as well as photodegradation kinetics and thermal stratification.

The presence of human metabolites of pharmaceuticals and their phototransformation products may also contribute to the ecotoxicological risk, as they may be more persistent than the parent compound and retain biological activity. Hence, the occurrence of various human metabolites of pharmaceuticals in Vidy Bay was also investigated. On average, the detected concentrations of human metabolites were similar to, or lower than, their associated parent compound. Moreover, the metabolites targeted in this study were determined to be more susceptible to environmental degradation processes than their parent. Nevertheless, their presence in the aquatic environment may still lead to an increase of the ecotoxicological risk.

In continuation, the propensity of selected human metabolites to undergo photodegradation and resulting photodegradation products was studied in detail. In particular, we determined the direct photolysis kinetics and identified the major photoproducts of four human metabolites of the antibiotic sulfamethoxazole, which is one of the substances that exceed water quality criteria in Vidy Bay. The majority of the investigated metabolites were found to be more photostable than the parent compound under environmentally relevant conditions, in contrast to observed field data, indicating that other transformation processes such as indirect photolysis processes and biodegradation may also contribute to the total degradation in the investigated environment. In addition, identification of the major phototransformation products of several human metabolites showed that one was retransformed back to the parent compound via a photoreduction. As such, human metabolites could represent a thus overlooked environmental source of pharmaceuticals in the environment.

This work has revealed new insights regarding the environmental impact of direct discharge of effluent wastewater into lakes. Moreover, it allowed for the identification of important processes and parameters affecting the fate of micropollutants in the aquatic environment, as well as of the problematic compounds which should be considered priority substances for wastewater treatment plant optimization and further monitoring campaigns. Applying a precautionary principle, the results of the present study underline the importance of reducing or preventing the release of micropollutants to the environment.

Key words: micropolluants, pharmaceuticals, human metabolites, antibiotics, sulfamethoxazole, UPLC-MS/MS, ecotoxicity, pesticides, wastewater, Lake Geneva, hydrodynamic model, photodegradation, environmental risk assessment.

Résumé

Invisibles à l'œil nu, ils sont pourtant partout… La présence et les risques potentiels des micropollutants dans l'environnement sont incontestés. Les stations d'épuration actuelles ne peuvent les éliminer des eaux usées ; ceux-ci se retrouvent dans les eaux de surface. Cette thèse étudie la présence et les transformations photoly-tiques des micropolluants dans la Baie de Vidy, au nord du lac Léman, ainsi que le risque environnemental qui en résulte. La Baie de Vidy est une zone potentiellement contaminée du Léman car elle reçoit les rejets des eaux de la station d'épuration (STEP) de la ville de Lausanne.

Les variations spatio-temporelles des concentrations de 39 micropolluants ont été étudiées lors d'une campagne de prélèvements de 10 mois dans la Baie de Vidy, à différentes positions et profondeurs, autour du point de rejet de l'émissaire de la STEP de Vidy. La présence d'un panache de micropolluants a ainsi pu être mise en évidence d'avril à octobre. La position de ce panache de pollution varie selon la stratification thermique du lac, il est plus profond lors de la saison chaude. Des concentrations de micropolluants plus élevées que la moyenne ont été détectées jusqu'à 1.5 km du point de rejet, cependant, les concentrations diminuent avec la distance de la source. Une forte corrélation entre la conductivité de l'eau et les concentrations de micropolluants issus des eaux usées a par ailleurs été mise en évidence. Cette relation peut être utile pour estimer les concentrations de ces micropolluants à l'aide de simples mesures de la conductivité. De novembre à janvier, le lac n'étant pas stratifié, le panache peut atteindre la surface, mais il n'est souvent pas observé en raison du plus fort mélange de la colonne d'eau. Contrairement aux produits pharmaceutiques, une concentration homogène pour la plupart des pesticides est observée dans la Baie de Vidy, ce qui indique qu'ils ne proviennent principalement pas du réseau d'eaux usées.

Pour obtenir une image précise et complète de la distribution des micropolluants issus de l'émissaire des eaux usées dans la Baie de Vidy, et pour contourner certaines limitations liées à l'échantillonnage ponctuel, un modèle couplant les mesures expérimentales avec les processus de transport et de dégradation a été développé. Ce modèle hydrodynamique 3D de traçage prend également en compte les phénomènes de photo-dégradation, en fonction de la profondeur. Finalement, les risques écotoxicologiques liés aux concentrations prédites de micropolluants ont été déterminés.

Le rejet des effluents de la STEP dans la Baie de Vidy crée une zone dans laquelle les concentrations de certains micropolluants sont supérieures aux critères de qualité des eaux de surface, qui visent à protéger la faune et la flore aquatique. Ces risques écotoxicologiques

sont particulièrement liés à trois substances parmi les 24 étudiées, toutes trois étant des antibiotiques. Comme attendu, la photodégradation est un processus important d'abattement de nombreuses substances et, avec le phénomène de dilution, contribue à la réduction des risques écotoxicologiques des effluents de la STEP, principalement lorsque le panache est proche de la surface. Par contre, lorsque la stratification thermique maintient le panache en profondeur, la photodégradation perd de son importance en raison de l'atténuation de la lumière par les couches superficielles. La modélisation démontre le rôle essentiel que jouent les vents pour la mise en place des courants hydrodynamiques et pour le processus de mélange des eaux alors que l'irradiation solaire est déterminante pour la cinétique de photodégradation et pour la stratification thermique des eaux.

La présence de métabolites humains de médicaments ainsi que de substances issues de photodégradation peuvent également contribuer à l'augmentation du risque écotoxicologique, car ils peuvent être plus persistants que leur substance parente, et tout autant toxiques. Pour ces raisons, la présence dans la Baie de Vidy de plusieurs métabolites humains a également été étudiée. Les concentrations mesurées des métabolites sont plus faibles ou similaires à celles de leur parent. Par ailleurs, les métabolites ciblés se sont révélés plus susceptibles à une dégradation environnementale que leur parent. Néanmoins, leur présence dans l'environnement aquatique ne peut qu'augmenter le risque écotoxicologique.

Finalement, les processus de photodégradation d'un antibiotique, le sulfamethoxazole (SMX), et ceux de ses métabolites humains, ont été étudiés plus en détail afin de vérifier les mesures de terrain et d'identifier leurs sous-produits. Le SMX est l'une des substances dont les concentrations observées dans la Baie de Vidy dépassent les normes de qualité pour les eaux de surface. Les cinétiques de dégradation du SMX et de ses principaux métabolites ont ainsi été déterminées. Contrairement aux observations de terrain, la plupart des métabolites se sont révélés plus résistants à la dégradation par le soleil que leur parent, ce qui indique que d'autres processus tels que la photodégradation indirecte ou la biodégradation contribuent également à leur élimination dans le milieu naturel. Cependant, l'identification des photoproduits a permis la mise en évidence d'une retransformation d'un métabolite en son principe actif parent par l'effet du soleil. Ainsi, les métabolites humains peuvent représenter une source de produits pharmaceutiques dans l'environnement.

Ce travail donne une meilleure compréhension sur l'étendue de l'impact environnemental d'un rejet direct d'eaux usées dans un lac. Il permet également de reconnaître les facteurs et les processus clés qui influencent la persistance ou la dégradation des micropolluants dans un environnement lacustre. Il identifie par ailleurs certains micropolluants problématiques comme cibles de futures campagnes de terrain et comme substances prioritaires pour l'optimisation des procédés de traitement des eaux usées. En respectant le principe de précaution, l'ensemble des résultats de cette étude souligne l'importance d'éliminer, ou tout au moins de réduire, les rejets de micropolluants dans l'environnement.

Mots clés : micropolluants, médicaments, métabolites humains, antibiotiques, sulfamethoxazole, UPLC-MS/MS, ecotoxicité, pesticides, eaux usées, lac Léman, modèle hydrodynamique, photodégradation, risque environnemental.

Contents

List of Figures

List of Tables

List of Abbreviations

ABR - antibiotic resistant bacteria
CDOM - chromophoric dissolved organic matter
DOC - dissolved organic carbon
DOM - dissolved organic matter
EC50 - effect concentration 50
HC - hazard concentration
HRT - hydraulic retention time
HRMS - high resolution mass spectrometry
LC - liquid chromatography
MEC - measured environmental concentration
MS - mass spectrometry
NOEC - no-observed effect concentration
NSAID - Non-steroidal anti-inflammatory drug
PEC - predicted environmental concentration
PNEC - predicted no-effect concentration
Q-TOF - quadrupole time-of-flight
RQ - risk quotient
SF - safety factor
SPE - solid phase extraction
SRT - solids retention time
SSD - species sensitivity distribution
TOF - time-of-flight
WQC - water quality criteria

1 Introduction

1.1 Introduction

Invisible to the human eye, yet ubiquitous... The occurrence and the potential adverse effects of micropollutants in the environment have been the object of many studies in recent years, and are starting to receive attention from the general public. In research, much focus has been laid on the so-called emerging pollutants, namely pharmaceuticals, which reach the sewer system and wastewater treatment plants mainly via domestic use. Technologies commonly applied for wastewater treatment are not designed to remove these micropollutants, and as a consequence the aquatic environment is ubiquitously contaminated with pharmaceuticals and other micropollutants (biocides, pesticides). A wide variety of micropollutants have been detected in the ng-μg·L^{-1} range in various land-use settings and climatic regions throughout the planet. Yet, research to date has focused on their fate during wastewater treatment and their occurrence in river waters. Though some studies have investigated their degradation in lake water columns, the variety of studied compounds is limited and the current state of knowledge on their fate in the environment is far from satisfying. To better preserve lakes as a freshwater resource and environmental habitat, it is essential to gain a better understanding of micropollutants in surface waters.

Lake Geneva represents the most important freshwater reservoir of Western Europe, providing potable water for over 700'000 people. The city of Lausanne on the northern shore of the lake benefits from this freshwater source, drawing water from the Vidy Bay. On the other hand, the city's effluent wastewater is discharged directly into the Bay, yielding a potentially contaminated site. This thesis investigates the presence of a selection of micropollutants in the Vidy Bay of Lake Geneva, quantifies the importance of photodegradation with respect to their fate in natural waters, and finally proposes a model to estimate the spread and persistence of micropollutants surrounding the wastewater outfall in Vidy Bay.

This introduction describes some relevant concepts and a provides a brief summary of relevant literature to date, leading the reader from the consumption of a pharmaceutical to its release into the environment, by describing the potential sources, pathways and transformation of a pharmaceutically active substance (section 1.2). Details pertaining to the study site of the Vidy Bay will be emphasized (blue box) when pertinent. This section also discusses some intimately linked issues such as the potential effects and risks of trace concentrations of these micropollutants in natural waters. Next, some important photodegradation principles will explained in relation to recent scientific work (section 1.3). Finally, the research objectives and the general approach of each research chapter will be presented (section 1.4).

1.2 Micropollutants in the environment- from source to sink

1.2.1 What are micropollutants?

Before leaping into the topic, let us define the term micropollutants and their main sources. Micropollutants are organic compounds present in the environment in low concentrations ($\mu g \cdot L^{-1}$ or $ng \cdot L^{-1}$) and originate from chemicals that form an integral part of our daily lives, such as human pharmaceuticals, biocides, pesticides, personal care products, industrial chemicals, etc. Over 100'000 chemicals are registered in the European Union, of which 30'000 to 70'000 are regularly used[1] and may find their way into the environment. This thesis focuses on a subset of compounds that were determined most pertinent for the Vidy Bay catchment[2]. The selection comprises mainly pharmaceuticals, but also the human metabolites of pharmaceuticals, as well as biocides, pesticides, fungicides and corrosion-inhibitors.

Pharmaceuticals will be a strong focus of this thesis, as they represent an important part of the chemical enterprise; thousands of tons of drugs are used every year, and consumption has been rising constantly. In the European Union, approximately 3000 substances are registered for pharmaceutical purposes[3]. Pharmaceuticals are defined as substances responsible for physiological or pharmacological action and are used in diagnosis, cure, mitigation, treatment or prevention of disease. Most pharmaceuticals are designed to be persistent enough to reach the target location in the human body, where the physiological effects are desired[4]. Yet this caracteristic becomes detrimental if these substances reach the environment. Many questions remain open as to their fate in the environment, and their effects on biota at the concentrations that have been observed. But how is it that pharmaceuticals find their way into the environment?

1.2.2 Sources of micropollutants

The main sources for pharmaceuticals in the environment are industry, hospitals, household consumers and veterinary drugs from livestock (Figure 1.4). Contamination of the environment can begin at the manufacturing plant where pharmaceuticals are disposed of as solid waste or in wastewater effluent. Pharmaceuticals disposed of as solid waste can be destroyed through incineration. On the contrary, solid waste disposed in landfills may persist in water drained from the landfill or percolate to groundwater aquifers (leaky landfill)[4]. Pharmaceuticals from households and hospitals are consumed, partially metabolized, and are either released in feces and urine to the sewer system or disposed of as solid waste. Improper disposal of unused drugs down the toilet constitutes another source of pharmaceuticals in wastewater. Once in wastewater, these compounds are transported by sewers to wastewater treatment plants (WWTPs). In some cases, they may be directly discharged into aquatic environments without treatment, e.g. during high rain events that lead to a surpass of the WWTP capacity, or through leaking sewers[5].

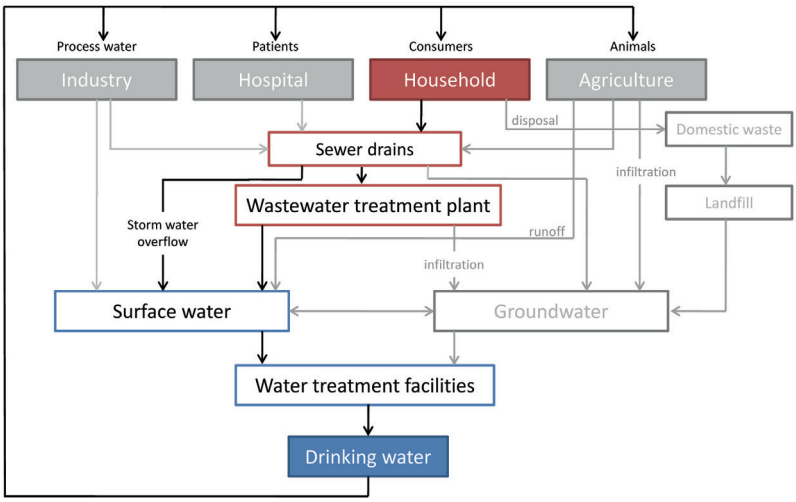

Figure 1.1: *Exposure routes of pharmaceuticals into wastewaters and the aquatic environment. Adapted from*[4].

Compounds transiting the WWTP may be removed by one of the mechanisms discussed below, yet studies have shown that many compounds are removed by less than 50%[4]. Therefore, centralized sewage treatment plants represent an important point source for micropollutants into the aquatic environment[4]. Compounds sorbed to sewage sludge sludge may find their way to the environment through application of sewage sludge as a soil fertilizer. In Switzerland, however, land application of sewage sludge has been forbidden since 2003; instead, sewage sludge is incinerated. The path taken by veterinary drugs to the environment is more direct, as the latter are more likely to directly contaminate soil, groundwater and surface waters without any sewage treatment. Indeed, surface and groundwater can be contaminated by runoff of manure from fields after rainfall[6].

The sources of pesticides and herbicides to the aquatic environment are multiple, and can be qualified as diffuse or point-source. Pesticides are evidently used for agricultural purposes, but are also applied in urban areas, on lawns, streets, building materials and for protection of materials (e.g. anti-fouling agents). Point sources of agricultural pesticides are generally due to misuse (over-application) and improper disposal (direct discharge to surface waters). However, the most significant pathways of agricultural pesticides into surface waters are diffuse pollution such as surface runoff, subsurface hydrological pathways, and spray drift[7]. On the other hand, most urban pesticides are likely to be flushed from gardens, streets and buildings into the sewer system and to the wastewater treatment plant, which, due to incomplete removal, also represent point sources of pesticides to the environment[8]. In Switzerland, agriculture is one of the dominant land uses. Accordingly, diffuse transport from land has been identified as an important source of pesticides to surface waters. However, in catchments of mixed land use, the contribution of urban area inputs may be at least as large as those from agricultural areas[9].

The Lake Geneva catchment falls into this mixed land-use category, hence both diffuse and point source (from WWTPs) pollution are expected. Approximately 40% of the catchment is arable or pastured land, presenting a potential diffuse source of pesticides. Another possible source of contamination to the lake is the Rhône river, which flows in from the west, and accounts for over 75% of the total input to the lake. The Rhône is influenced by agricultural practices, as well as several industrial sites along the Rhône Valley. Pollution associated to urban areas such as discharged WWTP effluents is expected to be important along the northern shore of the lake, as it accommodates the greater part of the population.
Effectively, the Vidy Bay, on the northern shore of Lake Geneva by the city of Lausanne (135'000 inhabitants), is thought to be one of the most contaminated areas of the lake. The Bay represents 0.3% of the lake's total volume. Aside from lake currents, a major input of water to Vidy Bay is the effluent discharge from Lausanne's wastewater treatment plant. Other sources of water to Vidy Bay are the Chamberonne River and the Flon stormwater outlet, which are impacted by agricultural and urban areas respectively, and, aside from diffuse run-off from land, may present sources of agricultural or urban pesticides. As to pharmaceuticals, wastewater from Lausanne's various hospitals and health care centers adds up to less than 0.4% of the total volume of treated wastewater. Hence household consumption, via discharge through WWTPs, likely represents the main source of pharmaceuticals into the Bay (bold in Figure 1.1).

Following this scheme, the next sections will focus on pharmaceuticals, from consumption, through the wastewater treatment system, to presence, fate and effects in the aqueous environment. Each section aims to give a brief overview of the important research to date, and highlight research needs.

1.2.3 Human metabolism and excretion of pharmaceuticals

After intake by humans, pharmaceuticals are metabolized to various extents, which is partly a function of the substance and the individual patient. The proportion of an ingested pharmaceutical that is excreted in unchanged form varies over a wide range[4,10,11]: only 5% of paracetamol and 26% of diclofenac are found unchanged in urine and feces, yet this fraction increases to 45% for the antibiotic ciprofloxacin and can reach 96% in the case of the betablocker atenolol[12].

Once absorbed by the human body, the active substance can undergo two main metabolic transformation processes (Figure 1.2). Phase I transformations involve the introduction of a functional group such as –OH, -SH, $(>C)_2O$ (epoxide), $-NH_2$, or –COOH (e.g. Figure 1.3, ring hydroxylation of propranolol). Frequently, this reaction is mediated by a cytochrome P450 enzyme.

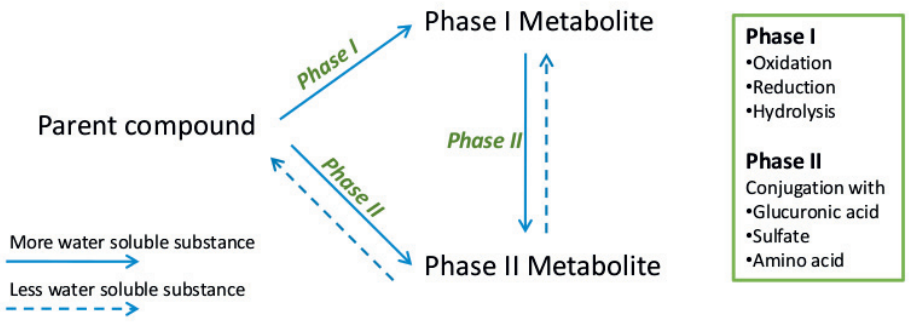

Figure 1.2: *Human metabolism of pharmaceuticals into phase I and phase II metabolites. Adapted from*[13,14].

Phase II metabolism, also refered to as conjugation, consists in the addition of a readily available *in vivo* molecule (generally glucuronic acid or sulfate) to a susceptible functional group (e.g. Figure 1.3, glucuronidation and sulfation of propranolol). Both transformation phases lead to an increase of polarity (and thus excretability) of the compound. Though drug metabolism was initially defined as a detoxication mechanism, current research now recognizes that metabolism does not necessarily transform the parent compound into a less toxic substance[15]. Thus, after consumption, a variable fraction of unchanged pharmaceutical and various metabolites are excreted via urine and feces, leading to presence of active substances in raw wastewater.

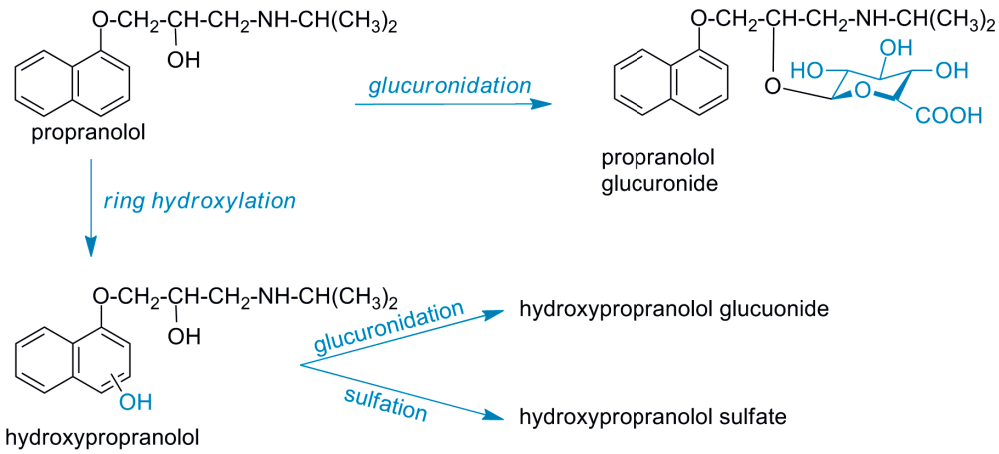

Figure 1.3: *Main metabolic pathways of betablocker propranolol in humans (adapted from*[16]*).*

1.2.4 Occurrence and fate in wastewater

The first studies reporting the presence of pharmaceuticals in raw and effluent wastewater go back to the 1980's. Ever since, the occurrence and fate of pharmaceuticals in wastewater has been the focus of numerous studies. Detected concentrations in raw and influent wastewater vary greatly between individual pharmaceuticals and among studies, ranging from the high ng·L^{-1} to low μg·L^{-1} range ([4,17] and references therein), however the undisputed conclusion remains that removal is incomplete for a large majority of compounds in conventional wastewater treatment plants (WWTP).

The physical-chemical properties of a compound, namely aqueous solubility, volatility, acidity and lipophilicity will influence its behaviour during the various steps of conventional wastewater treatment. Ultimately, the fate of an organic compound mainly depends on its capacity to associate with particles (physical-chemical removal) and its biodegradability. Descriptors of organic partitioning, such as K_{OW} (octanol-water partitioning coefficient) or K_d (sorption coefficient) are often used to predict the extent of sorption to sludge [18]; available data suggests that K_d is the most suitable parameter to estimate removal by adsorption [19–21]. Sorption can be considered a significant removal mechanism only for a small fraction of drugs; namely hydrophobic compounds with high K_{OW} (Log K_{OW} ca. 5.5–6) and/or K_d values greater than 300 kg·L^{-1} [20]. As such, preliminary and primary treatments, where sorption processes dominate, generally showed poor removal of pharmaceuticals [17]. Hence, the greatest removal occurs during the biological treatment [18]. Overall removal efficiencies vary from <5% to 95% [4]. This large variance can be explained in part by the different physico-chemical properties of each pharmaceutical. Nevertheless, no evident correlations have been identified between propensity to biodegrade and compound structure to allow for predictions of biological removal efficiencies [3]. Thus, we rely on empirical data (e.g. batch experiments [3]) and in situ observations to assess the extent of biological removal for a given compound.

Paracetamol, gemfibrocil, and bezafibrate are examples of compounds susceptible to biological removal, and will be considered in this thesis. Conversley, carbamazepine, diclofenac, sulfamethoxazole, gabapentine, or metoprolol are all relatively recalcitrant to conventional treatment ([18] and references therein).

Removal is also significantly influenced by operating conditions, such as the treatment process, the age of the activated sludge, hydraulic and solid retention time (HRT and SRT) and environmental conditions [17]. Several reviews highlight the opposing conclusions of various studies as to the effect or non-effect of varying HRT and SRT, as well as the influence of ambient temperature [18,22]. Nevertheless, with respect to temperature, the majority of investigations report enhanced degradation during warmer seasons [22]. Consequently, lower removal was observed during the cold season, as illustrated by a study on five pharmaceuticals (ibuprofen, naproxen, ketoprofen, diclofenac and bezafibrate), which found a three- to five-fold increase of concentrations in effluent water during the winter months [23].

Recent work investigated the occurrence and removal of 58 pharmaceuticals, endocrine disruptors, corrosion inhibitors, biocides, and pesticides in the Vidy WWTP of the city of Lausanne. The target compounds were selected through a prioritization study for the Lake Geneva region, based on consumption loads, the degree of human metabolism, estimated removal in WWTPs, and – if known – ecotoxicological relevance[2]. Average effluent concentrations of the chosen priority compounds ranged from 0.025 to 6 $\mu g \cdot L^{-1}$. Only a few of the compounds exhibited a removal efficiency greater than 50%. The low removal efficiencies were expected, as the priority compounds were selected in part based on their poor removal during WW treatment. The increased recalcitrance of some micropollutants in the present study compared to previous work might also be related to the low water temperatures in the WWTP during the sampling period (Febuary-March 2009)[24].

Available data shows that metabolites are present in wastewater effluent in concentrations comparable or higher than their parent compound. Leclercq et al. found 2–5 times higher concentrations of the main metabolite of carbamazepine (10,11-dihydro-10,11-trans-dihydroxycarbamazepine) in wastewater of three different treatment plants, in addition to other metabolites of this antiepileptic drug[25]. Hilton reported high concentrations of N4-acetylsulfamethoxazole, a metabolite of sulfamethoxazole, in treated sewage[26]. Other studies have also observed concentrations of metabolites (ibuprofene and diclofenac, among others) that regularly exceeded those of the parent compound[27–33]. Negative removal efficiencies observed during the treatment process for certain compounds led scientists to the problem of human metabolites in wastewater. Indeed, there is evidence that metabolites may be retransformed to the parent form during biological treatment, through cleavage of the glucuronide bond for example[32,34,35]. As some metabolites retain biological activity or may represent a source of parent compound in WWTPs, researchers agree on the need of including metabolites in water monitoring surveys and environmental risk assesments[36].

As mentioned earlier, urban pesticides, from lawns, streets and buildings, find their way to WWTPs, where, as for their pharmaceuticals, both detected concentrations and removal efficiencies vary largely[24].

Ongoing efforts focus on the improvement of wastewater treatment with regard to the removal of pharmaceuticals and other micropollutants. The addition of an advanced treatment step such as membrane filtration, activated carbon, ozonation, advanced oxidation or UV-treatment, to conventional treatment have shown promising results[18], but remain very energy-demanding[37].

Two advanced treatments, ozonation and adsorption onto powdered activated carbon coupled to ultrafiltration, were tested on a large scale in the WWTP of Vidy (Lausanne, Switzerland), yielding >80% removal of 58 investigated micropolluants, for a 30% energy requirement increase[38].

Further studies have shown that alternate treatment processes such as wetlands and lagoons also allowed for increased micropollutant removal[18]. Until such technologies become more widespread, concerning loads of pharmaceuticals are released to surface waters after wastewater treatment.

1.2.5 Occurrence in surface water

Owing to the constant release of pharmaceuticals via WW outfalls, the presence of micropollutants in surface waters is no surprise. Accordingly, since the 1980's, an increasing number of studies confirm the presence of a large variety of pharmaceuticals and other micropollutants in surface waters of various land-use settings around the world, with rising frequency of detection[13,39]. The reported concentrations vary with compound, but are generally remain below 100 ng·L^{-1}, though substantially higher concentrations have been observed (up to several μg·L^{-1}) . Non-steroidal anti-inflammatory drugs (NSAIDs) are the compound class showing highest concentrations (e.g. diclofenac and paracetamol). Other pharmaceuticals regularly detected in significant concentrations in surface waters include sulfamethoxazole (antibiotic), carbamazepine (anti-epileptic), gemfibrozil (lipid regulator) and atenolol (betablocker)[39]. To date, most investigations have focused on streams or rivers[39], whereas data pertaining to the occurrence of pharmaceuticals in lakes is scarce.

The observed concentrations of pharmaceuticals in surface waters are influenced by a number of factors: consumption in the catchment area, degree of human metabolism, extent of degradation during WW treatment, dilution factors in receiving surface waters, hydrological chacrteristics of the water body and environmental removal processes, to name a few. Accordingly, a number of studies reported the spatial, seasonal and temporal variability of observed concentrations in surface waters.

With respect to spatial distribution of pharmaceuticals, highest concentrations are generally observed close to point sources, such as discharges for WWTP effluent and tended to decrease with increasing distance from the contamination source[10,39]. When the analysis is extended over long river stretchs (e.g. the Rhine river, ca. 700 km), the concentrations of pharmaceuticals are expected to increase with increasing distance from river source, owing to increasing anthropogenic pressure[40,41]. Nevertheless, the reported spatial variations were rarely consistent among all the investigated compounds of a given study and among different studies[40,42]. This illustrates the influence of compound-specific physico-chemical properties and the physical characteristics of their surrounding environment.

Only a limited number of studies have examined the depth dependence of micropollutant concentrations. Conely et al. found a positive relation between surface and subsurface river samples of certain compounds, but owing to the small concentration difference concluded that the investigated river system was thoroughly mixed. Altogether, there is little comprehensive data describing fluctuations of pharmaceutical concentrations with depth, nor much information on spatial distribution of pharmaceuticals near point sources in lakes.

The temporal variations of micropollutants also depend on a variety of factors, which may explain the differences in reported seasonal trends. Though a number of studies found higher concentrations during winter and spring, this was not always the case. Higher concentrations observed in winter/spring were often attributed to cold-water temperatures, which may enhance the recalcitrance of given compounds during WW treatment, as well as their persistence in the natural environment[42–44]. Certain compounds, such as the anti-epileptic carbamazepine, displayed no significant variation by season[40,42]. Seasonal variability may also be the effect of varying flow conditions, precipitations and consumption patterns of pharmaceuticals (e.g. antibiotics are more frequently prescribed in winter[45]) [40,43,46].

Human metabolites were not only detected in wastewaters, but also in the receiving environment, though data remains scarce. Various authors report the presence of metabolites in streams receiving wastewater effluent, in drinking water (the main metabolite of carbamazepine) and even in bottled water (an N-acetylated metabolite of sulfamethazine)[29,30,47].

For pesticides, the first reports of surface water contamination date back to 1960's. Both diffuse surface runoff and point source input of urban pesticides from WWTPs contribute to pesticide pollution worldwide. Resulting concentrations in surface waters vary with compound and may reach the low $\mu g \cdot L^{-1}$ range. Several consecutive reviews reported that more than 95% of samples collected from streams across the United States contained at least one pesticide[48,49]. Frequently detected pesticides in the European environment include atrazine, mecoprop and isopropanol[50–52]. In comparison to pharmaceuticals, spatial and temporal patterns have been more extensively studied. This may be explained by both the earlier discovery in environmental waters and the intrinsic seasonal and spatial aspects of pesticide application. As expected, detected concentrations showed a strong seasonality and were linked to rainfall events, with highest concentrations detected during field application periods[50,52,53].

The monitoring of pesticides in Lake Geneva was initiated in 2001, whereas pharmaceutical occurrence data exist since 2005. Samples, taken two times a year at various depths above the deepest point of the lake (309 m) were analysed for an entire suite of pesticides (306 in 2010) and pharmaceuticals (109 in 2010). Though not peer-reviewed, the latest report confirmed the presence over 50 pesticides 10 and pharmaceuticals. In 2010, the sum of all pesticides ranged between 0.1 and 0.2 $\mu g \cdot L^{-1}$ and has been stable since 2008. Note that the sum of pesticides detected in the Venoge river on the eastern limit of the Bay was over 0.4 $\mu g \cdot L^{-1}$ in November 2009 and May 2010. For pharmaceuticals, the highest concentrations were observed for the anti-eplieptics carbamazepine (62 $ng \cdot L^{-1}$) and gabapentine (24 $ng \cdot L^{-1}$), and the anti-diabetic metformin (320 $ng \cdot L^{-1}$).

To date, regulations in Switzerland limiting the concentrations of pharmaceuticals in environmental waters remain vague. The water protection ordonnance (OEaux, 814.201) stipulates that surface waters must not contain synthetic substances that may be persistent and/or have adverse effects on biota. However, there are no numeric requirements for pharmaceuticals. Conversely, fixed limits are given for individual organic pesticides, for which concentrations must remain below 0.1 $\mu g \cdot L^{-1}$.

1.2.6 Occurrence in drinking water

Trace levels of several compounds have even been detected in finished drinking water. Commonly studied pharmaceuticals such as paracetamol, diclofenac, and carbamazepine were detected in drinking water across Europe and in North America[14,39,54]. Moreover, concentrations detected in Berlin tap water were found to be correlated to the proportion of groundwater recharge used as drinking water source ([54] and references therein). Carbamazepine and gemfibrocil were found in the drinking water of four Canadian cities that all used advanced water treatment, such as ozone or granular activated carbon, indicating that certain substances may pass through modern and advanced water treatment facilities. Nevertheless, the overall detection frequency remains low, and to date the contamination of drinking water does not pose an known appreciable risk to human health ([54,55] and references therein).

A recent news report on Swiss TV revealed the systematic presence of up to 10 micropollutants in tap water sampled around Lake Geneva, with the notable presence of the atrazine (pesticide), benzotriazole (corrosion inhibitor) and carbamazepine (anti-epileptic) (ABE (RTS), 30 October, 2012).

1.2.7 Potential effects on the aquatic environment

Pharmaceutical compounds are originally designed to be biologically active and influence specific metabolic pathways in humans and animals. Though measured concentrations in water are considerably lower than those producing targeted physiological effects, the continuous exposure of aquatic fauna and flora to low-levels of biologically active pharmaceuticals and pesticides is concerning. The potential effects of pharmaceuticals still remain largely unknown. Effects are commonly predicted from acute (short-term) and chronic (long-term) laboratory tests performed on species such as algae, crustaceans and fish, yielding threshold concentrations such as the EC50 (effect concentration 50% [1]) or NOEC (no-observed effect concentration).

Adverse effects of exposure to trace concentrations of individual pharmaceuticals and more complex mixtures have been revealed by a growing number of studies ([54,56,57] and references therein). One typical example is the feminization of male fish due to the endocrine disrupting effects of estrogens[58]. A recent critical review reported that 10–15% of pharmaceuticals present acute or chronic toxicity for certain biological endpoints[57]. However, it is relevant to note that ecotoxicological data is available for less than 15% of pharmaceuticals detected in the environment.

Most research to date has focused on acute effects of single compounds[59]. Available data show that acute effect concentrations are 2–3 orders of magnitude above actual environmental concentrations, suggesting that there is little risk of acute toxicity[57,60]. Yet, in the environment, organisms are exposed to an entire cocktail of substances over their entire life-time.It has been found that such mixtures can exhibit different and more harmful effects on growth, fertility, sex ratios or reproductive behavior of aquatic organisms than single compounds[14,54,56]. As to long-term effects, the common approach of deriving chronic ecotoxicity data from acute tests by means of applying a safety factor (or assessment factor) has been proven invalid for several compounds[59,61]. Overall, experts agree that there is a general lack of information regarding long-term effects of environmentally relevant mixtures. Moreover, available data on chronic effects often don't concern the key targets, nor consider different organisms[60]. Recent studies focus on the specific modes of action of pharmaceuticals to better identify the most sensitive trophic groups and measure pertinent biological endpoints[57].

Metabolites are generally expected to have an equal or lower toxicity than the parent compound[62], but may still lead to adverse effects on aquatic organisms. Norfluoxetine, the main metabolite of fluoxetine, was found to be 50% more toxic than the parent compound[36]. Several other metabolites, such as those of clofibric acid or propranolol, were determined to be at least as toxic as their parent compound[36,63]. As for the majority of pharmaceuticals, the ecotoxicological risks of metabolites are still to be determined, but a precautionary principle should be applied by also considering excreted metabolites in risk assessments.

[1] concentration at which 50% of the tested organism shows the targeted endpoint, generally mortality

Another area of concern is the spread of antibiotic-resistant bacterial strains. Effluent wastewater has been identified as a major source of antibiotic resistant bacteria (ARB) in surface waters[64,65], and the continual input of ARB and their resistance genes may ultimately lead to an increase of infections with resistant pathogens. ARB were detected in diverse aquatic environments[54,56]. In addition, trace concentrations of antimicrobials play a role in promoting resistance among environmental strains. Recent work showed that even extremely low antibiotic concentrations, similar to the concentrations found in natural environments, can select for resistant bacteria[66]. The question if the direct input of already resistant bacteria or low levels of antibiotics in surface waters represents a more important source of ARB in the environment was highlighted in a recent review[56]. To date, available data points toward the direct input of ARB as the most important source of resistance in the environment.

1.2.8 Environmental risk assessment of micropollutants

The increasing concern regarding the presence and effects of micropollutants in surface waters has led European and North American countries to propose water quality criteria (WQC) for micropollutants in surface waters ([67] and references therein). EU guidelines often use predicted no-effect concentrations (PNEC) as WQC[68]. PNECs represent concentrations below which an unacceptable effect will most likely not occur. PNECs are classically determined using ecotoxicity data (preferably chronic data, e.g NOEC) of three trophic levels. The PNEC for each substance is calculated by dividing the EC50 or NOEC of the most sensitive trophic level by a safety factor (SF), typically 100 or 1000. The safety factor expresses the degree of uncertainty in the extrapolation from the test data on a limited number of species to the actual environment and as mentioned earlier, will be higher if using results from acute tests. When enough ecotoxicity data is available (e.g. for many pesticides), the hazardous concentration 5 (HC5), a more robust WQC, can be derived from species sensitivity distribution curves (SSD). The HC5 represents the concentration that protects 95% of all aquatic species[67], and a PNEC equivalent can be calculated by dividing HC5 by a factor of 5[68].

The environmental risk is generally characterized by comparing the measured environmental concentrations (MEC) with specific WQCs (PNECs). The resulting risk quotient (RQ) for each individual substance i, shown in equation 1.1, must remain below one to ensure an acceptable risk to the environment[67].

$$\mathrm{RQ}_i = \frac{\mathrm{MEC}_i}{\mathrm{PNEC}_i} \tag{1.1}$$

However, in the aquatic environment, all substances are present contiguously, thus a realistic ecotoxicological risk assessment should consider the effect of all chemicals present.

Latest research recommends applying a concentration addition (CA) model as a conservative worst case estimation of mixture toxicity[69,70]. Explicitly, the risk of a chemical mixture, RQ_m, is the sum of the RQ of all n substances present in the mixture, RQ_i (equation 1.2):

$$RQ_m = \sum_{i=1}^{n} \frac{MEC_i}{PNEC_i} \tag{1.2}$$

The CA model by definition assumes all substances exhibit a similar mode of action, an assumption that is often not fulfilled in environmentally realistic mixtures[70]. Nevertheless, the concept of CA is recommended for a precautious risk assessment, and has been shown to provide excellent predictions of mixture toxicities[71,72].

1.2.9 Natural elimination in the environment

Organic micropollutants are subject to various removal processes which affect their concentration in environmental systems. These processes are largely influenced by the intrinsic physical and chemical properties of the compound, but also the environmental conditions and the surrounding matrix. The main removal processes in surface waters are biodegradation, sorption and photodegradation.

We can expect a minor importance of biodegradation for those micropollutants that showed incomplete removal during biological wastewater treatment and are released to the environment[60]. Moreover, the lower bacterial density and diversity in surface waters likely implies slower biodegradation than in sewage[56]. For example, a recent review reported that over 20 important antibiotics were not found to biodegrade readily in batch reactors (closed-bottle tests)[56,73].

Given the polar and hydrophilic nature of the large majority of pharmaceuticals (low octanol-water partition coefficient), removal through sorption processes is expected to be small. However, sorption is also affected by pH, stereochemical structure and chemical nature of the sorbent and sorbed compound[56]. This is well illustrated with the antibiotic ciprofloxacin, which, despite its low log K_{OW} (0.28, physprop database), was found to sorb to particulate organic matter[71], showing that ionic interactions between ionized groups of a pharmaceutical can also act as binding mechanisms to particles or dissolved organic matter. Planar aromatic structures may also favor sorption by intercalation in layers of some clay minerals[56].

Nevertheless, for those chemicals that do not undergo sorption to sludge nor biodegradation in WWTPs, photodegradation can be expected to be a major environmental removal process. Photolysis has been identified as an key degradation mechanism of many pharmaceuticals and other micropollutants in the environment[74–76]. Many compounds feature aromatic rings, heteroatoms and other functional groups capable of absorbing solar radiation and making them susceptible to transformation by the sun[75].

Compounds which do not directly absorb incident radiation may nonetheless undergo indirect transformation mechanisms via reaction with other photo-excited species such as various water constituents[11]. Direct and indirect photoprocesses yield various intermediate species, which in turn can trigger the other degradation mechanisms described above. Indeed photoproducts and intermediates are more polar and hydrophilic than their parent compounds, and may undergo further biodegradation and hydrolysis[77,78].

Important principles of direct and indirect photolysis will be described next, followed by a review of relevant literature regarding photodegradation in aquatic environments in section 1.3.

Direct Photolysis

Direct photolysis can occur when an organic pollutant directly absorbs incoming radiation. Light absorption implies an overlap of the sunlight emission spectrum with the absorbance spectrum of the given compound; however, not all absorbed light yields a photochemical transformation. Light absorption leads to the promotion of the compound to an excited state, namely the short-lived singlet-state. At this point the excited compound may convert to triplet state via intersystem crossing. The triplet excited state has lower energy than the singlet excited state, but a longer lifetime. Both excited states may, through physical processes, return to their ground state (no transformation), or undergo chemical reactions which involve the transformation of the compound.

Physical processes which return the excited molecule to the ground energy state include[19]:

Internal conversion: vibrational energy loss yielding heat

Luminescence: energy loss by light emission (e.g. fluorescence and phosphorescence)

Photosensitization: energy transfer to another molecule

Yet, we are more interested in potential chemical reactions, as these have environmental implications. Possible phototransformation reactions include cleavage, dimerization, electron transfer, hydrogen atom abstraction, intramolecular rearrangement and isomerization are listed below and some are depicted in figure 1.4[19].

The efficiency of a phototransformation reaction is given by the reaction quantum yield, $\Phi(\lambda)$. For a given wavelength (λ), it is defined as the ratio of the number of molecules transformed by photolysis to the number of photons absorbed:

$$\Phi(\lambda) = \frac{\text{number of molecules transformed by photolysis}}{\text{number of photons absorbed}} \tag{1.3}$$

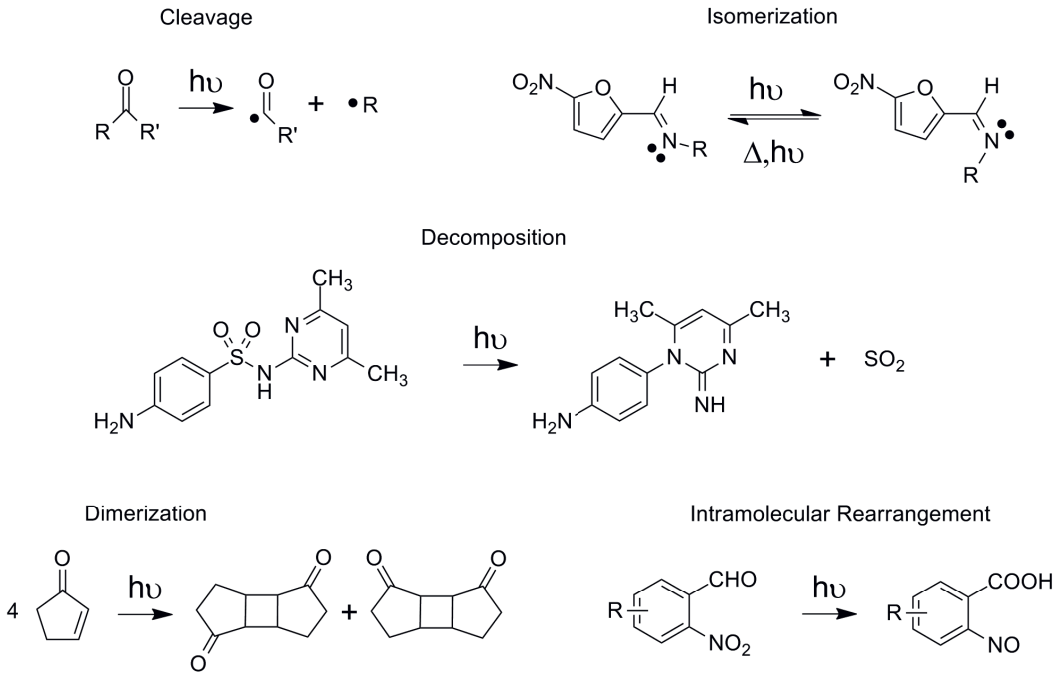

Figure 1.4: *Examples of phototransformation reactions (adapted from [79,80]).*

Quantum yields cannot be predicted (yet) on basis of the chemical structure of the compound, so they must be determined experimentally. Equation 1.3 evokes a wavelength dependence of the quantum yield. However in many cases the quantum yield can be assumed wavelength independent, except for compounds absorbing over a large wavelength range with several light absorption peaks [19].

As light absorption is a prerequisite for all photoprocesses, it is important to define necessary concepts of light absorption which will serve as a basis for calculating important photodegradation quantities, such as the quantum yield or the light screening factor. For a complete derivation of the equations, interested readers are referred to textbooks [19].

Two important absorption processes must be considered:

a) Light absorption by the bulk solution.

Light attenuation by the totality of chromophoric substances in solution impacts the amount of radiation available for photodegradation processes. The Beer-lambert law describes the absorbance of light by a solution by relating the amount of light emerging from the solution $I(\lambda)$ to the incident light intensity $I_0(\lambda)$:

$$I(\lambda) = I_0 \cdot 10^{-[\alpha(\lambda)+\varepsilon_i(\lambda)\cdot C_i]\cdot l} \tag{1.4}$$

where $\alpha(\lambda)$ is the attenuation coefficient of the solution in cm^{-1}, C_i is the concentration of the compound i under consideration, l the pathlength of light through the solution and $\varepsilon_i(\lambda)$ the decadic molar absorption coefficient of i, which describes the ability of the compound to absorb light at a particular wavelength.

The absorbance of the solution $A(\lambda)$ is then given by:

$$A(\lambda) = \frac{I_0(\lambda)}{I(\lambda)} = [\alpha(\lambda) + \varepsilon_i(\lambda)\cdot C_i]\cdot l \tag{1.5}$$

In natural systems, the trace concentrations of micropollutants have little influence on the total amount of light absorbed by a body of water, but other factors such backscattering and reflection of light come into play. In this case, $\varepsilon_i(\lambda)\cdot C_i$ is negligible, $\alpha_D(\lambda)$ replaces $\alpha(\lambda)$ to account for backscattering and reflection, and the pathlength l becomes z_{mix}:

$$A(\lambda) = \alpha_D(\lambda)\cdot z_{mix} = 1.2\cdot\alpha(\lambda)\cdot z_{mix} \tag{1.6}$$

where $\alpha_D(\lambda)$ is the diffuse attenuation coefficient and z_{mix} the depth of the mixed water column. $\alpha_D(\lambda)$ can be approximated by $1.2{\cdot}\alpha(\lambda)$ for non-turbidwaters and temperate latitudes [19]. Hence, the more light absorbed by the solution (large $\alpha(\lambda)$ due e.g. to presence of dissolved organic matter and/or deeper mixing depth), the less light will be available for absorption by the compound.

b)Light absorption by the compound itself

This quantity determines the amount of light absorbed by a compound of interest within a solution containing several chromophores. The specific rate of light absorption, $k_a(\lambda)$, expresses the amount of light absorbed per unit time per mole of compound I in a given system (characterized by $\alpha_D(\lambda)$ and z_{mix}). It is determined by the intersection of the absorbance spectrum of the compound i of interest ($\varepsilon_i(\lambda)$) , and the irradiance spectrum of the light ($I(\lambda)$).

$$k_a(\lambda) = \frac{I(\lambda)\cdot\varepsilon_i\cdot(1-10^{-\alpha(\lambda)\cdot z_{mix}})}{z_{mix}\cdot\alpha(\lambda)} \tag{1.7}$$

In the case of very little light absorption by the water column (i.e. shallow, near-surface conditions), the following approximation is valid:

$$1 - 10^{-\alpha(\lambda)\cdot z_{mix}} = 2.303 \cdot \alpha(\lambda) \cdot z_{mix} \tag{1.8}$$

The near-surface specific rate of light absorption at a given wavelength is then:

$$k_a^0(\lambda) = 2.303 \cdot I(\lambda) \cdot \varepsilon_i(\lambda) \tag{1.9}$$

This quantity is integrated over the wavelength range over which the compound absorbs

$$k_a^0 = 2.303 \cdot \int_\lambda k_a^0(\lambda)\,\mathrm{d}\lambda \cong 2.303 \cdot \sum k_a^0(\lambda)\,\Delta\lambda = 2.303 \cdot \sum I(\lambda) \cdot \varepsilon_i(\lambda)\,\Delta\lambda \tag{1.10}$$

Finally the reaction quantum yield (assuming independance of wavelength) can be related to the direct photolysis rate constant and the specific rate of light absorption by:

$$\Phi = \frac{\text{number of molecules transformed by photolysis}}{\text{number of photons absorbed}} = \frac{k_{\text{photolysis}}}{k_a^0} \tag{1.11}$$

Where $k_{\text{photolysis}}$ is the experimentally determined photolysis rate constant in the system under consideration.

A light screening factor describes the fraction of light absorbed by the water column, and is used to correct measurable parameters such as the observed photolysis rate constant, to account for the fact that not all incident light is available for photoprocesses, resulting in slower photodegradation. Note that it is the simplified ratio of k_a (equation 1.7) and near-surface k_a^0 (equation 1.9):

$$\mathrm{SF}(\lambda) = \frac{k_a(\lambda)}{k_a^0(\lambda)} = \frac{1 - 10^{-\alpha(\lambda)\cdot z_{mix}}}{2.303 \cdot \alpha(\lambda) \cdot z_{mix}} \tag{1.12}$$

Direct photolysis of organic compounds is only possible when there is overlap between the absorption spectrum of the compound and the solar spectrum. Therefore, compounds that do not absorb light above 290 nm are resistant to direct photodegradation. Nonetheless, they may be transformed by reaction with other excited species, through indirect photodegradation processes.

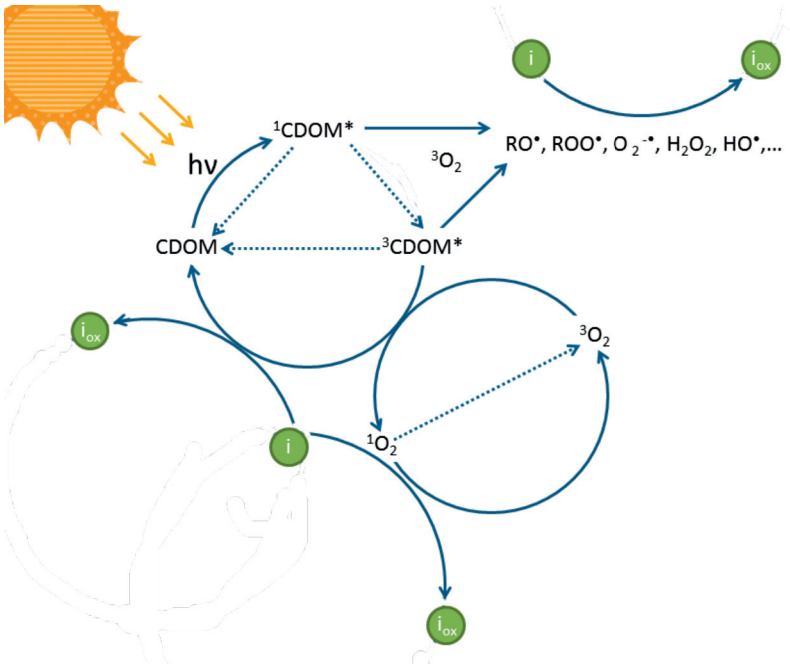

Figure 1.5: *Formation of several reactive intermediates from irradiation of DOM and subsequent indirect photolysis of an organic compound i. Dotted arrows represent radiationless transition (adapted from [19]).*

Indirect photolysis

Indirect photolysis involves an additional species capable of light absorption, which after excitation transfers this energy to or reacts with the compound . These excited species, known as sensitizers, are for instance formed after light absorption by natural water constituents (dissolved organic matter (DOM), nitrate and nitrite) or other organic contaminants.

DOM is present in all natural waters. It is one of the most highly absorbing compounds in the aqueous phase and therefore plays a major role in the photoprocesses of surface waters. The fraction of DOM which absorbs light is commonly refered to as chromophoric dissolved organic matter (CDOM). Light absorption promotes it to the singlet excited state, which, due to its short life-time, rapidly yields triplet excited state CDOM (^{3}CDOM). Figure 1.5 shows various reactive species generated from excited CDOM, which in turn may react with the compound. Molecular oxygen is the main quencher of excited CDOM, leading to formation of reactive singlet oxygen $^1O_2$. Other reactive species formed are for example superoxide anion ($^{\bullet}O_2^-$), oxyl- and peroxl radicals (RO$^{\bullet}$, ROO$^{\bullet}$), hydrogen peroxide (H_2O_2), hydroxyl radical (HO$^{\bullet}$) (though DOM is more sink than source) and solvated electrons (e^-_{aq}). The relevance of each of these reactive species in natural water chemistry is influenced by several factors such as their formation rate, lifetime and the specific reactions with organic compounds. More details pertaining to important reactive species, namely ^{3}CDOM, $^1O_2$ and $^{\bullet}$OH, in addition to other factors which have been found to influence the fate of micropollutants in surface waters are given in the following section 1.3.

1.3 State of research on environmental photolysis of micropollutants

In the objective of understanding the fate of micropollutants in natural waters, a substantial number of studies have focused on determining the propensity of these compounds to undergo photolysis. These experiments commonly investigate the direct and/or indirect photolysis kinetics via laboratory experiments using artificial light (lamp or solar simulator), or by exposing test beakers to natural sunlight. The photodegradation of pharmaceuticals can vary significantly from compound to compound and strongly depends on the characteristics of each individual substance (absorption spectrum, reaction quantum yield), as well as many environmental factors (season, latitude, pH, turbidity, water depth, temperature) and on the water constituents (presence of DOM and/or nitrate). Several reviews have noted the large variance in experimental set-ups: different light sources, reactor geometry, solution composition, initial compound concentration, actinometric methods, etc.[37,75]. These disparities may render the direct comparison between results difficult.

The following paragraphs highlight some examples from literature with the objective of showing how compound structure and water composition can influence the fate of a pharmaceutical in water.

1.3.1 Chemical structure of the pharmaceutical

The propensity of pharmaceuticals to undergo photodegradation can sometimes be predicted based on structural similarities to other compounds for which the photodegradation behavior has been investigated. For example, certain pesticides containing structural moieties, such as phenol, nitro, and napthoxyl groups are known to undergo direct photolysis. Therefore, pharmaceuticals containing these moieties can be expected to exhibit similar degradation behavior. This fact is well illustrated on the example of pesticides carbaryl and napropamide, which show fast photolysis and contain the napthoxyl chromophore, a moiety also found in the pharmaceuticals propanolol and naproxen (Figure 1.6a). Consequently, propanolol and naproxen were also found to be photolabile[75].

Indeed, propranolol rapidly undergoes direct photolysis through ring oxidation. In contrast, beta blockers atenolol and metoprolol, which are structurally different beta blockers (Figure 1.6b), with only one ring, showed much slower direct photolysis[81].

However, structural similarities are not always a sufficient indicator for photodegradation behavior. For example, although five-membered sulfadrugs have a fairly similar structure and differ only in their five-membered N-bond substituent, they possess relatively different direct photodegradation rate constants[82], suggesting that the five-membered ring governs photochemical behavior of such compounds. Figure 1.7 shows the potential direct photolysis cleavage sites. The main products reported by this and other studies result from cleavage at δ and γ site.

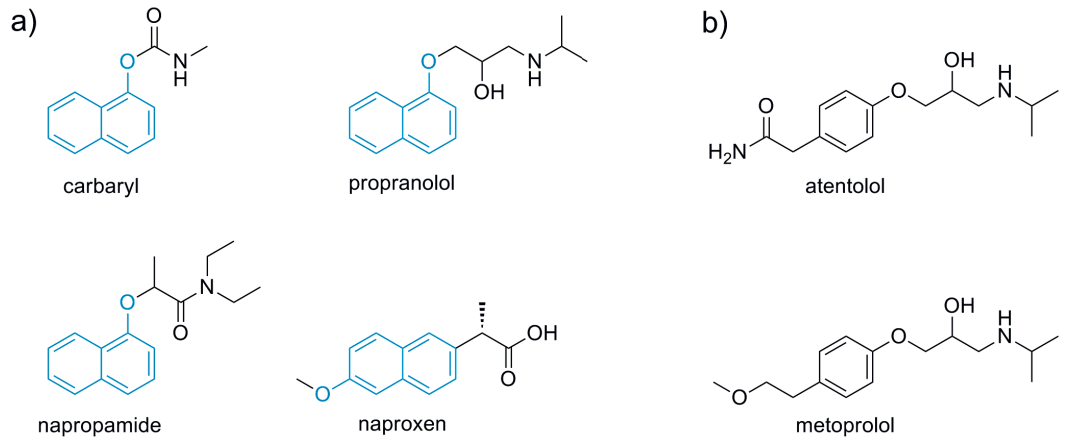

Figure 1.6: *a) Structural similarities between the pesticides carbaryl and napropamide and the pharmaceuticals propranolol and naproxen, which all contain the napthoxyl chromophore (emphasized in blue) (adapted from [75]). b) Chemical stucture of betablockers atenolol and metoprolol with only one ring.*

On the other hand, a significantly different photochemical behavior was observed for 6-membered sulfa drugs. These showed similar direct photolysis rate constants, however, unlike 5-membered sulfa drugs, which degrade mainly through direct photolysis, they also undergo indirect photolysis with triplet excited state dissolved organic matter, presumably by electron transfer or hydrogen atom abstraction[83]. However, the major products of six-membered sulfonamides were not the cleavage products expected based on their analogy with the five-membered structures, but resulted from of SO_2 extrusion (Figure 1.7, bottom).

This example shows that a slight change in structure may alter the extent and routes of photolysis, and though structure may at times aid to predict the propensity of a compound to photodegrade, a case-by-case study remains necessary.

1.3.2 Water composition

The generation of reactive species by natural water components is an important process for the removal of certain compounds, namely those persistent to direct photolysis. Surface waters with high levels of dissolved organic matter, nutrients and reactive transients have been shown to increase the overall degradation rates through photosensitizing effects. Such effects have been observed among others on carbamazepine, clofibric acid, diclofenac, ibuprofene, sulfonamides and several beta blockers[78,83–86]. DOM, singlet oxygen and hydroxyl radicals are the most studied and most relevant reactants for indirect transformations of compounds in a natural water system. The following paragraphs summarize their modes of action with several examples from literature.

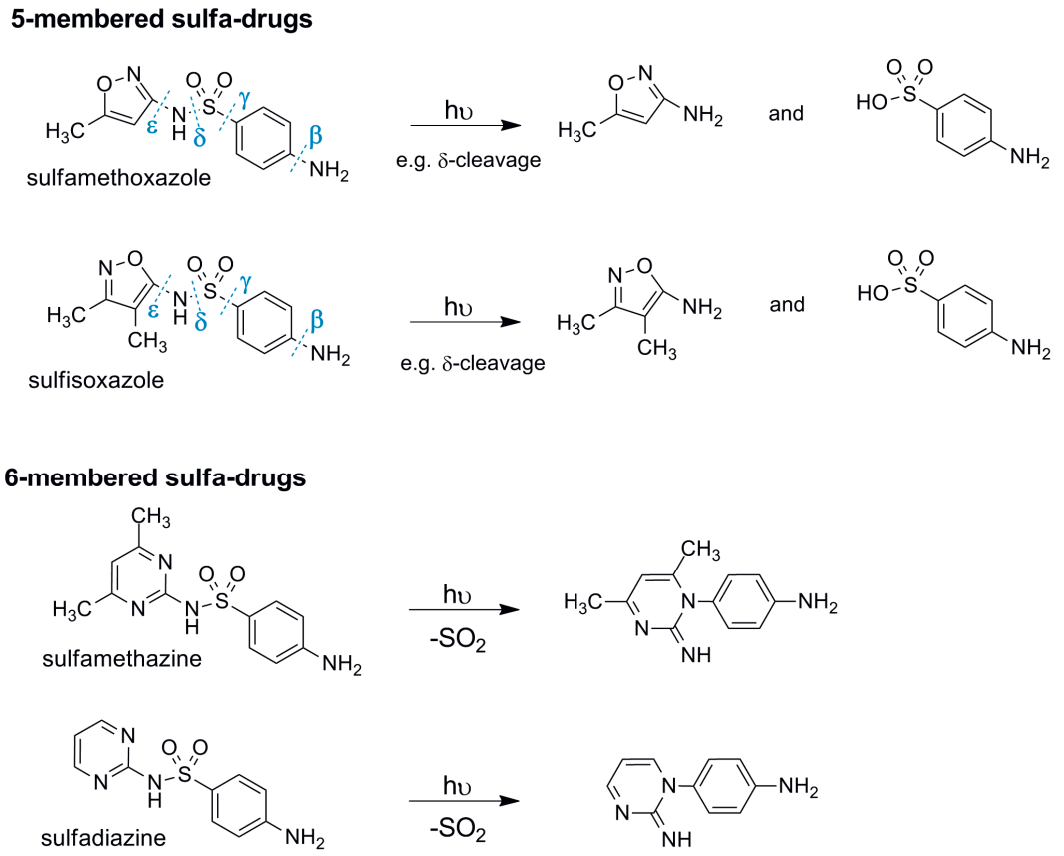

Figure 1.7: *Top: Structures of selected 5-membered sulfadrugs, potential direct photolysis cleavage sites and major products generated through d-cleavage*[82]*. Bottom: structures of selected 6-membered sulfadrugs and major products resulting from SO_2 extrusion*[83].

Dissolved organic matter

Dissolved organic matter, though still ill-defined, is known to contain a variety of chromophores capable of light absorption. Triplet excited state CDOM (^{3}CDOM) can then be generated after light absorption by CDOM. As presented in figure 1.5, an entire suite of reactive species are formed by reaction with ^{3}CDOM, namely $^1O_2$, RO$^\bullet$, ROO$^\bullet$, $^\bullet O_2^-$, H_2O_2 and HO$^\bullet$. ^{3}CDOM may also undergo direct reactions with pharmaceuticals by energy, electron- or hydrogen-transfer[19]. Electron or hydrogen transfer reactions typically occur with easily oxidizable compounds such as electron-rich phenols[87,88]. Tertiary amines and anilines are also expected to be readily oxdized by triplet states of CDOM-derived photooxidants, as illustrated earlier for six-membered sulfadrugs which degraded up to 2.8 times faster in river water compared to dionized water[83]. Moreover, a positive correlation was found between the dissolved organic carbon (DOC) content in water and degradation kinetics of betablockers atenolol, metoprolol, and propranolol, which presumably react via oxidation of their electron-rich ring structures[78]. Typical concentrations of DOC in natural waters range from 0.1-50 mg·L^{-1}[89].

But increasing concentrations of CDOM may on the contrary act as an inner filter through competitive light absorption of incident radiation, and thus yield decreased photodegradation rate constants[84]. Other inhibitory mechanisms of CDOM include scavenging of reactive oxidants (hydroxyl or carbonate radicals) by CDOM, and transformation of reaction intermediates back to the reduced parent compound. For example, Canonica et al. showed that increasing amounts of CDOM has an inhibitory effect on photodegradation of (among others) sulfamethoxazole, trimethoprim and propranolol due to backreduction of the oxidized photoproducts[90]. This particular inhibitory effect was also found to depend on the CDOM type; CDOM with high allochthonous (soil-derived) content (greater aromaticity) generally showed greater inhibition capacity[91].

Singlet oxygen

Singlet oxygen ($^1O_2$) denotes the first electronic excited state of molecular oxygen and is mainly formed by energy transfer from ^{3}CDOM to molecular oxygen ($^3O_2$). In natural waters, the life-time of $^1O_2$ (and steady-state environmental concentration) is essentially controlled by physical deactivation by water[92]. Other processes such as physical quenching by organic substrates, reaction with contaminants or radiative decay back to ground state are minor in environmental conditions, though quenching by DOM can become important for DOC levels above 20 mg C $\cdot L^{-1}$ ([19] and references therein). Typical steady state concentrations of $^1O_2$ in surface waters range from 10^{-13}–10^{-14} M[93], and can be up to three orders of magnitude larger within the DOM[94]. The efficiency of $^1O_2$ formation from CDOM was found depend on the type of the CDOM (aquatic or terrestrial) and the season[93,95]. However, several studies have shown that certain CDOM parameters, namely absorbance at 300 nm or DOC, can be used to estimate the environmental steady state concentrations of singlet oxygen within a factor of four[96].

Singlet oxygen is a selective oxidant, and reacts mainly with compounds exhibiting structural moieties (dienes) capable of [4 + 2] reactions (cycloaddition), compounds containing electron-rich double bonds (for example double bonds that are substituted with electron-donating groups), and with easily oxidizable moieties (e.g. sulfides, anilines, and phenols).

The reactivity of specific chemical structures and organic chemicals with $^1O_2$ has been extensively studied[97,98]. However, singlet oxygen being a rather selective oxidant, it is expected to play an important role in the environmental fate of only a few types of compounds, in particular those with high reaction rate constants (>10^8 $M^{-1}\cdot s^{-1}$)[99]. These predictions seem validated by the sparse research reporting reaction between pharmaceuticals or pesticides with singlet oxygen. Even though some pharmaceuticals such as cimetidine, naproxen and atorvastatin were found to react with singlet oxygen, this process was considered important in natural waters only for cimetidine[85,100,101]. Other compounds such as the antibiotics sulfamethoxazole and trimethoprim were found to generate singlet oxygen, via their triplet excited state, but the self-generated singlet oxygen did not affect their degradation[82,102,103].

OH radical

Of all the reactive intermediates mentioned, hydroxyl radical is the most reactive and non-selective, and consequently reacts with many organic compounds at nearly diffusion controlled rates [104,105].

The hydroxyl radical can be produced by several processes such as the photolysis of hydrogen peroxide, nitrate, nitrite, DOM, $FeOH^{2+}$ and by reaction of H_2O_2 with Fe^{2+} (Fenton reaction). Yet, the major sources of hydroxyl radical in surface waters appear to be the photolysis of NO_3^- and NO_2^- by the following reactions [19]:

$$NO_3 + h\nu \longrightarrow NO_3^{-*} \longrightarrow NO_2 + O^{\bullet -} \xrightarrow{H_2O} HO^{\bullet} + HO^- \tag{1.13}$$

$$NO_2^- + h\nu \longrightarrow NO_2^{-*} \longrightarrow NO + O^{\bullet -} \xrightarrow{H_2O} HO^{\bullet} + HO^- \tag{1.14}$$

The consumption of hydroxyl radicals is controlled by natural scavengers, namely carbonate, DOM and bromide in seawater, which in turn may give rise to longer-lived, selective radicals such as the carbonate radical ($CO_3^{\bullet -}$) and the bromine radical ($Br^{\bullet}$). Steady-state concentrations of hydroxyl radical in surface waters thus strongly depend on the chemical composition of water. Commonly reported concentrations range from 10^{-14}–10^{-18} M [106]. Moreover, hydroxyl radical formation and its scavenging can be related to the nitrate and DOM and bicarbonate content, respectively of a given water, allowing for a reasonable estimation of its concentration in various surface waters based on these parameters [106].

Typical reactions involve electrophilic addition to a double bond or an aromatic system and hydrogen atom abstraction (Figure 1.8). Compounds exhibiting aromatic rings and/or carbon-carbon double bonds with electron-donating substituents, as well as those with aliphatic groups from which an H-atom can be easily abstracted react at near diffusion controlled rates [19]. These specific reaction pathways have been useful in distinguishing degradation products from direct and indirect photolysis [107]. Conversely, hydroxyl radical was found least reactive with aliphatic polyhalogenated substances [19].

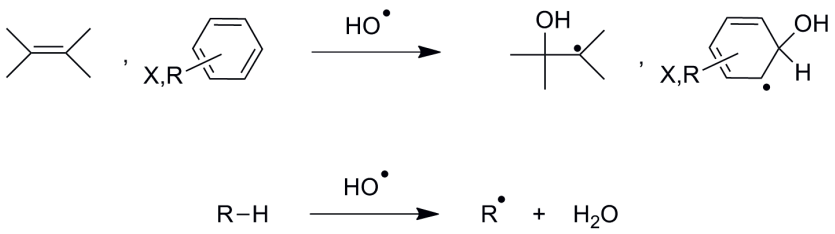

Figure 1.8: *Reactions with hydroxyl radical: electrophilic addition to a double bond or an aromatic system (above) or hydrogen atom abstraction from a carbon atom (below)* [19].

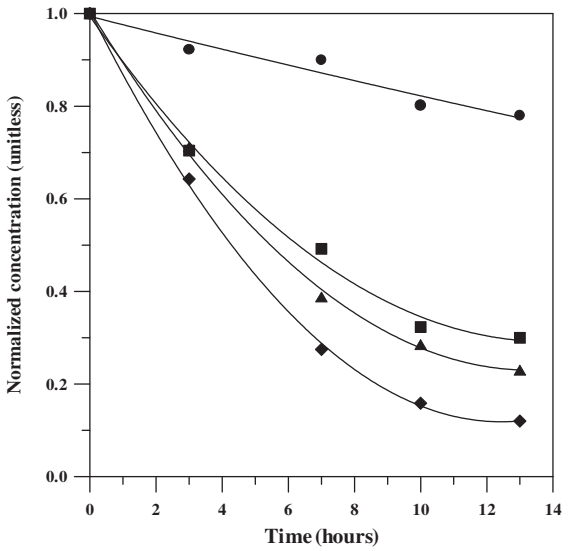

Figure 1.9: *Effect of nitrate and humic acids on the phototransformation of the antibiotic ofloxacin in bi-distilled water during exposure to spring sunlight at 25 °C. [Ofloxacin]= $1{\cdot}10^{-5}$ mol·L^{-1} (●: only ofloxacin; ■: with humic acids ($5{\cdot}10^{-3}$ g·L^{-1}); ▲: with humic acids ($5{\cdot}10^{-3}$ g·L^{-1}) and nitrate ($1{\cdot}10^{-2}$ g·L^{-1});♦: with nitrate ($1{\cdot}10^{-2}$ g·L^{-1})) (from [74]).*

Owing to their non-selective nature, hydroxyl radicals are expected to play a significant role in limiting the persistence of many organic micropollutants. Numerous studies have indeed confirmed both the role of nitrate in enhancing photolysis through hydroxyl radical generation and the important contribution of these radicals to the overall fate of contaminants in surface waters [74,85,103,106,108,109]. This is well illustrated by the enhanced degradation of the antibiotic ofloxacin in presence of DOM and/or nitrate (Figure 1.9).

1.3.3 Other parameters influencing photodegradation rates

pH influences the protonation state of the compound, and consequently its absorption spectrum (shape and/or maximal absorbance). Accordingly, though higher absorbance is not necessarily correlated with higher degradation rate constants, varying pH may influence direct photolysis rate constants. Five-membered sulfadrugs showed varying degradation kinetics at different pH-values; for example, sulfamethoxazole rapidly undergoes direct photolysis in its neutral state (at pH values below $pK_{a,2}$=5.7), whereas the anionic component present at environmentally relevant pH ranges photolyzes more slowly [82]. Similar pH-dependancies were observed for ciprofloxacin or propranolol, among others [78,110–113]. Changes in protonation state furthermore alters the electron density of a molecule, which may consequently also affect indirect photolysis processes via more specific transient species such as singlet oxygen [19,99].

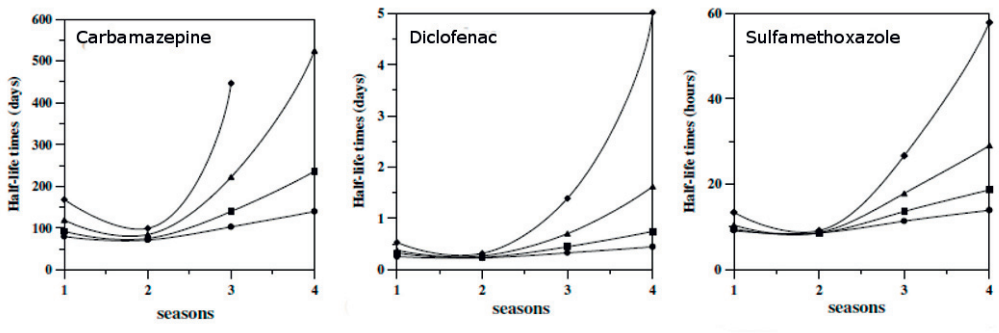

Figure 1.10: *Half-lives (in days) for the direct photolysis of selected pharmaceuticals at different seasons and latitudes. (1) spring; (2) summer; (3) fall; (4) winter. ●: 20 °N, ■: 30 °N; ▲: 40 °N; ♦: 50 °N (from [74]).*

Another water component which may influence photolysis of certain compounds is iron. Indeed, the macrolide antibiotic clarithromycin was only found to photodegrade efficiently when complexed by Fe(III). Generally, macrolide antibiotics do not absorb at wavelengths above 290 nm, yet complexed to iron(III) they become photochemically active [114].

Irradiation being the prerequisite for all photoprocesses, variations in the solar irradiation spectrum and intensity will clearly affect photodegradation rates. Hence season and/or latitude may have a large influence on the environmental fate of micropollutants. At temperate latitudes of 40°N, predicted pharmaceutical half-lives were up to 5 times longer in winter than during the summer season and the seasonal effect increases with increasing latitude, as shown in figure 1.10 [74]. Using similar model predictions, various studies show a significant decrease of photolysis rates in winter months [82,115,116]. Actual accumulation of pharmaceuticals, in winter months or at lower depths was also confirmed by environmentally measured concentrations [42,117,118].

1.4 Research objectives and approach

From the large scale of the Vidy Bay to the molecular level of an antibiotic, the following chapters intend to fill some research gaps identified throughout the literature review. The objectives and content of these chapters is described briefly as follows:

Chapter 2 Only scarce data is available concerning the environmental fate of pharmaceuticals and other micropollutants directly discharged from WWTPs into lakes. Moreover, the spatial and temporal distribution of pharmaceuticals in lakes has rarely been studied. By means of monthly sampling at various depths and locations across the Vidy Bay, this chapter aims to understand the impact of the wastewater outfall on the spatial distribution of 39 micropollutants in the Vidy Bay. The spatial occurrence of contaminants discharged from the wastewater outfall (pharmaceuticals) are compared to those typically entering the lake from streams or runoff from land, such as pesticides. Moreover, the seasonal variability of micropollutant concentrations and their profiles throughout the water column are examined, both of which may be impacted by summer stratification.

Chapter 3 The limitations of punctual water sampling in evaluating the spatial extent of pollution sources is readily understood. In such cases, modelling physical and chemical processes has been proven successful. This chapter describes a model developped to predict the spreading of wastewater-derived micropollutants arising from the WWTP outfall in Vidy Bay. The overall goal is to spatially and temporally define the area of potential ecotoxicological risk in Vidy Bay. Both hydrodynamics, from a flow model, and direct and indirect photolysis processes, determined experimentally, are coupled in a model that predicts the concentrations of micropollutants under typical wind scenarios and seasons relevant to Vidy Bay.

Chapter 4 To date, there is very little information on the environmental occurrence of human metabolites of pharmaceuticals. However, evidence of their potential capacity to transform back to the parent compound, along with the knowledge that some metabolites retain biological activity, are inciting reasons to include metabolites in the study of presence, fate and effects of micropollutants. This chapter is a continuation of the first chapter with regard to human metabolites. The goal is to determine the presence of a selection of human metabolites in Lake Geneva, to assess their fate with respect to degradation over time and space, and to evaluate their contribution to the overall ecotoxicological risk.

Chapter 5 The identification of phototransformation products was highlighted as an important research need. This final research chapter investigates the direct photolysis products of an antibiotic, sulfamethoxazole (SMX) and four of its human metabolites, with the objective of understanding the influence of the small structural differences between SMX and its metabolites on photolysis rates and pathways. In addition, the possibility of photolytic back-transformation of a metabolite to SMX is assessed for the first time.

2 Spatial and temporal presence of a wastewater-derived micropollutant plume in Lake Geneva

2.1 Introduction

The occurrence and potential adverse effects of micropollutants in the environ-ment have been the object of many recent studies. A wide variety of pesticides and, more recently, pharmaceuticals have been detected in the ng-μg·L^{-1} range in various aquatic environments throughout the planet[14]. Human pharmaceuticals enter the environment mainly via the discharge of wastewater effluent to surface waters. Only a fraction of the pharmaceuticals consumed are metabolized by the human body, whereas the remainder is excreted into the sewer system, and transported to the wastewater treatment plant (WWTP). Studies have shown that many pharmaceuticals are removed by less than 50% during wastewater treatment. Therefore, sewage treatment plant effluents represent an important point source of micropollutants into fresh water systems[18] . Moreover, during high rain events, when the WWTP capacity is surpassed, or due to leaking sewers, untreated wastewater may be directly discharged into aquatic environments[119]. Pesticides, in contrast, can enter surface waters by several diffuse mechanisms, such as runoff from land[9,120].

To date, most research on environmental occurrence and fate of pharmaceuticals has focused on the presence of these compounds in rivers and streams, often at sites close to discharges of WWTP effluent. These studies have reported higher concentrations of several pharmaceuticals downstream of WWTP effluent discharges compared to upstream, as well as decreasing concentrations with increasing downstream distance from the effluent discharge point[23,121]. This decrease was for the most part attributed to dilution with receiving waters, and natural degradation processes, mainly photolysis[42,118].

A modified version of this chapter was published as: *F. Bonvin, R. Rutler, J. Halder, N. Chevre and T. Kohn, Environmental Science & Technology, vol. 45, 2011*

Only scarce data exist, however, concerning the environmental fate of pharmaceuticals and other micropollutants directly discharged from WWTPs into lakes. A study conducted in the Great Lakes region observed the highest concentrations of most pharmaceuticals nearest to the WWTP discharges; however no depth profiles were acquired and only surface water samples were considered[122]. Another study on corrosion inhibitors in Swiss rivers and lakes found maximal concentrations at the surface and at -10 m water depth in Lake Zürich and Lake Geneva[123]. The authors speculated that the peak at -10 m was caused by WWTP effluent discharged directly into the lakes; however this hypothesis was never pursued.

When wastewater is discharged into a large body of water, it may not fully mix with the surrounding water mass, but instead stratify as a distinct layer (plume) at a point where its density corresponds to that of the surrounding water mass[124]. Several authors have investigated the dispersion and dilution of sewage outfall. Common wastewater plume tracers are microbiological, physical and chemical indicators, such as bacteria, salinity or conductivity, which can be associated with the outfall-plume[125–127]. Plumes can also be traced directly by added tracers such as fluorescent dyes or radioisotopes[128]. No data exist, however, on micropollutant concentrations in these plumes.

In this study, we aim to determine whether wastewater plumes represent a reservoir of micropollutants in lakes. Our study location, Lake Geneva, represents one of the largest potable water resources of Western Europe and is the main drinking water source to more than 700'000 people. Several WWTPs along the shoreline discharge effluent wastewater directly into the lake. The centralized Lausanne WWTP, which collects the wastewater of 220'000 inhabitant equivalents, discharges more than 100'000 m^3 of treated wastewater per day into Lake Geneva's Vidy Bay at -30 m depth. Previous work has shown that the wastewater effluent contains pharmaceuticals and other micropollutants in the 0.1-1 $\mu g \cdot L^{-1}$ range[24]. To date no research has investigated the 4-dimensional variations (space and time) of a large selection of micropollutant concentrations in a lake, in particular near a wastewater effluent discharged directly into the lake. The objectives of the present study were to determine the impact of the wastewater outfall on the spatial distribution of 39 micropollutants in the Vidy Bay. The spatial occurrence of contaminants discharged from the wastewater outfall (pharmaceuticals) was compared to those typically entering the lake from streams or runoff from land, such as pesticides. Moreover, the seasonal variability of micropollutant concentrations and their profiles throughout the water column were examined, both of which may be impacted by summer stratification. Finally, we assessed the potential ecotoxicological risks of elevated concentrations of micropollutants observed in the wastewater plume.

2.2 Experimental Section

2.2.1 Site description and sampling strategy

The study area, Vidy Bay, lies on the northern shore of Lake Geneva, and represents 0.3% of the lake's total volume (Figure 2.1) [129]. Aside from lake currents, a major input of water to Vidy Bay is discharge from Lausanne's wastewater treatment plant 700 m from shore at -30 m depth. During rain events the WWTP capacity is rapidly exceeded, and untreated wastewater flows directly into the lake [130]. Other sources of water to the Bay are the Chamberonne River and the Flon stormwater outlet. On the western limit of the bay, 3.1 km downstream of the WWTP outfall, the St. Sulpice drinking water plant (sand filtration) withdraws ca. 100'000 m^3 of raw drinking water per day.

Monthly water samples were collected at various depths and locations in Vidy Bay between April 2010 and January 2011. The central sampling location ("WWTP outfall") was above the discharge point of effluent wastewater. The two other sampling sites were located ca. 1.5 km upstream ("REF up") and downstream ("REF down") of the discharge point (Figure 2.1). Between 5 and 9 depths were sampled at each site. Samples were taken from the R/V "La Licorne" (Forel Institut, Geneva) equipped with a crane and a rosetta water sampler (1018 Rosette Sampling System, General Oceanics Inc.). The rosetta consisted of 11 Niskin bottles (1.7 L), coupled to a CTD device (OCEAN SEVEN 316Plus CTD, IDRONAUT Srl) which were externally powered via a sea cable and yielded instantaneous information on temperature and electrical conductivity. Temperature and electrical conductivity were processed with REDAS-5 Release 5.40 (IDRONAUT Srl). For selected months, the WWTP effluent was sampled in the WWTP pipeline before discharge into the lake. 24 h composite samples were taken on the same day as the lake campaign using an automatic sampler (full-size portable sampler ISCO 6712, Teledyne Isco, Inc.) located at the entrance of the pipeline.

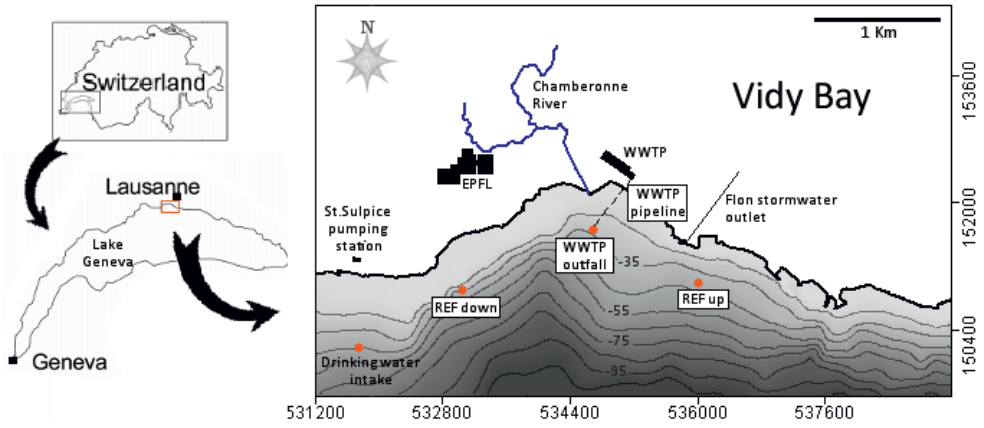

Figure 2.1: *Map of the Vidy Bay with sampling sites "WWTP pipeline", "WWTP outfall", "REF up", and "REF down". Coordinates are in Swiss Grid system with datum CH1903.*

The pipe receives treated wastewater combined with excess wastewater, which bypassed the WWTP. Although water samples could not be acidified during the automatic sampling, tests showed that even the most biodegradable compound of our selection of micropollutants (paracetamol) remained stable during the 24h sampling period.

2.2.2 Choice of substances

Previous studies identified priority micropollutants for the Lake Geneva region, based on consumption loads, the degree of human metabolism, removal in the WWTP, and – if known – ecotoxicological relevance[2]. After a preliminary sampling campaign to identify the substances present at detectable concentrations, a total of 39 micropollutants were retained as priority pollutants for this study, including 27 pharmaceuticals (analgesics, antibiotics, antilipemic agents, beta-blockers), and 12 other micropollutants (corrosion inhibitors, pesticides). A detailed list of the selected micropollutants and their applications is presented hereafter in table 2.1. The chemical structures, pK_a and $logK_{OW}$ are given in Appendix A

Chemicals and reagents. All chemicals and reagents used have been listed previously[24].

2.2.3 Sample manipulation

1 L water samples were collected in Niskin bottles and transferred into amber glass bottles, immediately acidified to pH 2 (with concentrated HCl) to inhibit all biological activity, and transported to the laboratory within 4 hours of sampling, where they were directly filtered through <1μm glass fiber filters (Whatman). Test experiments showed no significant difference between acidification before or after filtration, indicating that the partitioning of our selection of micropollutants between water and suspended matter was not influenced by acidification. Before further treatment, all filtrates were spiked with a set of 20 deuterated standards (final concentration 120 ng·L^{-1}) to account for losses during extraction, as described previously[24]. All glassware used for samples was immersed for 24h in a Contrad bath, machine-washed and finally rinsed with methanol and sample water before use.

2.2.4 Analytical method

A previously developed analytical method for the monitoring of various micropollutants involving solid-phase extraction (SPE) and ultra-performance liquid chromatography coupled to a tandem mass spectrometer (UPLC-MS/MS) (Acquity UPLC system, Waters) was adapted and applied to the lake water samples[24]. Briefly, the target compounds were extracted on hand-assembled 6 mL cartridges using an automated SPE system (GX-274 ASPEC, Gilson), eluted and evaporated to 200 μL and finally stored at -20°C until UPLC-MS/MS analysis. Within two weeks of sampling, stored extracts were diluted 1:1 with UPLC eluent and analyzed twice by UPLC-MS/MS. Reported values represent the average of the two separate measurements. UPLC-MS/MS parameters are described as Method 1 in Morasch et al.[24]. A set of 10 to 13

standards with concentrations between 1 and 700 $\mu g \cdot L^{-1}$ were analyzed in duplicate along with the samples. The analytical limit of quantification (LOQ) was defined as the concentration of the lowest standard with a signal-to-noise ratio > 10. Micropollutant concentrations in the sample concentrates were calculated based on calibration curves using at least 6 calibration points closest to the sample concentration. Correlation coefficients for the calibration curves were typically > 0.990. The few compounds with unreliable calibrations and high detection limits (Table 2.1) were not included in the spatio-temporal analysis described below. Extraction recoveries for each sampling day were determined for each of the 20 deuterated surrogates by averaging the recoveries in the individual samples. Compounds lacking deuterated surrogates were assigned one based on retention time in the liquid chromatography (see Appendix A, Table A.1). The concentrations in the original lake water samples were determined taking into account the extraction efficiencies of the associated deuterated standards and the exact sample masses weighed during sample preparation. The uncertainty associated with the sample concentrations, calculated as the relative standard deviation, was <30% for the large majority of the compounds. Details regarding the calculation of this uncertainty are given in Appendix A.

2.2.5 Statistical analyses

Statistical analyses and correlations were performed in Matlab (2009b, The Mathworks, Natick, MA).

2.2.6 Ecotoxicological risk assessment

The increasing concern regarding the presence and effects of micropollutants in surface waters has led European and North American countries to propose water quality criteria (WQC) for micropollutants in surface waters ([67] and references therein). EU guidelines often use predicted no-effect concentrations (PNEC) as WQC[68]. PNECs represent concentrations below which an unacceptable effect will most likely not occur. In the present study, the ecotoxicological risk was assessed by comparing the measured concentrations with specific WQCs defined for individual substances. The resulting risk quotient (RQ), which is the ratio of the environmental concentration and the WQC (PNECs), must remain below one to ensure an acceptable risk to the environment[67].

PNECs are classically calculated by dividing the effect concentration 50% (EC50) or no-observed effect concentration (NOEC) by a safety factor, typically 100 or 1000. When enough ecotoxicity data is available (e.g. for many pesticides), the hazardous concentration 5 (HC5), a more robust WQC, can be derived from species sensitivity distribution curves (SSD). The HC5 represents the concentration that protects 95% of all aquatic species[67], and a PNEC equivalent can be calculated by dividing HC5 by a factor of 5[68]. PNECs for the individual micropollutants, calculation methods and references are listed in Appendix A (Tables A.3, A.4 and A.5).

Table 2.1: *List of targeted micropollutants, their applications and average limit of quantification (LOQ) of the analytical method. *: Compounds not considered in spatio-temporal analysis due to poor calibration or lack of data*

Compound Name	Application	CAS	LOQ [ng·L^{-1}]
atenolol	beta blocker	29122-68-7	1.3
atrazin	pesticide (herbicide)	1912-24-9	1.3
azithromycin	antibiotic	83905-01-5	1.3
benzotriazol	corrosion inhibitor	95-14-7	6.6
bezafibrat	anticholesterol	41859-67-0	1.0
carbamazepin	antiepileptic	298-46-4	1.3
carbendazim	pesticide (fungicide)	10605-21-7	1.8
chloridazon	pesticide (herbicide)	82869-32-7	0.7
ciprofloxacin	antibiotic	85721-33-1	2.1
clarithromycin	antibiotic	81103-11-9	0.6
clindamycin	antibiotic	18323-44-9	1.1
clofibric acid*	antilipemic	637-07-0	5.0
diclofenac	analgesic (NSAID)	15307-86-5	1.8
diuron*	pesticide (herbicide, algicide)	330-54-1	8.4
gabapentin	antiepileptic	60142-96-3	2.2
gemfibrozil	anticholesterol	25812-30-0	2.2
iopamidol*	X-ray contrast media	62883-00-5	288.2
iopromid*	X-ray contrast media	73334-07-3	735.9
IPBC*	pesticide (fungicide)	85045-09-6	1.5
irgarol	pesticide (herbicide, algicide)	28159-98-0	1.6
isoproturon*	pesticide (herbicide, fungicide)	34123-59-6	2.0
ketoprofen	analgesic (NSAID)	22071-15-4	2.0
mecoprop	pesticide (herbicide)	93-65-2	2.1
mefenamic acid*	analgesic (NSAID)	61-68-7	17.6
methylbenzotriazol	corrosion inhibitor	29385-43-1	1.3
metoprolol	beta blocker	37350-58-6	0.7
metronidazol	antibiotic	443-48-1	1.4
naproxen*	analgesic (NSAID)	22204-53-1	3.6
norfloxacin	antibiotic	70458-96-7	1.9
ofloxacin	antibiotic	82419-36-1	1.4
paracetamol	analgesic	103-90-2	3.6
primidon	antiepileptic	125-33-7	2.0
propiconazol	pesticide (fungicide)	60207-90-1	0.7
propranolol	beta blocker	525-66-6	0.9
simvastatin	anticholesterol	79902-63-9	1.2
sotalol	beta blocker	3930-20-9	1.3
sulfamethoxazol	antibiotic	723-46-6	1.1
terbutryn	pesticide (herbicide, algicide)	886-50-0	1.2
trimethoprim	antibiotic	738-70-5	1.1

2.3 Results and Discussion

2.3.1 Occurrence of micropollutants in the Vidy Bay

Over the 10-month sampling period, almost 200 water samples were taken at different depths and locations in the Vidy Bay as well as in the outlet pipeline of the Lausanne WWTP. The majority of the compounds investigated were detected in more than 70% of the water samples. The frequency of detection was slightly higher above the WWTP outfall than in the other lake sampling sites. The highest concentrations were observed for the corrosion inhibitors benzotriazol and methylbenzotriazol, as well as the analgesic paracetamol. However, most of the targeted micropollutants showed concentration ranges below 20 $ng \cdot L^{-1}$ (Figure 2.2). Highest concentrations of pharmaceuticals were observed above the WWTP outfall, whereas this was not the case for all pesticides.

2.3.2 Presence of a wastewater plume with elevated micropollutant concentrations

The presence of effluent wastewater discharged into the lake was evident from conductivity depth profiles taken above the wastewater discharge point. During the warmer months, elevated conductivities (a common indirect plume tracer[126]), arising from high ion concentrations (e.g., Na+, Cl-) in wastewater (see Figure A.1, Appendix A) could be observed at variable depth in the water column, indicating the presence of a wastewater plume. Corresponding water samples taken within this plume exhibited elevated concentrations of a large fraction of the targeted micropollutants.

In these samples, pharmaceutical concentrations were up to 70-fold higher than those detected in the surrounding water column (Figure 2.3 a). Such micropollutant hotspots were consistently observed during the warmer seasons for substances entering the bay with effluent wastewater (i.e. most pharmaceuticals, as well as corrosion inhibitors), whereas no such feature was detected for most pesticides (Figure 2.3 d,e). The absence of a pesticide plume confirms that these substances mainly enter the Bay through runoff from land or with streams, but not via the WWTP outlet.

The wastewater plume and associated elevated micropollutant concentrations was initially detected at a depth of -10 m during the April sampling campaign. The plume depth decreased over the following months and finally was detected near the lake bottom at -25 m in October, as shown by the conductivity profiles in Figure 2.4. The formation and depth of these micropollutant hotspots can be explained by thermal lake stratification which occurs during the warmer months when the upper water layer is heated by the sun, leaving colder, denser water below. Stratification inhibits vertical transport from the lake bottom to the surface. Discharged wastewater, characterized by a specific temperature and conductivity, will stabilize at a level where its density corresponds to that of the surrounding water column.

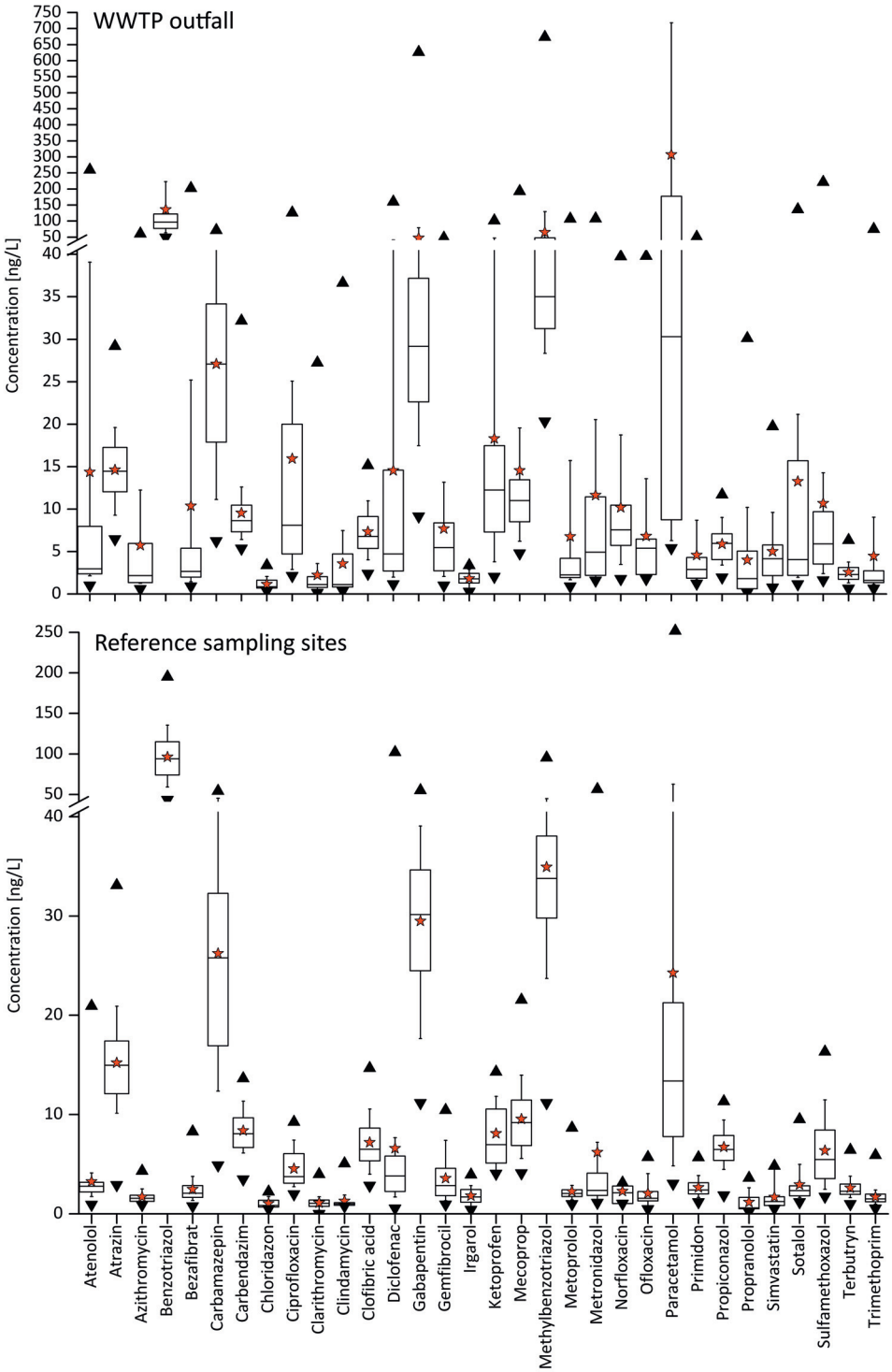

Figure 2.2: *Detected concentration ranges of micropollutants in the water column above WWTP outfall (above) and at the reference points (below). Boxes represent 25th percentile, median and 75th percentile. The whiskers are determined by the 5th and 95th percentiles. Stars, upward-, and downward-facing triangles show the mean, maximum and minimum values, respectively.*

Under stratified conditions, wastewater generally rose through the water column, but its density did not allow it to mix with the less dense, warmer water masses above the thermocline. The wastewater thus accumulated below the warmer upper layer, creating the micropollutant hotspots (plume) detected from April to October.

During the cold season, the temperature profiles straightened (Figure 2.4), and allowed mixing of the water column. Explicitly, this phenomenon caused the disappearance of the micropollutant hotspots above the WWTP outfall, and led to a homogeneous vertical concentration profile for all of the targeted substances. In November, the density of the unstratified water column appeared to be slightly higher than that of wastewater, allowing wastewater to rise and form a diluted, yet measurable concentration peak between -3 and -5 m (Figure 2.3 c).

Carvalho et al.[128] reported similar plume dynamics using dye tracers added to wastewater. Under stratified conditions the plume was trapped below the thermocline with low dilution by surrounding water (35-fold), yet when unstratified, the plume surfaced and the dilution increased (100-fold). The thermocline barrier effect was also observed in Vidy Bay in a previous phage tracer study, when bacteriophages injected at -30 m depth only surfaced under unstratified conditions[131].

In the present study, the measured dilutions of micropollutants from the wastewater effluent to the plume increased from 20-fold during thermal stratification up to 100-fold under homogenous water column conditions. Seasonal comparisons of plume concentrations are difficult to make because it was not known if the minimal dilution was captured on each sampling occasion. Several authors have acknowledged the challenge of plume tracing given the highly complex and patchy structure of plumes[131,132].

The full horizontal extent of the plume remains unknown, but past and present data provide evidence that the wastewater plume is not merely a local issue above the WWTP outfall. On one occasion, during the April sampling campaign, the plume was detected as far as the reference point 1.5 km downstream of the WWTP discharge (Figure A.3, Appendix A). Though such a large spreading was not observed in any of the following campaigns, previous research in the Vidy Bay also verified a similar horizontal extension. Tracer-phages added to the WWTP outfall were detected up to 1.8 km away[131]. More recent field studies in the Bay (summer 2010) also noted higher conductivity values above the WWTP outfall, with a patchy, horizontal extension of at least 400 m in all directions (Matthieu Masson, personal communication).

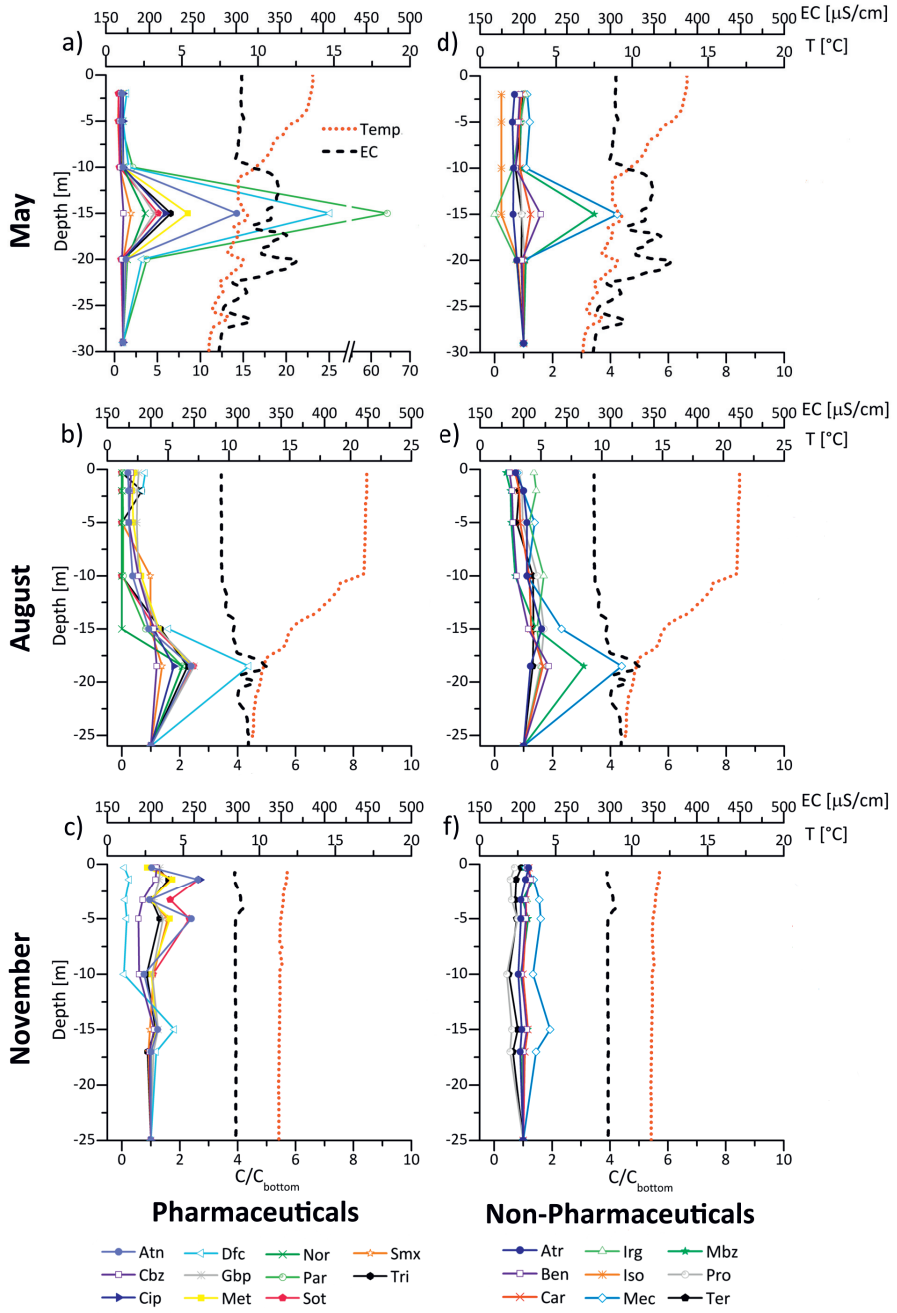

Figure 2.3: *Conductivity, temperature and concentration profiles of a selection of pharmaceuticals (a,b,c) and non-pharmaceuticals (d,e,f) relative to the concentration detected at the bottom. Shown profiles were taken above the WWTP outfall in May (a,d), August (b,e) and November (c,f) 2010. EC:electrical conductivity, T:temperature, Atn:atenolol, Cbz:carbamazepin, Cip:ciprofloxacin, Dfc:diclofenac, Gbp:gabapentin, Met:metoprolol, Nor:norfloxacin, Par:paracetamol, Sot:sotalol, Smx:sulfamethoxazol, Tri:trimetoprim, Atr:atrazin, Ben:benzotriazol, Car:carbendazim, Irg:irgarol, Iso:isoproturon, Mec:mecoprop, Mbz:methylbenzotriazol, Pro: propiconazol, Ter: terbutryn.*

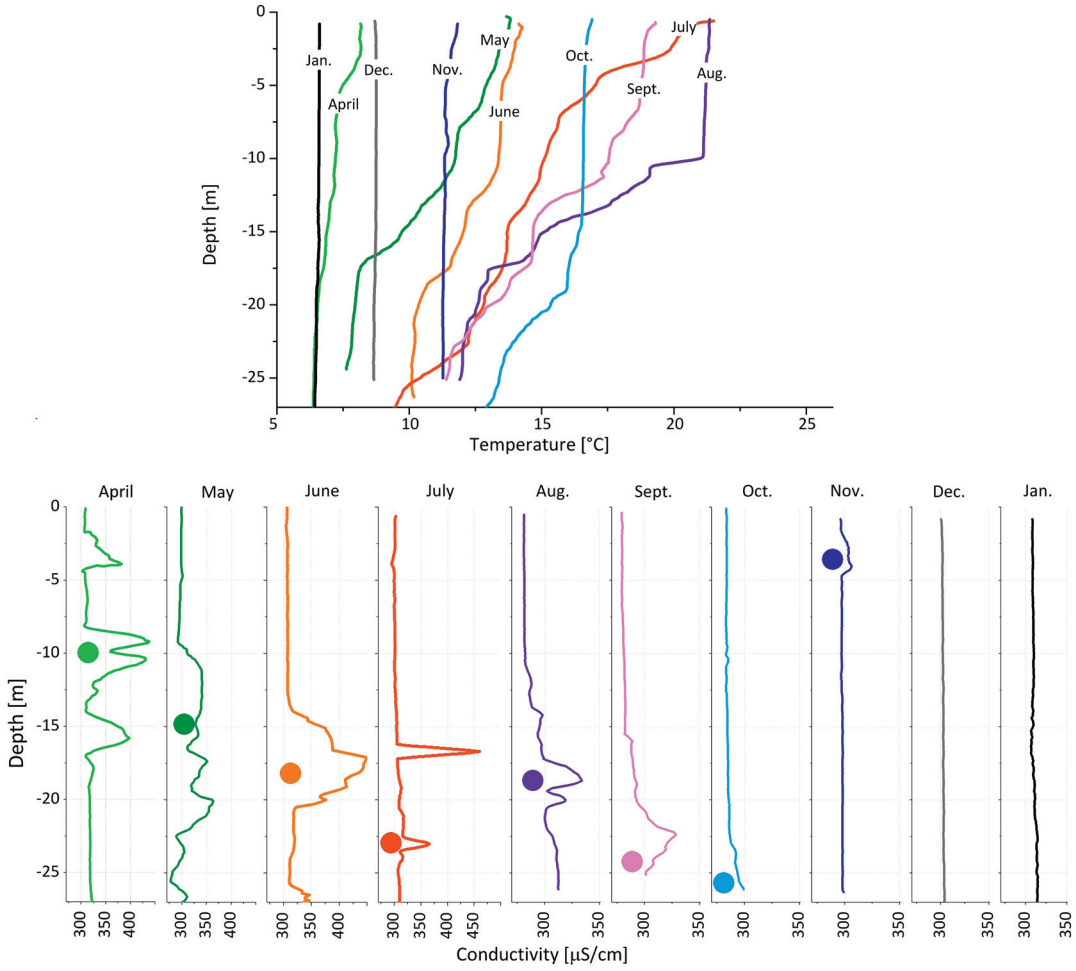

Figure 2.4: *Chronology of temperature and electrical conductivity profiles above the WWTP outfall. Peaks in conductivity indicate the location and depth of the wastewater plume. Round symbols indicate depth at which highest concentrations (plume) of micropollutants were detected in the water sample profile. Conductivity profiles coincide with the sampling cast, whereas temperature profiles were taken in the surrounding water column.*

2.3.3 Conductivity as an indicator for elevated micropollutant concentrations

Micropollutant hotspots could be identified by elevated conductivities. Further analyses showed that there exists a linear correlation between conductivity and the concentrations of wastewater-derived micropollutants in the plume, with correlation coefficients generally > 0.8 (Figure 2.5, blue bars). Given this strong correlation, it will be possible in the future to track the plume and estimate its wastewater-derived micropollutant concentrations using conductivity measurements alone. Pesticides, in contrast, exhibited a different trend, with insignificant or low correlation coefficients (between 0.2 and 0.6) (Figure 2.5, green bars), confirming the notion that their main input into the Vidy Bay is not associated with the WWTP effluent.

Some noteworthy exceptions to the observed trends (Figure 2.5, orange bars) include the anti-epileptic carbamazepin, which is known to be highly recalcitrant during wastewater treatment and has frequently been detected in wastewater effluent[28]. The poorly discernable plume peak (Figure 2.3 a,b), combined with the markedly lower correlation with conductivity (R=0.68), indicate that this pharmaceutical shows pesticide-like input trends. Carbamazepin is produced by several pharmaceutical industries in the Rhône Valley that discharge their effluents to the main tributary of Lake Geneva, the Rhône River. This induces a non-negligible source of carbamazepin into the lake. In fact, it has been estimated that >90% of carbamazepin in Lake Geneva is of industrial origin (Nathalie Chèvre, personal communication). Periodically high carbamazepin concentrations (1 μg·L^{-1}) have been observed in the Rhône River shortly before it reaches Lake Geneva[133]. Therefore, background carbamazepin concentrations are high enough to dominate the concentrations above the WWTP outfall.

The contrary was observed for two corrosion inhibitors and the fungicide carbendazim, which show the plume feature, similar to pharmaceuticals. Yet, this finding is in agreement with past research. The corrosion inhibitors benzotriazol and methylbenzotriazol are widely used in dish-washing detergents and have frequently been detected in WWTP effluent[123]. Carbendazim is applied for film preservation in paints and facade coatings, and considerable input of carbendazim to the aquatic environment through wastewater was observed in several Swiss rivers. Constant influent loads, rather than peaks during rain events from leaching facades, led to the hypothesis of an additional unknown source of carbendazim from households[134].

The pesticide mecoprop shows, as expected, no strong linear relation to conductivity (R=0.28) yet a small plume peak can be observed (Figure 2.3 d,e). Considered a classic urban pesticide[9], which is used as a herbicide on lawns and roadsides and as a protection agent for roofs, mecoprop may be washed out from these sources and directly enter the Bay via runoff, or leach to the sewage system and enter the Bay via the WWTP outfall. This dual source may lead to a reduced linear correlation, while maintaining a measurable peak in the plume.

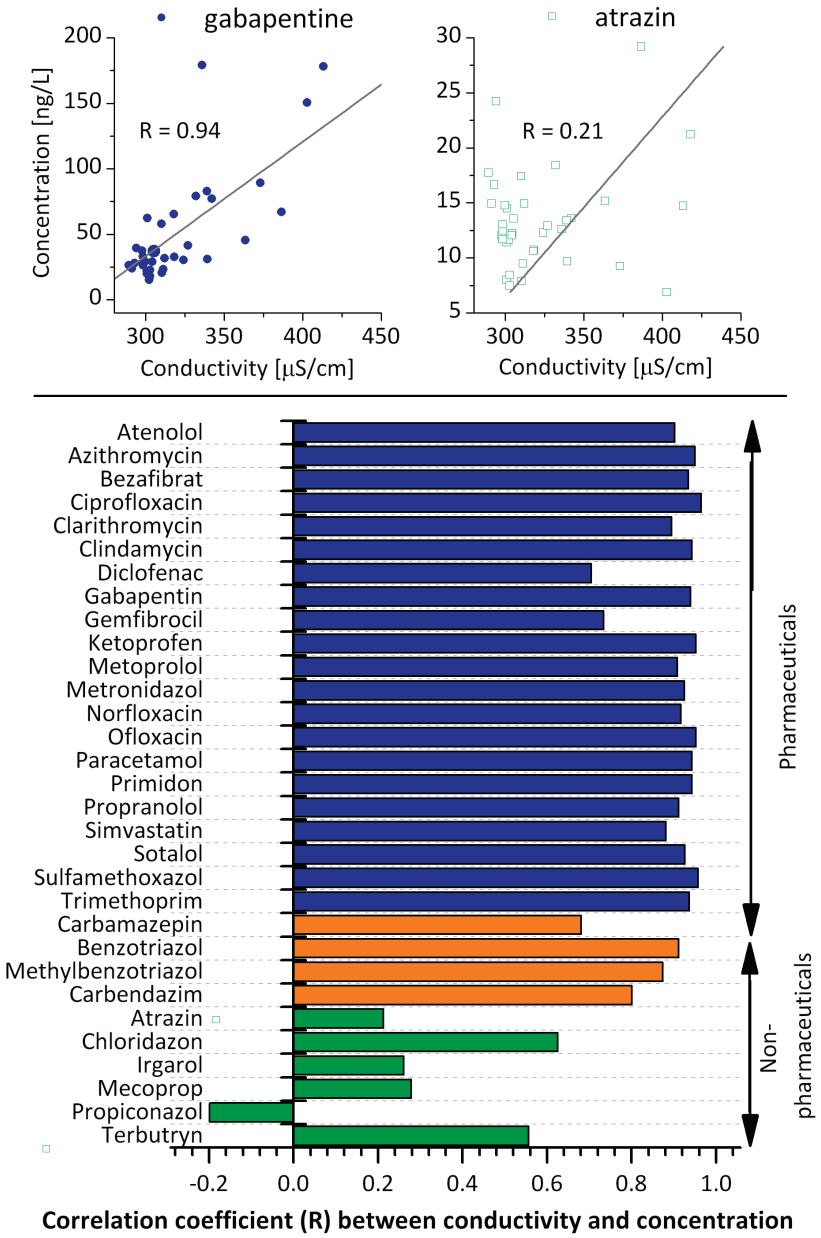

Figure 2.5: ***Above:*** *relation between electrical conductivity (EC) and concentration, computed for EC values above background levels for the antiepileptic gabapentin (left) and the pesticide atrazin (right). R=correlation coefficient.* ***Below:*** *Correlation coefficient between EC and concentration for all micropollutants. Blue: pharmaceuticals, orange: exceptions (see text), green: pesticides.*

2.3.4 Dilution and degradation of WWTP-derived micropollutants throughout the Vidy Bay

To determine the influence of the micropollutant plume on the overall water quality of the Vidy Bay, the spatial variations of micropollutant concentrations were examined. The concentrations measured above the WWTP outfall were compared to those detected at the reference points by means of a percentile analysis, in which uncharacteristic compounds, namely carbamazepin, benzotriazol, methylbenzotriazol and carbendazim, were removed for the analysis (Figure A.2, Appendix A). For all targeted pharmaceuticals except carbamazepin, the maximal concentrations in the Vidy Bay were observed above the WWTP discharge point. In contrast, as expected given their diffuse input, the observed concentrations of pesticides at WWTP and the reference points were similar.

Changes in concentrations with distance from the WWTP were particularly evident for antibiotics norfloxacin and ofloxacin, which were rarely detected at the reference points. Similarly, 75% of all concentrations of azithromycin and ciprofloxacin (antibiotics), diclofenac and paracetamol (anti-inflammatories) detected at the reference points were below the median values detected above the WWTP outfall. This difference was less perceptible in winter (November-January), which may be explained by enhanced mixing of the water masses due to stronger winds and the absence of stratification during this period. Other pharmaceuticals, such as gabapentin, primidon, sulfamethoxazol or trimetoprim showed smaller differences between sampling locations.

The observed decrease in micropollutant concentrations with distance from the WWTP discharge point can arise from both dilution and degradation processes. To assess the extent of micropollutant degradation occurring in the Vidy Bay, concentrations of all compounds at a given location and depth were normalized to the gabapentine concentration at this location, to remove the effect of dilution. Gabapentine hereby served as a conservative tracer, owing to its persistence in WWTPs and surface waters[24,135]. Given that dilution affects all compounds equally, and assuming generally constant ratios of the targeted compounds to gabapentine in effluent wastewater, this normalization eliminates the effect of dilution, and differences in normalized concentrations therefore indicate degradation processes or additional sources of the compound in question.

Normalized concentrations of the majority of pharmaceuticals showed a gradual decrease from the WWTP pipeline, to the plume and finally to the reference points (average value over entire water column). This indicates the occurrence of natural elimination processes during the passage of water through the Vidy Bay (Figure 2.6). The extent of degradation was variable, but typically ranged from 40 to > 90% between the WWTP effluent and the average water column concentration at the reference points.

Paracetamol, which is well-known to readily biodegrade, showed the greatest decrease from effluent wastewater to the reference point. An important removal was also observed for atenolol, bezafibrat and norfloxacin.

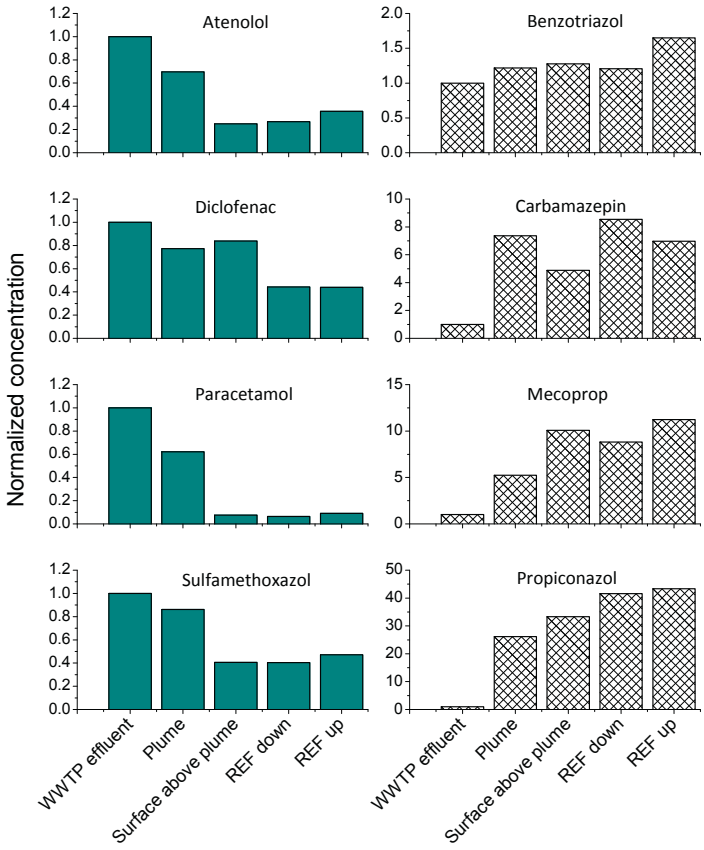

Figure 2.6: *Degradation of a representative selection of micropollutants (from WWTP effluent, to plume, surface above WWTP outfall and reference points up-and downstream). Detected concentrations are normalized by gabapentine and are shown relative to the concentration in the WWTP effluent (for better comparison between compounds).*

In contrast, less degradation occurred for the antibiotics sulfamethoxazol and trimetoprim, which is consistent with the small concentration differences observed between sampling locations and seasons. Moreover, these observations are in agreement with previous work reporting the conservative nature of sulfamethoxazol and trimetoprim in surface waters [127].

As the compounds investigated are known to neither hydrolyze, adsorb to particles, nor — with the exception of paracetamol – biodegrade very readily[2], the observed elimination can tentatively be attributed to photodegradation processes. Photodegradation as the main elimination mechanism is also consistent with the finding that the decrease in the concentrations of wastewater-derived compounds between the WWTP effluent and the reference points was greatest in the summer and smallest during winter (Figure A.2, Appendix A). The temporal variations of the ratio of photodegradation products to parent compound would be the best confirmation of this hypothesis. However, the identification and environmental detection of products of photolysis goes beyond the scope of the present study, but will be addressed in future work.

Non-wastewater-derived substances, mainly pesticides and carbamazepine, showed the opposite behavior, with a gradual increase of normalized concentration from the effluent to the reference points. Once more, this supports the assumption that the Lausanne WWTP does not represent the main source of pesticides and carbamazepin to the Vidy Bay.

2.3.5 Environmental significance

The wind regimes in the Vidy Bay lead to a predominantly circular current that retains both water and sediments within the Bay[136]. Coupled with the constant input of wastewater into the relatively shallow bay, this situation raises concerns regarding the ecotoxicological hazards associated with wastewater-derived micropollutants. Despite variable weather and wind conditions and changing seasons throughout the sampling campaign, a wastewater plume was consistently observed above the WWTP discharge point from April to October. The high concentrations of pharmaceuticals detected in the wastewater plume, along with the plume's extension over several hundred meters, may present a risk to the ecosystem. An individual risk (RQ>1) was observed for several pharmaceuticals in the plume, namely the antibiotics azithromycin, ciprofloxacin and sulfamethoxazol (Figure 2.7) and the pesticide irgarol.

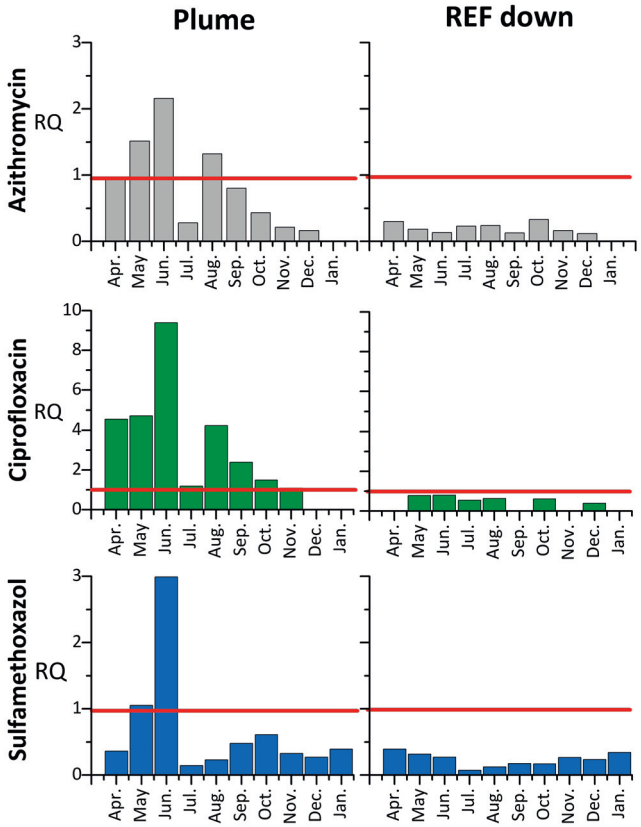

Figure 2.7: *Time course of risk quotient (RQ) for azithromycin, ciprofloxacin, and sulfamethoxazol for concentrations detected in the plume (left) and average water column concentrations detected at REF down (right). RQ>1 (red line) indicates a potential ecotoxicological risk.*

RQ of ciprofloxacin remained critical for the greater part of the campaign, whereas the critical RQ was surpassed only in May, June and August for azithromycin and sulfamethoxazol. However, it is uncertain that the minimal dilution of the plume was captured on any occasion by the water samples, thus the RQ may have been exceeded for these compounds during the other months as well. Of the remaining compounds, diclofenac, carbendazim, propranolol and terbutryn consistently came within an order of magnitude of an RQ of 1 (Figure A.4, Appendix A).

Average monthly concentrations detected at the reference point 1.5 km downstream of WWTP outlet were always lower than recommended WQC, except for the pesticide irgarol, which exceeded the RQ on five occasions. With the exception of this compound, the ecotoxicological risk posed by micropollutants in the Vidy Bay can be considered acceptable, except in the vicinity of the WWTP outlet. However, this localized risk should not be neglected, in particular owing to the unknown extent of spreading of effluent wastewater around the outlet. Moreover, though many substances have an RQ <1, the effect of mixtures of substances with a similar mode of action is not considered in the individual RQ. However, assessing the risk of mixtures, especially in the case of substances with very different mechanism of action goes beyond the scope of this study and will be the matter of a future publication.

Overall, the presence of micropollutant plumes and associated ecotoxicological risks should be considered when discharging wastewater directly into lakes. However, further research is needed to depict a more accurate picture of the spatio-temporal evolution of the wastewater plume, and to better assess the ecotoxicological risk posed by the micropollutant mixture. In the case of the Lausanne WWTP, current pilot projects are testing advanced wastewater treatment to further decrease the discharged micropollutant load in the near future.

3 Micropollutant dynamics in Vidy Bay-coupled hydrodynamic-photolysis model to assess the spatial extent of ecotoxicological risk

3.1 Introduction

The direct discharge of wastewater effluent into the Vidy Bay of Lake Geneva results in the seasonal formation of an effluent plume, presenting locally high concentrations of wastewater-derived micropollutants. A 10-month sampling campaign showed that the plume depth followed the thermocline, which moved to deeper depths over the course of the seasons. In absence of thermal stratification, between November and January, the plume surfaced or was not detected due to enhanced mixing of the water column. The locally elevated concentrations of micropollutants near the wastewater (WW) outfall present a potential ecotoxicological risk. Although the high concentrations of micropollutants were observed as far as 1.5 km from the outfall on one occasion, the spatial extent of this risk zone remains unclear. Nevertheless, a sampling approach to determine the risk zone represents a costly, tedious and unrealistic task. In this sense, models are increasingly used in the field of environmental risk assessment of organic micropollutants to overcome the limitations of sampling or to augment punctual environmental measurements.

In Vidy Bay, factors that contribute to the dispersion of the wastewater-derived micropollutant plume and the associated risk zone are multiple. On the one hand physical mixing processes contribute to dilution of micropollutants by surrounding water masses and are largely influenced by the hydrodynamics of currents in the Bay. On the other, biotic and abiotic degradation and removal processes will affect the fate micropollutants and their concentrations within the Bay.

The hydrodynamics of water masses in Vidy Bay have been the object of a recent study investigating the effect of dominant meteorological conditions on the currents in the Bay[137].

In this study water flow in Lake Geneva was modeled using a 3D finite-difference hydrodynamic model (Delft3D-FLOW), forced by high resolution meteorological data (COSMO-2). The simulations revealed that the main currents in the Bay were highly affected by overlying wind conditions and were generally parallel to shore (eastward and westward) above the wastewater outfall. Moreover, certain wind conditions were found to result in the formation of a gyre. Such circular currents retaining water and sediments within the Bay have also been reported previously[136].

Aside from dilution, several mechanisms, such as photolysis, biodegradation or sorption may influence the concentration of micropollutants in water. The compounds of interest for this study were selected in part due to their low removal efficiencies during wastewater treatment; accordingly, these compounds are likely not very susceptible to biodegradation and/or sorption to settling particles[31,75,78]. Therefore, photodegradation is expected to be their main elimination mechanism in surface waters. This assumption is consistent with a number of studies, which acknowledge the importance of direct and indirect photolysis processes for micropollutants in various aquatic environments[74–76].

Both lake hydrodynamics and photolysis processes are highly affected by season. Warm summer temperatures induce thermal lake stratification, preventing mixing of the top and bottom layers of the water column. In addition, the increased solar irradiance leads to faster photolysis kinetics in the summer[19]. Conversely, during the cold season, solar irradiance is reduced, but homogeneous temperature profiles lead to enhanced mixing throughout the entire water column.

A number of models integrating both physical mixing processes and degradation mechanisms have been developed to determine the fate of micropollutants in aquatic environments. Commonly applied models include river catchment models (GREAT-ER or PhATE™) and 2D lake models (e.g. AQUASIM). A number of studies report the use of such models which incorporate photodegradation kinetics to predict concentrations of pharmaceuticals in rivers and lakes[116,117,138,139], but none relate 3D dynamics with depth-dependent processes in lakes. In hydrodynamics, particle tracking is often used for plume studies as it is designed to describe the detailed spatial pattern of water parcels ("particles") over the mid-field range (<15 km). Hence, particle-tracking represented the ideal method to combine 3D plume spreading and depth-dependent photolysis processes.

This work aims to couple water hydrodynamics and photodegradation of micropollutants in the vicinity of the effluent wastewater outfall to estimate the concentration of micropollutants under typical wind scenarios and seasons relevant in Vidy Bay. Specifically, we determined the direct and indirect photolysis rate constants for 24 wastewater-derived micropollutants, and implemented this data into a hydrodynamic flow model, which tracked the movement of water parcels from the WW outfall through the Vidy Bay. Modeling results were validated with monthly field data collected in 2010. The ultimate goal of this study was to spatially and temporally define the area of potential ecotoxicological risk in Vidy Bay.

3.2 Material and methods

3.2.1 Site description, water sampling strategy and analysis of micropollutants

The Vidy Bay, lies on the northern shore of Lake Geneva, by the city of Lausanne, and represents 0.3% of the lake's total volume[129]. Aside from lake currents, the main input to Vidy Bay is discharge from Lausanne's wastewater treatment plant. Between one and three $m^3 \cdot sec^{-1}$ of treated wastewater is released 700 m from shore at -30 m depth. Other minor sources of water to the Bay are the Chamberonne River and the Flon stormwater outlet. Three locations were sampled on a monthly basis at various depths between April 2010 and January 2011, namely "WWTP outfall", directly above the discharge point of effluent wastewater and two references sites "REF-up" and "REF-down", respectively 1.5 km east and west of the WWTP outfall sampling site (Figure 3.1). Samples were analyzed within 24 h to determine the concentrations of 35 micropollutants (pharmaceuticals, pesticides, corrosion inhibitors). Of these, most pharmaceuticals as well as the corrosion inhibitors were found to be wastewater-derived, whereas the majority of pesticides entered the lake via diffuse sources. The analysis proceeded through solid phase extraction followed by detection via ultra-performance liquid chromatography coupled to a tandem mass spectrometer. Details regarding sampling strategy, choice of substances, and the analytical method have been described previously[24,140].

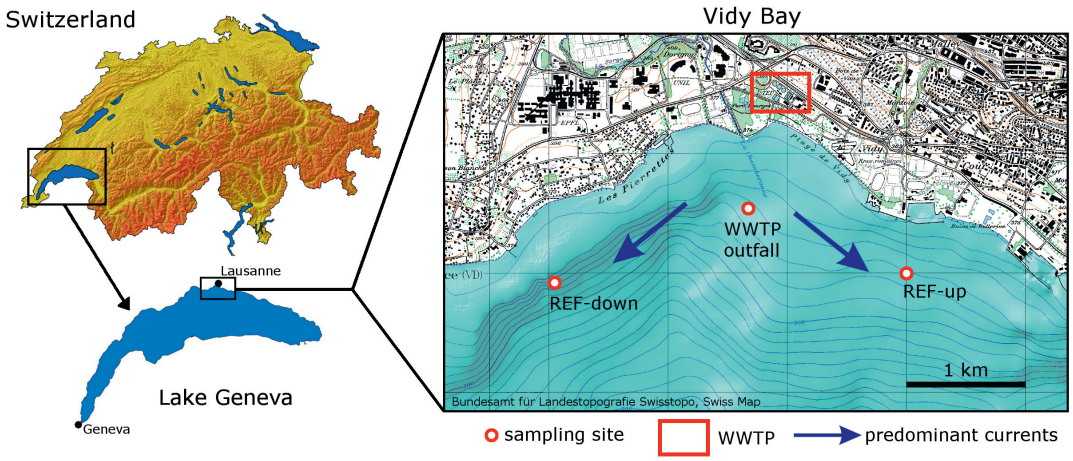

Figure 3.1: *Situation and map of the Vidy Bay showing the sampling locations WWTP outfall (Swiss coordinates : 534'672/ 151'540), REF-up (Swiss coordinates : 536'000/151'000) and REF down (Swiss coordinates : 533'048/150'920). Coordinates are in the Swiss Grid system with datum CH1903. Arrows show the predominant current directions which are generally parallel-to-shore*[137].

3.2.2 Particle tracking to model spreading of the plume

The hydrodynamic spreading of the wastewater plume in Vidy Bay was simulated using a particle tracking model (Delft3D-PART), a module of Delft3D which considers both advection and dispersion processes. The transport of particles in Delft3D-PART was driven by current velocity fields from a 3D finite-difference hydrodynamic flow model (Delft3D-FLOW), validated for Lake Geneva [137].

Particles tracks were computed for four scenarios, with differing wind and lake stratification conditions. The dominant winds regimes affecting Lake Geneva and more specifically Vidy Bay are the "Bise" (north wind), the "Vent" (west wind). Thus, the four chosen scenarios comprise moderate Bise (10°, 3 m·s^{-1}) and Vent (240°, 3 m·s^{-1}) both in stratified (summer) and unstratified (winter) conditions. As the particle tracking module does not model the initial spreading and mixing (near-field) of discharged water from an outfall, the dynamics of release near the outfall were modeled by starting the simulation from a circular plume with an estimated radius of 10 m for the Vidy Bay outfall situation. The release depth was chosen to be the depth of the thermocline (14–16 m) for stratified scenarios and the surface (0–1 m) for unstratified conditions, based on field observations and theoretical concepts. An instananeous release of 5'000 particles at the given depth above the WWTP outfall location was simulated for each scenario. Simulations using 2'000 and 3'000 particles showed no significant differences with release of 5'000 particles. The simulation yields the position (x-y-z(depth)) of each particle at each timestep (15 min), which was used as the input for the photodegradation model described below. Details concerning the parameters used for each simulation are available in the SI and described thoroughly by Razmi et al. [141].

The particle tracking model was validated using measured concentrations of conservative micropollutants (e.g. gabapentine) in the Bay. Explicitly, currents in Lake Geneva were modelled using 2010 meteorological data using Delft3D-FLOW [137]. Thereafter, simulations were computed using Delft3D-PART for field sampling days of 2010 and results compared nicely to actual measured concentrations [141].

3.2.3 Photolysis experiments and photodegradation in surface waters

The direct and indirect photolysis kinetics of target micropollutants necessary for the photodegradation model were determined experimentally under a solar simulator.

Chemicals. The commercial origin of the selected micropollutants has been listed previously [24]. Stock solutions were made in HPLC grade methanol. All other solvents used were of analytical grade quality. All aqueous solutions were made using Nanopure water. Further chemicals used in the photodegradation experiments were p-nitroanisole (Sigma-Aldrich), pyridine (Acros), sodium bicarbonate (Fluka) and sodium nitrate (Fluka).

Direct photolysis experiments. Solutions of a mixture of up to nine micropollutants, with individual concentrations ranging between 15 and 80 $\mu g \cdot L^{-1}$ in 1 mM bicarbonate-buffered Nanopure water (pH 8.4) were irradiated between 2 and 76 h by a Sun 2000 Solar Simulator (ABET Technologies, Milford, Connecticut) equipped with a 1000 W Xe lamp and an AM1.5 filter. The starting concentration of each compound corresponded to 10-times its limit of detection (LOD). As such, we monitored a 90% decay, while minimizing light screening by the target compounds. The compounds were grouped into mixtures based on their susceptibility to direct photolysis determined in preliminary experiments.

The irradiance of the solar simulator was determined spectroradiometrically (Model ILT-900-R, International Light) before and after each experiment. The absolute irradiance was calibrated using chemical actinometry (p-nitroanisole (pNA)) and was 76 $W \cdot m^{-2}$ between 280 and 430 nm and showed no day-to-day variation (lamp spectrum shown in SI, Figure xx). The irradiated solutions (400 mL) in amber glass beakers were continuously stirred , and their temperature was maintained at ca. 19°C using a water-filled tray, connected to a recirculation cooler (F240 Recirculating Cooler, Julabo). Identical solutions were left in the dark during each experiment to serve as dark controls. Moreover, mixtures containing double the starting concentration of each compound (between 30 and 160 $\mu g \cdot L^{-1}$) were photolyzed concurrently, to determine if second-order reactions between compounds in the mixture were contributing to the observed degradation. At selected time points (minimum 7), 1.2 mL samples were collected to monitor the parent compound concentration decrease over time. The samples were transferred to amber glass vials, were maintained at 4°C after collection and were analyzed within 48 h by ultra-performance liquid chromatography (Acquity UPLC system, Waters) coupled to a tandem mass spectrometer (MS/MS, XEVO, Waters). The experiments were repeated three times. Data acquisition and processing was performed using Masslynx. In parallel, absorbance spectra for all solutions were collected with a UV-vis 2550 Spectrophotometer (Shimadzu Scientific Instruments) at various irradiation time points to assess the change in absorbance over time and wavelength. Time-averaged values were used to correct for light screening. The chromatographic conditions and analytical methods were described previously[24,140].

Indirect photolysis experiments. To determine the contribution of indirect photolysis, two sets of experiments were conducted: in the first set, micropollutants were irradiated as described above, but water from Lake Geneva was used as the matrix. These experiments were used to determine the importance of transient species (e.g., singlet oxygen, triplet state organic matter) formed during irradiation of this particular lake water. These experiments, however, contained <0.4% methanol arising from the micropollutant stock solutions. Because methanol is an efficient hydroxyl radical quencher, the contribution of hydroxyl radicals to micropollutant degradation could therefore not be assessed. Instead, a second set of experiments were conducted in 1 mM bicarbonate buffer amended with nitrate (15 $mg \cdot L^{-1}$) as a sensitizer for hydroxyl radicals. For these experiments, the compounds were added to the buffer from stock solutions of the individual compounds prepared in methanol-free Nanopure water.

Quantum yield calculations. The degradation of all compounds followed first order kinetics and degradation rate constants ($k_{direct,i}$) were calculated using the slope of $\ln(A_t/A_0)$ plotted against time, where A_t refers to the peak area of chromatograms at time t, and A_0, the initial peak area. A light-screening factor was used to account for the fact that in some solutions the average light intensity in the beaker was lower than in optically dilute solutions, due to self-screening by the compounds in solution or transformation products forming. The observed direct photolysis degradation rate constant, $k_{direct,i}$, for each compound i was corrected to yield a photolysis rate constant representative of an optically dilute system, $k^0_{direct,i}$. The direct photolysis quantum yield(Φ_i) was determined for each compound (i). It represents the efficiency of direct photolysis and was calculated as follows:

$$\Phi_i = \frac{k^0_{direct,i}}{k^0_{abs,i}} \tag{3.1}$$

where $k^0_{abs,i}$ is the specific rate of light absorbtion, a measure of the spectral overlap of light irradiance and compound absorbance.

Details regarding light screening corrections, quantum yield calculations and calibration of light intensity by chemical actinometry and error calculations are described in Appendix C.

Contribution of indirect photolysis. The reaction rate constant ($k^0_{tot,i}$) determined in the indirect photolysis experiments encompasses both direct and indirect photolysis processes. The importance of indirect photolysis by reaction with hydroxyl radical ($k'_{\bullet OH,i}$) generated through nitrate photolysis was assessed after subtracting the direct photolysis rate constant from the total observed rate constant. Second order reaction rate constants ($k_{\bullet OH,i}$) between hydroxyl radical and each target compound were then determined from equation 3.2:

$$k^0_{tot,i} - k^0_{direct,i} = k'_{\bullet OH,i} = [^\bullet OH]_{ss} \cdot k_{\bullet OH,i} \tag{3.2}$$

where $[^\bullet OH]_{ss}$ represents the steady state concentration of OH-radicals in solution. This quantity was determined from the decay of one of the compounds within the micropollutant mixtures for which $k_{\bullet OH,i}$ was known (see Appendix B). The importance of other transient species was determined analogously by comparing the total degradation rate constants ($k^0_{tot,i}$) in the lake water experiment to the direct photolysis rate constant, $k^0_{direct,i}$, determined in buffered Nanopure water.

Extrapolation to environmental conditions. The direct photolysis quantum yields determined experimentally, Φ_i, were used to calculate the environmental direct photolysis rate constants, $k_{env,direct,i}$, for the different scenarios following equation 3.3.

$$k_{env,direct,i}(z) = \Phi_i \cdot k^0_{abs,sun,i} \cdot \mathrm{SF}_{lake}(z) \tag{3.3}$$

where $k^0_{abs,sun,i}$ is the specific rate of light absorption of the pollutant under solar irradiation, a quantity which depends on the substance itself, as well as on the intensity of solar irradiance. A theoretical solar irradiation was computed (SMARTS), at 47°N latitude, for the 21^{st} of June (stratified scenario) and 21^{st} of December (unstratified scenario), assuming clear sky conditions. The reduced photolysis rate due to light absorption by the lake water is accounted for in the lake water screening factor, SF_{lake},and is a function of depth z. Explicitly, the near-surface specific rate of light absorption for a given substance i, can be calculated as follows over the relevant wavelength absorption range:

$$k^0_{abs,sun,i} = 2.303 \cdot \sum_{280\mathrm{nm}}^{\lambda_{\mathrm{range}}} \varepsilon_i(\lambda) \cdot \mathrm{I}_{sun}(\lambda) \tag{3.4}$$

ε_i denotes the decadic molar extinction coefficient for substance i and was determined at pH 8.3 using a UV-vis 2550 Spectrophotometer (Shimadzu Scientific Instruments). $I_{sun}(\lambda)$ represents the computed solar irradiance for the chosen scenario (summer or winter).

The lake water screening factor for a given depth z is the ratio of the specific rate of light absorption at that depth, $k^z_{abs,sun,i}$, and the near-surface specific rate of light absorption, $k^0_{abs,sun,i}$:

$$\mathrm{SF}_{lake}(z) = \frac{k^z_{abs,sun,i}}{k^0_{abs,sun,i}} = \frac{\mathrm{I}_{sun}(\lambda) \cdot \varepsilon_i \cdot (1 - 10^{-z \cdot \alpha_D(\lambda)})}{\mathrm{I}_{sun}(\lambda) \cdot \varepsilon_i \cdot 2.303 \cdot z \cdot \alpha_D(\lambda)} = \frac{1 - 10^{-z \cdot \alpha_D(\lambda)}}{2.303 \cdot z \cdot \alpha_D(\lambda)} \tag{3.5}$$

Where $\alpha_D(\lambda)$ denotes the diffuse attenuation coefficient of lake water. It can be approximated by[19]:

$$\alpha_D(\lambda) = 1.2 \cdot \alpha_{lake}(\lambda) \tag{3.6}$$

Though wavelength-dependent, it can be approximated by using the value from a single wavelength where k_{abs} is maximal, which in the case of nitrate and most of the targeted compounds is near 320 nm. For Lake Geneva water, an average lake water absorbance at 320 nm, α_{lake}(320 nm), of 0.02 cm^{-1} was measured. The absorbance values did not vary significantly over the entire sampling period.

Indirect photolysis processes are particularly relevant for compounds resistant to direct photodegradation. The importance of reaction with $^1O_2$ or excited triplet state organic matter were found negligible for Lake Geneva water (see Results section); therefore the environmental indirect photolysis rate constant, $k_{env,indir,i}$, considers only reaction with hydroxyl radical:

$$k_{env,indir,i}(z) = k_{\bullet OH,i} \cdot [^{\bullet}OH]_{ss,lake} \cdot \mathrm{SF}_{lake}(z) \tag{3.7}$$

The steady state concentration of hydroxyl radicals in Lake Geneva, $[^{\bullet}OH]_{ss,lake}$, was calculated based on average measured levels of nitrate (0.029 mM) and scavenging species, such as HCO_3^-, CO_3^{2-} and dissolved organic carbon content (see Appendix B). The estimation of the steady state concentration of hydroxyl radicals extrapolated to 24 h on a sunny day yields maximal values of $1.7 \cdot 10^{-17}$ and $3 \cdot 10^{-18}$ M for the summer and winter scenarios respectively. The SF in equation 3.7 accounts for the reduction in hydroxyl radical production with depth, as less light becomes available for the photolysis of nitrate. Finally, the total environmental photolysis rate constant for each pollutant (assuming midday irradiance) can be written as:

$$k^{noon}_{env,tot,i}(z) = k_{env,direct,i}(z) + k_{env,indir,i}(z) \tag{3.8}$$

The midday rate constant can be extrapolated to the average irradiance over 24 hours by a factor of 0.4 [19]:

$$k^{24h}_{env,tot,i}(z) = 0.4 \cdot k^{noon}_{env,tot,i}(z) \tag{3.9}$$

The photolysis component of the proposed model is based on well-acknowledged theoretical concepts. The equations above have been derived previously and more details are given in Schwarzenbach et al. [19].

The photodegradation equations used herein have been repeatedly applied for simple estimation of photodegradation half-lives of micropollutants in water (e.g. [74,82]), in "back of the envelope"-type calculations, to assess the importance of photolysis compared to other removal mechanisms [117], and in more complex models which modeled photolysis rates in rivers as a function of the distance of single "particles" from the surface [116]. Moreover, several studies compared predicted environmental direct photolysis rate constants (calculated from laboratory-determined quantum yields (i.e. equation 3.3 above)) to experimental rate constants (measured in natural sunlight) and found similar results for a variety of compounds [82,138]

3.2.4 Mixture toxicity assessment

Recent work revealed a potential ecotoxicological risk for individual micropollutants above the outfall[140]. The individual risk of pollutants is commonly estimated using the risk quotient (RQ), which is the ratio of the measured or predicted environmental concentration (MEC or PEC) to the predicted no effect concentration (PNEC)[70]. A potential risk exists when RQ surpasses one. The PNEC-values of the selected micropollutants were compiled previously[140].

$$\mathrm{RQ}_i = \frac{\mathrm{PEC}_i}{\mathrm{PNEC}_i} \tag{3.10}$$

In the aquatic environment, all substances are present contiguously, thus a realistic ecotoxicological risk assessment should consider the effect of all chemicals present. Latest research recommends applying a concentration addition (CA) model as a conservative worst case estimation of mixture toxicity[69,70]. Explicitly, the risk of a chemical mixture, RQ_m, is the sum of the RQ of each substance present in the mixture, RQ_i (equation 3.10):

$$\mathrm{RQ}_m = \sum_i \mathrm{RQ}_i \tag{3.11}$$

Though the CA model by definition assumes all substances exhibit a similar mode of action, which is often unverified in environmentally realistic mixtures[70], it is nevertheless suggested for a precautious risk assessment, and has been proven to provide excellent predictions of mixture toxicities[71,72].

3.2.5 Coupling photodegradation and hydrodynamics

The spatial distribution of environmental concentrations near the outfall was estimated by combining particle tracking (section 3.2.2) and photolysis kinetics (section 3.2.3). The modeled area of the Bay (4 km by 3 km, starting at the north-eastern coordinate 532'600/152'450, Swiss coordinate system) was discretized into a 50-by-50 m grid, over layers of 2 m depth. The hydrodynamic model yielded the 3D position $p_{n,t,j}$ of each parcel of water n (total of 5'000 parcels ("particles") released), for each timestep t (15 min intervals=$\Delta(t)$)), up to 3 days following the time of release.

$$p_{n,t,j} = j^{th} \text{ component of the position for particle } n \text{ at time } t \tag{3.12}$$

with $j = 1$: x coordinate, $j = 2$: y coordinate and $j = 3$: depth z (in m)

The number of particles in each cell of the grid (x, y, z) at each timestep t is then given by:

$$\mathrm{N}_{x,y,z,t} = \sum_{n} \delta_{p_{n,t,1},x} \cdot \delta_{p_{n,t,2},y} \cdot \delta_{p_{n,t,3},z} \qquad \begin{matrix} \text{with } x = 1,2,...,300 \\ y = 1,2,...,200 \\ z = 1,2,...,25 \end{matrix} \tag{3.13}$$

$$\text{and with } \delta \text{ the Kronecker delta}: \delta_{\alpha,\beta} = \begin{cases} 1 & \text{if } \alpha = \beta, \\ 0 & \text{if } \alpha \neq \beta. \end{cases} \tag{3.14}$$

Thereafter, the concentration of each substance in every cell of the grid was determined separately, for each timestep. To do so, all n particles were attributed a hypothetical mass M_0^i at the time of release ($t = 0$). M_0^i is compound-dependent, and chosen such that the sum of all particle masses in the release volume match the concentration of a given compound (i) that was actually observed during the 2010 sampling campaign (i.e. the concentrations measured in the surface plume in November 2010 were used for the unstratified scenario and those detected in June 2010 for the stratified scenario). Assuming no degradation, the mass of each particle is constant in time, and the concentration of compound i in a given cell (x, y, z) at a specific timepoint t is given by:

$$\mathrm{C}_{x,y,z,t}^{conservative,i} = \frac{\mathrm{N}_{x,y,z,t} \cdot \mathrm{M}_0^i}{\mathrm{V}} \tag{3.15}$$

where V is the cell volume (50 × 50 × 2 m). In this conservative case, only dilution due to currents affects the concentration in each cell of the modelled area.

However, most compounds being susceptible to photodegradation, each of the 5'000 particles released undergoes a depth-dependent degradation. Hence, the mass of each particle evolves over time according to its relative distance from the surface, following a 1^{st} order degradation:

$$\mathrm{M}_{n,t}^i = \mathrm{M}_0^i \cdot e^{-\Delta t \cdot \sum_{\tilde{t}=0}^{t-1} k_{n,\tilde{t}}^i} \tag{3.16}$$

with $\Delta t = 15$ min, and $k_{n,\tilde{t}}^i$ the depth-dependent degradation rate constant of particle n for a given micropollutant i. $k_{n,\tilde{t}}^i$ was calulated according to equation 3.9 and is a function of the propensity of compound i to undergo photolysis, the incoming irradiance, I_{sun} (summer or winter), and the depth. Due to the finite resolution, we used the average depth between timesteps $(p_{n,\tilde{t},3} + p_{n,\tilde{t}-1,3}/2)$:

$$k_{n,\tilde{t}}^i = f(i, p_{n,\tilde{t},3}, p_{n,\tilde{t}-1,3}, \mathrm{I}_{sun}) \tag{3.17}$$

When both dilution and photolysis processes are considered, the concentration of compound i in a given cell at time t is:

$$C^{photo,i}_{x,y,z,t} = \frac{\sum_n \delta_{p_{n,t,1},x} \cdot \delta_{p_{n,t,2},y} \cdot \delta_{p_{n,t,3},z} \cdot M^i_{n,t}}{V} \tag{3.18}$$

Finally, to reflect the actual conditions of effluent WW discharge in Vidy Bay, which is continuous and not instantaneous, a continuous release situation was mimicked by addition of the concentrations in each cell over all timesteps, until reaching steady state conditions. Accordingly the steady state predicted environmental concentration (PEC) in a given cell assuming only dilution processes (cloudy skies) is given by:

$$PEC^{conservative,i,ss}_{x,y,z} = \sum_t C^{conservative,i}_{x,y,z,t} \tag{3.19}$$

When both dilution and photodegradation are occurring, the predicted environmental concentration becomes:

$$PEC^{photo,i,ss}_{x,y,z} = \sum_t C^{photo,i}_{x,y,z,t} \tag{3.20}$$

Ultimately, the ecotoxicological risk of the plume was calculated following equation 3.11, considering 24 wastewater-derived substances and the predicted environmental concentrations from the coupled hydrodynamic-photolysis model. All computations were performed using Matlab R2011b.

3.3 Results and discussion

3.3.1 Photolysis experiments

The direct photolysis rate constants measured under the solar simulator, corresponding quantum yields and calculated environmental half-lives are listed in Table 3.1. The data span a wide range of values, from the photolabile substances such as ketoprofen and diclofenac with direct photolysis rate constants between 0.4 and 9 h^{-1}, to the compounds which were more recalcitrant to direct photodegradation, with rate constants on the order of 0–0.1 h^{-1}. The calculated quantum yields also spanned a large range from $1.4{\cdot}10^{-4}$ to 0.75. The quantum yields determined in the present study were compared to literature values (often single-wavelength Φ), when available. The values obtained herein compared relatively well to literature, with values between 1.1 and 9 times those reported in previous studies.

The total photolysis rate constants determined in the experiments conducted in Lake Geneva water showed no significant difference with experiments buffered Nanopure water($k^0_{tot,i}$ were within 20% of $k^0_{direct,i}$). This indicates that indirect processes via triplet state organic matter or singlet oxygen are negligible for this particular lake water. Note that these experiments contained methanol from the compound stock solution, hence hydroxyl radical reactions were suppressed. On the other hand, for a large number of compounds significantly faster degradation was observed in experiments (without traces of methanol) amended with 15 $mg{\cdot}L^{-1}$ nitrate, a hydroxyl radical sensitizer. These radicals being very reactive and non-selective, they are known to react with many organic compounds at nearly diffusion controlled rates [104,105]. Accordingly, the bimolecular rate constants with hydroxyl radical determined in the present study or from literature vary from $1–22{\cdot}10^9$ $M^{-1}{\cdot}s^{-1}$ (Table 3.1). Though the actual nitrate levels in Lake Geneva are typically well below the experimental concentrations (ca. 1-2.5 $mg{\cdot}L^{-1}$ [142]), hydroxyl radicals nevertheless play an important role in the overall degradation of a number of compounds (see "contribution of indirect to total photolysis" in Table 3.1) , namely those that are not susceptible to direct photolysis.

Based on their environmental half-lives, calculated according to equations 3.8 and 3.9, the targeted wastewater-derived micropollutants were classified in 4 groups; 5 degraded very rapidly (τ_{summer} < 1h) in near-surface, summer conditions, 5 degraded fast (τ_{summer} < 1 day), 2 fall into the moderately persistent category (1 day < τ_{summer} < 50 days), and the remainder (12 compounds) were classified as persistent (τ_{summer} > 50 days). Note that all compounds relying mainly on indirect phototransformation processes (contribution of indirect to total photolysis > 70 %) fall in the persistent category, indicating that for the compounds targeted in this study, direct photolysis still represents the most efficient removal process for the given lake parameters.

Diclofenac, sulfamethoxazole and gabapentine were chosen as representative compounds for the "very fast", "fast" and "persistent" categories. They will be considered below for the analysis of the spatial extent of elevated concentrations around the wastewater outfall.

Table 3.1: *Direct and indirect photolysis parameters determined for the 24 target micropollutants: $k^0_{direct,i}$: direct photolysis rate constant measured in buffered solution under the solar simulator, and resulting quantum yield (QY). These values are not applicable (n.a.) to compounds which do not absorb light beyond 280 nm. $k_{\bullet OH,i}$: bimolecular rate constant between compound and hydroxyl radical; τ_{summer} and τ_{winter}: predicted environmental half-life based on $k^{24h}_{env,tot,i}$ (equation 3.9);Percent indirect: contribution of indirect to total photolysis; PNEC: predicted no-effect concentration.*

Compound Name	$k^0_{direct,i}$ (h^{-1})	Φ	**Φ-literature**	$k_{\bullet OH,i}$ ($M^{-1}\cdot s^{-1}$)	**Reference for** $k_{\bullet OH,i}$	τ_{summer} (h)	τ_{winter} (h)	**Percent indirect**	**PNEC** ($ng\cdot L^{-1}$)
atenolol	0.018 ± 0.002	0.019 ± 0.004		7.5 ± 0.3	Ji et al.[109]	2916	20525	87%	33400
azithromycin	n.a.	n.a.		2.9	Dodd et al.[143]	9539	55327	100%	10
benzotriazol	0.11 ± 0.01	0.015 ± 0.004	0.009 ± 0.0002[144]	14 ± 2	Vel Leitner et al.[145]	1474	10861	86%	30000
bezafibrat	0.061 ± 0.004	0.055 ± 0.011		7.4 ± 1.2	Huber et al.[146]	3737	21682	100%	1191
carbamazepin	0.006 ± 0.001	0.00015 ± 0.00004	0.0003 ± 0.0004[105,144]	5.0 ± 0.6	Wols et al.[105]	1293	9860	27%	2500
carbendazim	0.009 ± 0.001	0.00051 ± 0.00012	0.002[105]	5.9 ± 0.1	Wols et al.[105]	4319	27237	95%	100
ciprofloxacin	10 ± 1	0.037 ± 0.009	0.012 ± 0.002[105]	5.94 ± 1.72	Wols et al.[105]	0.26	1.2	0%	5
clindamycin	n.a.	n.a.		22 ± 21	*this study*	1254	7275	100%	1000000
diclofenac	28 ± 3	0.76 ± 0.19	0.17 ± 0.18[105,144]	8.4 ± 0.8	Wols et al.[105]	0.41	2.1	0.01%	100
gabapentin	n.a.	n.a.		1.4 ± 0.4	*this study*	19497	113084	100%	1000000
gemfibrozil	0.22 ± 0.06	0.018 ± 0.006		10 ± 1	Razavi et al.[147]	18	75	0.56%	751000
ketoprofen	115 ± 60	0.21 ± 0.01	0.3 ± 0.01[105]	3.5 ± 0.2	Wols et al.[105]	0.68	3.2	0.01%	15600
methylbenzotriazol	0.09 ± 0.01	0.008 ± 0.002		4.45 ± 1.11	*this study*	890.52	14175.66	27%	75000
metoprolol	0.057 ± 0.005	0.071 ± 0.013	0.035 ± 0.04[105]	7.5	Wols et al.[105]	1927	18595	70%	3200
metronidazol	0.84 ± 0.05	0.003 ± 0.001	0.0034 ± 0.0001[105]	4.7 ± 0.7	Wols et al.[105]	3.6	16	0.05%	25000
norfloxacin	8.3 ± 2.1	0.032 ± 0.01	0.043 ± 0.005[148]	1.7 ± 0.7	*this study*	0.33	1.5	0%	40100
ofloxacin	1.1 ± 0.1	0.006 ± 0.001	0.0030 ± 0.0002[148]	16 ± 4.7	*this study*	3.0	13	0.15%	500
paracetamol	0.038 ± 0.004	0.010 ± 0.003	0.002 ± 0.003[105]	7.1 ± 4.7	Wols et al.[105]	716	5698	22%	9200
primidon	n.a.	n.a.		6.7 ± 0.02	Real et al.[149]	4128	23947	100%	54171
propranolol	0.60 ± 0.05	0.024 ± 0.005	0.0052[76]	8.7 ± 0.3	Chen et al.[150]	12	91	0.43%	50
simvastatin	n.a.	n.a.		3.1 ± 0.2	Razavi et al.[101]	8810	51098	100%	9600
sotalol	4.2 ± 0.3	0.39 ± 0.08		1.6 ± 0.6	*this study*	0.98	4.1	0%	15935
sulfamethoxazol	1.4 ± 0.1	0.028 ± 0.005	0.038 ± 0.011[105]	5.1 ± 0.74	Wols et al.[105]	23	102	0.37%	27
trimethoprim	0.46 ± 0.04	0.0007 ± 0.0002	0.001 ± 0.0001[105]	6.3 ± 0.85	Wols et al.[105]	1545	16059	49%	16000

3.3.2 Predicted plume extension for representative compounds

During the colder months when the lake temperature is homogeneous throughout the water column, the warmer wastewater discharged at -30 m depth rises through the colder, denser water to the lake surface. Figure 3.2 shows the subsequent distribution and attenuation of diclofenac, sulfamethoxazole and gabapentine in the surface water (0–2 m depth) surrounding the wastewater outfall. In order to show the area impacted by discharged WW containing elevated concentrations of micropollutants, the individual concentration plumes are shown down to 0.5 ng·L^{-1}, regardless of background concentrations measured in the lake. Values measured in the surface plume in November 2010 were used as the concentration at the outfall (after initial near-field mixing of the plume) [140]. Two weather conditions were distinguished: the left column illustrates the predicted concentrations based on only dilution by lake currents. This situation represents the plume dynamics on a cloudy day. In the right column, both dilution and photodegradation are considered, representing a sunny day (averaged over 24 h). If only dilution is considered, the area impacted by effluent wastewater varies from compound to compound, due to the different initial concentrations at the source. Among the compounds considered, gabapentin shows the largest area of elevated concentrations, followed by diclofenac. If photolysis is taken into account, however, the spatial extent of the diclofenac plume is significantly reduced. On the other hand, photolysis only slightly reduces the area of the sulfamethoxazole plume. Though this antibiotic degrades rather fast at the water surface in summer sunlight, the estimated winter half-life is over 80 h (Table 3.1). As the timescale of dilution (ca. 12 h travel time until reaching concentrations <1 ng·L^{-1}, see Figure B.1, Appendix B) is considerably smaller than that of photolysis processes, only little reduction of the concentration due to photolysis is observable in Figure 3.2. Finally, gabapentine, owing to its persistent nature, relies exclusively on dilution for the attenuation of its concentration. The presence of sunlight therefore does not influence the extent of its plume.

3.3.3 Predicted extent of the diclofenac-plume near the WW outfall for different wind and stratification scenarios

Given the important influence of sunlight on the spatial extent of diclofenac discharged from the WWTP, the footprint of the diclofenac plume was considered for each scenario (Bise and Vent; stratified and well-mixed) and weather condition (cloudy (only dilution) and sunny (dilution and photolysis)). In sunny weather conditions (Figure 3.3, right panel), results from the coupled hydrodynamic-photolysis model showed a larger extension of the diclofenac plume in stratified conditions compared to mixed ones, owing to decreased photodegradation due to entrapment of the WW plume below the thermocline. The largest extent of the plume under stratified conditions was observed for the Bise scenario (Figure 3.3 d). The smaller extent of the plume in the stratified-Vent scenarios can be attributed to the stronger dilution of particles, which are pushed against the shore, experience a return flow along the lake bed and are thus distributed to deeper depths compared to the Bise conditions [137] (Figure 3.4 (F) and Figure B.2 in Appendix B)

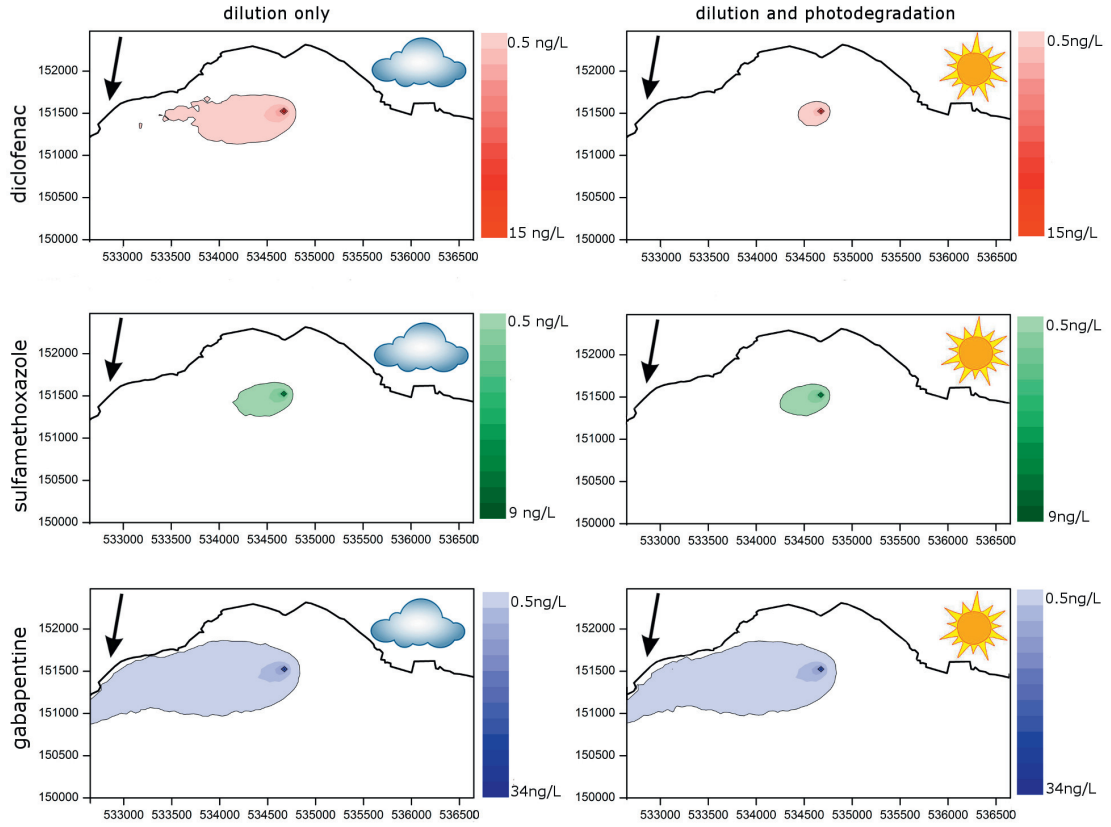

Figure 3.2: *Predicted concentrations in the surface layer (0–2 m depth) of diclofenac (top), sulfamethoxazole (middle) and gabapentine (bottom) around the wastewater outfall, assuming a small surface plume in unstratified conditions, under the influence of Bise (arrow shows wind direction). The concentrations are shown down to 0.5 ng·L^{-1}, under cloudy (only dilution, left panel) and sunny weather conditions (dilution & photolysis, right panel). The size of the sun differentiates winter (small sun) and summer (large sun) irradiance. Axes show the latitudinal and longitudinal coordinates (Swiss Grid system with datum CH1903).*

In the absence of sunlight (Figure 3.3, left panel) similar plume extensions were observed for stratified and unstratified conditions when the Bise is blowing (ca. 1 km). However, the largest plume extension of all weather conditions (sunny vs cloudy) and scenarios was observed for the combination of an unstratified lake and Vent. This may be explained by higher current velocities under these conditions. Indeed, the magnitude of currents induced by friction between air and underlying water is proportional to the the maximal distance an air mass travels across a lake, the fetch. The long fetch associated with Vent (20 km) leads to the formation of large gyres in the lake, which in turn generate high along-shore current velocities and in consequence a higher dispersion of the plume when it is at the surface. In contrast, owing to land topography and wind direction, the fetch of Bise in the Vidy Bay is understandably smaller. Accordingly, surface current velocities and plume dispersion are smaller as well.

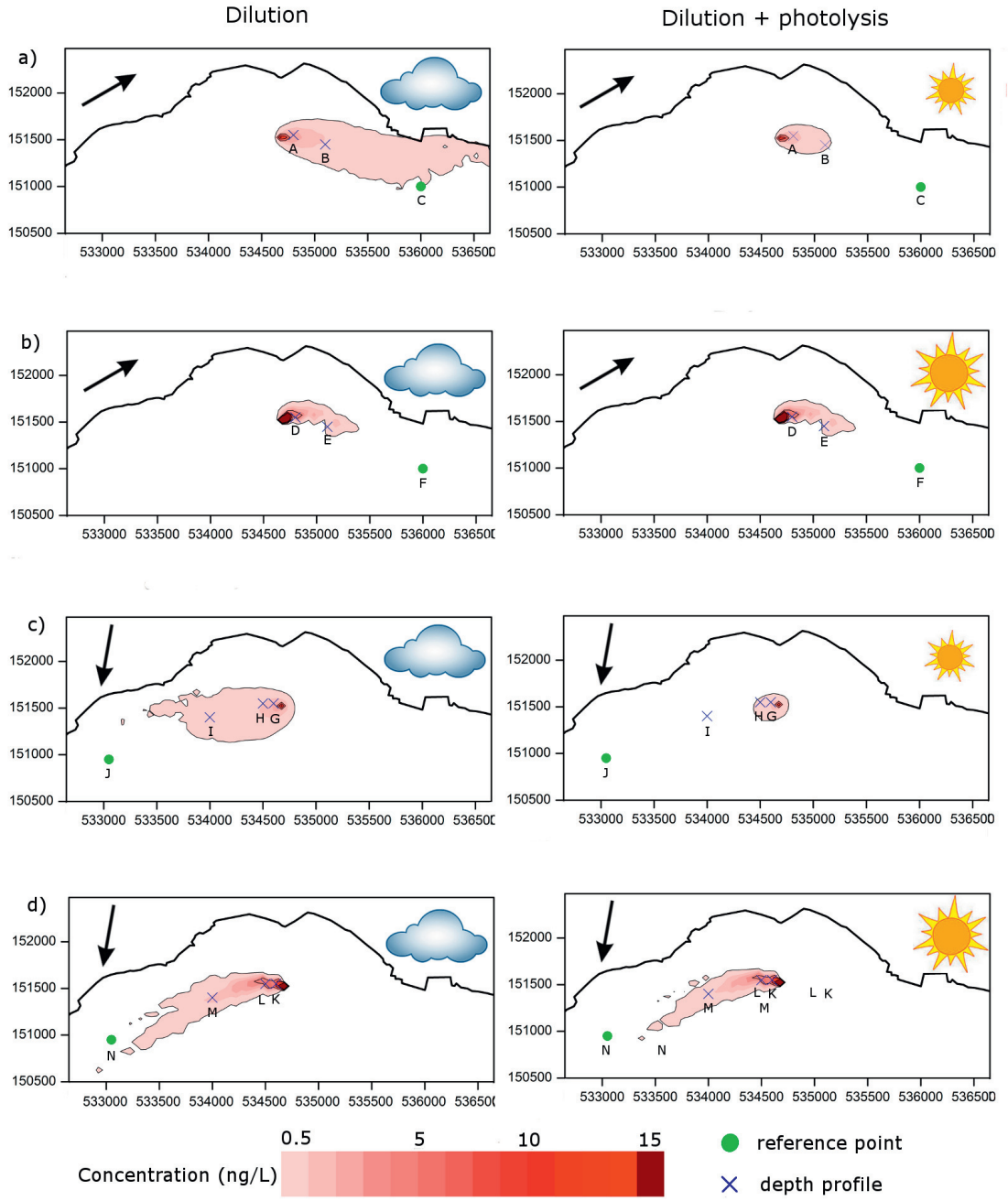

Figure 3.3: *Predicted concentrations of diclofenac around the WW outfall for different scenarios. a) Vent-unstratified b) Vent-stratified c) Bise-unstratified d) Bise-stratified, under cloudy (only dilution, left panel) and sunny (dilution & photodegradation, right panel) weather conditions. Depth profiles are given in Figure 3.4 for the blue crosses and the reference points (green dots). Arrows indicate the wind direction. Maps show the layer of particle release: 0–2 m in unstratified conditions and 14–16 m in stratified conditions. Axes show the latitudinal and longitudinal coordinates (Swiss Grid system with datum CH1903).*

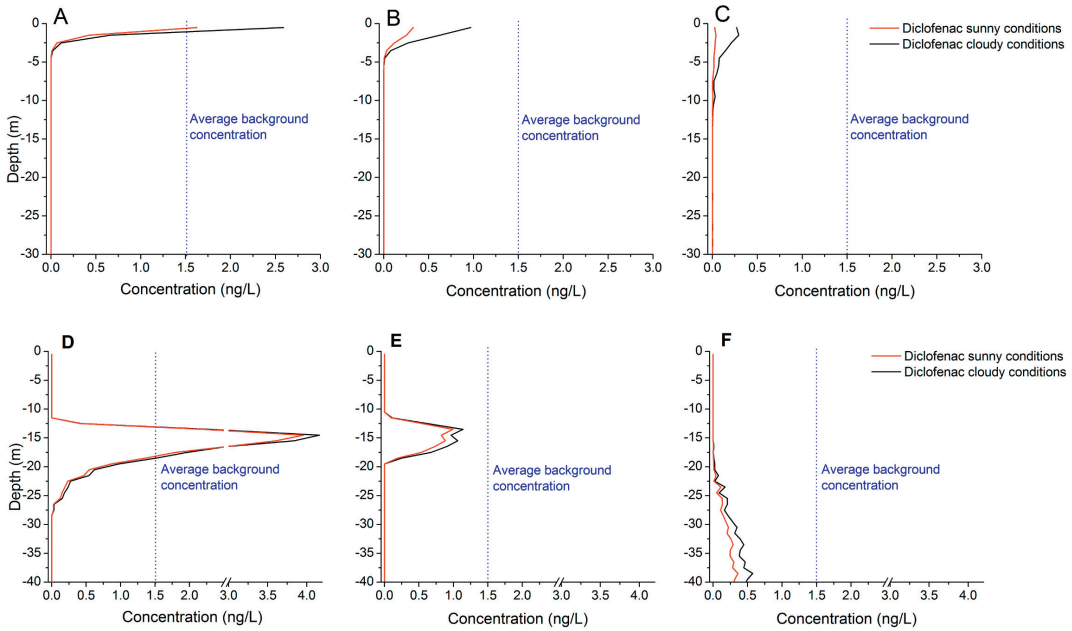

Figure 3.4: *Modeled concentration depth profiles for diclofenac under unstratified Vent (top), and stratified Vent (bottom) for the locations A-F marked by blue crosses in Figure 3.3.*

The previous figures delineate the WW plume assuming pristine surrounding waters (micropollutant concentrations <0.5 ng·L^{-1}). However, actual measured background concentrations of diclofenac in the lake are approximately 1.5 ng·L^{-1} [140].

The actual spatial extent of the zone with concentration greater than the background concentration is depicted in figure 3.5 for the case of diclofenac. Similar extents were predicted for other wastewater-derived micropollutants. The maximal extension observed under stratified Bise conditions extends 300 m away from the outfall. In contrast, in unstratified conditions, the footprint of the wastewater plume is barely discernible from the background concentrations, owing to the enhanced near-field mixing of up-welling wastewater. Accordingly, during the cold season the chances of detecting a plume at the surface are diminished. Indeed, during the 10-month sampling campaign, a surface plume was detected only on one occasion, whereas it was regularly detected when the lake was stratified.

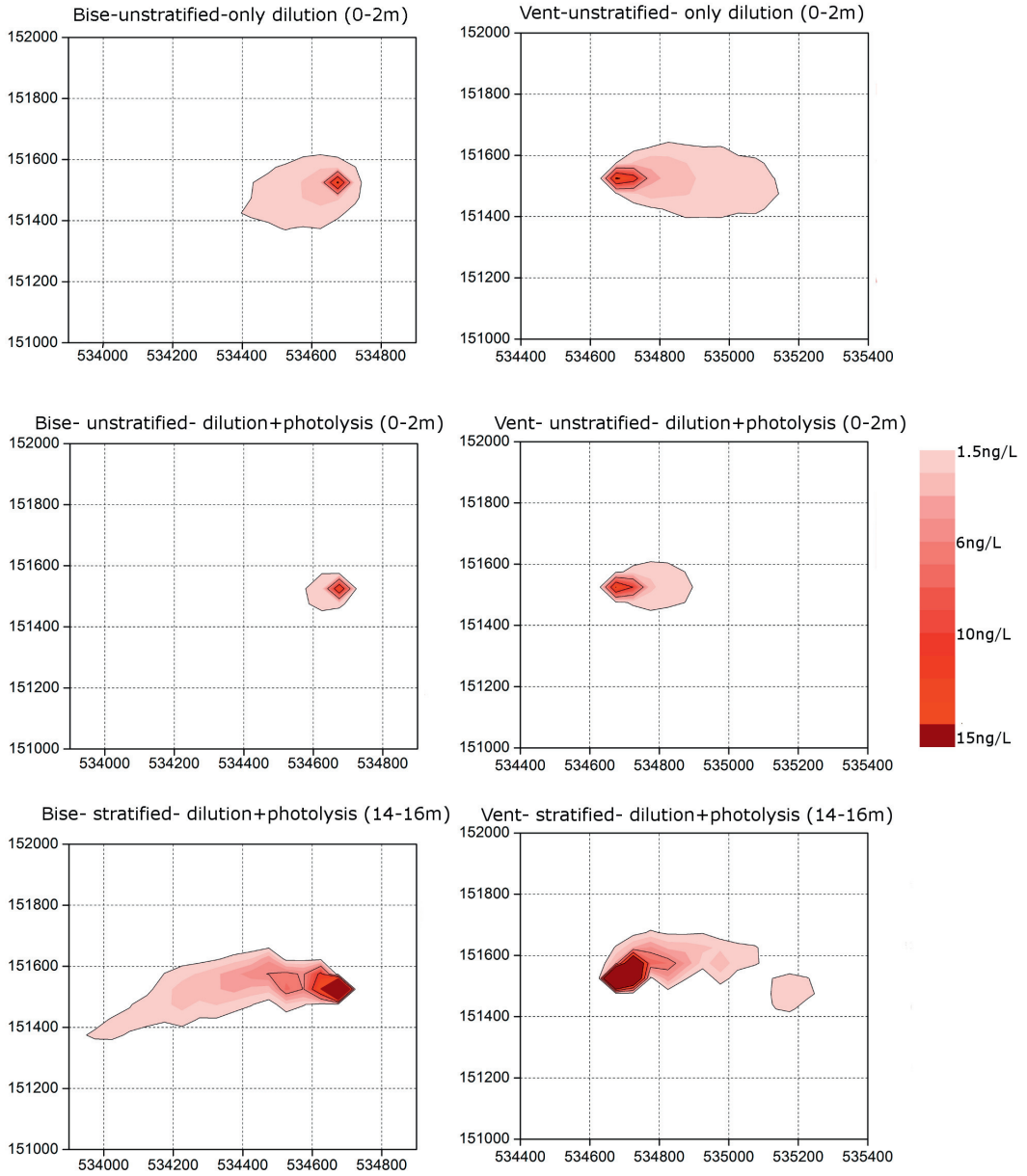

Figure 3.5: *Spatial extent of the diclofenac concentration which exceeds the lake background concentration (1.5 ng·L^{-1}) for the different wind conditions: Bise (left panel) and Vent (right panel); and climatic scenarios: well-mixed cloudy conditions (top), well-mixed sunny conditions (middle) and stratified sunny conditions (bottom).Axes show the latitudinal and longitudinal coordinates (Swiss Grid system with datum CH1903)*

3.3.4 Extent of the ecotoxicological risk zone around the WWTP outfall

The ecotoxicological risk exerted the wastewater plume, comprising a entire suite micropollutants, cannot be determined based on the behavior of individual substances alone. For a realistic ecotoxicological risk assessment, the entirety of micropollutants present in the mixture, which differ in concentration, susceptibility to photolysis, and ecotoxicological relevance should be considered.

Herein, the overall ecotoxicological risk of the 24 targeted micropollutants was determined based on the combination of the individual risk of each substance according to equation 3.11. The zone with RQ_m >1 was defined as the zone with a potential ecotoxicological risk. It should be noted, however, that possible mixture effects at low doses, well below the NOEC (no-observed effect concentration) remain a major ecotoxicological concern [151]. Furthermore, inclusion of additional compounds in the study would likely induce an even larger RQ_m. To account for these uncertainties, the area with RQ_m values between 0.1 and 1 is was additionally defined as a precautionary risk zone for the purpose of this study.

Calibrated with measured concentrations in the plume at the level of the thermocline, a maximal value of RQ_m=12.9 was obtained at the WW outfall location. Through dilution and degradation processes, this extremely high RQ rapidly decreased with distance from the outfall. Model results showed that the risk zone (red in Figure 3.6) was generally larger under stratified (summer) conditions (Figure 3.6 b,d) than under well-mixed (winter) conditions (Figure 3.6 a,c). The risk zone was largest during stratified Bise, in the thermocline layer (Figure 3.6 b). Indeed, for these conditions we predicted a horizontal spread of over 300 m. The precautionary risk zone was also largest for this scenario, with a westward expansion of >1 km. The area of potential adverse effects was significantly smaller in well-mixed conditions. Under Vent conditions, the zone affected by RQ_m >1 area was slightly smaller. Nevertheless, the precautionary risk zone (orange in Figure 3.6) almost matched the Bise extension (ca. 700 m) and extended to deeper depths mainly to the east (upstream) of the WW outfall (Figure 3.7).

The mixture toxicity near the outfall was dominated by five substances, namely, in order of the importance of their contribution, the antibiotics ciprofloxacin, sulfamethoxazole, and azithromycin, carbendazim, an urban pesticide and diclofenac, an anti-inflammatory drug. With increasing distance from the source, we observe a shift in the compounds that dominate the overall risk, owing to photodegradation processes. For instance, in unstratified conditions, 1 km from the outfall, sulfamethoxazole, azithromycin and carbendazim still contributed significantly to RQ_m, but other compounds such as paracetamol, propranolol and carbamazepine became increasingly relevant.

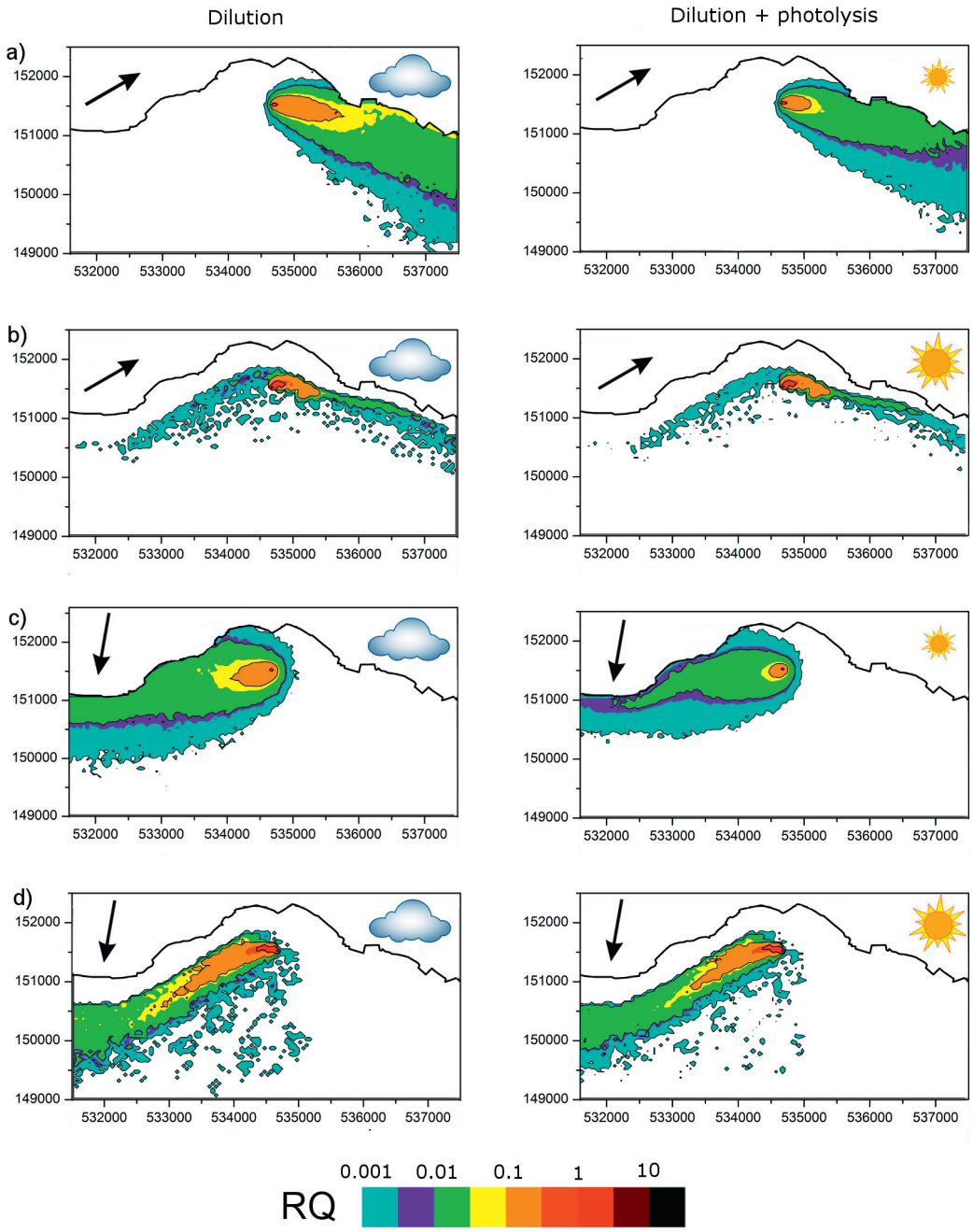

Figure 3.6: *Delineation of the risk zone (RQ_m>1, red) and precautionary risk zone (0.1<RQ_m<1, orange) for the four scenarios and 2 weather conditions (cloudy: left panel and sunny: right panel) in the layer of release (0–2 m for unstratified conditions and 14–16 m for stratified conditions). a) Vent-unstratified; b) Vent-stratifed; c) Bise-unstratified; d) Bise-stratified. The size of the sun differentiates winter (small sun) and summer (large sun) irradiance. Arrows indicate the wind direction and axes show the latitudinal and longitudinal coordinates (Swiss Grid system with datum CH1903).*

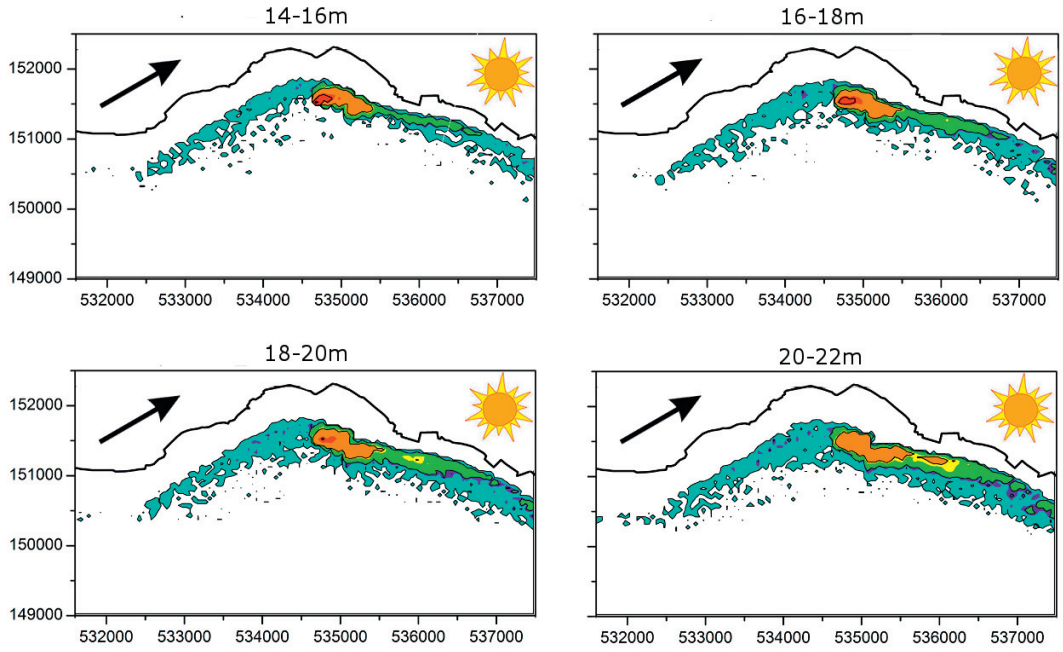

Figure 3.7: *3D extension of the risk quotient for stratified vent scenario. The highest risk is observed in the release layer (14–16 m), but the precautionary risk zone extends further at lower depths (20–22 m). Arrows indicate the wind direction and axes show the latitudinal and longitudinal coordinates (Swiss Grid system with datum CH1903).*

Note that area of potential ecotoxicological risk determined here only accounts for wastewater-derived micropollutants targeted in this study. However, an entire suite of organic chemicals have been detected in Lake Geneva, which undoubtedly affect the overall risk. For example, the additional risk that can be attributed to measured background concentrations of a small selection of non-wastewater derived substances (i.e pesticides also measured during the 2010 sampling campaign[140]), adds up to 0.1.

3.3.5 Comparison of measured and predicted concentrations

The coupled hydrodynamic photolysis model predicts the extent of a micropollutant plume discharged from a point-source. The location of this source was chosen to be not the actual WW outfall at -30 m depth, but rather the depth to which the plume rises before it spreads. Under stratified conditions, this corresponds to the level of the thermocline (14–16 m) and for the well-mixed, winter scenario to the surface layer (0–2 m). The release of particles was assumed to be continuous at these depths. In reality, the thermocline depth will vary slightly on a daily, even hourly basis, along with the WWTP discharge flow. In addition, the hydrodynamic driving force (wind speed and direction), which was assumed constant for each of the 4 scenarios, also fluctuates at times on an hourly scale[137].

A recent campaign depicted the near-field (<300 m) spatial and temporal variability of the wastewater plume via dense measurements of conductivity profiles around the outfall[152]. Results showed that within 100 m of the outfall, the number and depth of elevated conductivity peaks varied with sampling site around the outfall, but no relation was found with respect to the distance or direction of the sampling location from the outfall. Moreover, day to day variations were observed. These results confirm the complex current dynamics within the Bay, due in part to the variability of the parameters discussed above, and illustrate the near-field heterogeneity of the wastewater plume. Nevertheless, though the wind field may be remarkably variable, Bise and Vent are the two wind directions which occur regularly over the lake[153]. Therefore with this model we do not claim to give an exact picture of the micropollutant plume, yet to depict the worst-case extent of the plume on a larger scale (mid-field) under typical wind conditions and solar irradiation.

Exact validation of the coupled hydrodynamic-photolysis model is delicate due to the lack of sampling points between the source and the reference points, which were generally beyond the plume. Nevertheless, the plume was captured on one occasion at REF-down at -10 m depth, which allowed for the validation of the hydrodynamic component of the model, as phototransformation processes are not relevant at this depth.

When comparing results of the coupled model with actual measurements, it is important to note that sampling observations capture both the plume signal as well as background concentrations. On the other hand, the hydrodynamic-photolysis model assumes the unique source of micropollutants is above the wastewater outfall at the level of the thermocline (or the surface). The importance of photolysis processes, seasonality and distance from the outfall is well depicted in Figure 3.8 which shows the measured concentration ranges in the near-surface (0–3 m) and near-bottom (17–30 m) layers of the Bay in stratified (June–August) and unstratified (November–January) conditions. Firstly, under stratified conditions average concentrations in the surface layers (orange boxes) are generally smaller than below the thermocline (blue boxes) at both the outfall sampling location and at REF-down. Lower surface concentrations may be attributed to enhanced photolysis of micropollutants in the surface layers as well as their entrapment beneath the thermocline. Correspondingly, differences are more pronounced for compounds that photolyze relatively fast (diclofenac, atenolol and benzotriazole), than for the persistent compounds (gabapentine). From the model results it is evident that the large majority of the particles released at the thermocline effectively remain below the thermal boundary, where photolysis is reduced, leading to increased concentrations in the summer (Figure 3.4, bottom). On the other hand, under well-mixed conditions, the measured concentrations did not differ significantly in the top and bottom layers of the water column. This corresponds well to the modeled depth profiles (Figure 3.4, top), which show that background concentrations are rapidly reached under unstratified conditions.

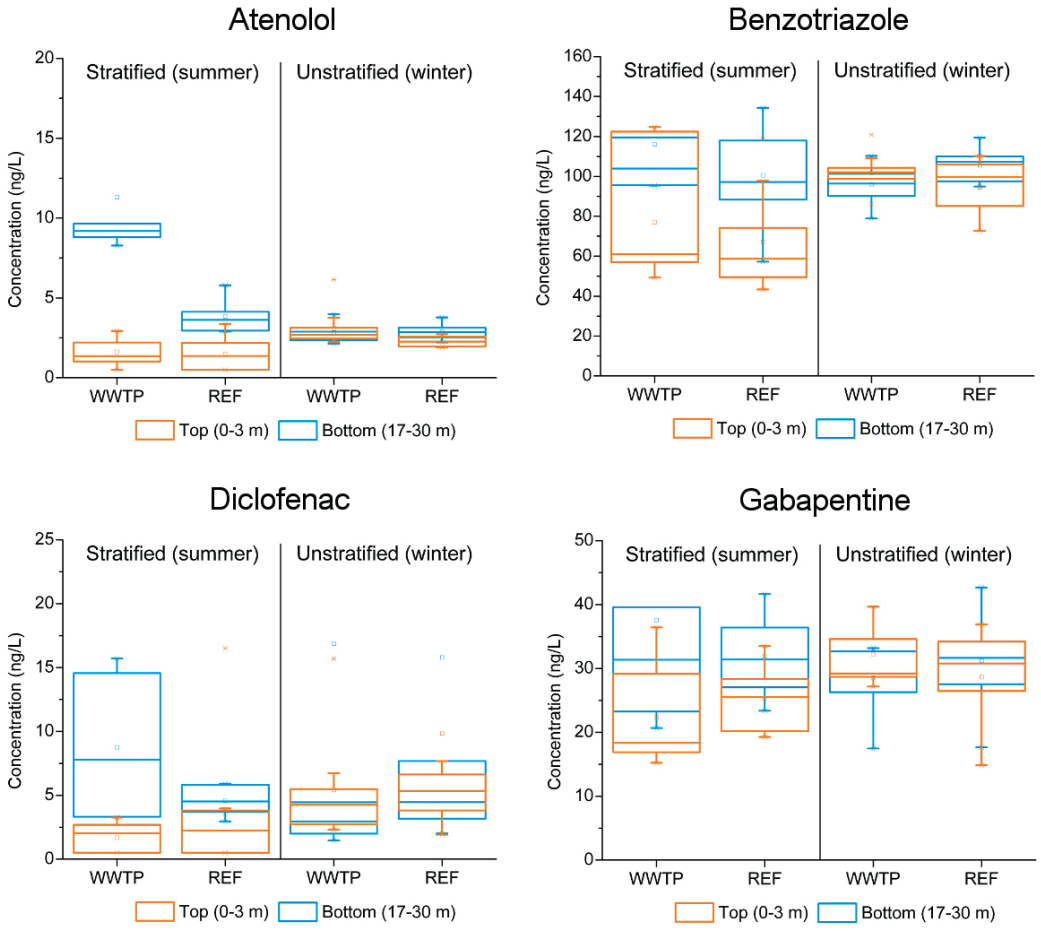

Figure 3.8: *Range of concentrations measured at WWTP outfall and the reference points during the 2010 sampling campaign in the near-surface (0–3 m, orange box) and near-bottom (17–30 m, blue box) layers of the Bay in stratified (June–August) and unstratified (November–January) conditions. Boxes represent the 25^{th} percentile, mean and 75^{th} percentile. The whiskers are determined by the 5^{th} and 95^{th} percentiles.*

3.4 Conclusions

This work illustrates the importance of photolysis as well as the key factors affecting the fate of organic contaminants in aquatic environments; namely solar irradiance (influencing photolysis rates and lake stratification), water absorbance (influencing photolysis kinetics) and mixing processes (influencing relative distance of the contaminant from the surface). These factors were also found crucial in determining the extent of the WW plume in Vidy Bay.

Similarly, past research in UK and US rivers found that direct photolysis significantly reduced the predicted environment concentrations of the beta-blocker propranolol in the water phase[116]. The highest reductions were predicted in summer, for long rivers with low turbidity and low flow conditions. Likewise, direct photolysis was also identified as the main elimination process of diclofenac and triclosan in a small Swiss lake[117,138]. In the latter study, Tixier et al. successfully matched field data with (2D) modeled concentrations in the water column of the lake. Photolysis was found to take place only in the upmost 50 cm of this particular lake, where 95% of sunlight is absorbed[138].

In the field of environmental risk assessment of organic micropollutants, models are increasingly used to overcome the limitations of sampling or as complimentary information to augment punctual environmental measurements. The coupled hydrodynamic-photolysis model allowed for the identification of critical scenarios. Simulations show that owing to the thermal stratification, the zone of ecotoxicological risk is largest in summer and extends horizontally over 300 m from the WW outfall. Finally, modeling the ecotoxicological risk helped to pin-point priority substances which contribute significantly to increasing the zone of potential adverse effects. Several antibiotics showed an important contribution to the total ecotoxicological risk. Antibiotics thus exhibit a dual problematic role in the environment: not only do they cause the well-acknowledged problematic of promoting antibiotic resistance, but they are also among the most relevant compounds with respect to detrimental ecotoxicological effects. Clearly, these are the substances that should be the focus of future monitoring campaigns and pollution mitigation strategies.

4 Pharmaceuticals and their human metabolites in Lake Geneva: occurrence, fate and ecotoxicological relevance

4.1 Introduction

4.1.1 Micropollutants in the aquatic environment

Over the past two decades, an increasing number of studies have documented the presence of low concentrations (ng·L^{-1} range) of various anthropogenic organic substances, or micropollutants, in surface and groundwaters [1,10,14,154,155]. Anthropogenic micropollutants include pharmaceuticals, personal care products, pesticides, xenoestrogens, biocides and other substances of human origin. These substances can enter the aquatic environment via runoff from agriculture and urban landscapes, atmospheric deposition, and industrial and municipal wastewater streams. Despite the abundance of occurrence data, less is known about the fate of micropollutants once they reach the environment. Main degradation pathways in surface waters are believed to include photolytic degradation or biodegradation [75,156], but knowledge of the corresponding transformation rates and products is incomplete. Information is even scarcer regarding the effects that these individual substances or their mixtures exert on the ecosystem. Some studies report shifts in microbial populations [157], feminization of fish [158] or of frogs [159]. However, much remains to be understood regarding the mechanisms of action underlying these effects. As such, micropollutants in the environment have emerged as one of the preeminent research fields in water quality.

A modified version of this chapter was published as: *F. Bonvin, R. Rutler, N. Chevre and T. Kohn, Archives des Sciences, vol. 65, 2012*

4.1.2 Micropollutants in Lake Geneva

In Europe, approximately 50 new substances are authorized for use in commercial and industrial markets every year, adding to the 100'000 of compounds already in use[160]. Through point-source and disperse pollution sources, many of these compounds are expected to enter rivers and lakes. In Lake Geneva, a large selection of micropollutants has effectively been detected on a regular basis throughout the water column, within the framework of the International Commission for the Protection of Lake Geneva[161–163], as well as in other studies[24,140]. The range of detected compounds includes a suite of pesticides and biocides, several classes of pharmaceuticals, X-ray contrast media, corrosion inhibitors and endocrine disruptors. Pesticides mainly originated from diffuse sources, such as runoff from land. The presence of some pharmaceuticals could be related to industrial discharge into the Rhône River, the main tributary of Lake Geneva. However, most pharmaceuticals, corrosion inhibitors and selected biocides were found to be associated with wastewater discharge into the lake. Recent work has shown that during the summer stratification period of the lake, the discharged wastewater does not readily mix with the surrounding water column, but instead forms a plume of significant spatial extent below the thermocline[140]. Within this plume, the concentrations of several micropollutants exceeded the predicted no-effect concentrations (PNEC), indicating a potential ecotoxicological risk to the environment. Thus, the practice of direct discharge of wastewater into the lake is of particular concern with respect to ecotoxicological effects of micropollutants.

4.1.3 Pharmaceuticals and their human metabolites

Among the different micropollutant classes detected in Lake Geneva and worldwide, pharmaceuticals are of exceptional interest. Because they are designed to fulfill a specific biological function, they are prone to exert undesired biological effects in the environment. In particular antibiotics have been a priority, as they may not only exert ecotoxicologial effects, but may also promote antibiotic resistance in the environment[56].

An important route of pharmaceuticals into the environment is the ingestion by humans and subsequent excretion into the sewage system[4]. After intake by humans, pharmaceuticals are metabolized to various extents. Thus, a variable fraction of the active pharmaceutical, along with its metabolites, is released via urine and feces into raw wastewater. Due to incomplete removal during wastewater treatment[18], many pharmaceuticals are ultimately discharged into receiving waters. Therefore, centralized sewage treatment plants represent an important point source for pharmaceuticals and their metabolites into the aquatic environment.

The presence of metabolites in the environment has received little attention to date. Nevertheless, available data shows that metabolites are present in wastewater effluent in concentrations comparable to or higher than their parent compound[27–31,33,164].

Leclercq et al. found 2–5 times higher concentrations of the main metabolite of carbamazepine (10,11-dihydro-10,11-trans-dihydroxycarbamazepine) in wastewater of three different treatment plants, in addition to other metabolites of this antiepileptic drug[25]. Hilton reported high concentrations of N4-acetylsulfamethoxazole, a metabolite of sulfamethoxazole, in treated sewage[26]. Human metabolites were not only detected in wastewaters, but also in the receiving environment, though data remains scarce. Trace concentrations of human metabolites were found in streams receiving wastewater effluent, in drinking water (the main metabolite of carbamazepine) and even in bottled water[29,30].

Human metabolites of pharmaceuticals are generally more polar and less biologically active than their parent substance, though some metabolites are known to retain biological function[165,166]. Furthermore, human metabolites have been found to back-transform to the parent substance via both biotic[167] and abiotic processes[168,169]. Human metabolites could thus present a source of pharmaceuticals to the environment. Finally, despite their increased polarity, some human metabolites have been found to be more persistent to typical environmental degradation processes, such as photolysis, compared to their parent substance[168,170]. Combined, these arguments make a compelling case that human metabolites should be included in the study of presence, fate and effects of micropollutants.

The goal of this study was to determine the presence of a selection of human metabolites in Lake Geneva, to assess their fate with respect to degradation over time and space, and to evaluate their contribution to the overall ecotoxicological risk. We have focused our work on the Vidy Bay, as this area was found to exhibit high micropollutant concentrations, likely due to the discharge of effluent wastewater from the Vidy treatment plant.In the present study, we focus on the human metabolites of a selection of pharmaceuticals. Specifically, we investigated human metabolites of three antibiotics (clarithromycin, norfloxacin and sulfamethoxazole), one analgesic (diclofenac) and an anti-epileptic (carbamazepine). The spatio-temporal distribution of the parent compounds was already examined in a previous study; the first four were found to originate primarily from wastewater effluent, and were previously reported in concentrations close to or beyond the PNEC. Conversely, carbamazepine, though also present in wastewater effluent, mainly enters the lake from industrial inputs into the Rhône River.

4.2 Materials and Methods

4.2.1 Site description and sampling strategy

The study area, Vidy Bay, lies on the northern shore of Lake Geneva, and represents 0.3% of the lake's total volume (Figure 4.1) [129]. Aside from lake currents, 100'000 m^3 of wastewater effluent are discharged per day into Vidy Bay from Lausanne's wastewater treatment plant (WWTP). The WWTP outfall is located 700 m from shore at -30 m depth. During rain events the WWTP capacity is rapidly exceeded, and untreated wastewater is released directly into the lake [130]. Other sources of water to the Bay are the Chamberonne River and the Flon stormwater outlet.

Monthly water samples were collected at various depths and locations in Vidy Bay between April 2010 and January 2011, as described in an earlier publication [140]. The central sampling location ("WWTP outfall") was above the discharge point of the effluent wastewater. The two other sampling sites were located ca. 1.5 km upstream ("REF-up") and downstream ("REF-down") of the discharge point (Figure 4.1). They will be considered together and referred to as reference sites or REF. Between 5 and 9 depths were sampled at each site. Samples were taken from the R/V "La Licorne" (Forel Institut, Geneva) equipped with a crane and a rosetta water sampler (1018 Rosette Sampling System, General Oceanics Inc.). The rosetta consisted of 11 Niskin bottles (1.7 L), coupled to a CTD device (OCEAN SEVEN 316Plus CTD, IDRONAUT Srl) which were externally powered via a sea cable and yielded instantaneous information on temperature and electrical conductivity. Temperature and electrical conductivity were processed with REDAS-5 Release 5.40 (IDRONAUT Srl).

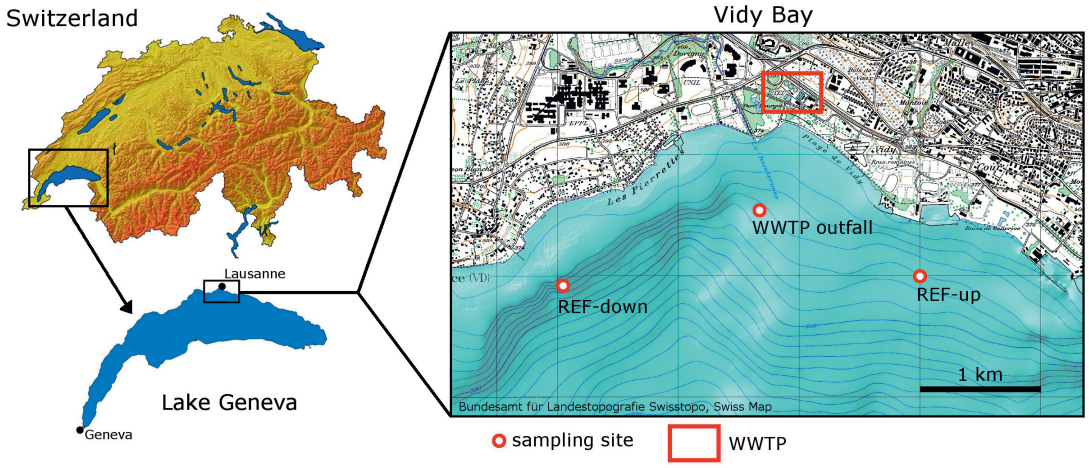

Figure 4.1: *Situation and map of the Vidy Bay showing the sampling locations WWTP outfall (Swiss coordinates : 534'672/ 151'540), REF-up (Swiss coordinates : 536'000/151'000) and REF down (Swiss coordinates : 533'048/150'920). Coordinates are in Swiss Grid system with datum CH1903.*

4.2.2 Choice of substances

Previous research in Vidy Bay retained a selection of 27 pharmaceuticals as priority pollutants for this area based on consumption loads, the degree of human metabolism, removal in the WWTP, previous detection in the Vidy bay, and – if known – ecotoxicological relevance[2,140].

A subset of these chemicals, namely carbamazepine (CBZ), clarithromycin (CLA), diclofenac (DCF), norfloxacin (NOR) and sulfamethoxazole (SMX), were chosen herein for analysis of their human metabolites. Deciding factors included their ecotoxicological impact in Vidy Bay, the commercial availability of their metabolites, and previous evidence for their presence in wastewater or surface waters in literature. The targeted metabolites included: trans-10,11-dihydro-10,11-dihydroxy carbamazepine (DiOH-CBZ), carbamazepine 10,11-epoxide (epoxy-CBZ), 10,11-dihydro-10-hydroxy carbamazepine glucuronide (DiOH-CBZ-glu), N-desmethyl clarithromycin (desm-CLA), 4'-hydroxy diclofenac (4-OH-DCF), N-acetyl norfloxacin (acetyl-NOR), sulfmethoxazole β-D glucuronide (SMX-glu) and N-acetyl sulfamethoxazole (acetyl-SMX). The structures of the selected micropollutants and their corresponding human metabolites are shown in Figure 4.2.

4.2.3 Chemicals and reagents

Most human metabolites were purchased from Toronto Research Chemicals (Canada). N-acetyl sulfamethoxazole was obtained from CHEMOS GmbH (Germany), and carbamazepine 10,11-epoxide from Sigma Aldrich (Switzerland). Other chemicals and reagents used in the analytical procedure have been listed previously[24].

4.2.4 Sample manipulation

1 L water samples were collected in Niskin bottles and transferred into amber glass bottles, immediately acidified to pH 2 with concentrated HCl to inhibit biological activity, and transported to the laboratory within 4 hours of sampling, where they were directly filtered through > 1 μm glass fiber filters (Whatman). Before further treatment, all filtrates were spiked with a set of deuterated standards (final concentration 120 ng·L^{-1}) to account for losses of the parent compound during extraction, as described previously[24]. As deuterated standards of the metabolites were not available for spiking at the time of sampling, their losses during extraction were determined in experiments using spiked lake water, as described in the following paragraph. All glassware used for samples was immersed for 24 h in a Contrad bath, machine-washed and finally rinsed with methanol and sample water before use

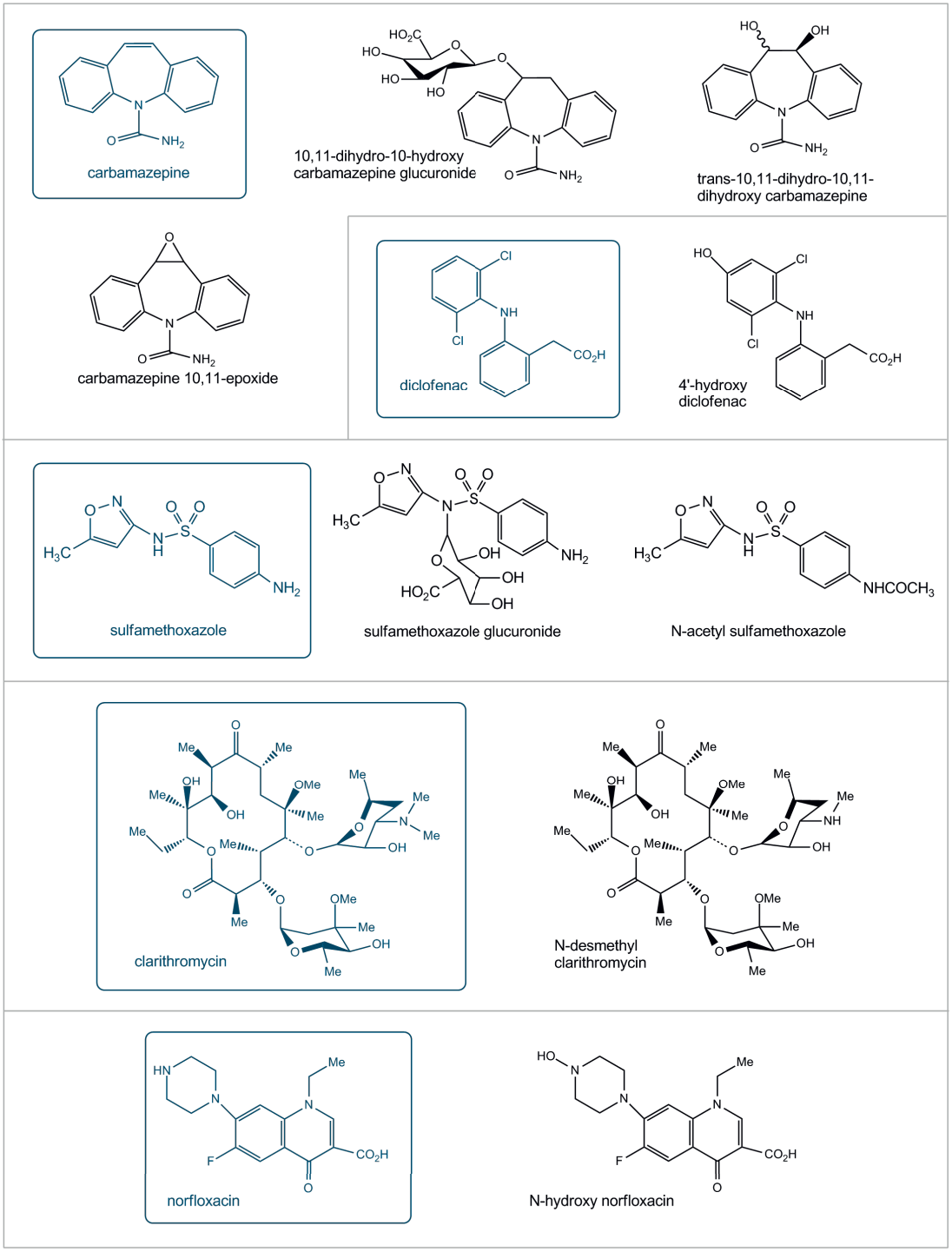

Figure 4.2: *Structures of the targeted pharmaceuticals (blue box) and their selected human metabolites.*

4.2.5 Analytical method

The concentrations of the parent compounds in lake water samples were analyzed following a previously developed analytical method involving solid-phase extraction (SPE) and ultra-performance liquid chromatography coupled to a tandem mass spectrometer (UPLC-MS/MS)[24,140]. Additionally, an analytical method for the detection of human metabolites was developed. Briefly, the target compounds were extracted on hand-assembled 6mL cartridges using an automated SPE system, eluted and evaporated, under a flux of nitrogen, at 40°C, to 200 μL and finally stored at -20°C until UPLC-MS/MS analysis. Analytical details regarding the determination of the parent compound concentration have been described previously[140]. For analysis of targeted metabolites, the stored extracts were diluted 1:6 with UPLC eluent (A) and analyzed twice by UPLC-MS/MS. Reported values represent the average of the two separate measurements. Compounds were separated on a Waters ACQUITY UPLC HSS T3 1.8 μm column. The mobile phases were (A) 95% H_2O; 5% MeOH; 1% formic acid; 5 mM ammonium formate and (B) 95% MeOH; 5% H_2O; 1% formic acid; 5 mM ammonium formate. The first minute the fraction of mobile phase A decreased from 90 to 60%, followed by a linear gradient for 7 min to 5% A. Thereafter the initial conditions were restored and held for 3 minutes. The injection volume was 10 μL, and the flow rate 0.3 mL·min^{-1}. UPLC-MS/MS parameters for our selection of human metabolites are listed in Table 4.1; a positive ionization potential (ESI-mode) was applied for all compounds. A set of 10 to 13 standards with concentrations between 1 and 700 μg·L^{-1} were analyzed in duplicate along with the samples. The analytical limit of quantification (LOQ; Table 4.1) was defined as the concentration of the lowest standard with a signal-to-noise ratio > 10.

Table 4.1: *Details of the analytical method for MS/MS analysis of targeted human metabolites and PNEC used in risk assessment.*

Name	Precursor ion [*m/z*]	Fragment ions [*m/z*]	Cone [V]	Collision [V]	Retention time [min]	LOQ[1] [ng/L]	Extraction efficiency	PNEC[2] [ng/L]
epoxy-CBZ	253.27	167.15	22	36	3.8	<1	0.3 ± 0.08	2500
		179.7	22	22				
DiOH-CBZ	271.33	210.18	22	14	3.5	<1	1.8 ± 0.23	2500
		236.18	22	12				
acetyl-SMX	296.22	65.01	34	36	3.1	<1	1.39 ± 0.19	28
		134.12	34	28				
4-OH-DCF	312.22	230.14	20	36	6.1	1.1	1.12 ± 0.19	100
		266.15	20	12				
acetyl-NOR	362.43	231.15	58	38	4.6	<1	0.7 ± 0.08	40100
		274.24	54	34				
SMX-glu	430.3	156.08	26	30	2.1	1	0.99 ± 0.11	28
		254.16	26	14				
DiOH-CBZ-glu	431.29	194.18	24	34	3.3	19	n.d.	2500
		237.14	24	12				
desm-CLA	734.8	83.14	30	54	6.3	<1	0.62 ± 0.04	60
		144.18	30	24				

[1] LOQ: limit of quantification

[2] PNEC (predicted no-effect concentration). PNEC of the corresponding parent compound was used for human metabolite PNEC (see text for details).

Human metabolite concentrations in the sample concentrates were calculated based on calibration curves using at least 6 calibration points closest to the sample concentration. Correlation coefficients for the calibration curves were typically > 0.990. Extraction recoveries (Table 4.1) and repeatability were determined by a method reproducibility test, in which 6 replicates of lake water spiked with all metabolites to 50 ng·L^{-1} were processed by the entire sample workup procedure. The concentrations in the original lake water samples were determined taking into account the extraction efficiencies determined by this test. The reproducibility of the entire method was high, resulting in a relative standard deviation of less than 25% of the calculated concentration.

4.2.6 Risk assessment

For a single compound i, the risk for aquatic organisms is normally evaluated by comparing the measured environmental concentration (MEC) in the aquatic system under consideration to either the predicted no-effect concentration (PNEC[68]) or the hazardous concentration (HC[171]). In this study, we calculated the risk based on the PNEC, as not enough data was available for the compounds under consideration to determine a HC The ratio of MEC_i to $PNEC_i$ (RQ_i, equation 4.1) must be smaller than one to ensure that a given chemical i presents an acceptable risk to the environment.

$$RQ_i = \frac{MEC_i}{PNEC_i} < 1 \tag{4.1}$$

For mixtures of compounds exhibiting a similar mode of action, the mixture effect can be predicted by the concept of concentration addition (CA)[171]. As no ecotoxicological information was available for the metabolites, we assumed that the mode of action of a metabolite is similar to that of its parent compound, and therefore defined the PNEC of metabolites as equivalent to the PNEC of the parent compound. This assumption will be discussed in the Results and Discussion section. The risk quotient for mixtures (RQ_m) of a parent compound and its metabolites thus corresponds to the sum of the individual RQ_i (Equation 4.2). The RQ_m must remain smaller than one to ensure that a mixture of chemicals presents an acceptable risk to the environment:

$$RQ_m = \sum_{i=1}^{n} RQ_i = \sum_{i=1}^{n} \frac{MEC_i}{PNEC_i} < 1 \tag{4.2}$$

PNECs of the individual parent compounds (and hence of their metabolites; Table 4.1) that were used to calculate RQ have been determined in a previous study ([140] and references therein).

4.3 Results and discussion

4.3.1 Occurrence of human metabolites in Lake Geneva

Over 140 lake water samples were analyzed for the presence of five pharmaceuticals along with a selection of their human metabolites. The frequency of detection and the observed concentrations varied with time and compound. Two metabolites, namely CBZ-glucuronide and N-acetyl NOR, were never detected over the entire sampling period. SMX-glucuronide and 4-OH-DCF showed a relatively low overall frequency of detection of 9 and 21% respectively. These compounds were mainly detected at the WWTP outfall sampling site. Higher frequencies of detection were observed for DiOH-CBZ, desm-CLA, acetyl-SMX and epoxy-CBZ, which were detected in 96, 89, 50 and 43% of all samples, respectively. Some difficulties were encountered with the detection of epoxy-CBZ which was unstable during analysis; thus the reported detection frequencies and concentrations for this compound may underestimate the actual occurrence.

Generally, the detected concentrations of human metabolites were in the same range or below those of their parent compound (Figure 4.3). The absolute range of concentrations was compound specific: CBZ and its metabolite epoxy-CBZ showed the highest concentrations with a median of 20 $ng{\cdot}L^{-1}$. The concentrations of all the other compounds and metabolites were generally below 10 $ng{\cdot}L^{-1}$. In a few samples, namely those obtained in close vicinity to the wastewater outfall, significantly higher concentrations of up to > 100 $ng{\cdot}L^{-1}$ were detected.

Though numerous human metabolites have been identified for CBZ, the major metabolic route involves transformation to epoxy-CBZ, which is subsequently hydrated to DiOH-CBZ. In addition, DiOH-CBZ can be conjugated with a glucuronide. Therefore DiOH-CBZ and the corresponding glucuronide are the main metabolites of CBZ[172]. Several studies have effectively detected DiOH-CBZ in influent and effluent wastewater samples, as well as in surface waters in concentrations up to three times those of the parent compound CBZ[25,28,173]. Conversely, the present study found significantly lower concentrations of DiOH-CBZ than its parent. This was attributed to the industrial sources of CBZ to Lake Geneva[140], which maintain relatively high and stable concentrations of the parent compound throughout the water column. Accordingly, significant differences of detected concentrations were observed between the WWTP outfall and the reference point only for the human metabolites and not CBZ. The other major metabolite, CBZ-glucuronide has never been reported to date in environmental samples, however there is evidence for cleavage of the glucuronide acid moiety in wastewater treatment plants ([25] and references therein). The CBZ-glucuronide standard was highly unstable in aqueous and organic solutions; hence its absence in lake water samples is not surprising.

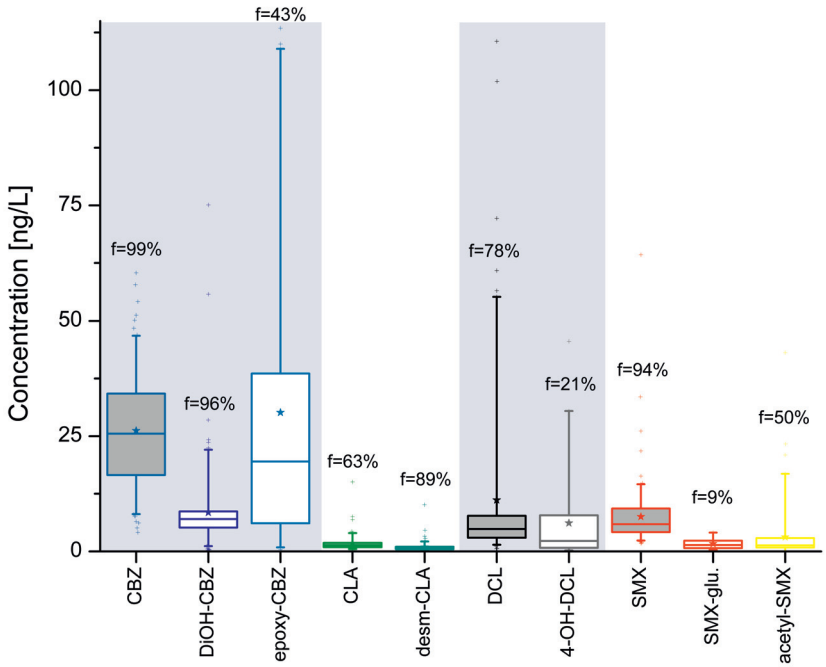

Figure 4.3: *Range of concentrations detected at all sampling sites over the entire sampling period of the parent compounds (shaded box) and their corresponding human metabolites. The frequency of detection (f) is given for each compound. Boxes represent 25th percentile, median and 75th percentile. The whiskers are determined by the 5th and 95th percentiles. Stars show the mean value.*

Concentrations of clarithromycin were relatively low (<5 ng·L^{-1}) and corresponding metabolite concentrations were significantly lower. Though the desmethylated metabolite of clarithromycin was detected in many samples, the detected concentrations were frequently below the limit of quantification. To our knowledge, this is the first report of the occurrence of a human metabolite of clarithromycin in wastewater or surface water samples.

Up to 50% of ingested diclofenac is excreted as the hydroxylated metabolite 4-OH-DCF and its corresponding glucuronide, while less than 10% remains unaltered [174]. Thus the presence of the major metabolites in untreated sewage is to be expected. Indeed, various studies have found 4-OH-DCF in both influent and effluent wastewater, with only partial removal (<50%) via various wastewater treatment processes [32,33]. The concentrations were sometimes as elevated as those of the parent compound in effluent samples. Averaged over all samples (Figure 4.3), the present study found similar concentration ranges of 4-OH-DCF and its parent in the Vidy Bay. More detailed analysis of individual sample concentrations, however, show generally higher concentrations of the metabolite above the WWTP outfall, whereas the inverse is observed at the reference sites.

Approximately 14% of ingested sulfamethoxazole is excreted unchanged; the remaining fraction is metabolized mainly to acetyl-SMX (47%) and SMX-glucuronide (10%) [175]. Acetyl-SMX has been detected in wastewater effluent [27] as well as surface waters at concentrations

comparable to its parent compound[121]. For SMX-glucuronide, in contrast, this is the first evidence of its occurrence in surface waters. Its low frequency of detection (15%) was expected given the unstable nature of the glucuronide bond, which can be microbially cleaved[167]. The overall concentrations of acetyl-SMX detected in this study were significantly lower than those of SMX. As for DCF, however, a sample-by-sample analysis revealed that in samples taken above the WWTP outfall, the metabolite concentration was significantly higher than that of the parent compound.

4.3.2 Peak metabolite concentrations in wastewater plume

The presence of a wastewater plume originating from the direct discharge of treated (and during high rain events, also untreated) wastewater into the Vidy Bay was reported in a recent study[140]. Locally high concentrations of pharmaceuticals were observed above the WWTP outfall site. The plume depth followed the thermocline during thermal lake stratification, which moved to lower depths over the course of the warm seasons. Additionally, a strong linear correlation between electrical conductivity and concentrations of wastewater-derived micropollutants was identified. In absence of thermal stratification, from November to January, no plume was observed.

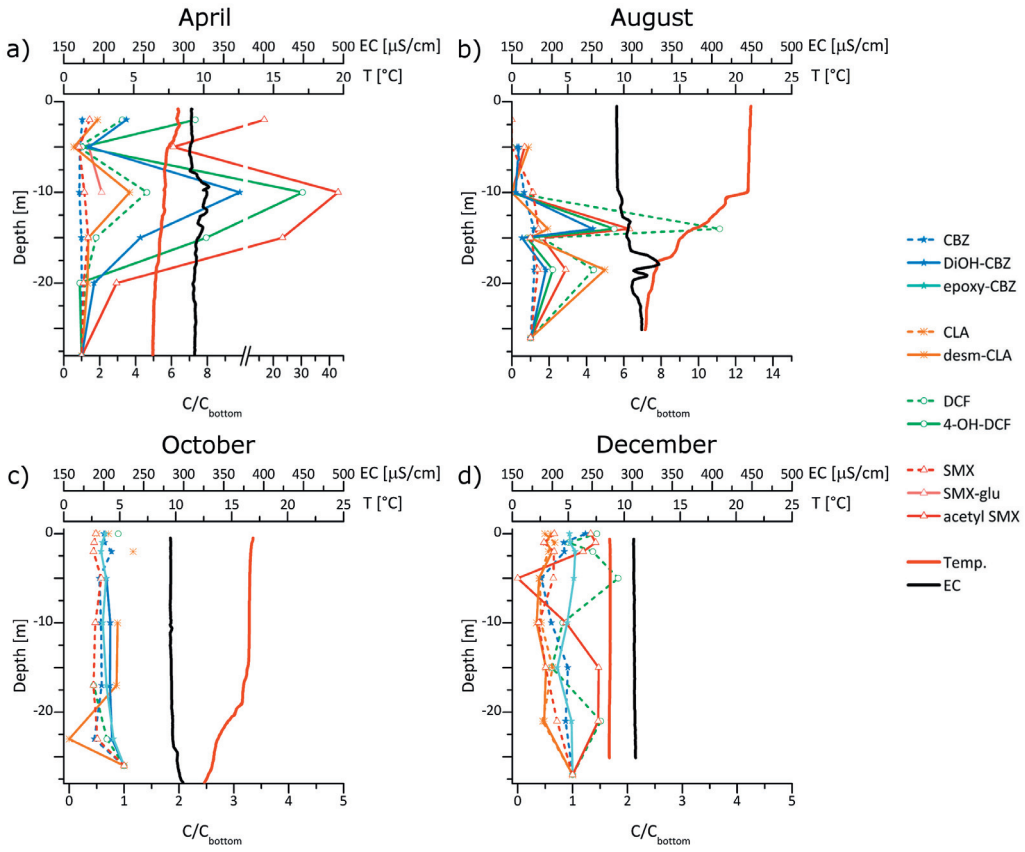

Figure 4.4: *Depth profiles of relative concentrations of the targeted human metabolites (full lines) and their corresponding parent compound (dashed lines) for a) April, b) August, c) October and d) December 2010. Temp: temperature; EC: electrical conductivity.*

The presence of human metabolites of pharmaceuticals in wastewater has been well-established[25,27,32]; hence the latter should logically show the plume feature. Indeed, notably higher concentrations of our targeted human metabolites were observed in vicinity to the WWTP outfall in April (Figure 4.4 a) and August (Figure 4.4 b). These high concentrations coincided with an elevated conductivity, which is indicative of wastewater. A slight plume feature could still be observed at -26 m depth in October (Figure 4.4 c); whereas homogenous concentrations are established in December (Figure 4.4 d) when complete mixing of the water column was restored. In general, the relative peak concentrations of the metabolites were more pronounced than their associated precursor. This could either be due to faster degradation of the metabolite with regard to its parent, or to high background concentrations of the parent, which may diminish the peak amplitude. For example, carbamazepine, which enters the lake with the Rhône River, showed little to no peak feature in the wastewater plume. Conversely, its human metabolite, DiOH-CBZ, showed evident concentration peaks above the WWTP outfall, in accordance with the hypothesis that its main source is wastewater.

The unstable nature of SMX-glucuronide mentioned earlier was confirmed by a low detection frequency in the water column. However, it was detected in the plume in April and August, as well as in other months (not shown), displaying a strong plume feature.

4.3.3 Spatio-temporal variations of metabolite concentrations in Vidy Bay

During thermal stratification, the locally high concentrations of human metabolites associated with the wastewater plume led to notably elevated median concentrations at the WWTP outfall site (Figure 4.5). Additionally, the 25-75% quantile ranges were large due to this plume feature. Conversely, after mixing of the wastewater with the surrounding water mass and travel to the reference sites, the water column concentrations of the targeted human metabolites were lower and more homogeneous. These homogeneous conditions, depicted by a narrow 25-75% quantile range in figure 4.5, were also observed during the cold months (November to January) at the WWTP outfall site. This can be explained by enhanced mixing throughout the water column, as temperature profiles straighten during the winter. Generally, metabolite concentration trends at the reference sites closely tracked those of the wastewater plume. Among the metabolites considered, only acetyl-SMX exhibited noticeable concentration differences at the reference sites between the warm and cold seasons, consistent with the higher concentrations in the plume during the same period. Notably, however, all metabolites appeared to decrease in concentration during the month of August.

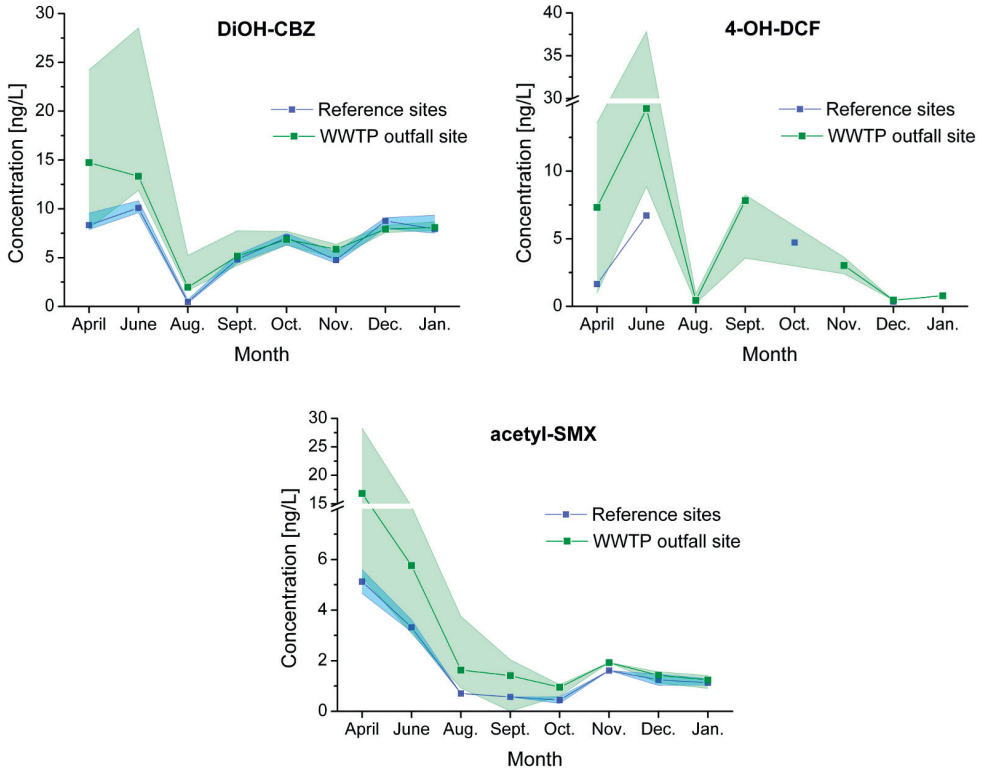

Figure 4.5: *Temporal and spatial variation of detected concentrations of DiOH-CBZ (left), 4-OH-DCF (middle) and acetyl-SMX (right). The solid line shows the median concentration and shaded area the 25-75% quantile range.*

4.3.4 Degradation within the Vidy Bay

After discharge from the WWTP, and upon dispersion of the wastewater plume, wastewater-derived micropollutant concentrations decrease with distance from the WWTP outlet due to dilution with surrounding water masses. In addition, environmental degradation processes, such as biodegradation or photolysis, can decrease micropollutant concentrations in the water column. The substances studied herein have previously been reported to undergo various extents of degradation in the Vidy Bay[24,140]: The concentrations of CLA and DCF were found to readily diminish, whereas SMX was more recalcitrant. As CBZ's main source was not the WWTP, no apparent decrease in concentration was found throughout the Vidy Bay. Furthermore, CBZ is known to be particularly recalcitrant to environmental degradation[117].

Compared to their parent compounds, human metabolites may be more susceptible to environmental degradation processes. For example, in a laboratory batch reactor, 4-OH-DCF was found more susceptible to biodegradation than its parent[32]. However, incomplete removal of this compound during wastewater treatment[32,33] indicates that biodegradation proceeds at a slow rate. Furthermore, both acetyl-SMX and SMX-glucuronide were reported to undergo biodegradation back to SMX during wastewater treatment[35] and in sediment tests[167].

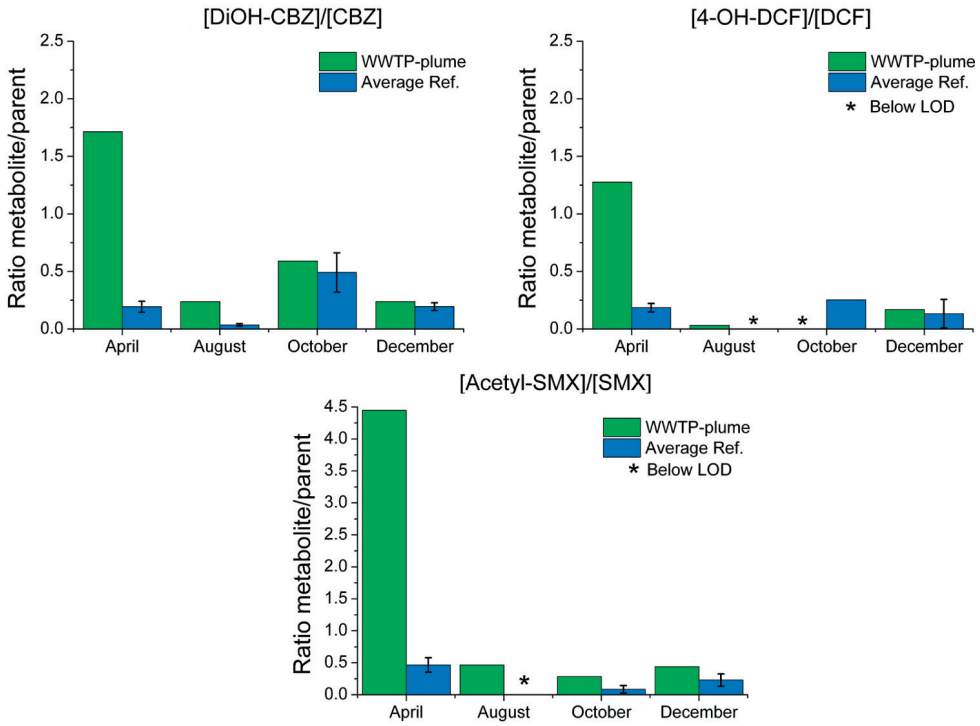

Figure 4.6: *Seasonal and spatial (WWTP-plume vs reference sites) variation of the metabolite/parent compound ratio.*

Finally, SMX-glucuronide has recently been found to be more photolabile than SMX, whereas acetyl-SMX was slightly more photostable [168].

To assess if human metabolites undergo environmental degradation in the Vidy Bay, and to determine the relative extent of degradation compared to the parent substance, we calculated the ratio of metabolite/parent concentration close to the wastewater outfall, as well as at the reference points located 1.5 km up- or downstream (Figure 4.6). Both metabolites and parents are equally affected by dilution; consequently, the difference in ratio between the wastewater discharge and the reference indicates the relative propensity of the metabolite to undergo environmental degradation during passage through the Vidy Bay. This analysis could only be conducted for those substances for which both parent and metabolites concentrations were detected at a high frequency.

As can be seen in figure 4.6, the metabolite/parent ratio was generally greater for samples taken near the wastewater outlet than in the corresponding reference samples. The difference was most drastic in April, where the wastewater sample captured a particularly pronounced plume feature, and thus consisted of poorly diluted wastewater (Figure 4.4). Correspondingly, metabolites were present at concentrations up to 4.5-fold greater than their parent compound, consistent with the notion that pharmaceuticals are mainly excreted into sewage in their metabolized form. In both April and August, the metabolite/parent ratio dropped off steeply between the plume and the reference points, indicating that metabolites underwent more rapid environmental degradation than their parent compounds.

During the months of October and December, the difference in ratio was less pronounced. This could be due to enhanced mixing of the discharged wastewater with the surrounding water column during the colder months (Figure 4.4). Furthermore, both biodegradation and photolysis processes are less efficient in fall and winter. Compared to dilution, the degradation of metabolites may thus play a smaller role during the cold period.

Overall, it can be stated that the metabolites considered herein are less recalcitrant in the environment than their parent compounds. As it is not fully clarified which products are formed during environmental degradation, however, it cannot be concluded that metabolites therefore are of lesser ecotoxicological concern. In particular for those metabolites which can be back-transformed to their parent compound, environmental degradation may lead to an increase in ecotoxicological risk.

4.3.5 Ecotoxicological risk assessment

Given the presence of metabolites in Lake Geneva, the important question arises whether these compounds are of ecotoxicologial relevance. Explicitly, our final goal was to determine if metabolites make a significant contribution to the ecotoxicological risk presented by the parent compounds. As was determined previously, DCF and SMX both presented an ecotoxicological risk (i.e., RQ > 1) in several plume samples[140]. In contrast, the detected concentrations of CLA and CBZ were always below the corresponding PNEC.

Even if metabolites are taken into account, a negligible risk is estimated for all mixtures of parent compound and metabolites at the reference point (Figure 4.7, right). At the plume, however, a risk is highlighted for DCF and metabolites in June and for SMX and metabolites in April and June (Figure 4.7, left). Taking into account metabolites leads to both a more frequent excess of the RQ of 1, as well as to higher overall RQs. For SMX, the RQ reaches a value of 3.3 in June, compared to 2.4 taking into account only the parent compound, suggesting that this pharmaceutical may be of environmental concern. Similarly, for DCF in June, the RQ only exceeded 1 if metabolites were considered, whereas it amounted to 0.56 for the parent alone.

Similarly, other studies have reported that the combination of several xenoestrogens led to ecotoxicological effects, even if each individual compound was present at no effect concentrations[176]. This highlights the importance of taking into account not only individual substances, but classes of compounds with the same mechanisms of action.

To our knowledge, no ecotoxicological information is available to date on human metabolites of pharmaceuticals; therefore it is not possible to determine accurate PNECs. In this study, we therefore assumed the PNEC of the metabolites to be similar to those of the parent compound. This assumption is supported by the study of Boxall et al.[170], who showed that 81% of the degradates are less or similarly toxic as the parent compound. However, one has to note that 19% of the metabolites are more toxic that the parent compound. We can therefore not exclude that we underestimated the toxicity of any given metabolite.

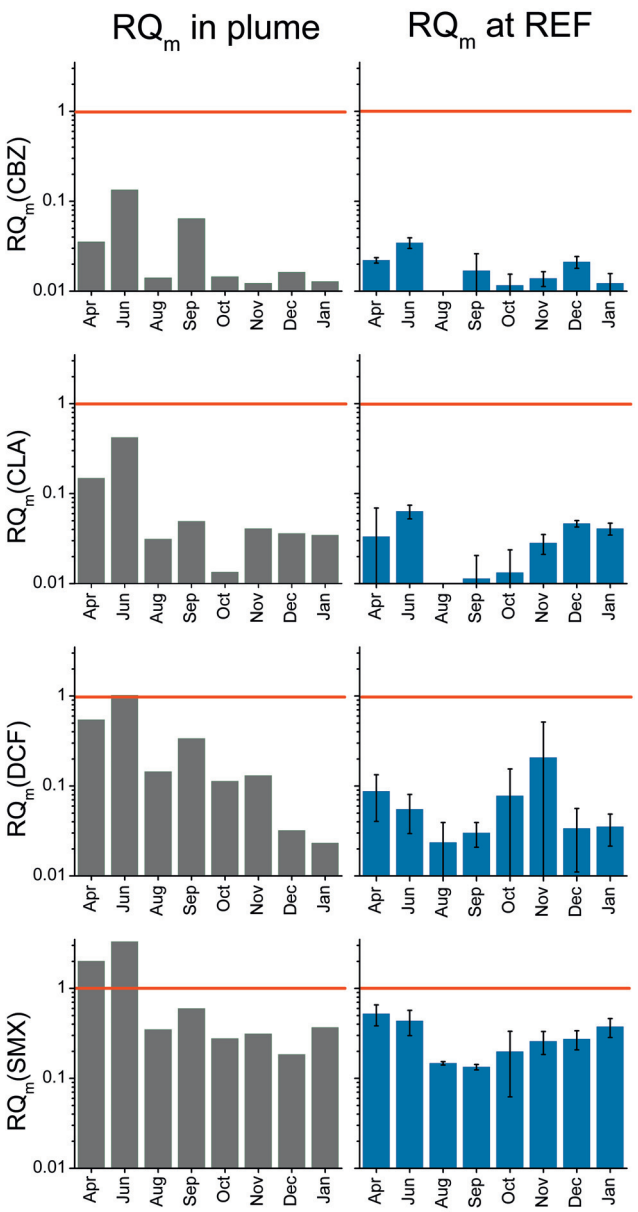

Figure 4.7: *Time course of mixture risk quotient (RQ_m) for the sum of pharmaceuticals carbamazepine (CBZ), clarithromycin (CLA), diclofenac (DCF) and sulfamethoxazole (SMX) and their associated metabolites for concentrations detected in the plume (left) and average water column concentrations detected at REF down (right). RQ > 1 (red line) indicates a potential ecotoxicological risk.*

Furthermore, by applying the concentration addition model we assumed that the metabolites have the same mode of action as the parent compound. To our knowledge, this was never evaluated in environmental organisms. From a pharmacological point of view, i.e. in humans, this assumption is correct for many, but not all metabolites. For example, the mode of action of 4-hydroxy-tamoxifen is similar to its parent compound, the anti-cancer drug tamoxifen[177]. In contrast, another metabolite of tamoxifen, endoxifen, has a different mode of action[177]. Furthermore, even in humans, the mode of action of pharmaceuticals and metabolites are not always well understood. The CA approach applied in this study is therefore used as a worst case scenario, as proposed by Backhaus et al.[171], when the mode of action of the chemicals in a mixture are not known.

4.4 Conclusion

Over a period of 10-months, the concentrations of five environmentally relevant pharmaceuticals and eight of their human metabolites were monitored at several locations and depths in Lake Geneva's Vidy Bay. Among the targeted metabolites, six were detected with variable frequency in the lake water samples. The highest concentrations were detected above the WWTP outfall, supporting the assumption that wastewater effluent represents the main source of human metabolites to the lake. The concentration profiles at the WWTP discharge location displayed a plume-like feature corresponding to the wastewater plume. On average, the detected concentrations of human metabolites were similar to, or lower than, their associated parent compound. Moreover, the metabolites targeted in this study were found to be less recalcitrant to typical environmental degradation processes than their parent. Nevertheless, their presence in the aquatic environment may still lead to an increase of the ecotoxicological risk. Assuming a worst-case scenario, in which pharmaceuticals and their metabolites present a similar ecotoxicological impact, we found a critical increase of the environmental risk for two compounds with their metabolites, namely SMX and DCF. The actual PNECs of human metabolites are still to be determined for a more precise evaluation of the environmental risk. However, the precautionary principle and the results of the present study underline the importance of including human metabolites of pharmaceuticals in environmental studies.

5 Direct photolysis of human metabolites of the antibiotic sulfamethoxazole: Evidence for abiotic back-transformation

5.1 Introduction

Antibiotics are now well-acknowledged contaminants of natural aquatic systems. The chronic exposure of bacteria and other aquatic organisms to trace concentrations of antibiotics raises concerns regarding their ecotoxicological effects, but also their potential to induce bacterial resistance. Among the target compounds measured, the antibiotic sulfamethoxazole (SMX) has regularly been detected in wastewaters and natural aquatic environments with median concentrations between 60 and 150 ng·L^{-1} [140,155]. Moreover, the PNEC (predicted no effect concentration) of SMX, a level which should not be surpassed to ensure an acceptable risk to the environment, has been repeatedly exceeded. The frequent detection of this antibiotic in surface waters can be explained by its extensive use in both human and veterinary medicine[35], its poor elimination in conventional wastewater treatment plants [18,24,178,179] and its relative persistence in the environment[39]. Much effort has been spent on investigating the presence and fate of SMX in the aquatic environment [155,180]. Photodegradation was identified as the major degradation pathway for SMX in surface waters[75], thus direct and indirect photodegradation kinetics of SMX have been extensively studied [74,82,102,103,107]. More recently, research interests have shifted towards identifying photolysis products of pharmaceuticals, as well as the presence and fate of their human metabolites, as both may present a risk to the aquatic ecosystem. Selected photoproducts have been shown to be more persistent than the corresponding parent compound and to retain biological activity [166,181]. Similarly, though human metabolites are generally more polar than the parent compounds, they are not always less toxic[36,175]. Only 14% of ingested SMX is excreted in its original form, yielding a large fraction of metabolites [175] (Figure 1, right panel). The most prominent metabolite is N-acetyl sulfamethoxazole (Ac-SMX), which represents 50% of the excreted administered dose.

A modified version of this chapter was published as: *F. Bonvin, J. Omlin, R. Rutler, W. B. Schweizer, P. Alaimo, T. Strathmann, K. McNeill and T. Kohn. Environmental Science & Technology, 2013.*

Other metabolites include sulfamethoxazole β–D-glucuronide (SMX-glucuronide) (9%), N-hydroxy sulfamethoxazole (OH-SMX) (2.2%), and minor fractions of 4-nitroso sulfamethoxazole (NO-SMX) and 4-nitro sulfamethoxazole (NO_2-SMX) [175].

The presence and fate of these metabolites in wastewater and receiving waters has received little scrutiny to date. NO-SMX was determined to be even more cytotoxic than SMX itself [182], but has never been reported in environmental studies. Acetyl-SMX has been detected in wastewater effluent [27] as well as surface waters at concentrations comparable to its parent compound [121]. In addition, there is evidence that Ac-SMX may be transformed back to the parent compound during wastewater treatment [35]. Biological back-transformation was also reported for both Ac-SMX and SMX-glucuronide in water sediment tests [167] Moreover, a potential abiotic back-transformation of NO_2-SMX, was recently revealed under strongly reducing conditions [169]. Photolytic back-transformation, however, has not been investigated to our knowledge.

Understanding the photochemical fate of SMX metabolites and their photoproducts is essential to fully evaluate the risk associated with SMX in the environment. Therefore, the present study aims to investigate the photolysis kinetics and products of a selection of SMX metabolites, namely the ones most abundantly found in urine [175], Ac-SMX and SMX-glucuronide, as well as OH-SMX, NO-SMX and NO_2-SMX. The possibility of photolytic back-transformation to SMX was assessed, and the influence of the small structural differences between SMX and its metabolites on photolysis rates and pathways was investigated. Finally, the influence of the photolability of metabolites on their fate and expected distribution in surface waters is discussed and compared to actual concentrations measured in Lake Geneva near a wastewater treatment plant effluent discharge point.

5.2 Materials and methods

5.2.1 Chemicals

SMX, Ac-SMX, OH-SMX, NO-SMX (>90%), NO_2-SMX, SMX-glucuronide were obtained from Toronto Research Chemicals. 4-(Acetylamino)benzensulfonic acid, 3-amino-5-methylisoxazole, 4-nitrobenzenesulfonamide, N-phenylacetamide, aniline and sulfanilic acid were all analytical grade from Sigma-Aldrich. (5-Methylisoxazol-3-yl)sulfamate was synthesized via sodium (5-methylisoxazol-3-yl)sulfamate using an adaptation of a procedure by Spillane et al.[183]. Details regarding this synthesis and confirmation of the product are available in Appendix C. All solutions were made using Nanopure water from either a Millipore Synergy UV or a Barnstead NANOpure Diamond Water Purification System (resistivity >18.2 MΩ cm). Stock solutions were made in HPLC grade methanol and other solvents used were all analytical grade quality. Further chemicals were used in buffer solutions and eluents, namely ammonium acetate (Sigma-Aldrich), acetic acid (Fluka), disodium tetra borate decahydrate (Merck), sodium bicarbonate (Fluka), pyridine (Acros), p-nitroanisole (Sigma-Aldrich).

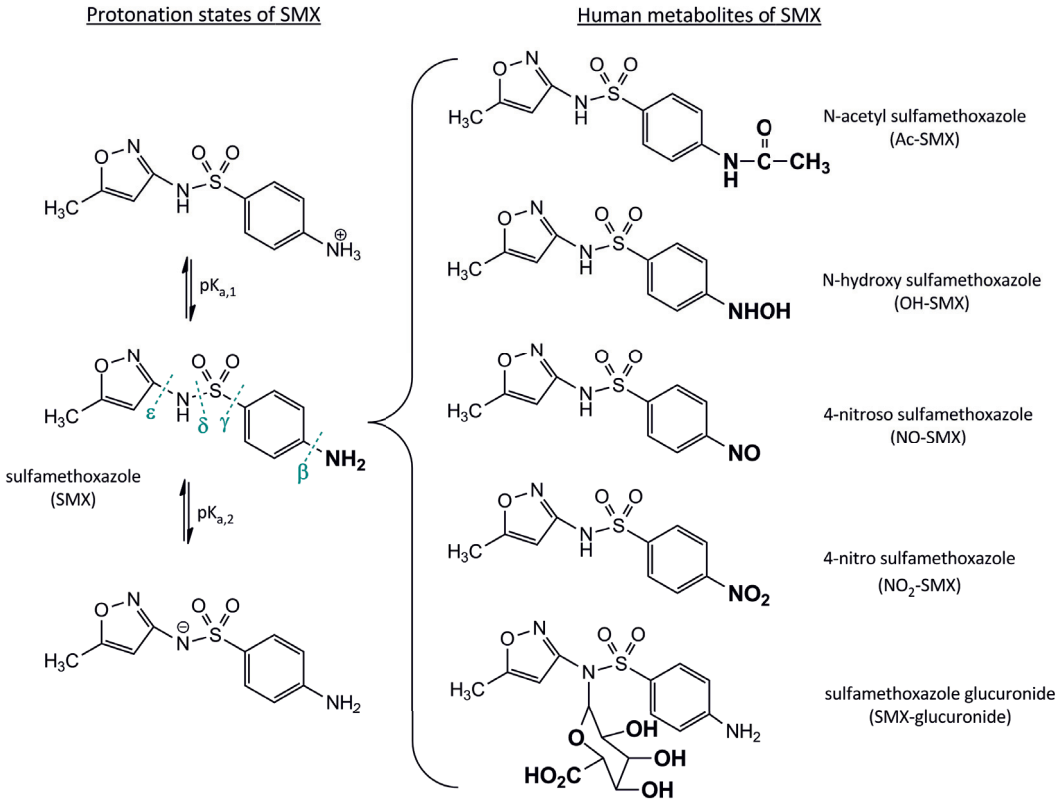

Figure 5.1: *Left panel: structure of parent compound sulfamethoxazole (SMX), protonation states and main cleavage sites of SMX photolysis. Right panel: major human metabolites of sulfamethoxazole.*

5.2.2 Spectrophotometric titration for $pK_{a,2}$ determination

The absorbance spectra of aqueous solutions (Nanopure water) of each individual metabolite (5 mg·L^{-1}) were measured with a 2550 Spectrophotometer (Shimadzu Scientific Instruments) in the pH range from 2 to 11. pH was adjusted using HCl and NaOH. $pK_{a,2}$ values were determined by a least square fit of absorbance versus pH data at a single wavelength, with the inflection point representing the $pK_{a,2}$ value (Figure C.2, Appendix C).$pK_{a,1}$ values of sulfa-drugs are generally below pH 2 and thus not relevant to natural water systems.

5.2.3 Direct photolysis experiments

The direct photolysis kinetics of SMX and metabolites were measured utilizing two different setups.

Solar simulator setup.
In the solar simulator setup, solutions of individual target compounds (1 mg·L^{-1}) in buffered Nanopure water were irradiated between 1 and 24 h from above by a Sun 2000 Solar Simulator (ABET Technologies, Milford, Connecticut) equipped with a 1000 W Xe lamp and an AM1.5 filter to mimic solar radiation. The irradiance for this setup was determined spectroradiometrically (Model ILT-900-R, International Light) before and after each experiment. The absolute irradiance was calibrated using chemical actinometry (p-nitroanisole (pNA)) and was 76 W·m^{-2} between 265 and 430 nm and showed no day-to-day variation (lamp spectrum is shown in Appendix C, Figure C.1). The irradiated solutions (400 mL) in amber glass beakers were kept homogenous by stirring, and their temperature was maintained at ca. 19°C using a water-filled tray, connected to a recirculation cooler (F240 Recirculating Cooler, Julabo). Identical solutions were left in the dark during each experiment to serve as dark controls. 1.2 mL samples were collected at selected time points (min. 10) to monitor the parent compound concentration decrease over irradiation time. The samples in amber glass vials were maintained at 4°C after collection and analyzed within 48 h by ultra-performance liquid chromatography (Acquity UPLC system, Waters) coupled to a tandem mass spectrometer (MS/MS, Acquity TQD, Waters). Each experiment was conducted at least twice. Data acquisition and processing was performed using Masslynx. In parallel, absorbance spectra for all solutions were collected with a UV-vis 2550 Spectrophotometer (Shimadzu Scientific Instruments) at various irradiation time points to assess the change in absorbance over time and wavelength. Averaged values were used to correct for light screening. As pH can affect the protonation state and thus the photolysis kinetics of organic compounds[82], direct photolysis experiments were conducted under acidic (pH 3.2) and mildly basic (pH 8.4) conditions. The various buffers, chromatographic conditions and analytical methods are described in Appendix C.

Rayonet setup.
The second setup used a turn-table apparatus inside a photochemical reactor (Rayonet) equipped with six 300 nm bulbs (Southern New England Ultraviolet Co. RPR-3500 *Å*). The bulb spectrum is shown in Appendix C (Figure C.1). The irradiation intensity, also calibrated with a chemical actinometer (pNA) from 265 to 430 nm, was 44.4 $W \cdot m^{-2}$. In this setup, solutions containing 12–30 $mg \cdot L^{-1}$ of the target compound in borate-buffered (pH 9) Nanopure water were irradiated in borosilicate glass test tubes for 1 to 24 h. Higher concentrations were used to facilitate and enhance photo-product identification. Two 150 μL aliquots were taken at various time points, and analyzed in parallel via two complementary methods: the first used a HPLC (Dionex) equipped with a UV detector to obtain quantitative kinetic data; the second allowed for high resolution mass determination of photoproducts by UPLC separation of compounds (NanoAcquity, Waters) and detection on a high-resolution mass spectrometer (HRMS, Thermo Exactive Orbitrap) (details below). Dark controls of the experimental solutions were monitored for parent compound decay over the duration of the photolysis experiments. Data acquisition and processing was done using Chromeleon (HPLC-UV) or Excalibur and Toxid (UPLC-HRMS). Again, to account for light screening, the absorbance (200–600 nm) of the solutions was monitored over time using a Cary 100 Bio (Varian) UV/Visible spectrophotometer. Solutions of a chemical actinometer pNA with pyridine[184] were photolyzed concurrently with SMX and metabolites as a measure of the effective light seen by the compounds in solution. The analytical methods are described thoroughly in Appendix C.

5.2.4 Product identification

Samples were directly analyzed by UPLC-HRMS and MS data was recorded scanning from *m/z* 90 to *m/z* 600 in both positive and negative ESI mode. Full mass spectra in both modes were explored for appearance of peaks with increasing irradiation time. Chemical formulas with theoretical exact masses within 5 ppm of the detected mass were considered as possible products. Thereafter, formulas which made the most chemical sense with respect to the starting material were investigated further. In absence of MS/MS fragmentation, no structural elucidation *per se* was possible. However the presence of fragments appearing at the same retention time due to in source fragmentation aided the structural elucidation. The identity of a selection of photoproducts could be fully confirmed by matching exact mass and retention time to authentic standards (commercially available or synthesized). Identification of HPLC-UV peaks was achieved through fractionation of concentrated photolysate. Explicitly, after reduction of the photolyzed experimental solution to ca. 1 mL via evaporation, the concentrated solution was fractionated by HPLC and the fractions directly injected on the HRMS to determine the exact mass of the peak captured in the fraction.

5.2.5 Direct photolysis calculations

The direct photolysis rate constants were determined under various conditions (pH, light source and concentration). The degradation of all metabolites followed first order kinetics (Figure C.4 a, Appendix C) and the observed degradation rate constants for each compound i, $k_{obs,i}$, were calculated using the slope of $\ln(A_t/A_0)$ plotted against time, where A_t refers to the peak area of chromatograms at time t, and A_0, the initial peak area. For experiments with relatively high concentrations of target compound and/or large volumes, a light-screening factor was used to account for the fact that the average light intensity in the tube was lower than in optically dilute solutions, due to self-screening by the compound itself or transformation products forming. The observed degradation rate constant, $k_{obs,i}$, was corrected to yield a photolysis rate constant representative of an optically dilute system, $k^0_{obs,i}$.

The direct photolysis quantum yield(Φ_i) was determined for each compound (i). It represents the efficiency of direct photolysis and was calculated as follows:

$$\Phi_i = \frac{k^0_{obs,i}}{k^0_{abs,i}} \tag{5.1}$$

where $k^0_{abs,i}$ is the specific rate of light absorbtion, a measure of the spectral overlap of light irradiance and compound absorbance (see Appendix C, Figure C.5). Details regarding light screening corrections, quantum yield calculations, calibration of light intensity by chemical actinometry and error calculations are given in Appendix C.

Finally, knowledge of the quantum yield and solar irradiance allows for the estimation of environmental half-lives. Accordingly, these were calculated by multiplying the quantum yield by the specific rate of light absorption of each compound under a theoretical solar irradiation (SMARTS), at 47°N latitude, on the 21^{st} of June (summer scenario) and 21^{st} of December (winter scenario), assuming continuous exposure, half-light attenuation and omitting indirect photolysis processes.

5.2.6 Surface water concentrations

The presence of Ac-SMX and SMX-glucuronide along with the parent compound SMX was investigated in water samples collected on a monthly basis at various depths of two sampling sites (reference sites) in the Vidy Bay of Lake Geneva between April 2010 and January 2011. Sampling strategy, sample preparation, extraction and analytical methods have been described previously[140,185].

5.3 Results and discussion

5.3.1 Acid-base speciation of SMX metabolites

SMX is a diprotonic acid (Figure 5.1, left panel), yet only the transition from the neutral to the anionic form through deprotonation of the sulfonamide NH ($pK_{a,2}$) is relevant for natural waters. For SMX and its human metabolites, Ac-SMX, NO-SMX and NO_2-SMX, $pK_{a,2}$ values of 5.89±0.07, 5.07±0.08, 4.71±0.1 and 3.66±0.01, respectively, were obtained (Figure C.2, Appendix C). Boreen et al. found a comparable $pK_{a,2}$ for SMX of 5.7[82]. No values were determined herein for SMX-glucuronide or OH-SMX. SMX-glucuronide is missing this acidic functionality and thus remains in its neutral form over the entire tested pH range (2-10). OH-SMX was rapidly converted to NO-SMX in neutral and basic aerated solutions, and due to this instability in experimental conditions, its $pK_{a,2}$ was not determined, nor was it considered for further experiments.

5.3.2 Direct photolysis kinetics, quantum yields and environmental half-lives

The protonation state of organic compounds affects their absorbance (Figure C.3, Appendix C) resulting in differences in direct photolysis kinetics[82]. For this reason, direct photolysis experiments were performed at different pH values and the resulting photolysis rate constants of the predominantly neutral form (pH 3.2) and anionic form (8.4 and 9.2) are listed in Table 5.1. The pH dependence of the photolysis kinetics was evident, with faster reaction kinetics in acidic conditions for most compounds. In accordance with previous research[82,102], the neutral form of SMX (prevalent at pH 3.2) was found to be more photolabile than the anionic form. SMX metabolites also degraded faster under acidic conditions, showing up to 30-times faster degradation kinetics of the neutral form. The accelerated direct photolysis in acidic solution was not observed for SMX-glucuronide. This result was expected as SMX-glucuronide is missing the sulfonamide NH acidic functionality; therefore, in contrast to SMX and the other metabolites, it remains in its neutral and more photoreactive form at environmental pH. The specific rate of light absorption of each compound (Table 5.1) in its neutral or anionic form was compared to its corresponding reaction rate constant. Both SMX and Ac-SMX showed a positive correlation between absorbed light and rate constant, with higher absorbance of the neutral compounds leading to faster kinetics. In contrast, despite greater light absorption of NO-SMX and NO_2-SMX in their anionic form, the neutral form degraded more readily.

Among the target compounds at pH 3.2, the fastest degradation was observed for SMX. The degradation of SMX-glucuronide and Ac-SMX were nearly as fast as SMX, whereas NO-SMX and NO_2-SMX were orders of magnitude slower. At pH 8.4 and 9.2, SMX-glucuronide showed the fastest degradation kinetics of all investigated compounds followed by the parent compound SMX. On the other hand, NO-SMX, Ac-SMX and NO_2 SMX showed significantly lower rate constants (Table 5.1).

Table 5.1: *Specific rate of light absorbtion ($k^0_{abs,i}$), direct photolysis degradation rate constants ($k^0_{obs,i}$), experimental half-lives, quantum yield and computed environmental half-lives (τ) for SMX and its human metabolites observed in the solar simulator setup (sol.sim.) and in the Rayonet setup. Errors represent 95% confidence intervals (details in Appendix C).* [a] *Observed direct photolysis reaction rate constant corrected for light screening;* [b] *Corrected for light screening;* [c] *n=number of replicas;* [d] *Environmental half-life: calculated using the direct photolysis quantum yield determined in the Rayonet setup and SMARTS irradiance values for solar irradiation on a sunny summer day, τ_{summer}, (21st June)/winter, τ_{winter}, day (21st December) at 47°N. Light attenuation by the water column was incorporated by assuming half-light attenuation correlates with a halving of the direct photolysis reaction rate constant*[82]*;* [e] *n.d.:not determined due to high photostability observed in solar simulator setup.*

Compound	**pH**	**Irradiance setup**	**Concentration** ($mg{\cdot}L^{-1}$)	$k^0_{abs,i}$ ($\cdot 10^{-3}\ h^{-1}$)	$k^0_{obs,i}$ [a] (h^{-1})	**Experimental half-life**[b] (h)	**n**[c]	**Quantum yield**	τ_{summer} [d] (h)	τ_{winter} [d] (h)
SMX	3.2	sol.sim.	1	6.45 ± 1.48	22.3 ± 1.86	0.031 ± 0.002	2	0.959 ± 0.235	10.4 ± 0.4	44 ± 2
	8.4	sol.sim.	0.5–3	5.36 ± 0.87	1.42 ± 0.08	0.494 ± 0.018	4	0.074 ± 0.013		
	9.2	Rayonet	22	16.95 ± 2.88	1.36 ± 0.10	0.440 ± 0.018	4	0.028 ± 0.005		
Ac-SMX	3.2	sol.sim.	1	2.32 ± 0.38	6.19 ± 0.49	0.111 ± 0.006	2	0.543 ± 0.132	61.5 ± 2.5	246 ± 10
	8.4	sol.sim.	0.5–3	3.17 ± 0.72	0.207 ± 0.017	3.43 ± 0.22	4	0.025 ± 0.005		
	9.2	Rayonet	31	11.24 ± 1.66	0.096 ± 0.008	6.14 ± 0.353	3	0.003 ± 0.0005		
NO-SMX	3.2	sol.sim.	1	35.42 ± 8.15	0.303 ± 0.034	2.29 ± 0.19	2	0.002 ± 0.0006	10.7 ± 0.3	47 ± 1
	8.4	sol.sim.	0.5–3	79.64 ± 12.95	0.184 ± 0.010	3.87 ± 0.15	4	0.0006 ± 0.0001		
	9.2	Rayonet	12–24	212.65 ± 25.60	0.540 ± 0.056	1.10 ± 0.05	5	0.0009 ± 0.0001		
NO_2-SMX	3.2	sol.sim.	1	11.49 ± 2.64	0.062 ± 0.020	11.3 ± 3.25	2	0.0015 ± 0.0006	337 ± 30	1515 ± 135
	8.4	sol.sim.	1	29.40 ± 4.78	0.0029 ± 0.0005	79.3 ± 3.15	1	0.00003 ± 0.00001		
	9.2	Rayonet	n.d[e]	n.d[e]	n.d[e]	n.d[e]	0	n.d[e]		
SMX-Glucuronide	3.2	sol.sim.	1	12.84 ± 2.95	16.27 ± 1.43	0.042 ± 0.003	2	0.352 ± 0.087	1.3 ± 0.1	5.9 ± 0.7
	8.4	sol.sim.	1	11.23 ± 1.83	12.41 ± 1.03	0.043 ± 0.002	3	0.307 ± 0.064		
	9.2	Rayonet	12	34.91 ± 4.01	15.57 ± 0.71	0.045 ± 0.001	2	0.124 ± 0.015		

Finally, self-sensitization by the compound itself was ruled out, as experiments performed at different concentrations showed no significant differences in kinetics (Figure C.4 b, Appendix C).

The majority of investigated compounds differ only in their aromatic-ring substituent, yet large differences were observed within direct photolysis rate constants. Hence, the different ring substituents influence the photochemical behavior of these compounds, as discussed in detail below. Similarly, previous research found different direct photolysis behavior among five sulfa drugs with varying five-membered heterocyclic substituents[82]. Direct photolysis is thus clearly sensitive to both ring functionalities of the molecule, though differences in five-membered ring substituents led to relatively small variations compared to the aromatic-ring substituents investigated here.

Similar trends as for rate constants could be observed for quantum yields (Table 5.1). The quantum yields of the neutral components (pH 3.2) were greater than of the anionic form of the compound, except for SMX-glucuronide, which remained in its neutral form in all experimental conditions. Furthermore, both SMX-glucuronide and SMX showed relatively high quantum yields, compared to values 2–3 orders of magnitude lower for Ac-SMX, NO-SMX and NO_2-SMX.

Quantum yields determined in the solar simulator setup were systematically higher than those determined using the Rayonet setup, with the exception of NO-SMX. A recent review reported a wavelength specific quantum yield for SMX of $\Phi = 0.038 \pm 0.002$[105], which is comparable to the one measured in the Rayonet setup (λ_{max}=300 nm), $\Phi_{Rayonet} = 0.028 \pm 0.005$, but lower than the quantum yield determined by Zhou and Moore, $\Phi_{257} = 0.084 \pm 0.016$ at pH 9[102]. The latter found values closer to the quantum yields determined under natural sunlight $\Phi_{sunlight} = 0.09 \pm 0.01$[82], which in turn match the ones determined here using the solar simulator setup $\Phi_{sol.sim} = 0.074 \pm 0.012$.

The sensitive nature of quantum yield calculations has been reported[186] and may explain variance among different experimental setups. The molar absorptivity of all compounds at pH 9.2 and 8.4 are identical and accordingly did not affect the quantum yields. In the present case, however, owing to the small spectral overlap of molar absorptivity and solar simulator irradiance for certain compounds (all but NO-SMX and NO_2-SMX) (Figure C.5, Appendix C), slight errors in their determination may largely influence the rate of light absorption, $k^0_{abs,i}$, and hence lead to differences in quantum yields. In contrast to the solar simulator irradiance which begins at 280 nm, the Rayonet irradiance spans a wavelength range from 250 to 400 nm, allowing for a larger spectral overlap with the target compounds (Figure C.5, Appendix C) and leading to a likely more robust quantum yield. On the other hand, NO-SMX shows a large spectral overlap in both experimental setups due to its absorption range up to 430 nm; it is thus more robust with respect to small inaccuracies in the absorbance and irradiance measurements. Correspondingly it is the only compound with comparable quantum yields in both setups. Furthermore, quantum yields may be wavelength-dependent, which may also

account for the observed differences with various light sources. Environmental half-lives were computed using the Rayonet quantum yields, which we consider to be more robust.

The minimum environmental half-lives were computed for a sunny summer day (τ_{summer})at 47° N latitude (Geneva, Switzerland) and ranged from 1.3 hours for SMX-glucuronide to 14 days for NO_2-SMX. In the winter, the calculated half-lives (τ_{winter}) increased to range from 6 h to 63 days (Table 5.1). In a lake environment, such as Lake Geneva, summer stratification constrains the mixing of the water column and consequently prevent inflowing micropollutants entering below the thermocline to reach the surface and undergo photolysis. Additionally, they may accumulate below the thermocline[140]. In winter months, photodegradation is greatly reduced; however, the enhanced mixing of the water column ensures a more homogeneous sunlight exposure throughout the water column. Therefore, the reduced winter photolysis may not have a significant impact on concentrations of SMX and its metabolites in the lake.

5.3.3 Product identification

Various studies have examined photoproducts arising from direct photolysis of SMX. The majority of reported photoproducts arise from cleavage of the molecule at various positions (Figure 5.1, left panel). Several authors have identified δ-cleavage, yielding sulfanilic acid, as the prevailing mechanism[82,166], though at least one study reported photoisomerization of the five-member isoxazole as the main mechanism[102].

The percent conversion was used to quantify the relative importance of confirmed photoproducts of SMX and its metabolites. Explicitly, the conversion corresponds to the percentage of irradiated target compound converted to a given first-generation product; it is calculated from the ratio of the initial rates of product concentration growth and target compound concentration loss. The conversion of the target compounds to first generation products could only be calculated for products with available standards.

SMX

The concentrations of quantifiable photoproducts of SMX over time are depicted in figure 5.2a, and the corresponding structures and conversion rates are shown in figure 5.3. Similarly to previous research, sulfanilic acid (*m/z* 172) was found to be the most important quantifiable product of SMX photolysis, with a conversion of 20%. SMX also produced (5-methylisoxazol-3-yl)sulfamate (*m/z* 176), a product which has not been reported to date and could be confirmed by matching exact mass, retention time and UV spectra with the synthesized standard (validation of standard (NMR, crystal structure, IR, HRMS) given in Appendix C). Generated through γ-cleavage, it accounts for 11% of degraded SMX. Further products that could be confirmed with authentic standards include aniline (5%, *m/z* 94) and 3-amino-5-methylisoxazole (2%, *m/z* 99). Both have previously been reported as photoproducts of SMX, and result respectively from γ- and δ-cleavage[102,166].

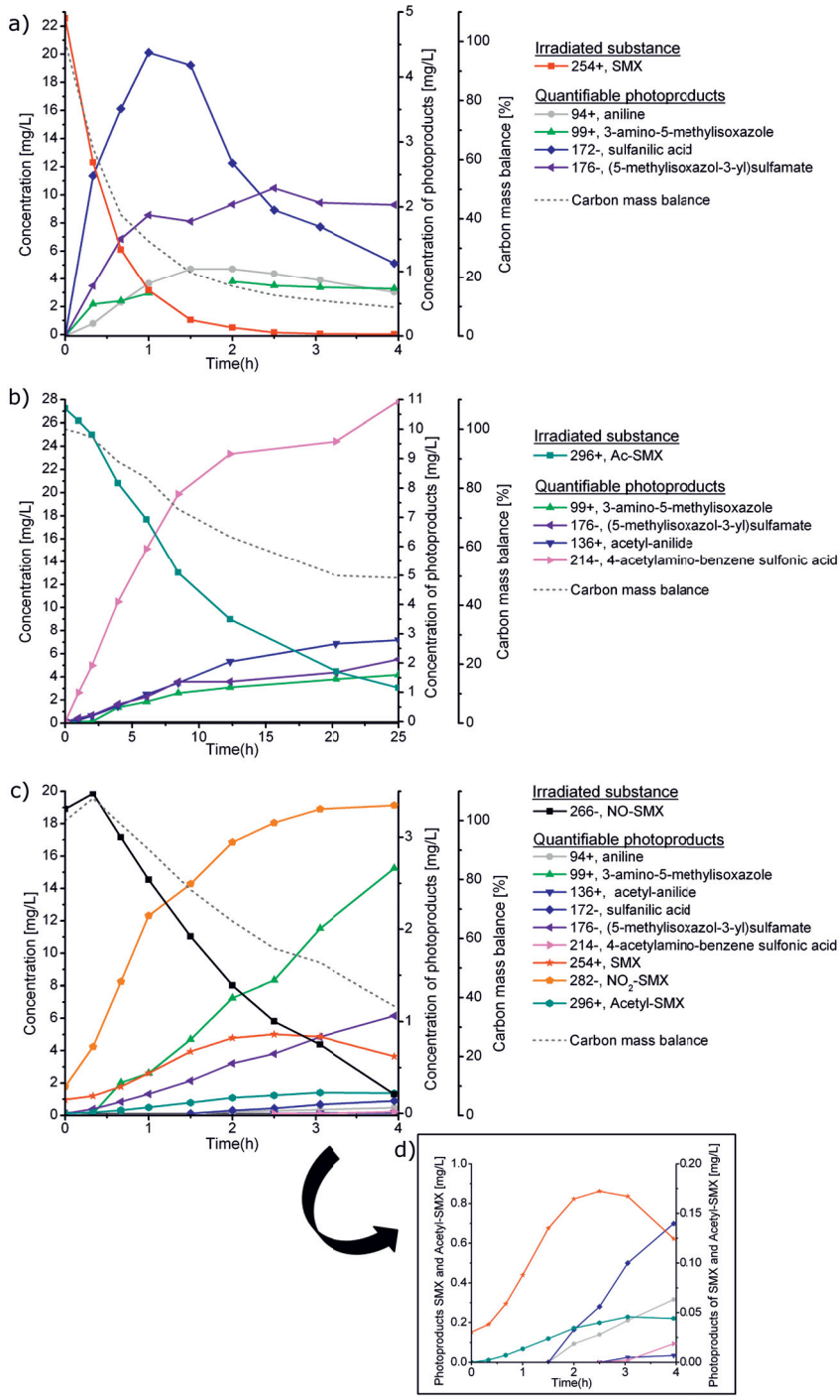

Figure 5.2: *Photolysis (at pH 9.2) of SMX (a), Ac-SMX (b) and NO-SMX (c) over time with appearance of quantifiable photoproducts and carbon mass balance. Left axis shows concentration of irradiated substance (mg·L^{-1}), first right-axis the concentration of each quantifiable photoproduct (mg·L^{-1}) and second right-axis the carbon-mass balance (%). (d) Enlargement of (c) with concentration of SMX and Ac-SMX (1st or 2nd generation products of NO-SMX) on the left axis (mg·L^{-1}) and their corresponding photoproducts on the right axis (mg·L^{-1}). +: MS positive ionization mode, - : MS negative ionization mode.*

As mentioned above, Zhou and co-workers reported an isomer of SMX, generated through photo-rearrangment of the isoxazole ring, as the major product with a yield of 30%[102]. They also identified a hydrated product of 2H-azirine, with mass $[m\text{-}H]^-$= 270.0550[102]. Though these have not systematically been observed in more recent studies[82], the exact masses of both an SMX isomer and hydrated 2H-azirine were observed in the present study. These, however, could not be confirmed, due to a lack of authentic standards or/and mass spectral fragmentation data.

A number of additional products were formed during SMX photolysis. Their exact masses in combination with mass spectral data, when available, were used to propose structures (Table C.3, Appendix C). Among the proposed structures are hydroxylated products, such as isomers of OH-SMX $[m+H]^+$=270.0533 (at several retention times), the hydroxylated sulfamate (4-hydroxy-5-methylisoxazole-3-yl)sulfamic acid ($[m\text{-}H]^-$=192.9915), hydroxyaminobenzene sulfonic acid ($[m\text{-}H]^-$= 188.0013), hydroxysulfonic acid ($[m\text{-}H]^-$=172.9906), and benzene sulfonic acid ($m\text{-}H]^-$= 156.9954. β-cleavage may also be occurring, with removal of the NH_2 group, yielding $[m+H]^+$=239.0478. A recent study on photolysis of other sulfonamides and their acetylated-metabolites found desulfonated products to be the most relevant photodegradation products identified[187]. In our work, the exact mass signal corresponding to the SO_2-extrusion product of SMX was also weakly visible.

Ac-SMX

The degradation of Ac-SMX and the growth of confirmed products over time are shown in figure 5.2b. Total conversion was highest for Ac-SMX, which was mainly transformed to 4-acetamidobenzenesulfonic acid (88%, *m/z* 214), the acetylated equivalent of sulfanilic acid, generated through δ-cleavage. Other first-generation products from direct irradiation of Ac-SMX include N-phenylacetamide (13%, *m/z* 136) and (5-methylisoxazol-3-yl)sulfamate (2%, *m/z* 176), both produced through γ-cleavage. The production of 3-amino-5-methylisoxazole (*m/z* 99), already observed during SMX photolysis, was also confirmed with an authentic standard. The highest concentrations of most photoproducts were attained after 8h of photolysis.

A further selection of products can be proposed on the basis of exact mass information. As observed for SMX photolysis, $[m+H]^+$=239.0485 is the proposed product of a β-cleavage. $[m+H]^+$=270.0536 could be observed at various retention times and may represent isomers of hydroxy-SMX. In contrast to SMX, a mass likely corresponding to the SO_2-extrusion product of Ac-SMX ($[m+H]^+$=232.1073) appeared after 1 h irradiation with a high intensity at a retention time of 10.52 min. The exact masses of all confirmed and proposed photoproducts are within 5 ppm of calculated masses of the proposed elemental composition and can be found Table C.4, Appendix C.

SMX-Glucuronide

SMX-glucuronide underwent δ-cleavage, yielding sulfanilic acid (*m/z* 172), which was, with aniline (*m/z* 94), the only confirmed photoproduct for this compound. Though exact masses corresponding to glucopyranuric acid ($[m+H]^+$=194.0659) and glucuronic acid ($[M-H]^-$=193.0354) appeared with increasing irradiation-time, supporting cleavage of the glucuronide, no production of the parent compound SMX was detected. The accurate mass corresponding to the desulfonated product of SMX-glucuronide ($[M+H]^+$=366.1294) was also observed. Proposed structures are presented in Table C.5, Appendix C.

NO-SMX

NO-SMX showed the highest number of identified products, mainly due to the production of SMX and Ac-SMX, which subsequently photolyzed to some of the above mentioned products. This notable back-transformation of NO-SMX to SMX (*m/z* 254 in Figure 5.2c) is the first evidence for photolytic back-transformation of a metabolite to its parent compound. However, the relative magnitude of this pathway remains small: the initial 18.6 mg·L^{-1} NO-SMX yielded no more than 0.5 mg·L^{-1} of SMX, which rapidly degraded to form sulfanilic acid (*m/z* 172) and aniline (*m/z* 94). Similarly, Ac-SMX (*m/z* 296) was observed right from the first sampled time point (0.3 h), but its maximum concentration remained below 0.5 mg·L^{-1}. In accordance with the slower photolysis kinetics of Ac-SMX, its respective photoproducts appeared with a slight time shift relative to SMX photoproducts.

Direct reduction of NO-SMX to SMX and Ac-SMX is chemically improbable, therefore both are likely at least second generation products of NO-SMX photolysis. The contribution of buffer components to the unexpected observation of Ac-SMX could be ruled out, as Ac-SMX was systematically observed with various types of buffers, only one containing an acetylated derivative (acetic acid). Moreover, a second order reaction involving NO-SMX itself could be excluded as doubling the initial concentration of NO-SMX did no more than double the production of Ac-SMX.

The largest fraction of NO-SMX was transformed to the most stable metabolite, NO_2-SMX (*m/z* 282 in Figure 2c), with a conversion of 55%. It seems that the NO-substituent favors modifications of the substituent (to NO_2, NH_2 and $NHCOCH_3$) rather than cleavage reactions, which predominated in SMX and Ac-SMX photolysis. As for SMX and Ac-SMX, (5-methylisoxazol-3-yl)sulfamate (*m/z* 99) was detected after 0.66 h of irradiation. Its emergence before SMX and Ac-SMX products (after 2 and 3 h respectively), yet with a slight delay on NO-SMX degradation, leads us to believe it is not a 1^{st} generation product; thus there is no evidence that γ-cleavage occurs directly on NO-SMX.

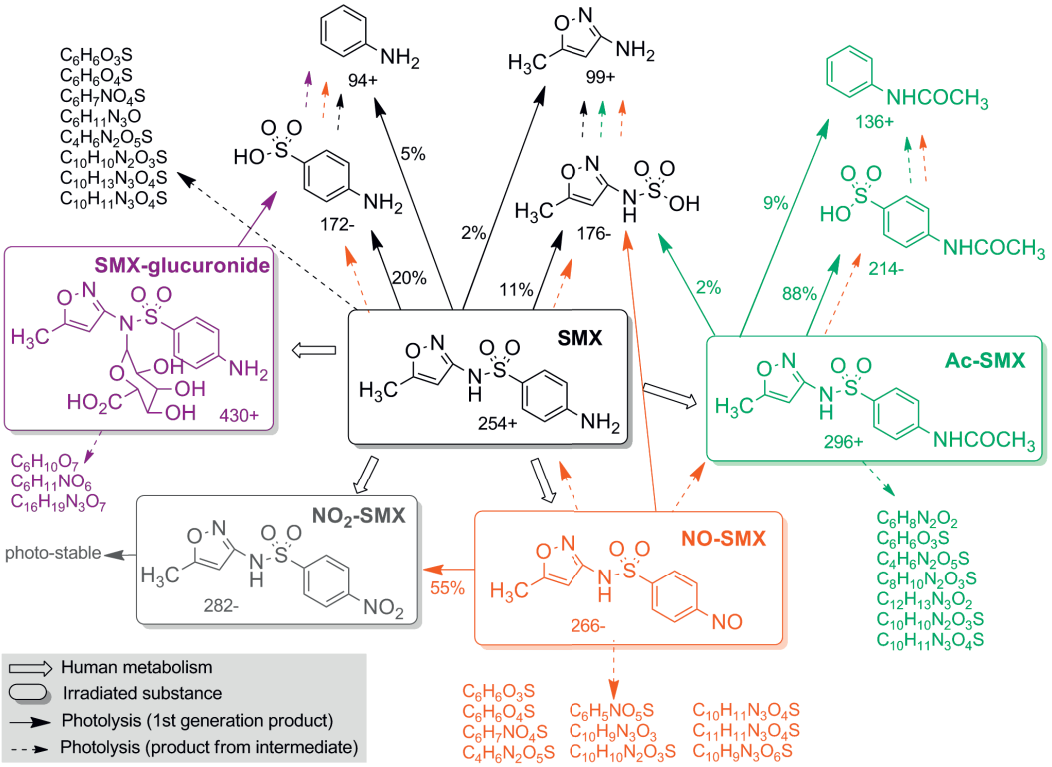

Figure 5.3: *Photolyzed substances and structures of confirmed photoproducts. Formulas are given for proposed products which were not validated with authentic standards; proposed structures for these formulas are given in tables C.3–C.6 in Appendix C.*

Apart from the new products discussed above and previously mentioned products from SMX and Ac-SMX, three new structures can be proposed, and supported by in-source fragmentation information: the nitro-derived products, nitro-benzenesulfonic acid ($[m\text{-}H]^-$ = 201.9812) and hydroxylated nitro-SMX ($[m\text{-}H]^-$ = 298.0143) and a product likely corresponding to addition of a methyl group on the aromatic ring of NO-SMX ($[m\text{-}H]^-$ = 280.0401). All confirmed products as well as proposed structures are shown in Table C.6, Appendix C.

A comparison of the conversion rates illustrates that the different ring substituents on the metabolites not only affect direct photolysis reaction rates, but also the principal photolysis pathways (Figure 5.3). Among the confirmed products, cleavage reactions were predominant for SMX and Ac-SMX, whereas the nitro-group was very resistant to phototransformation and the nitroso group mainly underwent modifications of the substituent. Despite the nitro-group being a very potent chromophore, nitroaromatics are known to have very short triplet life-times[188]; this may explain the low reactivity of NO_2-SMX. Irradiation experiments with nitrobenzene effectively found it to be photostable under natural sunlight[189]. The photochemistry of nitroso-aromatics has also received much attention, and some have been shown to oxidize photochemically to nitro-compounds[190,191]. Several reaction schemes, involving either C-N bond dissociation or excitation to the first singlet state, followed by intersystem crossing were proposed, but none could be ascertained[191].

Whatever the pathway, these observations are in line with the photooxidation of NO-SMX to NO_2-SMX observed here. The transformation of NO-SMX to SMX constitutes a photoreduction, and thus requires the presence of an electron donor. In our experimental system, trace amounts of methanol may have played this role. In environmental systems, potential electron donors include organic matter or chloride, though their effect on the photoreduction of NO-SMX was not specifically addressed herein.

The main products of SMX and Ac-SMX resulted from δ- and γ-cleavage. The acetyl-group may have a stabilizing effect on the C-S bond as δ-cleavage was predominant, while both N-S and C-S bonds seemed equally susceptible to cleavage during SMX-photolysis. β-cleavage, involving cleavage of the substituent, was observed for all target compounds, but was not quantified due to the lack of analytical standard. Accurate masses corresponding to the desulfonation-products of SMX and its metabolites were observed for every compound. Extrusion of SO_2 was already identified as an important direct photolysis pathway for similar sulfa-drugs (sulfapyridine and sulfmethazine) and their acetylated metabolites [187]. The relative importance of this pathway could not be quantified here due to lack of standards. Finally it may be worth recalling that nitroso- and nitro-substituted compounds already showed opposite behavior to SMX and Ac-SMX regarding the correlation between spectral overlap and reaction rate constant. Thus it seems that the nitro-/nitroso- group affects the photo-excitation and resulting pathways of sulfonamides. Evidently, further research using model compounds would be required to fully elucidate the mechanisms.

5.3.4 Contribution of direct photolysis to the degradation of SMX metabolites in Lake Geneva

Water samples from Lake Geneva were investigated to confirm the presence of human metabolites of SMX in the environment, and to analyze observed concentrations with respect to their excretion fractions and relative photolability. Over 70 lake water samples from 2 sampling sites and various depths (0–30 m) in Lake Geneva were analyzed for the presence of the two most abundantly excreted metabolites of SMX, Ac-SMX and SMX-glucuronide. Both metabolites were detected, but their frequency of detection varied with compound, sampling site and season. SMX-glucuronide was only detected at a low frequency (9% of samples). The observed concentrations were systematically and significantly lower than SMX (Figure 5.4), despite their comparable excretion fractions. This is consistent with our finding that SMX-glucuronide is the most photolabile of all compounds targeted in this study. Given the rapid photolysis, combined with the unstable nature of the glucuronide bond, which can also be microbially cleaved [167], a low frequency of detection and low environmental concentrations are expected. Ac-SMX, on the other hand, is excreted in higher amounts than SMX, but nevertheless was detected at a lower frequency (Ac-SMX: 43%; SMX: 94%). Furthermore, the concentrations of Ac-SMX detected in the lake were significantly lower than SMX.

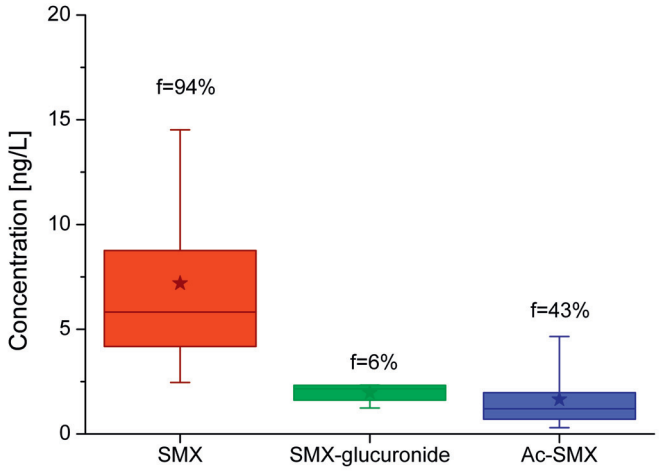

Figure 5.4: *Measured concentrations (ng·L^{-1}) of SMX and its human metabolites SMX-glucuronide and Ac-SMX in Lake Geneva. f=frequency of detection. Boxes represent 25th percentile, median and 75th percentile. The whiskers are determined by the 5th and 95th percentiles and the stars show the mean value*

The present study found Ac-SMX to be slightly more resistant to direct photolysis than SMX, hence the lower concentrations observed for Ac-SMX in lake water may indicate that other processes such as indirect photolysis processes and biodegradation may also contribute to the total degradation in the investigated environment. In fact, previous research showed that Ac-SMX biodegrades twice as fast as SMX in water-sediment tests [167]. Considering lake parameters and past research [82], we expect a minor contribution of indirect photolysis processes to the total degradation of SMX. However, the susceptibility of human metabolites of SMX to indirect processes is still to be determined.

5.4 Environmental relevance

This study observed an abiotic production of SMX from NO-SMX. In the present case, owing to the low fraction SMX excreted as NO-SMX, the low conversion back to the parent compound and the relatively high photolability of SMX, the back-transformation of NO-SMX to SMX may not be of high environmental relevance. However, actual environmental concentrations of NO-SMX in lake water would be necessary for a better assessment. Nevertheless, this is the first evidence that photolytic back-transformation of a human metabolite to its parent compound can occur, which in essence presents an environmental source of SMX. Likewise, it is pertinent to recall that NO_2-SMX, the main photoproduct of NO-SMX photolysis, was also found to retransform to SMX under reducing conditions [169], thus representing an additional abiotic source of SMX. As such, further studies should be pursued to investigate the yield of NO-SMX back-transformation under different environmental conditions, where the process may be more significant. Moreover, the back-transformation of other nitroso-metabolites should also be considered. Furthermore, a recent study effectively found a potential increase of the ecotoxicological risk due to the presence of, among others, SMX metabolites in surface waters [185]. The knowledge that some metabolites retain certain biological activity, combined with their potential to retransform to the parent compound, underlines the importance of considering human metabolites in environmental field work and including product identification in degradation studies.

6 Conclusion and Perspectives

Contamination of surface waters with trace levels of pharmaceuticals and other chemical residues from everyday life applications is an acknowledged environmental concern world-wide. The environmental implications of low concentrations of these compounds in the aquatic environment are still far from being understood, yet an extensive area of research has developed around the thematic of micropollutants in surface waters.

In the case of Lake Geneva, the presence of micropollutants is a legitimate worry, considering that over 70% of the 1.5 million inhabitants surrounding the lake rely on this immense natural reservoir as their drinking water resource. Moreover, the lake also serves for recreational purposes and as a natural habitat to an abundance of fauna and flora. Finally, it functions as a natural treatment plant in that it receives effluent wastewater from numerous treatment plants along the lake, which are well-acknowledged point-sources of pharmaceuticals to surface waters.

The sustainable development of this and other lakes world-wide is a global necessity, given the growing water demand and anthropogenic pressure associated with the increasing population. In order to preserve and contribute to a durable development of Lake Geneva, with respect to water quality, it is necessary to assess the physical, chemical, microbiological, and ecological dynamics of mid-sized lakes which are influenced by anthropogenic activity. Accordingly, in regard to micropollutants, understanding the dynamics, fate and consequences of the release of these substances in water is essential to evaluate potential risks. Such insight involves an entire suite of research fields, namely analytical, environmental and organic chemistry, ecotoxicology and hydrology. The interdisciplinarity of the problematic was illustrated throughout the four research chapters of this thesis. The work has led to the following key conclusions:

Direct discharge of effluent wastewater into lakes leads to the formation of a plume with elevated micropollutant concentrations during the period of thermal stratification

The first step in assessing the risk associated with the presence of micropollutants in Lake Geneva consisted in determining their concentrations in the lake. A large variety of pharmaceuticals and other micropollutants have been observed in surface waters around the world, with rising frequency of detection. Often, however, the spatio-temporal aspects of concentration fluctuations were not considered. Moreover, the impact of direct discharge of effluent wastewater into a lake had never been investigated. These aspects were highlighted in Chapter 2, which investigated the occurrence of 39 priority micropollutants (pharmaceuticals from various classes, pesticides and corrosion-inhibitors). A 10-month water sampling campaign in the Vidy Bay of Lake Geneva showed that wastewater directly discharged into the lake does not readily mix with the surrounding water column during certain periods of the year. Indeed, during the warm season, thermal stratification prevents vertical mixing between the surface and the bottom layers of the lake. This leads to a plume of elevated concentrations of micropollutants above the outfall at the level of the thermocline. In winter, homogeneous temperature profiles allow enhanced mixing of the water column and, consequently, uniform micropollutant concentrations at all depths.

Over 200 water samples were collected and analyzed during this campaign in order to confirm the presence of a plume and get a sense of its spatio-temporal variability and extent. Despite rapid recent advances in sample preparation techniques and detection methods, determining concentrations of these pollutants in water samples still remains a tedious and costly task. This illustrates one of the limitations of punctual field sampling when investigating dynamic and variable processes.

In this sense, the relation between micropollutants and electrical conductivity discovered in this study represents a simple tool to estimate the concentrations of these compounds around the wastewater outfall. Indeed, the concentrations of wastewater-derived micropollutants within the plume were found to be closely correlated to the value of electrical conductivity. Ultimately, it is a measure of the wastewater dilution, thus the correlation is conserved for conductivity measurements greater than the background, i.e. within the plume. This relation was observed for the specific setting of Vidy Bay, and is likely validated in other aquatic environments receiving effluent wastewater, owing to the high ion concentrations of the latter.

The spreading of the plume can be captured beyond individual sampling points by combining hydrodynamic considerations with environmental degradation processes

To fully evaluate the implications of the micropollutant plume, both its spatial extent and temporal variability must be known. Models represent a complementary approach to overcome the limitations of punctual sampling and/or to augment measured data. As the spatial distribution of a chemical is simultaneously affected by transport and transformation processes, knowledge of these processes and their underlying physical-chemical parameters is required. In surface waters, photolysis has been recognized as a major transformation process for many polar organic contaminants, in particular those having resisted biological treatment in wastewater treatment plants. The inherent interdisciplinarity of understanding the spreading of the micropollutant plume was exemplified in Chapter 3. It proposed a model coupling 3D particle tracking, the product of an associated project on lake hydrodynamics, and photodegradation of micropollutants. Though unconventional, particle tracking represented the ideal method to combine depth-dependent photolysis and 3-dimensional plume spreading in the objective of predicting the concentration of micropollutants in the vicinity of the wastewater outfall under typical wind scenarios and seasons relevant to Vidy Bay. To assess the importance of photolysis for the targeted compounds in Vidy Bay, photolysis kinetics were determined via a series of direct and indirect photolysis experiments under a solar simulator and then extrapolated to environmental conditions.

As expected, photodegradation was an important removal mechanism for many micropollutants and thus contributed to a reduction in their concentrations over time and distance from the WW outfall, especially for surface plumes in winter. In contrast, during thermal stratification, the importance of photodegradation processes in attenuating the plume extent was greatly reduced, due to light screening by the water column.

The micropollutant plume causes a potential ecotoxicological risk

Ultimately, the underlying motivation of delineating the plume and its concentrations is to assess whether the measured and predicted concentrations of micropollutants in Vidy Bay exhibit an environmental risk. Though present at low concentrations, pharmaceuticals are designed to be biologically active and the existence of adverse effects on aquatic fauna and flora is well-acknowledged. Moreover, in the environment, a myriad of compounds are present; these can interact with each other resulting in additive or potentially even synergistic mixture effects. The zone of potential ecotoxicological risk for the mixture of targeted micropollutants was delineated by combining the individual risk of each substance determined using ecotoxicity data obtained from literature.

Direct discharge of effluent wastewater into the Bay resulted in a limited zone that surpassed water quality criteria for micropollutant concentrations. The coupled hydrodynamic-photolysis model confirmed the field measurements, which indicated that the risk is most

pronounced and the affected zone is largest in summer: a stretch of up to 300 m to the east and the west of the wastewater outfall may exhibit a potential ecotoxicological risk. It should be noted, however, that this risk assessment only takes into account the (24) wastewater-derived micropollutants targeted in this study. Hence, the inclusion of additional compounds would likely increase the ecotoxicological risk and the affected area.

The total ecotoxicological risk can be mainly attributed to a few compounds

Overall, the coupled hydrodynamic-photolysis model applied to ecotoxicological risk assessment allows for the identification of critical situations and well as important parameters. Analysis of various scenarios showed that wind conditions and solar irradiation play an essential role in determining the zone of potential ecotoxicological risk. On the one hand, winds govern hydrodynamic currents and mixing processes. On the other, the intensity of solar irradiation will influence photodegradation kinetics and thermal stratification. Thus, the risk zone varies greatly according to these environmental factors, over which we have no control.

Nevertheless, we may exert our influence by preventing the release of micropollutants to the environment. Indeed, as ultimately only a few compounds contributed significantly to the total ecotoxicological risk, these should be considered priority substances for wastewater treatment plant optimization and further monitoring campaigns. Among the problematic compounds, antibiotics were the major pharmaceutical class that contributed to the risk. This ecotoxicological risk adds on to the existing concern of the spreading of antibiotic resistant bacteria also associated to the presence of antibiotics in surface waters.

Human metabolites of pharmaceuticals lead to an increased ecotoxicological risk and may present a source of parent compound in the environment

Recent research efforts have shifted towards identifying photolysis products of pharmaceuticals, as well as the presence and fate of their human metabolites, as both may also present a risk to the aquatic ecosystem. Some metabolites are not only more pharmacologically active than the parent compound, but were also found to back-transform to the active pharmaceutical, for example during biological wastewater treatment. Similarly, photodegradation processes may yield photoproducts that are more persistent than the parent compound and retain toxicological relevance.

The occurrence of various human metabolites of pharmaceutical in Vidy Bay was investigated in Chapter 4. Their concentration profiles at the WWTP discharge location displayed a plume-like feature, confirming that wastewater effluent represents the main source of human metabolites to the lake. Nevertheless, the metabolites targeted in this study were determined to be more susceptible to environmental degradation processes than their parent.

In continuation, the propensity of selected human metabolites to undergo photodegradation was more fundamentally addressed in Chapter 5. Unlike observed field data, almost all investigated metabolites were found to be more photostable that the parent compound, indicating that other transformation processes such as indirect photolysis processes and biodegradation may also contribute to the total degradation in the investigated environment.

Assuming a worst-case scenario, in which pharmaceuticals and their metabolites present a similar ecotoxicological impact, the presence of human metabolites led to an increased environmental risk. In addition, identification of the major phototransformation products of several human metabolites showed that one was retransformed back to the parent compound via a photoreduction. This is the first evidence for photolytic transformation of a human metabolite back to its parent compound. As such, human metabolites could represent an environmental source of pharmaceuticals in the environment.

Future research needs

In the past decade, notable advances have been made in assessing the occurrence, fate, effects and risks of pharmaceuticals in the environment. Yet, throughout this work, a number of unanswered questions arise pertaining to the limitations of current methods in assessing the fate of contaminants and the actual consequences of their presence in the environment.

Understanding the fate of contaminants in water constitutes an essential step in the ecotoxicological risk determination. For instance, some compounds may be toxicologically relevant, but exhibit low persistence and thus do not represent a threat to the environment. An entire field of research is dedicated to assessing the propensity of individual compounds to undergo various degradation processes and to identifying the factors that influence these transformations. The necessary parameters required to model their fate in water, such as for instance the quantum yield of direct photolysis, may be determined in the well-controlled environment of a laboratory via simple black-box type experiments. However, a fundamental understanding of the factors influencing these processes finally gives rise to molecular or intramolecular-level models to predict e.g. the magnitude of indirect processes based on water characteristics, and perhaps in the near future the quantum yields of direct photolysis based on chemical structure. To date, a number of intrinsic compound properties and structural information allow estimations of partitioning between phases or reaction rates with given compounds (QSAR, quantitative structure activity relationships). Research is developing in the field to predict biotransformation pathways (QSBR, quantitative structure-biodegradation relationships) and oxidative transformation processes. A promising, yet challenging area of research thus constitutes the prediction of susceptibility to photodegrade or even the nature of phototransformation products, based on chemical structure and quantum chemical calculations. Such predictions would address the lack of experimental data which is needed to parameterize exposure or risk models.

Similarly, a lack of pertinent experimental data may be noted in the field of ecotoxicology. Common toxicity tests use a small selection of laboratory organisms and focus on acute effects. Yet, aquatic organisms are generally exposed to low levels of micropollutants over their entire lifetime, inducing chronic toxicity or more subtle effects, which are still unknown. Additional questions arise regarding toxicity of human metabolites of pharmaceuticals and transformation products. Considering the overwhelming number of compounds, human metabolites and transformation products, complete experimental assessment of their toxicity is unrealistic. Therefore, future research should focus on the development of simple screening tests (effect-based approach) coupled to computational prediction methods (i.e. methods that estimate metabolite or transformation product toxicity based on the structure and toxicity of the parent) as a first-tier toxicity assessment. In this sense, pre-existing clinical information of pharmaceuticals may also be useful to infer adverse effects, or to assess relative effects of transformation products or metabolites compared to parent compounds. Filling in these gaps will lead to more realistic risk assessments with lower uncertainty

Finally, models are insignificant without environmental or experimental data. The field of analytical chemistry has made tremendous advances, with on-line extraction devices and high-resolution mass spectrometry. Nonetheless, progress can still be made in sample preparation techniques, coping with matrix effects, lowering detection limits and identifying non-target compounds and transformation products.

So, there's a micropollutant plume in the lake... now what?

With respect to the sustainable development of Lake Geneva, which is above all an immense drinking water reservoir, what solutions can be envisioned? Knowledge of a baseline concentration of various micropollutants in the lake, along with at least one localized zone of elevated toxicity associated with micropollutants should trigger some reactions within the affected population and their decision makers.

End-of-pipe solutions, consisting in the improvement of wastewater treatment technologies to decrease the load discharged to surface waters represent an efficient and timely solution. The ineffectiveness of conventional wastewater treatment systems is a key component in the problematic presence of these compounds in surface waters. Alternative approaches and advanced technologies show promising results with respect to removal of micropollutants; nevertheless, currently no treatment technology can completely remove all pharmaceuticals and other contaminants. This highlights the importance of identifying the micropollutants which present a high risk to the environment as was done in this work. Ultimately, a handful of pharmaceuticals and one pesticide contributed significantly to the ecotoxicological risk. These priority micropollutants should be the focus of treatment optimization, all while preventing the formation of toxic by-products, which may occur with some technologies.

Centralized treatment plants, such as the Vidy WWTP, lead to massive point-source release. This may be prevented by decentralization of sewage treatment, which delocalizes the discharge and increases the dilution of effluent,hence avoiding the formation of micropollutant hot spots. Yet, this approach does not solve the issue of overall micropollutant release if conventional treatment technologies are maintained. As such, passive treatment systems, such as constructed wetlands or lagoons present a promising alternative in areas where land space is sufficient.

On a longer-term, preventing entry of micropollutants into the sewer system should also be considered. Various approaches along the “pipeline” of micropollutants are already under investigation, namely segregation of sources (no-mix toilet, separate treatment of hospital wastewater), improvement of drug disposal information, more considerate prescription of pharmaceuticals by doctors and correct usage by patients, and green-pharmaceutical industry.

The adverse effects associated with the presence of trace concentrations of micropollutants in surface waters are undisputed. Many questions remain as to their full extent and the potential human health risks. Currently, there is little evidence showing adverse effects on human health. Yet, facing these uncertainties, the precautionary principle should be applied and preventing entry of micropollutants to the environment is worth the extra cost.

A Appendix - Chapter 2

Antibiotics

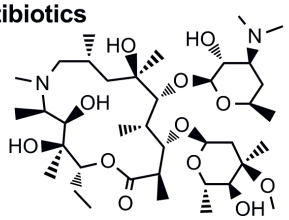

azithromycin
$\log K_{OW}$ =4.02 ; pK_a=8.7

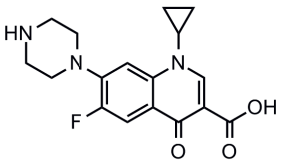

ciprofloxacin
$\log K_{OW}$ = 0.28; pK_a=6.1

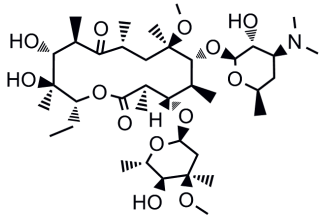

clarithromycin
$\log K_{OW}$ =3.16; pK_a=8.4,12.5

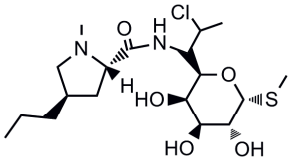

clindamycin
$\log K_{OW}$ = 2.16; pK_a=7.5

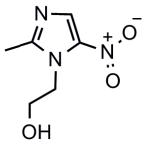

metronidazole
$\log K_{OW}$ = -0.02; pK_a=2.5

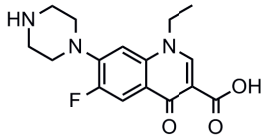

norfloxacin
$\log K_{OW}$ = -1.03; pK_a=6.4, 8.7

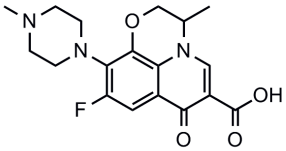

ofloxacin
$\log K_{OW}$ =-0.39; pK_a=5.7, 7.1

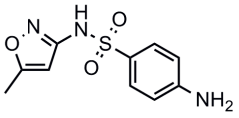

sulfamethoxazole
$\log K_{OW}$ = 0.89; pK_a=1.6, 5.7

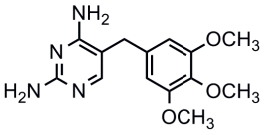

trimetoprim
$\log K_{OW}$ = 0.91; pK_a=7.1

Analgesics/Anti-inflammatories

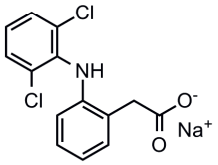

diclofenac
$\log K_{OW}$ = 4.51; pK_a=4.1

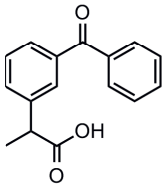

ketoprofen
$\log K_{OW}$ = 3.12; pK_a=4.5

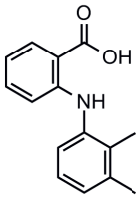

mefenamic acid
$\log K_{OW}$ = 5.12; pK_a=4.2

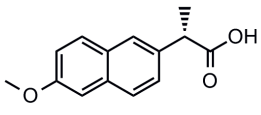

naproxen
$\log K_{OW}$ = 3.18; pK_a=4.2

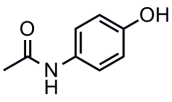

paracetamol
$\log K_{OW}$ = 0.46; pK_a=9.4

Beta blockers

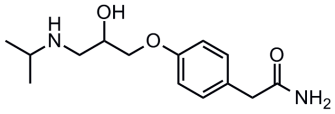

atenolol

$\log K_{OW}$ = 0.16; pK_a=9.6

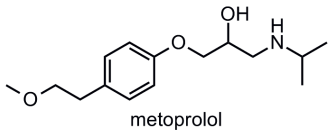

metoprolol

$\log K_{OW}$ = 1.88; pK_a=9.7

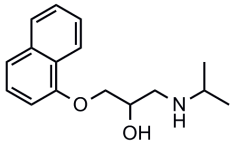

propranolol

$\log K_{OW}$ = 3.48; pK_a=9.4

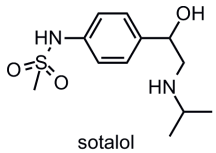

sotalol

$\log K_{OW}$ = 0.24; pK_a=8.2, 9.1

Lipid regulators

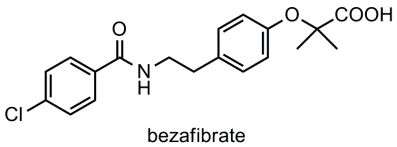

bezafibrate

$\log K_{OW}$ = 4.25; pK_a=NA

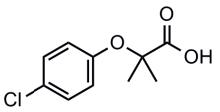

clofibric acid

$\log K_{OW}$ = 2.57; pK_a=3.5

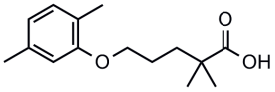

gemfibrozil

$\log K_{OW}$ = 4.77; pK_a=4.7

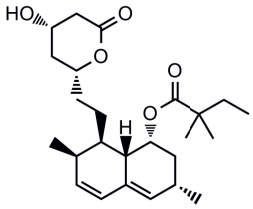

simvastatin

$\log K_{OW}$ = 4.68; pK_a=13.5

Antiepileptics

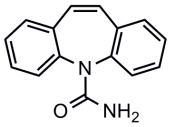

carbamazepine

$\log K_{OW}$ = 2.45; pK_a=7.0

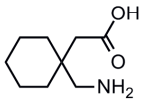

gabapentine

$\log K_{OW}$ = -1.1; pK_a=3.7

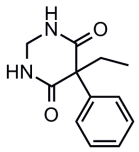

primidon

$\log K_{OW}$ = 0.91; pK_a=NA

X-ray contrast media

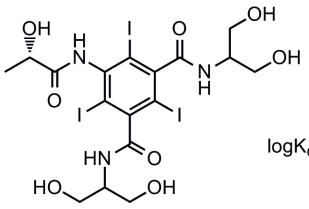

iopamidol

$\log K_{OW}$ = -2.24; pK_a=NA

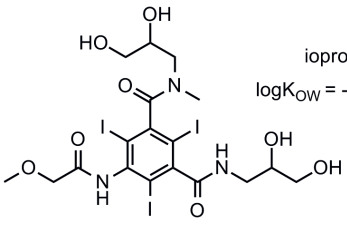

iopromide

$\log K_{OW}$ = -2.05; pK_a=NA

Herbicides

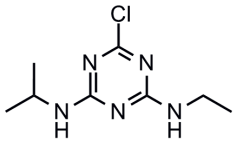

atrazin

$\log K_{OW}$ = 2.61; pK_a=1.7

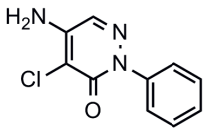

chloridazon

$\log K_{OW}$ = 1.14; pK_a=3.4

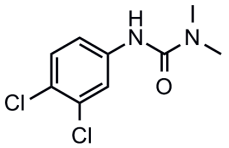

diuron

$\log K_{OW}$ = 2.68; pK_a=NA

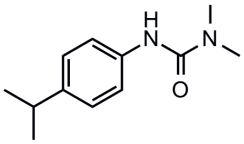

isoproturon

$\log K_{OW}$ = 2.87; pK_a=NA

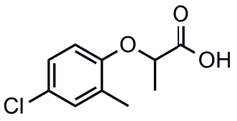

mecoprop

$\log K_{OW}$ = 3.13; pK_a=3.1

Fungicides

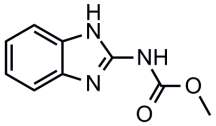

carbendazim

$\log K_{OW}$ = 1.52; pK_a=4.2

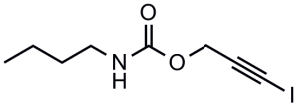

IPBC

$\log K_{OW}$ = 2.54; pK_a=NA

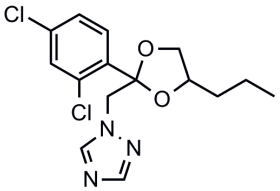

propiconazole

$\log K_{OW}$ = 3.72; pK_a=1.1

Algicides

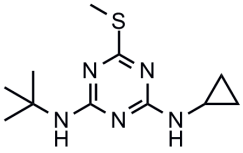

irgarol

$\log K_{OW}$ = 4.07; pK_a=NA

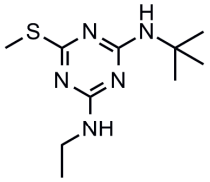

terbutryn

$\log K_{OW}$ = 3.74; pK_a=4.3

Corrosion inhibitors

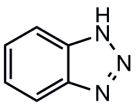

benzotriazole

$\log K_{OW}$ = 1.44; pK_a=8.4

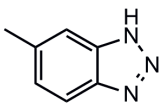

methylbenzotriazole

$\log K_{OW}$ = 1.71; pK_a=NA

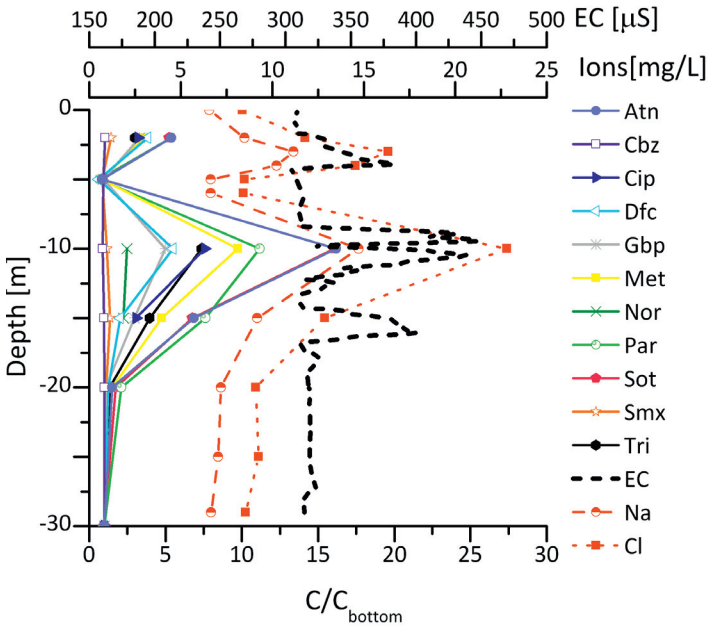

Figure A.1: *Profiles of electrical conductivity (EC), ions Na^+ and Cl^- and pharmaceuticals above the WWTP discharge point in April 2010.*

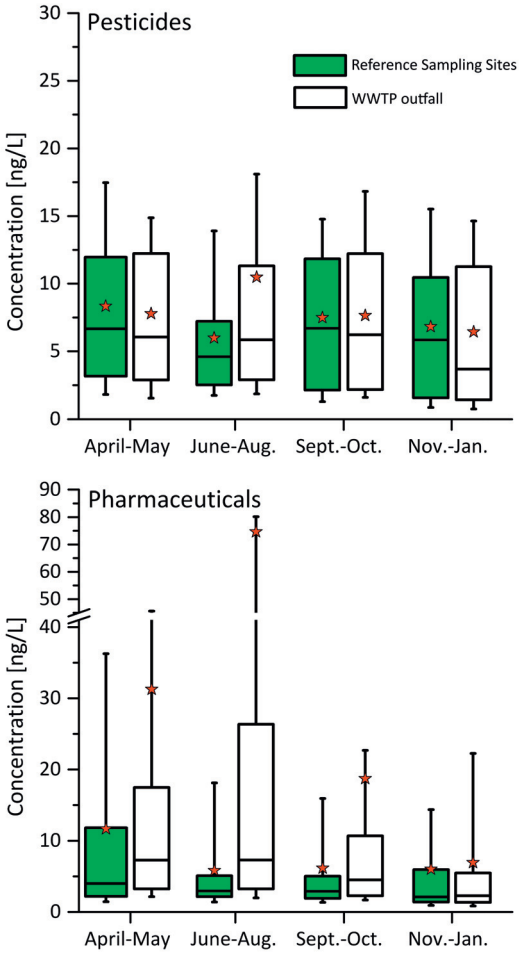

Figure A.2: *Seasonal comparison of measured concentrations of pharmaceuticals (top figure) at the WWTP outfall (white) and at the reference points (green). Concentrations are generally lower at the reference point with a more perceptible difference in summer. In contrast, concentrations of pesticides (bottom figure) show no significant differences between WWTP outfall and reference points (note that uncharacteristic compounds, namely carbamazepin, benzotriazol, methylbenzotriazol and carbendazim, were removed for the analysis). Boxes represent* 25^{th} *percentile, median and* 75^{th} *percentile. The whiskers are determined by the* 10^{th} *and* 90^{th} *percentiles. Stars show the mean value. Mean values of pharmaceuticals are pulled towards higher values by outliers (e.g. high concentrations in plume).*

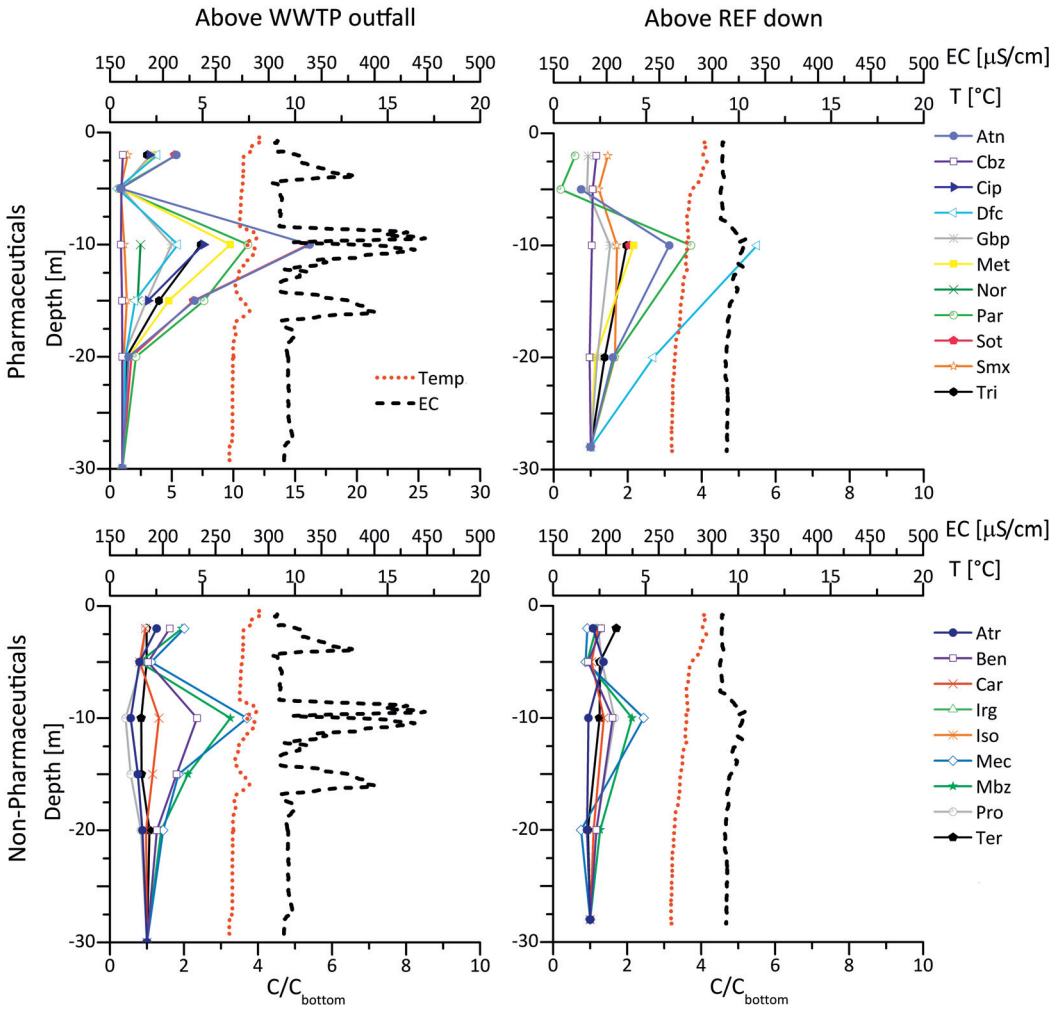

Figure A.3: *Concentration depth profiles for pharmaceuticals (top) and non-pharmaceuticals (bottom) above the WWTP discharge point (left) and above the down-stream reference point (REF down) (right) in April 2010. Concentrations are relative to the concentration detected at the bottom. A small concentration peak at REF down (-10 m) was observed only on this occasion (April 2010). EC: electrical conductivity, T: temperature, Atn: atenolol, Cbz: carbamazepin, Cip: ciprofloxacin, Dfc: diclofenac, Gbp: gabapentin, Met: metoprolol, Nor: norfloxacin, Par: paracetamol, Sot: sotalol, Smx: sulfamethoxazol, Tri: trimetoprim, Atr: atrazin, Ben: benzotriazol, Car: carbendazim, Irg: irgarol, Iso: isoproturon, Mec: mecoprop, Mbz: methylbenzotriazol, Pro: propiconazol, Ter: terbutryn.*

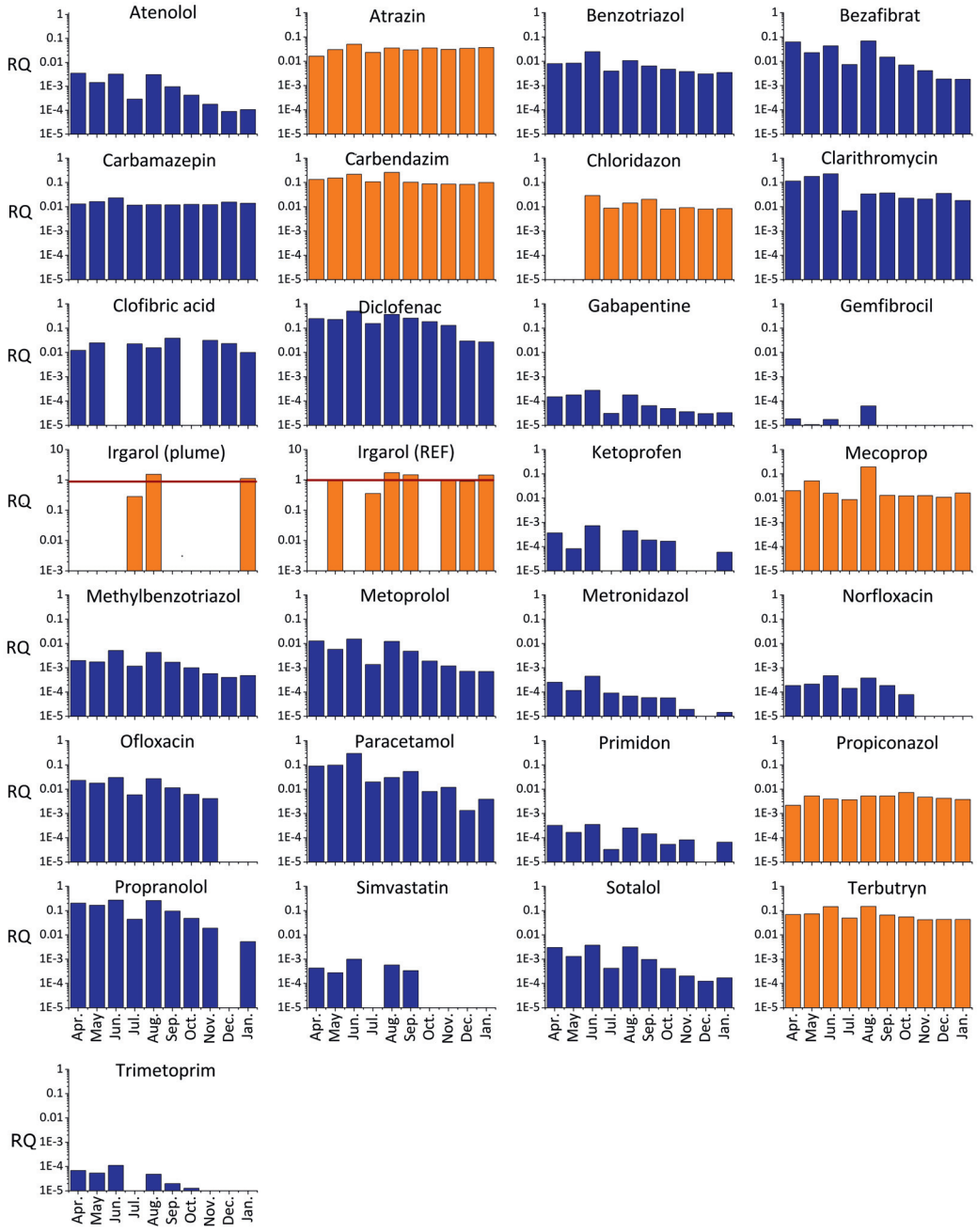

Figure A.4: *Chronology of risk quotient (RQ) in plume for all micropollutants. Pharmaceuticals in blue and non-pharmaceuticals in orange.*

Table A.1: *Retention times (RT) and deuterated surrogate standard (Surr. Std) or assigned deuterated surrogate standard with corresponding mean relative recovery (25^{th} and 75^{th} percentile of averaged monthly recoveries).*

Compound	UPLC RT [min]	Surr. Std	Mean Recovery
atenolol	3.5	atenolol-d7	0.99-1.08
atrazin	13.2	atrazine-d5	0.63-0.67
azithromycin	11.5	azithromycin-d3	0.90-1.01
benzotriazol	7.2	benzotriazol-d4	0.64-0.74
bezafibrat	14.1	bezafibrat-d4	1.26-1.41
carbamazepin	12.7	carbamazepine-d10	0.82-0.92
carbendazim	6.0	gabapentine-d4	
chloridazon	9.3	primidon-d5	
ciprofloxacin	8.4	ciprofloxacin-d8	0.43-0.75
clarithromycin	14.0	bezafibrat-d4	
clindamycin	12.0	carbamazepine-d10	
clofibric acid	13.8	ketoprofen-d3	
diclofenac	15.0	diclofenac-d4	0.71-0.88
diuron	13.0	atrazine-d5	
gabapentin	5.8	gabapentine-d4	1.06-1.13
gemfibrozil	15.8	simvastatin-d6	
iopamidol	1.7	paracetamol-d3	
iopromid	4.0	iopromide-d3	1.09-1.19
IPBC	13.0	atrazine-d5	
irgarol	13.4	irgarol-d9	0.39-0.48
isoproturon	13.3	isoproturon-d6	0.89-0.98
ketoprofen	13.7	ketoprofen-d3	1.40-1.46
mecoprop	14.2	bezafibrat-d4	
mefenamic acid	15.7	mefenamic acid-d3	0.27-0.51
methylbenzotriazol	10.1	azithromycin-d3	
metoprolol	9.3	primidon-d5	0.98-1.02
metronidazol	2.4	paracetamol-d3	
naproxen	13.9	ketoprofen-d3	
morfloxacin	8.1	ofloxacin-d8	
ofloxacin	7.9	ofloxacin-d8	0.59-0.74
paracetamol	3.3	paracetamol-d3	0.82-0.94
primidon	9.2	primidon-d5	1.05-1.21
propiconazol	15.2	diclofenac-d4	
propranolol	11.7	azithromycin-d3	
simvastatin	16.3	simvastatin-d6	0.49-0.69
sotalol	2.4	paracetamol-d3	
sulfamethoxazol	7.8	sulfamethoxazol-d4	0.68-.89
terbutryn	13.0	atrazine-d5	
trimethoprim	7.0	metoprolol-d5	

Uncertainty budget

The main sources of uncertainty of determined concentrations are i) the uncertainty associated to recovery, ii) the uncertainty linked to repeatability of measurements and iii) the uncertainty associated with calibration. Each uncertainty is quantified as a standard deviation (SD) (gaussian distribution) to show the extent of the variance around the cited value. The main sources of uncertainty are clarified below:

Recovery uncertainty (SD_R) Extraction recoveries were determined for the 20 deuterated surrogates and for each sampling day. Measured sample concentrations of each substance were corrected by the average extraction efficiency of its corresponding deuterated surrogate. The uncertainty of recovery arises from the uncertainty linked to using the monthly average recovery, rather than individual sample recoveries, to determine the micropollutant concentrations in each sample. The uncertainty of recovery was thus expressed as the SD of all individual recoveries for a given compound over the entire sampling period. Substances lacking deuterated surrogates were attributed the SD_R of their assigned surrogate compound.

Repeatability uncertainty (SD_{rep}) The uncertainty associated with repeatability is represented by the variability of the overall method reproducibility tests. In these tests, two sets of eight replicates of lake water were spiked with all 39 micropollutants to concentration of 3 and 70 ng·L^{-1}, respectively, and were put through the entire sample workup procedure (extraction-UPLC-MS/MS-calculation of concentration via calibration curves). For replicates spiked to 70 ng·L^{-1}, the SD of entire procedure was lower than 15% of the calculated concentration for the large majority of the compounds. The SD increased for replicates spiked to 3 ng·L^{-1}, yet remained below 20% for most compounds. The SD from reproducibility tests performed with 3 ng·L^{-1} was used to calculate the total uncertainty.

Calibration uncertainty (SD_{cal}) The uncertainty of calibration is linked to using a calibration curve technique to interpolate the concentration of a given compound in the sample. This source of uncertainty was found to be smaller than i) and ii) and is already included in the uncertainty budget in ii). Indeed, the higher SD for replicates spiked with only 3 ng·L^{-1} is due to an increase in uncertainty of the calibration. Indeed, the lower concentration lies towards the lower end of the calibration curve, thus uncertainty increases.

The total uncertainty combines the individual sources of uncertainty according to the following equation, assuming individual uncertainties are not correlated:

$$SD_{tot} = \sqrt{SD_R^2 + SD_{rep}^2 + SD_{cal}^2} \tag{A.1}$$

As SD_{cal} is small and already included SD_{rep}, the worst case total SD simplifies to:

$$SD_{tot} = \sqrt{SD_R^2 + SD_{rep}^2} \tag{A.2}$$

The above described method used to estimate uncertainties in analytical procedures using chromatographic techniques was adapted from the method proposed by Koneiczka et al. [192]. SD_R and SD_{rep}, as well as the total relative uncertainty linked to each individual compound are listed in table A.2 hereafter.

Table A.2: *Total uncertainty of each individual compound computed from STD_{rep2} (or when missing SD_{rep1}) and SD_R according to equation A.2.*

Compound	SD_{rep1}[1]	SD_{rep2}[2]	**SD_R**	**SD_{tot}**
atenolol	0.07	0.25	0.14	**0.28**
atrazin	0.08	0.14	0.3	**0.33**
azithromycin	0.1	0.11	0.18	**0.21**
benzotriazol	0.07	0.09	0.22	**0.24**
bezafibrat	0.15	0.33	0.18	**0.38**
carbamazepin	0.06	0.15	0.22	**0.27**
carbendazim	0.08	0.07	0.18	**0.31**
chloridazon	0.07	0.08	0.16	**0.35**
ciprofloxacin	0.11	0.2	0.3	**0.27**
clarithromycin	0.23	0.09	0.18	**0.16**
clindamycin	0.07	0.09	0.22	**0.23**
clofibric acid	0.25	0.22	0.21	**0.47**
diclofenac	0.08	0.29	0.34	**0.38**
diuron	0.14	0.13	0.3	**0.25**
gabapentin	0.08	0.11	0.18	**0.51**
gemfibrozil	0.1	0.24	0.55	**0.28**
iopamidol	0.09	0.08	0.2	**0.56**
iopromid	0.1	-	0.21	**0.23**
IPBC	0.18	0.3	0.3	**0.42**
irgarol	0.11	0.16	0.41	**0.21**
isoproturon	0.16	0.29	0.25	**0.29**
ketoprofen	0.14	0.1	0.21	**0.11**
mecoprop	0.17	0.15	0.18	**0.15**
mefenamic acid	0.25	0.26	0.49	**0.26**
methylbenzotriazol	0.06	0.09	0.18	**0.09**
metoprolol	0.06	0.09	0.14	**0.1**
metronidazol	0.07	0.13	0.2	**0.23**
naproxen	0.24	0.16	0.21	**0.16**
norfloxacin	0.11	0.11	0.25	**0.11**
ofloxacin	0.18	0.12	0.25	**0.13**
paracetamol	0.09	0.06	0.2	**0.06**
primidon	0.06	0.09	0.16	**0.09**
propiconazol	0.09	0.14	0.34	**0.14**
propranolol	0.07	0.18	0.18	**0.18**
simvastatin	0.08	0.24	0.55	**0.25**
sotalol	0.08	0.11	0.2	**0.11**
sulfamethoxazol	0.1	0.13	0.35	**0.13**
terbutryn	0.11	0.2	0.3	**0.21**
trimethoprim	0.06	0.12	0.14	**0.12**

[1] SD_{rep1}: SD of eight replicate samples spiked with 39 micropollutants to a concentration of 70 ng·L^{-1}

[2] SD_{rep2}: SD of eight replicate samples spiked with 39 micropollutants to a concentration of 3 ng·L^{-1}

Table A.3: *Predicted no-effect concentrations (PNECs) of individual compounds and method used to derive PNEC.*

	PNEC ($ng \cdot L^{-1}$)[3]	Method[4]	**Source**
atenolol	33'400	SF	Perazzolo et al. 2010[2]
atrazin	420	SSD	Chèvre et al. 2006[67]
azithromycin	10	SF	present study (Table A.4)
benzotriazol	30'000	-	OekotoxZentrum[193]
bezafibrat	1'191	SF	Perazzolo et al. 2010[2]
carbamazepine	2'500	SF	Perazzolo et al. 2010[2]
carbendazim	100	SSD	Junghans et al. 2010[194]
chloridazon	97	SF	present study (Table A.4)
ciprofloxacin	5	SF	Perazzolo et al. 2010[2]
clarithromycin	60	-	OekotoxZentrum[193]
clindamycin[5]	-	-	-
clofibric acid	397	SF	Perazzolo et al. 2010[2]
diclofenac	100	SF	Perazzolo et al. 2010[2]
gabapentin	1'000'000	SF	Perazzolo et al. 2010[2]
gemfibrozil	751'000	SF	Perazzolo et al. 2010[2]
irgarol	1.6	SSD	present study (Table A.5)
ketoprofen	15'600	SF	present study (Table A.4)
mecoprop	1'000	SSD	Chèvre et al. 2007[195]
methylbenzotriazol	75'000	-	OekotoxZentrum[193]
metoprolol	3'200	SF	Perazzolo et al. 2010[2]
metronidazol	25'000	SF	present study (Table A.4)
norfloxacin	40'100	SF	Perazzolo et al. 2010[2]
ofloxacin	500	SF	present study (Table A.4)
paracetamol	9'200	SF	present study (Table A.4)
primidon	54'171	SF	Perazzolo, unpublished data
propiconazol	1'220	SSD	Chèvre et al. 2007[195]
propranolol	50	SF	Perazzolo et al. 2010[2]
simvastatin	9'600	SF	Perazzolo, unpublished data
sotalol	15'935	SF	Perazzolo et al. 2010[2]
sulfamethoxazol	26.8	SF	Perazzolo et al. 2010[2]
terbutryn	40	SSD	Chèvre et al. 2006[67]
trimethoprim	160'000	SF	present study (Table A.4)

[3] PNEC or PNEC-equivalent in $ng \cdot L^{-1}$

[4] Method used to determine PNEC:
SF: derived from NOEC or EC50 and corrected with a safety factor (SF);
SSD: HC5 was derived from a species sensitive distribution curve (SSD) (see Table A.5 for an example), and reported PNEC is a PNEC-equivalent equal to HC5/5.

[5] no ecotoxicity data

Table A.4: *PNEC values with ecotoxicity data for the three trophic levels (algae, crustaceans, fish). PNEC values were derived according to the method reported in Perazzolo et al.[2], and safety factors chosen based on recommendations in the Technical guidance document on risk assessment[68]. PNEC: predicted no-effect concentration; NOEC: no-observed effect concentration; EC50: Effect Concentration 50% (concentration at which 50% of the tested (generally acute tests) organism shows the targeted endpoint, generally mortality); SF: safety factor used to derive PNECs.*

	PNEC ($\mu g \cdot L^{-1}$)	**SF**	**Algae (type)** ($\mu g \cdot L^{-1}$)	**Crustaceans** ($\mu g \cdot L^{-1}$)	**Fish** ($\mu g \cdot L^{-1}$)	**Sources**
azithromycin	**0.0094**	100	0.94 (EC50)	4.4 (NOEC)	84'000 (NOEC)	[196]
chloridazon	**0.097**	1000	97 (EC50)	180 (EC50)	199'000 (LC50)	[197]
ketoprofen	**15.6**	1000	15'600 (EC50)[6]	97'000 (EC50)	64'000 (LC50)	[196]
metronidazol	**25**	500	12'500 (EC50)	100'000 (EC50)	500'000 (NOEC)	[196]
ofloxacin	**0.5**	10	5 (NOEC)	10'000 (NOEC)	16'000 (NOEC)	[198]
paracetamol	**9.2**	1000	134'000 (EC50)	9'200 (EC50)	378'000 (EC50)	[199]
trimethoprim	**160**	100	16'000 (EC50)	100'000 (NOEC)	100'000 (NOEC)	[196]

Table A.5: *Ecotoxicity data (NOEC) and corresponding sources used to derive HC5 for pestide irgarol using a species sensitive distribution (SSD) curve (see figure A.5). Algae being the most sensitive taxon to irgarol, only algal species were considered for the SSD. NOEC: No-observed effect concentration; HC5: Hazardous concentration 5% (concentration that affects 5% of aquatic species). ETX 2.0 software (Normal distribution based hazardous concentration and fraction affected; software by RIVM, Bilthoven, the Netherlands, 2004)*

Species Scientific Name	**NOEC in μg·L^{-1}**	**Source**
Apium nodiflorum	0.2	Lambert et al. 2006[200]
Chara vulgaris	0.001	Lambert et al. 2006[200]
Chlorella fusca ssp. Vacuolata	0.506	Arrhenius et al. 2006[201]
Chroococcus minor	1	Zhang et al. 2008[202]
Dunaliella tertiolecta	0.09	DeLorenzo et al.[203]
Eisenia bicyclis	0.757	Okamura et al. 2000[204]
Elodea Canadensis	0.8	Nyström et al. 2002[205]
Enteromorpha intestinalis	0.05	Scarlett et al. 1997[206]
Fucus serratus	8	Braithwaite et al. 2005[207]
Lemna gibba	0.4	Van Wezel et al. 2004[208]
Myriophyllum spicatum	2	Lambert et al. 2006[200]
Navicula accomoda	0.1	Nyström et al. 2002[205]
Navicula pelliculosa	0.017	Van Wezel et al. 2004[208]
Nitzschia sp.	0.1	Nyström et al. 2002[205]
Porphyra yezoensis	0.543	Okamura et al. 2000[204]
Potamogeton pectinatus	2.53	Nyström et al. 2002[205]
Scenedesmus subspicatus	0.23	Van Wezel et al. 2004[208]
Scenedesmus vacuolatus	0.507	Arrhenius et al. 2006[201]
Selenastrum capricornutum	1.803	Van Wezel et al. 2004[208]
Skeletonema costatum	0.01	Zhang et al. 2008[202]
Thalassiosira pseudonana	0.1	Zhang et al. 2008[202]
HC5 (computed using ETX 2.0)= 0.008 μg·L^{-1} $\Rightarrow$ PNEC-equivalent = HC5/5 = 1.6 ng·L^{-1}		

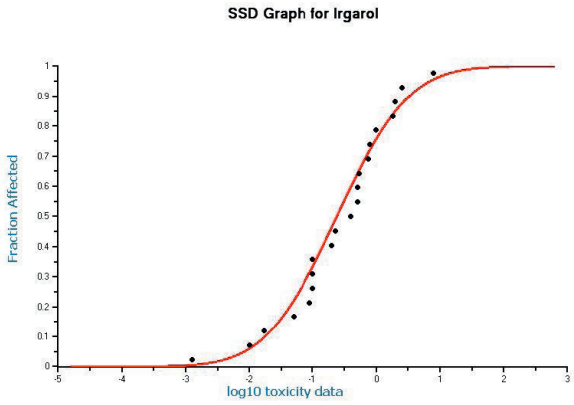

Figure A.5: *Species sensitivity distribution for irgarol, using data from table A.5*

B Appendix - Chapter 3

Calculation of bimolecular reaction rate constant with hydroxyl radical

Equation 3.2 from text:

$$k^0_{tot,i} - k^0_{direct,i} = k'_{OH,i} = [^\bullet OH]_{ss} \cdot k_{\bullet OH,i}$$

Values from literature (Table 3.1) were used to estimate the $[^\bullet OH]_{ss}$ in each experimental beaker containing a mixture of substances with known (from literature) and unknown bimolecular rate constants with $^\bullet$OH, via equation 3.2. Consequently, unknown bimolecular rate constants were calculated with the estimated $[^\bullet OH]_{ss}$ from the corresponding experimental beaker.

Calculation of $[^\bullet OH]_{ss,lake}$

The concentration of hydroxyl radicals in surface waters can be approximated by the ratio of the rates of production and consumption of $^\bullet$OH[19]:

$$[^\bullet OH] = \frac{k_{abs,NO_3^-} \cdot \Phi_{f,NO_3^-} \cdot [NO_3^-] + k_{abs,NO_2^-} \cdot \Phi_{f,NO_2^-} \cdot [NO_2^-]}{k'_{\bullet OH,DOC} \cdot [DOC] + k'_{\bullet OH,HCO_3^{2-}} \cdot [HCO_3^{2-}] + k'_{\bullet OH,CO_3^-} \cdot [CO_3^-]} \quad \text{(B.1)}$$

The values used in equation B.1 are given in Table B.1.

Table B.1: *Parameters used in equation B.1*

	Summer	**Winter**	**Unit**	
k_{abs,NO_3^-}	$1.31 \cdot 10^{-5}$	$1.89 \cdot 10^{-6}$	$M^{-1} \cdot s^{-1}$	specific rate of light absorption of nitrate, noon
Φ_{f,NO_3^-}	0.007	0.007	-	quantum yield of $^\bullet$OH formation by nitrate
$[NO_3^-]$	$2.9 \cdot 10^{-5}$	$2.9 \cdot 10^{-5}$	M	nitrate concentration (measured)
$[NO_2^-]$	0	0	M	nitrite concentration (measured)
$k'_{\bullet OH,DOC}$	$2.5 \cdot 10^4$	$2.5 \cdot 10^4$	$(mg\ C)^{-1} s^{-1}$	reaction rate constant between $^\bullet$OH and DOC[106]
[DOC]	1.4	1.1	$mg\ C \cdot L^{-1}$	dissolved organic carbon concentration (measured[142])
$k'_{\bullet OH,HCO_3^{2-}}$	$1 \cdot 10^7$	$1 \cdot 10^7$	$M^{-1} \cdot s^{-1}$	reaction rate constant between $^\bullet$OH and HCO_3^{2-}[209]
$[HCO_3^{2-}]$	$2.25 \cdot 10^{-3}$	$2.25 \cdot 10^{-3}$	M	bicarbonate concentration (calculated) (a)
$k'_{\bullet OH,CO_3^-}$	$4 \cdot 10^8$	$4 \cdot 10^8$	s^{-1}	reaction rate constant between $^\bullet$OH and CO_3^-[209]
$[CO_3^-]$	$3.73 \cdot 10^{-5}$	$9.8 \cdot 10^{-6}$	$M^{-1} \cdot s^{-1}$	carbonate concentration (b)
$[OH]_{ss,noon}$	$3.95 \cdot 10^{-17}$	$6.79 \cdot 10^{-18}$	M	$^\bullet$OH steady state concentration, noon
$[OH]_{ss,24h}$	$1.74 \cdot 10^{-17}$	$3 \cdot 10^{-18}$	M	$^\bullet$OH steady state concentration, 24h

(a) $[HCO_3^{2-}] = 2 \cdot [Ca^{2+}]$

(b) $\log[CO_3^-] = pH - pK_a - \log[HCO_3^{2-}]$

Important model parameters (more details found in Razmi et al.[141]):

Wind speed, direction: Bise: 3 $m \cdot s^{-1}$, 10° ; Vent: 3 $m \cdot s^{-1}$, 240°

Radius of release: 10 m

Vertical dispersion coefficient: 0.0001-0.00001 (depending on the stratification)

Density of water: 1000 $kg \cdot m^3$

Horizontal dispersion coefficient: $t^{0.01}$ (t= particle age), recommended by Delft3D-PART

Stratification: a classic stratification for Lake Geneva in summer time with the thermocline around 14-16 m depth in Vidy Bay.

Time to steady state:

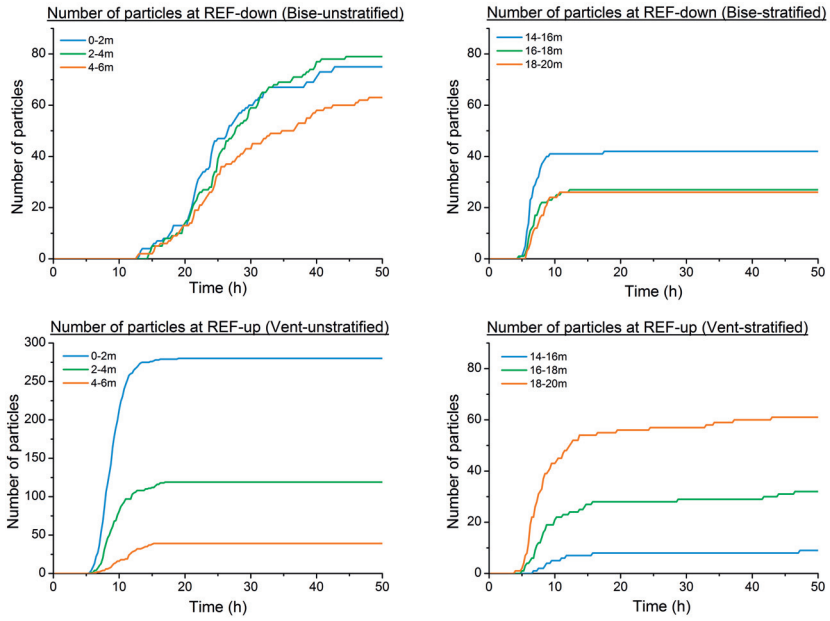

Figure B.1: *Number of particles over time in different layers at REF-down (top figures) and REF-up (bottom figures) for the Bise and Vent scenarios, respectively. The initial increase of particles indicates the minimal travel-time from the WWTP outfall to the considered reference location. Steady state is reached once the number of particle stabilizes.*

Concentration depth profiles for Bise conditions:

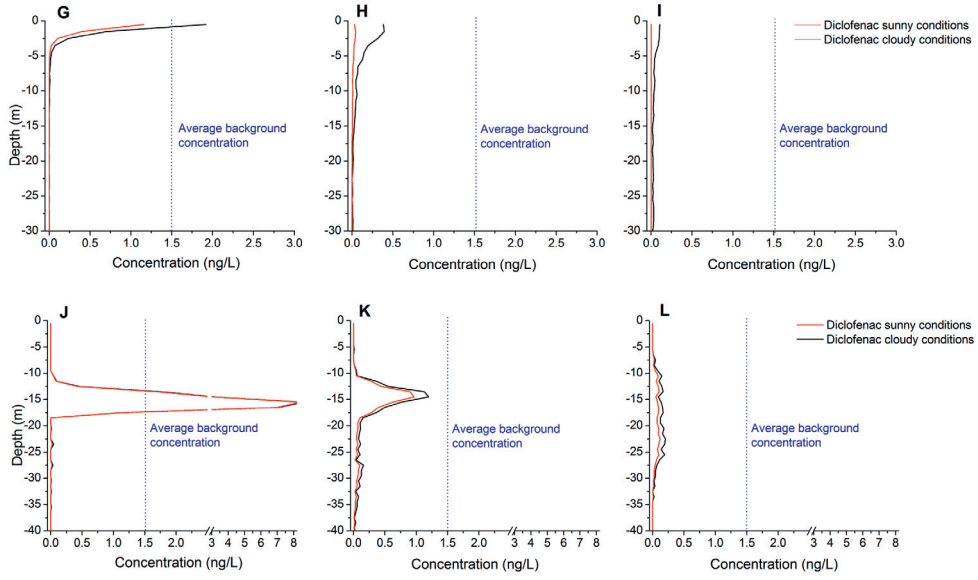

Figure B.2: *Modeled concentration depth profiles for diclofenac under unstratified Bise (top), and stratified Bise (bottom) for the locations G-L marked by blue crosses in figure 3.3.*

C Appendix - Chapter 5

Absolute and normalized spectrum of 300 nm bulbs, solar simulator and simulated solar spectrum (SMARTS)

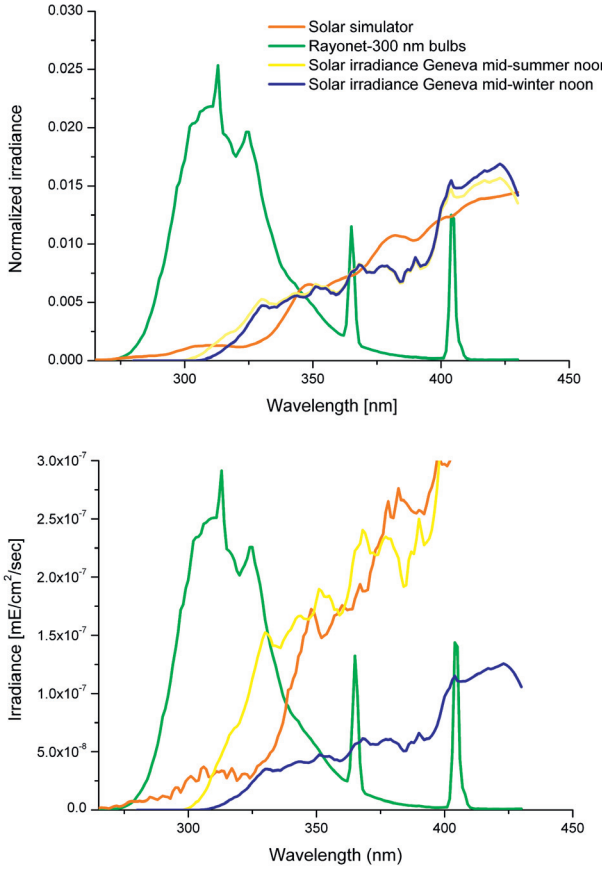

Figure C.1: *Top: Normalized irradiance of the different experimental light sources (Rayonet -measured from within the test tubes- and solar simulator) and of the computed SMARTS solar irradiance for a sunny day at 47° N (Geneva) for a summer scenario (21st June) and winter scenario (21st December) Values are normalized over the relevant wavelength interval of 265–430nm. Note that, though the solar simulator spectrum extends below 280 nm, excess UVB compared to the solar spectrum only amounts to 1% of the total intensity. Bottom: Absolute irradiance of the different experimental light sources (Rayonet -measured from within the test tubes- and solar simulator) and of the computed SMARTS solar irradiance for a sunny day at 47° N for a summer scenario (21st June) and winter scenario (21st December).*

Absorbance versus pH for $pK_{a,2}$ determination

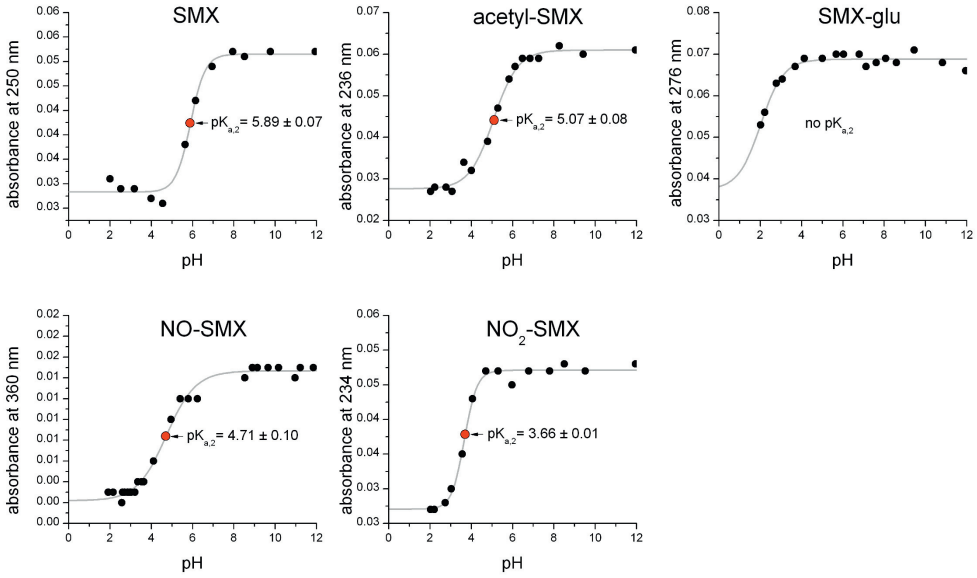

Figure C.2: *Absorbance values at a single wavelength versus pH for SMX and its human metabolites. Grey line represents the least square fit of sigmoidal Boltzman function* $y = \frac{A_1 - A_2}{1+e^{\frac{x-x_0}{dx}}} + A_2$*, where* x_0 *is the inflection point (i.e* $pK_{a,2}$ *value) and* A_1 *and* A_2 *are, respectively, the lower and upper asymptotes. Error reflects the standard deviation of* x_0*.*

Molar absorptivity at pH conditions used in photolysis experiments

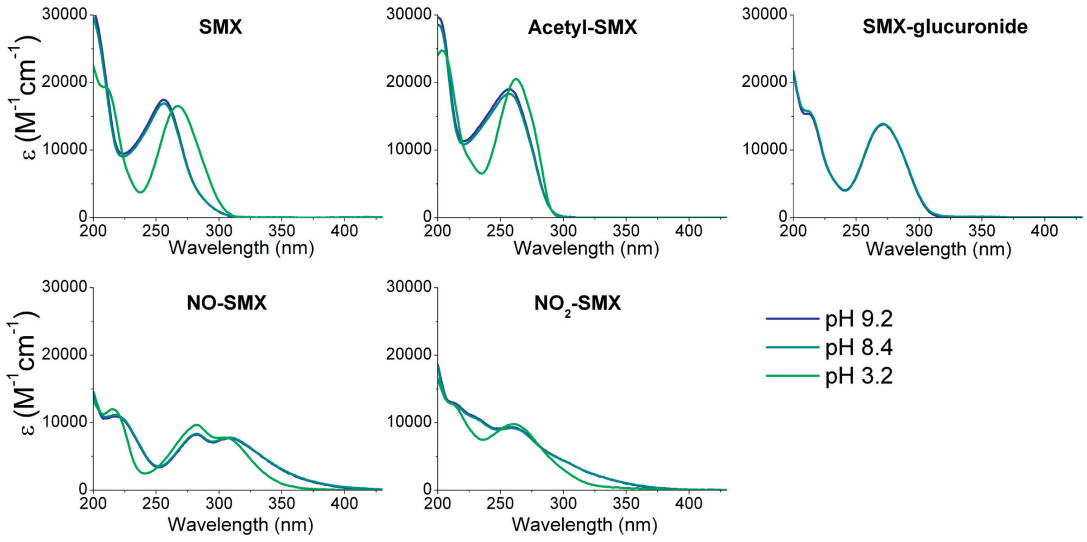

Figure C.3: *Absorption spectra (Molar absorptivity* ε*) of the irradiated target compounds at the different experimental pH-values.*

Direct photolysis kinetics

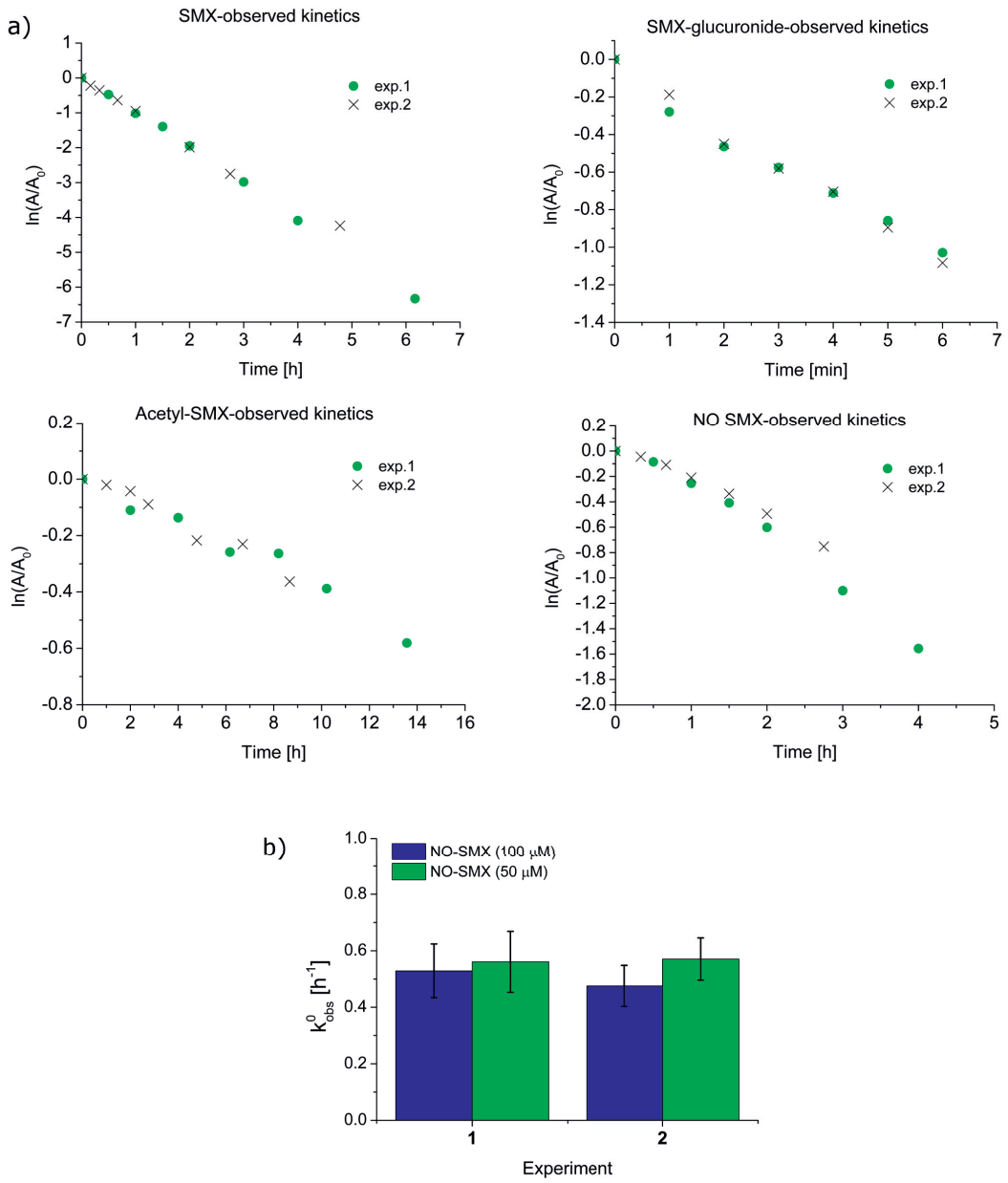

Figure C.4: *Direct photolysis kinetics: a)First-order direct photolysis kinetics for SMX and its human metabolites; b) comparison of direct photolysis rate constants for experiments with single (50 µM, green bars) and double concentration (100 µM blue bars).*

Examples of spectral overlap of compound absorbance and irradiance

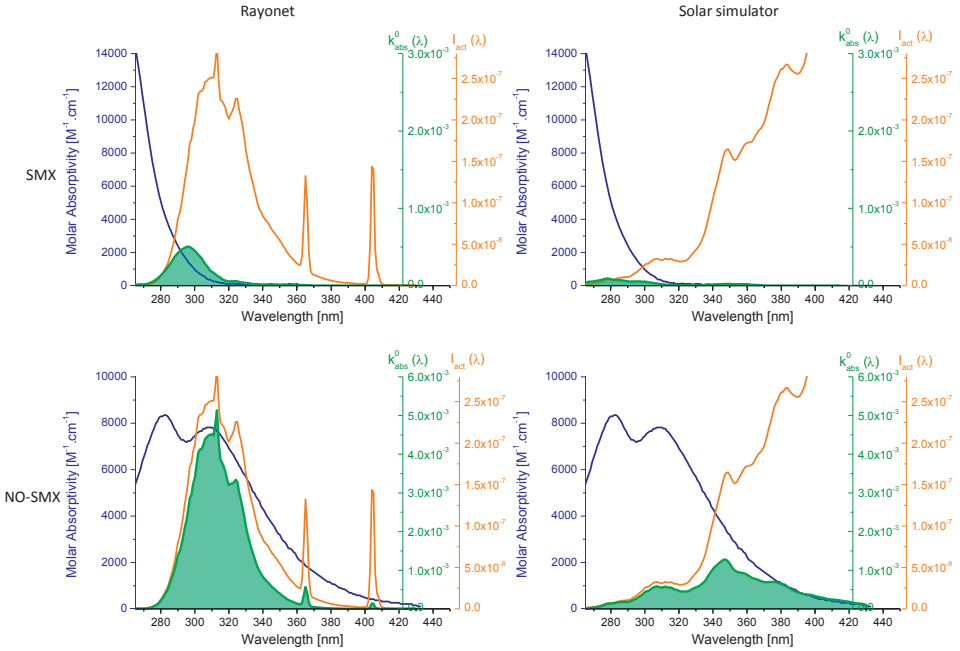

Figure C.5: *Top panels: Spectral overlap (specific rate of light absorption $k^0_{abs,i}$) of SMX in the Rayonet setup (left) and Solar simulator setup (right). Bottom panels: Spectral overlap (specific rate of light absorption $k^0_{abs,i}$) of NO-SMX in the Rayonet setup (left) and Solar simulator setup (right). *Spectral overlap (green shaded area): overlap of compound absorbance spectrum (blue line) and spectrum of light source (orange line). Attention is brought to the small overlap of SMX (and similarly absorbing compounds: Acetyl-SMX and SMX-glucuronide) in the solar simulator setup.*

Analytical methods

Composition of irradiated solutions

The irradiated solutions of the target compounds in Nanopure water were buffered using various chemicals, depending on the desired pH, in order to maintain a stable pH in solution. pH values measured before experiments always remained stable for the entire irradiation time. The composition and pH of the various buffers are described below:

- **acidic experiments** (pH 3.2, solar simulator setup): acidic experiments (pH 3.2, solar simulator setup): 0.1 mM citric acid, 0.5 mM HCl.
- **basic experiments** (pH 8.4, solar simulator setup): 2 mM sodium bicarbonate.
- **basic experiments** (pH 9.2, Rayonet setup): 1 mM sodium tetraborate decahydrate.

Description of isocratic and gradient modes from Table C.1

Gradients are expressed as % of eluent A over time

- **Isocratic 1** run time : 5 min, 60% eluent A-40% eluent B
- **Gradient 1** run time : 14 min. 0-3 min: 80% A, 3–4 min: ramp to 75%, 4–6 min: ramp to 72%, 6–8 min: ramp to 5%, 8–10 min: 5%, 10–11 min: ramp to 80%, 11–14 min: equilibrate at 80%.
- **Gradient 2** run time : 11 min. 0 min: 95% A, 1–7 min: ramp to 75%, 7–8 min: ramp to 5%, 8–9 min: ramp to 95%, 9–11 min: equilibrate at 95%.
- **Gradient 3** run time : 45 min. 0–11 min: 100% A, 11–12 min: ramp to 87%, 4–6 min: ramp to 72%, 12–36 min: 87%, 36–37 min: ramp to 100%, 37–45 min: equilibrate at 100%.
- **Gradient 4** run time : 42 min. 0–4 min: 99% A, 4–8 min: ramp to 79%, 8–17 min: 79%, 17–19 min: ramp to 63%, 19–28 min: 63%, 28–29 min: ramp to 10%, 29–31 min: 10%, 31–32 min: ramp to 99%, 32–42 min: equilibrate at 99%.

Table C.1: *Analytical methods used to perform quantitative analysis for the different setups. ESI:electrospray ionization; n.a.: not applicable. Gradients are described below the table.*

Experimental setup	Compounds	Instrument	Chromatography column	Eluent A	Eluent B	Flow	Injection volume	Flow rate	ESI mode	Detection wavelength
Solar Simulator	SMX, Ac-SMX, NO_2-SMX, SMX-glucuronide	Aquity UPLC w/ TQD MS/MS, Waters	Acquity UPLC BEH C18 1.7µM	95% H_2O, 5% MeOH, 1% formic acid, 5mM ammonium formate	5% H_2O, 95% MeOH, 1% formic acid, 5mM ammonium formate	Gradient 1	7.5 µL	0.3 mL/min	+/-	n.a.
	NO-SMX	Aquity UPLC w/ TQD MS/MS, Waters	Acquity UPLC BEH C18 1.7µM	100% H_2O, 5 mM ammonium formate	100% ACN	Gradient 2	7.5 µL	0.3 mL/min	-	n.a.
Rayonet with 6 300 nm bulbs	SMX and metabolites	Dionex HPLC UV	Supelco Discovery C16 RP amide (15 cm × 173 4.6 mm, 5 µm dia. 174 particles	95% H_2O, 5% ACN, 20mM ammonium acetate	100 % ACN	Gradient 3	100 µL	1 mL/min	n.a.	230 nm
Rayonet with 6 300 nm bulbs	SMX and metabolites	nanoAquity UPLC w/ Thermo exactive MS	Phenomenex	100% H_2O, 0.1% formic acid	100% ACN, 0.1% formic acid	Gradient 4	2 µL	20 µL/min	+/-	n.a.
Rayonet with 6 300 nm bulbs	PNA	Dionex HPLC UV	Supelco Discovery C16 RP amide (15 cm × 173 4.6 mm, 5 µm dia. 174 particles	95% H_2O, 5% ACN, 20mM ammonium acetate	100 % ACN	Isocratic 1	100 µL	1 mL/min	n.a.	314 nm

Direct photolysis calculations

The direct photolysis rate constants were determined at 3 pH values and various conditions (light source and concentration). The degradation of all metabolites followed first order kinetics and degradation rate constants $k_{obs,i}$ were calculated using the slope of $\ln(A_t/A_0)$ plotted against time, where A_t refers to the peak area of chromatograms at time t, and A_0, the initial peak area. For experiments with relatively high concentrations of target compound and/or large volumes, a light-screening factor was used to account for the fact that the average light intensity in the tube was lower than in optically dilute solutions, due to self-screening by the compound itself. The screening factor depends on the absorbance of solution, $\alpha(\lambda)$, and on the depth of the well mixed solution, z, according to equation C.1.

$$\mathrm{SF}(\lambda) = \frac{1-10^{-\alpha(\lambda)\cdot z}}{2.303\cdot\alpha(\lambda)\cdot z} \tag{C.1}$$

The observed degradation rate constant, $k_{obs,i}$, can then be corrected to yield a photolysis rate constant representative of an optically dilute system:

$$k^0_{obs,i} = \frac{k_{obs,i}}{\mathrm{SF}(\lambda)} \tag{C.2}$$

All reported values are corrected for light screening.

The direct photolysis quantum yields (Φ_i) for the metabolites (i) were then calculated as follows:

$$\Phi_i = \frac{k^0_{obs,i}}{k^0_{abs,i}} \tag{C.3}$$

The specific rate of light absorbtion, $k^0_{abs,i}$, in an optically dilute solution is a function of the light intensity, I_λ, and the decadic molar extinction coefficient of the compound, ε_λ:

$$k^0_{abs,i} = 2.303\cdot\sum_\lambda I_\lambda\cdot\varepsilon_\lambda \tag{C.4}$$

The light intensity, I_λ , of each light source was calibrated using a chemical actinometer, p-nitroanisole (pNA). To do so, the light intensity measured spectroradiometrically, $I_m(\lambda)$, was normalized by the total measured intensity over the relevant wavelength interval to give the normalized light intensity, ρ_λ :

$$\rho_\lambda = \frac{I_m(\lambda)}{\sum_\lambda^{280-430\mathrm{nm}} I_m(\lambda)} \tag{C.5}$$

The actual total light intensity, I_{act}, was determined using a pNA actinometry

$$I_{act} = \frac{k_a ct}{2.303 \cdot \Phi_{act} \sum_{\lambda} (\varepsilon_{\lambda,act} \times \rho_{\lambda})} \tag{C.6}$$

where k_{act} is the 1st order degradation rate constant of pNA photolysis, Φ_{act} the known quantum yield of pNA[184] and $\varepsilon_{act}(\lambda)$, the decadic molar extinction coefficient of the actinometer.

The absolute intensity at a given wavelength is then:

$$I_{\lambda} = I_{act} \cdot \rho_{\lambda} \tag{C.7}$$

Error calculations

The direct photolysis rate constants correspond to average values of 2–5 experiments, each with its respective error (95% confidence interval). Accordingly, the errors associated to the average direct photolysis rate constant correspond to the propagated errors of single experiments. The uncertainty associated with calculated values, such as the specific rate of light absorption or the quantum yield, was also calculated using basic propagation of uncertainty rules and certain assumptions regarding the errors of certain quantities. More explicitly we assume a 10% error on the irradiance measurements as for the molar absorptivity of each compound. We also assume that the errors are independent of wavelength.

Synthesis of Sodium (5-methylisoxazol-3-yl)sulfamate

General synthetic methods. All reaction glassware was oven-dried (110 °C, overnight), assembled hot, and cooled under a stream of nitrogen. Reagents and solvents were purchased as ACS grade and were used as received, unless otherwise noted. Pyridine was dried for 2 d over 4$\AA$ molecular sieves prior to use. 3-Amino-5-methylisoxazole was dissolved in dry CH_2Cl_2, dried over 4$\AA$ molecular sieves for 2 d, filtered, and evaporated to dryness prior to use. NMR spectra were obtained on a Bruker AVANCE III 400 MHz NMR spectrometer, and are referenced to residual protiated solvent (HOD, 4.79 ppm). Accurate mass measurements were performed by direct injection using negative-mode electrospray ionization (ESI) on a Thermo Exactive Mass Spectrometer. Sodium (5-methylisoxazol-3-yl)sulfamate has been reported once before; however, the yield was only 2.4%. Thus we synthesized it by adapting a more recent procedure by Spillane and co-workers[183]. Sodium (5-methylisoxazol-3-yl)sulfamate. A dry 50 mL two-neck round bottom flask equipped with a magnetic stirbar was fitted with a septum and a dry septum-capped pressure-equalizing addition funnel. The flask was charged with dry pyridine (22.5 g, 280 mmol), and the flask was cooled to -15°C in a bath of ice, acetone and NaCl. Chlorosulfonic acid (3.26 g, 28 mmol) was transferred to the addition funnel using a fixed-needle glass syringe because of the corrosiveness of chlorosulfonic acid with plastic syringes and disposable needles. The chlorosulfonic acid was added dropwise over 30 min to the vigorously stirred pyridine, and the reaction mixture was then stirred for an additional 75 min at -15°C. Dry 3-amino-5-methylisoxazole (2.75 g, 28 mmol) was dissolved in dry pyridine (4 mL) and added to the cold reaction mixture by syringe over 3 min. The ice bath was removed, the reaction mixture was allowed to warm to room temperature, and the mixture was stirred overnight. In air, the reaction was quenched by the addition of 2M NaOH (30 mL) to give a solution of pH 10. The resulting solution was extracted with ether (3 x 50 mL), and the aqueous layer was evaporated in vacuo to give pale yellow crystals, which were recrystallized from hot 95% EtOH to give the sulfamate product (1.714 g, 9.62 mmol, 34.3%). Mp = 148 -– 255°C, slow decomp. 1H NMR (400 MHz, D2O): δ 6.01 (s,1H), 2.34 (s,3H) ppm. 13C NMR (100 MHz, D_2O): δ 170.3, 163.9, 95.7, 11.7 ppm. IR (ATR): 3350, 1617, 1515, 1488, 1344, 1277, 1212, 1064, 1034, 847, 780, 665, 550, 608, 534, 591 cm^{-1}.[210]. IR: 3400-3190 (N-H), 1240-1210 (asym SO_3), 1203-1170 (sym SO_3), 1072–1040 (sym SO_3), 730-660 (N-S) cm^{-1}. HRMS (ESI) m/z calculated for $C_4H_5N_2O_4S$ [M-Na]– 176.9976; found, 176.9969.

X-ray Analysis. The X-ray intensity data was measured on a Bruker Kappa Apex-II Duo CCD system equipped with a graphite monochromator. Frame integration, data reduction and cell refinement was done with the Bruker SAINT software package. The structure was solved and refined with SHELXS and OLEX2 . Hydrogen positions could be localized in a difference electron density map and were refined with isotropic temperature factors. The crystallographic data have been deposited with the Cambridge Crystallographic data Centre, deposition number CCDC 901298.

Table C.2: *X-ray Analysis results for Sodium (5-methylisoxazol-3-yl)sulfamate*

Empirical formula	$C_4H_7N_2NaO_5S{\cdot}H_2O$
Formula weight	236.18
Temperature	100(2) K
Wavelength	0.71073 $\AA$
Crystal system, space group	Orthorhombic, Pbcm
Unit cell dimensions	a = 13.6257(9) $\AA$ b = 9.8236(5) $\AA$ c = 6.9584(5) $\AA$
Volume	931.41(10) A^3
Z, Calculated density	4, 1.684 mg/m^3
Absorption coefficient	0.401 mm^{-1}
F(000)	488
Crystal size	0.57 x 0.36 x 0.30 mm
Theta range for data collection	1.49° to 30.01°
Limiting indices	-19≤h≤10, -13≤k≤13, -9≤l≤9
Reflections collected / unique	5241 / 1387 [R(int) = 0.0151]
Completeness to theta = 30.01 °	94.60%
Absorption correction	SADABS, multi-scan
Max. and min. transmission	0.8892 and 0.8036
Refinement method	Full-matrix least-squares on F^2
Data / restraints / parameters	1387 / 6 / 105
Goodness-of-fit on F^2	2.372
Final R indices [I>2s(I)]	R1 = 0.0258, wR2 = 0.1064
R indices (all data)	R1 = 0.0264, wR2 = 0.1068
Extinction coefficient	0.028(5)
Largest diff. peak and hole	0.530 and -0.410 e·$\AA$-3

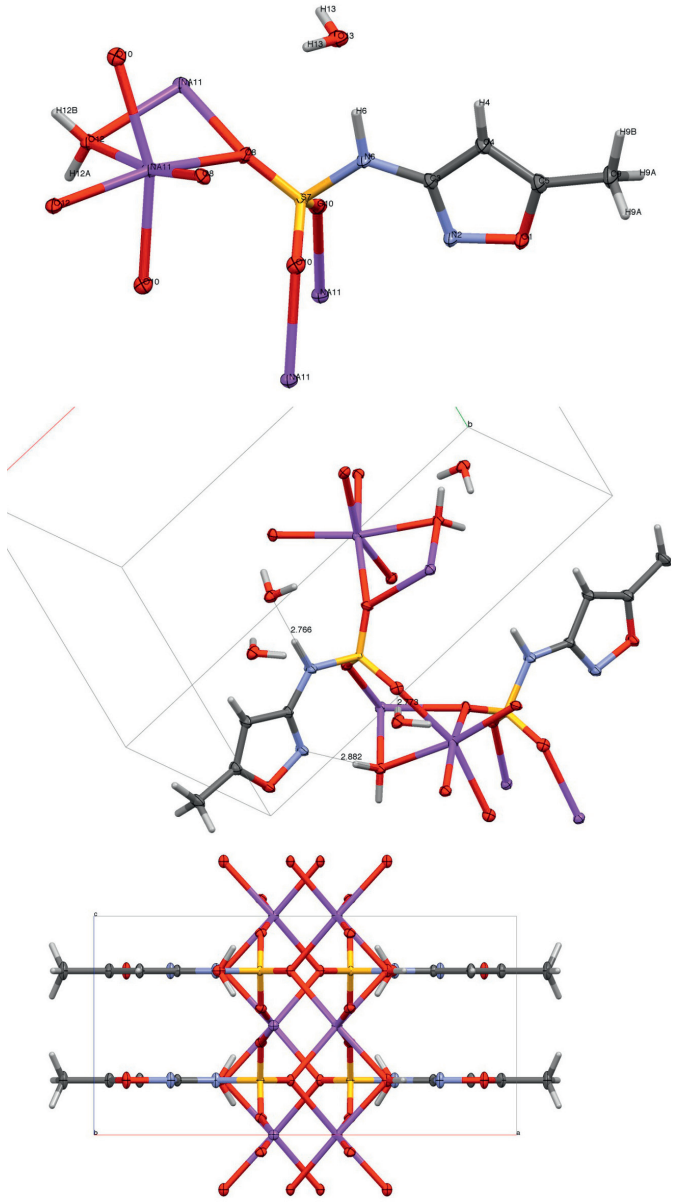

Figure C.6: *Crystal structure of synthesized sodium (5-methylisoxazole-3-yl)sulfamate. Atomic displacement parameters are drawn at the 50%.*

Confirmed photoproducts and proposed structures of SMX direct photolysis

Table C.3: *Photoproducts of SMX direct photolysis, with chromatographic retention time (RT) and accurate mass observed by HR-MS in a given ionization mode (positive or negative). A structure is proposed for each given elemental composition and was confirmed for certain products with authentic standards.*

Name	Fragment	RT (min)	ESI mode (+/-)	observed mass	calculated mass	Error (ppm)	Elemental composition	proposed structure	confirmed with standard
Target substance									
SMX	**254**	**14.50**	**+**	**254.0586**	**254.0594**	**3.15**	**C10H11N3O3S**	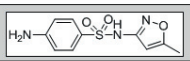	**yes**
Photoproducts									
aniline	94	2.85	+	94.0652	94.0651	-1.06	C6H7N		yes
3-amino-5-methylisoxazole	99	5.91	+	99.0552	99.0553	1.01	C4H6N2O		yes
benzene sulfonic acid	156	8.98	-	156.9954	156.9965	7.01	C6H6O3S		no
sulfanilic acid	172(a)	2.32	-	172.0063	172.0074	6.40	C6H7NO3S	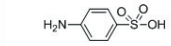	yes
hydroxysulfonic acid	172(b)	3.63	-	172.9906	172.9914	4.62	C6H6O4S	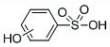	no
(5-methylisoxazol-3-yl)sulfamate	176	5.55	-	176.9966	176.9976	5.65	C4H6N2O4S	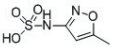	yes
4-(hydroxyamino)benzenesulfonic acid	188	2.23	-	188.0013	188.0023	-5.32	C6H7NO4S	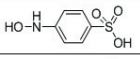	no
desulfonated-SMX (N1-(5-methylisoxazol-3-yl)benzene-1,4-diamine)	190	7.85	+	190.0973	190.0975	-1.05	C6H11N3O	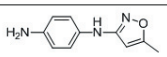	no
(4-hydroxy-5-methylisoxazole-3-yl)sulfamic acid	192	5.65	-	192.9915	192.9925	5.18	C4H6N2O5S	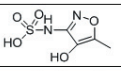	no
N-(5-methylisoxazol-3-yl)benzenesulfonamide	239	21.77	+	239.047	239.0485	6.27	C10H10N2O3S	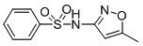	no
SMX isomer (structure reported in Zhou et al. 1994)	254	9.43	+	254.0586	254.0594	3.15	C10H11N3O3S	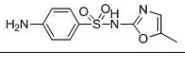	no
product 270 reported in Zhou et al., 1994	270-	9.20	-	270.055	270.0554	1.48	C10H13N3O4S	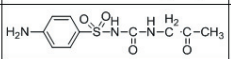	no
isomers of OH-SMX	270+	various RT	+	270.0533	270.0543	3.70	C10H11N3O4S		no

Confirmed photoproducts and proposed structures of Ac-SMX direct photolysis

Table C.4: *Photoproducts of Ac-SMX direct photolysis, with chromatographic retention time (RT) and accurate mass observed by HR-MS in a given ionization mode (positive or negative). A structure is proposed for each given elemental composition and was confirmed for certain products with authentic standards.*

Name	Fragment	RT (min)	ESI mode (+/-)	observed mass	calculated mass	Error (ppm)	Elemental composition	proposed structure	confirmed with standard
Target substance									
Ac-SMX	**296**	**16.10**	**+**	**296.0689**	**296.0700**	**3.72**	**C12H13N3O4S**	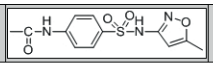	**yes**
Photoproducts									
3-amino-5-methylisoxazole	99	5.96	+	99.0554	99.0553	-1.01	C4H6N2O		yes
acetyl-anilide	136	11.75	+	136.0755	136.0757	-1.47	C8H9NO	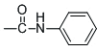	yes
N-(5-methylisoxazol-3-yl)acetamide	141	9.48	+	141.0657	141.0659	1.42	C6H8N2O2	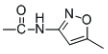	no
benzene sulfonic acid	156	8.98	-	156.9956	156.9965	5.73	C6H6O3S		no
(5-methylisoxazol-3-yl)sulfamate	176	5.55	-	176.9967	176.9976	5.08	C4H6N2O4S	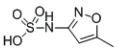	yes
(4-hydroxy-5-methylisoxazole-3-yl)sulfamic acid	192	5.65	-	192.9918	192.9925	3.63	C4H6N2O5S	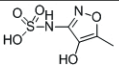	no
4-acetylamino-benzensulfonic acid	214	7.35	-	214.0174	214.0180	2.80	C8H9NO4S	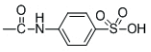	yes
N-(4-sulfamoylphenyl)acetamide	215	8.80	+	215.0480	215.0485	2.33	C8H10N2O3S	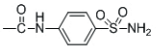	no
desulfonated-acetyl-SMX (N-(4-((5-methylisoxazol-3-yl)amino)phenyl)acetamide)	232	10.52	+	232.1073	232.1081	3.45	C12H13N3O2	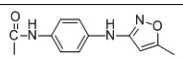	no
N-(5-methylisoxazol-3-yl)benzenesulfonamide	239	21.77	+	239.0478	239.0485	2.93	C10H10N2O3S	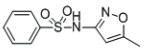	no
isomer of NO-SMX	266(b)	20.78	-	266.0237	266.0241	1.50	C10H9N3O4S		no
isomers of OH-SMX	270	15.17	+	270.0536	270.0543	2.59	C10H11N3O4S		no

Confirmed photoproducts and proposed structures of Glu-SMX direct photolysis

Table C.5: *Photoproducts of Glu-SMX direct photolysis, with chromatographic retention time (RT) and accurate mass observed by HR-MS in a given ionization mode (positive or negative). A structure is proposed for each given elemental composition and was confirmed for certain products with authentic standards.*

Name	Fragment	RT (min)	ESI mode (+/-)	observed mass	calculated mass	Error (ppm)	Elemental composition	proposed structure	confirmed with standard
Target substance									
SMX-glucuronide	**430**	**10.63**	**+**	**430.0923**	**430.0915**	**-1.86**	**C16H19N3O9S**	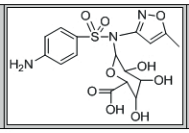	**yes**
Photoproducts									
aniline	94	2.72	+	94.0654	94.0651	-3.19	C6H7N		yes
sulfanilic acid	172(a)	2.29	-	172.0067	172.0074	4.07	C6H7NO3S	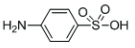	yes
glucuronic acid	193	2.26	-	193.0348	193.0354	3.11	C6H10O7	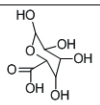	no
Glucopyranuronic acid	194	1.87	+	194.0660	194.0659	-0.52	C6H11NO6		no
desulfonated-SMX glucuronide	366	2.12 and 5.66	+	366.1294	366.1296	0.55	C16H19N3O7	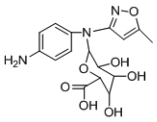	no

Confirmed photoproducts and proposed structures of NO-SMX direct photolysis

Table C.6: *Photoproducts of NO-SMX direct photolysis, with chromatographic retention time (RT) and accurate mass observed by HR-MS in a given ionization mode (positive or negative). A structure is proposed for each given elemental composition and was confirmed for certain products with authentic standards.*

Name	Fragment	RT (min)	ESI mode (+/-)	observed mass	calculated mass	Error (ppm)	Elemental composition	proposed structure	confirmed with standard
Target substance									
NO-SMX	**266**	**24.43**	-	**266.0238**	**266.0241**	**1.13**	**C10H9N3O4S**	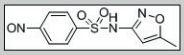	**yes**
Photoproducts									
aniline	94	2.85	+	94.0654	94.0651	-3.19	C6H7N		yes
3-amino-5-methylisoxazole	99	5.91	+	99.0556	99.0553	-3.03	C4H6N2O		yes
acetyl-anilide	136	11.75	+	136.0758	136.0757	0.73	C8H9NO	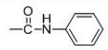	yes
benzene sulfonic acid	156	8.98	-	156.9956	156.9965	7.01	C6H6O3S		no
sulfanilic acid	172(a)	2.32	-	172.0068	172.0074	3.49	C6H7NO3S	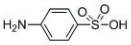	yes
hydroxysulfonic acid	172(b)	3.63	-	172.9908	172.9914	4.62	C6H6O4S	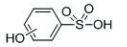	no
(5-methylisoxazol-3-yl)sulfamate	176	5.55	-	176.9969	176.9976	3.95	C4H6N2O4S	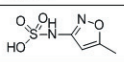	yes
4-(hydroxyamino)benzenesulfonic acid	188	3.52	-	188.002	188.0023	-5.32	C6H7NO4S	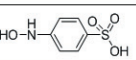	no
(4-hydroxy-5-methylisoxazole-3-yl)sulfamic acid	192	5.65	-	192.9915	192.9925	5.18	C4H6N2O5S	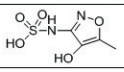	no
4-nitrobenzenesulfonic acid	201	12.02	-	201.9812	201.9816	1.98	C6H5NO5S	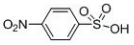	no
4-acetylamino-benzensulfonic acid	214	7.35	-	214.0175	214.018	2.34	C8H9NO4S	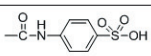	yes
desulfonated-NO_2-SMX (5-methyl-N-(4-nitrophenyl)isoxazol-3-amine)	220	22.05	+	220.0715	220.0717	0.91	C10H9N3O3	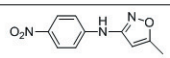	no
N-(5-methylisoxazol-3-yl)benzenesulfonamide	239	21.77	+	239.0484	239.0485	0.42	C10H10N2O3S	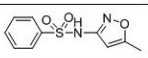	no
SMX	254	14.55	+	254.0595	254.0594	-0.39	C10H11N3O3	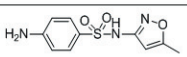	yes
isomers of OH-SMX	270	various RT	+	270.0542	270.0543	0.37	C10H11N3O4S		no
methyl-N-(5-methylisoxazol-3-yl)-4-nitrosobenzenesulfonamide	280	14.65	-	280.0401	280.0398	-1.07	C11H11N3O4S	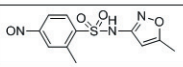	no
NO_2-SMX	282	23.97	-	282.0193	282.019	-1.06	C10H9N3O5S	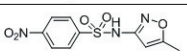	yes
acetyl-SMX	296	16.11	+	296.0698	296.07	0.68	C12H13N3O4S	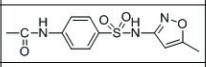	yes
N-(4-(N-(5-methylisoxazol-3-yl)sulfamoyl)phenyl)acetamide	298	22.18	-	298.0143	298.0139	-1.34	C10H9N3O6S	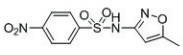	no

Bibliography

1. Schwarzenbach, R. P., Escher, B. I., Fenner, K., Hofstetter, T. B., Johnson, C. A., von Gunten, U., and Wehrli, B. *Science* **313**(5790), 1072–1077 (2006).

2. Perazzolo, C., Morasch, B., Kohn, T., Magnet, A., Thonney, D., and Chevre, N. *Environmental Toxicology and Chemistry* **29**(8), 1649–1657 (2010).

3. Joss, A., Zabczynski, S., Gobel, A., Hoffmann, B., Loffler, D., McArdell, C. S., Ternes, T. A., Thomsen, A., and Siegrist, H. *Water Research* **40**(8), 1686–1696 (2006).

4. Ternes, T. A. and Joss, A., editors. *Human pharmaceuticals, hormones and fragrances-the challenge of micropollutants in urban water management.* IWA Publishing, London, (2006).

5. Fono, L. and Sedlak, D. L. *Abstracts of Papers of the American Chemical Society* **228**, 186–ENVR (2004).

6. Lee, L. S., Carmosini, N., Sassman, S. A., Dion, H. M., and Sepulveda, M. S. In *Advances in Agronomy, Vol 93*, volume 93 of *Advances in Agronomy*, 1–68. Elsevier Academic Press Inc, San Diego (2007).

7. Carter, A. *Pesticide Outlook* **11**(4), 149–156 (2000).

8. Gerecke, A. C., Scharer, M., Singer, H. P., Muller, S. R., Schwarzenbach, R. P., Sagesser, M., Ochsenbein, U., and Popow, G. *Chemosphere* **48**(3), 307–315 (2002).

9. Wittmer, I. K., Bader, H. P., Scheidegger, R., Singer, H., Luck, A., Hanke, I., Carlsson, C., and Stamm, C. *Water Research* **44**(9), 2850–2862 (2010).

10. Heberer, T. *Toxicology Letters* **131**(1-2), 5–17 (2002).

11. Arnold, W. A. and McNeill, K. In *Analysis, Fate and Removal of Pharmaceuticals in the Water Cycle*, Petrovic, M. and Barcelo, D., editors, volume 50 of *Comprehensive Analytical Chemistry*, 361 – 385. Elsevier (2007).

12. Documed. *Compendium Suisse des Medicaments* (2012).

13. Halling-Sorensen, B., Nielsen, S. N., Lanzky, P. F., Ingerslev, F., Lutzhoft, H. C. H., and Jorgensen, S. E. *Chemosphere* **36**(2), 357–394 (1998).

14. Daughton, C. G. and Ternes, T. A. *Environmental Health Perspectives* **107**, 907–938 (1999).

15. Nassar, A. F. *Drug Metabolism Handbook: Concepts and Applications.* Wiley, (2009).

16. Marathe, P. H., Shen, D. D., and Nelson, W. L. *Drug Metabolism and Disposition* **22**(2), 237–247 (1994).

17. Verlicchi, P., Al Aukidy, M., and Zambello, E. *Science of the Total Environment* **429**, 123–155 (2012).

18. Oulton, R. L., Kohn, T., and Cwiertny, D. M. *Journal of Environmental Monitoring* **12**(11), 1956–1978 (2010).

19. Schwarzenbach, R. P., Gschwend, P. M., and Imboden, D. M. *Environmental Organic Chemistry, 2nd Edition.* John Wiley &L Sons, Inc., (2003).

20. Carballa, M., Omil, F., and Lema, J. M. *Water Research* **39**, 4790–4796 (2005).

21. Horsing, M., Ledin, A., Grabic, R., Fick, J., Tysklind, M., Jansen, J. l. C., and Andersen, H. R. *Water Research* **45**, 4470–4482 (2011).

22. Onesios, K. M., Yu, J. T., and Bouwer, E. J. *Biodegradation* **20**, 441–466 (2009).

23. Vieno, N. M., Tuhkanen, T., and Kronberg, L. *Environmental Science & Technology* **39**(21), 8220–8226 (2005).

24. Morasch, B., Bonvin, F., Reiser, H., Grandjean, D., de Alencastro, L. F., Perazzolo, C., Chevre, N., and Kohn, T. *Environmental Toxicology and Chemistry* **29**(8), 1658–1668 (2010).

25. Leclercq, M., Mathieu, O., Gomez, E., Casellas, C., Fenet, H., and Hillaire-Buys, D. *Archives of Environmental Contamination and Toxicology* **56**(3), 408–415 (2009).

26. Hilton, M. J. and Thomas, K. V. *Journal of Chromatography A* **1015**(1-2), 129–141 (2003).

27. Gobel, A., McArdell, C. S., Suter, M. J. F., and Giger, W. *Analytical Chemistry* **76**(16), 4756–4764 (2004).

28. Miao, X. S., Yang, J. J., and Metcalfe, C. D. *Environmental Science & Technology* **39**(19), 7469–7475 (2005).

29. Hummel, D., Loffler, D., Fink, G., and Ternes, T. A. *Environmental Science & Technology* **40**(23), 7321–7328 (2006).

30. Diaz-Cruz, M. S., Garcia-Galan, M. J., and Barcelo, D. *Journal of Chromatography A* **1193**(1-2), 50–59 (2008).

31. la Farre, M., Perez, S., Kantiani, L., and Barcelo, D. *Trac-Trends in Analytical Chemistry* **27**(11), 991–1007 (2008).

32. Perez, S. and Barcelo, D. *Trac-Trends in Analytical Chemistry* **27**(10), 836–846 (2008).

33. Stulten, D., Zuhlke, S., Lamshoft, M., and Spiteller, M. *Science of the Total Environment* **405**(1-3), 310–316 (2008).

34. Carballa, M., Omil, F., Lema, J. M., Llompart, M., Garcia-Jares, C., Rodriguez, I., Gomez, M., and Ternes, T. *Water Research* **38**(12), 2918–2926 (2004).

35. Gobel, A., Thomsen, A., McArdell, C. S., Joss, A., and Giger, W. *Environmental Science & Technology* **39**(11), 3981–3989 (2005).

36. Celiz, M. D., Tso, J., and Aga, D. S. *Environmental Toxicology and Chemistry* **28**(12), 2473–2484 (2009).

37. Fatta-Kassinos, D., Vasquez, M. I., and Kümmerer, K. *Chemosphere* **85**(5), 693–709 (2011).

38. Margot, J. and Magnet, A. *GWA* **7**, p. 487–493 (2011).

39. Mompelat, S., Le Bot, B., and Thomas, O. *Environment International* **35**(5), 803–814 (2009).

40. Sacher, F., Ehmann, M., Gabriel, S., Graf, C., and Brauch, H.-J. *Journal of Environmental Monitoring* **10**, 664–670 (2008).

41. Madureira, T. V., Barreiro, J. C., Rocha, M. J., Rocha, E., Cass, Q. B., and Tiritan, M. E. *Science of the Total Environment* **408**, 5513–5520 (2010).

42. Conley, J. M., Symes, S. J., Schorr, M. S., and Richards, S. M. *Chemosphere* **73**(8), 1178–1187 (2008).

43. Lissemore, L., Hao, C., Yang, P., Sibley, P. K., Mabury, S., and Solomon, K. R. *Chemosphere* **64**(5), 717–729 (2006).

44. Kim, S. C. and Carlson, K. *Environmental Science & Technology* **41**, 50–57 (2007).

45. Neumark, T., Brudin, L., Engstrom, S., and Molstad, S. *Scandinavian Journal of Primary Health Care* **27**, 18–24 (2009).

46. Zhao, J.-L., Ying, G.-G., Liu, Y.-S., and Chen, F. *Environmental Toxicology and Chemistry* **29**, 1377–1384 (2010).

47. Metcalfe, C. *Drug Metabolism Reviews* **38**, 38 (2006).

48. Gilliom, R. J., Barbash, J. E., Kolpin, D. W., and Larson, S. J. *Environmental Science & Technology* **33**(7), 164A–169A (1999).

49. Gilliom, R. J. *Environmental Science & Technology* **41**(10), 3408–14 (2007).

50. Konstantinou, I. K., Hela, D. G., and Albanis, T. A. *Environmental Pollution* **141**(3), 555–570 (2006).

51. Blanchoud, H., Moreau-Guigon, E., Farrugia, F., Chevreuil, M., and Mouchel, J. M. *Science of the Total Environment* **375**(1–3), 168–179 (2007).

52. Gonzalez, S., Lopez-Roldan, R., and Cortina, J.-L. *Environmental Pollution* **161**(0), 83–92 (2012).

53. Vryzas, Z., Vassiliou, G., Alexoudis, C., and Papadopoulou-Mourkidou, E. *Water Research* **43**(1), 1–10 (2009).

54. Khetan, S. K. and Collins, T. J. *Chemical Reviews* **107**(6), 2319–2364 (2007).

55. Jones, O. A. H., Voulvoulis, N., and Lester, J. N. *Critical Reviews in Environmental Science and Technology* **35**(4), 401–427 (2005).

56. Kummerer, K. *Journal of Environmental Management* **90**(8), 2354–2366 (2009).

57. Brausch, J. M., Connors, K. A., Brooks, B. W., and Rand, G. M. *Reviews of environmental contamination and toxicology* **218**, 1–99 (2012).

58. Waring, R. H. and Harris, R. M. *Molecular and Cellular Endocrinology* **244**(1–2), 2–9 (2005).

59. Cunningham, V. L., Buzby, M., Hutchinson, T., Mastrocco, F., Parke, N., and Roden, N. *Environmental Science & Technology* **40**(11), 3456–3462 (2006).

60. Fent, K., Weston, A. A., and Caminada, D. *Aquatic Toxicology* **76**(2), 122–159 (2006).

61. Crane, M., Watts, C., and Boucard, T. *Science of the Total Environment* **367**(1), 23–41 (2006).

62. Fenner, K. Technical report, June 2009 (2009).

63. Kosjek, T., Heath, E., Perez, S., Petrovic, M., and Barcelo, D. *Journal of Hydrology* **372**(1-4), 109–117 (2009).

64. Kummerer, K. *Journal of Antimicrobial Chemotherapy* **54**(2), 311–320 (2004).

65. Baquero, F., Martinez, J.-L., and Canton, R. *Current Opinion in Biotechnology* **19**(3), 260–265 (2008).

66. Gullberg, E., Cao, S., Berg, O. G., Ilback, C., Sandegren, L., Hughes, D., and Andersson, D. I. *Plos Pathogens* **7**, 1553–7366 (2011).

67. Chevre, N., Loeppe, C., Singer, H., Stamm, C., Fenner, K., and Escher, B. I. *Environmental Science & Technology* **40**(2), 426–435 (2006).

68. EuropeanCommission. Office for official publications of the european communities, Institute for Health and Consumer Protection, European Chemicals Bureau, European Commission (EC), (2003).

69. Vaj, C., Barmaz, S., Sorensen, P. B., Spurgeon, D., and Vighi, M. *Ecotoxicology and Environmental Safety* **74**(8), 2156–2166 (2011).

70. Backhaus, T. and Faust, M. *Environmental Science & Technology* **46**(5), 2564–2573 (2012).

71. Belden, J. B., Gilliom, R. J., and Lydy, M. J. *Integrated environmental assessment and management* **3**(3), 364–72 (2007).

72. Cedergreen, N., Christensen, A. M., Kamper, A., Kudsk, P., Mathiassen, S. K., Streibig, J. C., and Sorensen, H. *Environmental Toxicology and Chemistry* **27**(7), 1621–1632 (2008).

73. Alexy, R., Kumpel, T., and Kummerer, K. *Chemosphere* **6**, 505–512 (2004).

74. Andreozzi, R., Raffaele, M., and Nicklas, P. *Chemosphere* **50**(10), 1319–1330 (2003).

75. Boreen, A. L., Arnold, W. A., and McNeill, K. *Aquatic Sciences* **65**(4), 320–341 (2003).

76. Lin, A. Y. C. and Reinhard, M. *Environmental Toxicology and Chemistry* **24**(6), 1303–1309 (2005).

77. Baran, W., Sochacka, J., and Wardas, W. *Chemosphere* **65**(8), 1295–1299 (2006).

78. Liu, Q. T., Cumming, R. I., and Sharpe, A. D. *Photochemical & Photobiological Sciences* **8**(6), 768–777 (2009).

79. Wayne, C. E. and Wayne, R. P. *Photochemistry*. Oxford UP, (1996).

80. Smith, M. B. and March, J. *March's Advanced Organic Chemistry: Reactions, Mechanisms, and Structure, 5th Edition*. (2000).

81. Liu, Q. T. and Williams, H. E. *Environmental Science & Technology* **41**(3), 803–810 (2007).

82. Boreen, A. L., Arnold, W. A., and McNeill, K. *Environmental Science & Technology* **38**(14), 3933–3940 (2004).

83. Boreen, A. L., Arnold, W. A., and McNeill, K. *Environmental Science & Technology* **39**(10), 3630–3638 (2005).

84. Doll, T. E. and Frimmel, F. H. *Chemosphere* **52**(10), 1757–1769 (2003).

85. Packer, J. L., Werner, J. J., Latch, D. E., McNeill, K., and Arnold, W. A. *Aquatic Sciences* **65**(4), 342–351 (2003).

86. Werner, J. J., McNeill, K., and Arnold, W. A. *Chemosphere* **58**(10), 1339–1346 (2005).

87. Faust, B. C. and Hoigne, J. *Environmental Science & Technology* **21**(10), 957–964 (1987).

88. Canonica, S., Jans, U., Stemmler, K., and Hoigne, J. *Environmental Science & Technology* **29**(7), 1822–1831 (1995).

89. Thurman, E. M. *Organic geochemistry of natural waters*. Kluwer, (1985).

90. Canonica, S. and Laubscher, H.-U. *Photochemical & Photobiological Sciences* **7**(5), 547–551 (2008).

91. Wenk, J., von Gunten, U., and Canonica, S. *Environmental Science & Technology* **45**(4), 1334–1340 (2011).

92. Blough, N. and Zepp, R. In *Active Oxygen in Chemistry,* Foote, C., Valentine, J., Greenberg, A., and Liebman, F., editors, pp. 280– 333. (1995).

93. Haag, W. R. and Hoigne, J. *Environmental Science & Technology* **20**(4), 341–348 (1986).

94. Latch, D. E. and McNeill, K. *Science* **311**(5768), 1743–1747 (2006).

95. Paul, A., Hackbarth, S., Vogt, R. D., Roder, B., Burnison, B. K., and Steinberg, C. E. W. *Photochemical & Photobiological Sciences* **3**(3), 273–280 (2004).

96. Peterson, B. M., McNally, A. M., Cory, R. M., Thoemke, J. D., Cotner, J. B., and McNeill, K. *Environmental Science & Technology* **46**(13), 7222–7229 (2012).

97. Tratnyek, P. G., Hoigné, J., Zeyer, J., and Schwarzenbach, R. *Science of the Total Environment* **109–110**(0), 327–341 (1991).

98. Wilkinson, F., Helman, W. P., and Ross, A. B. *Journal of Physical and Chemical Reference Data* **24**(2), 663–1021 (1995).

99. Scully Jr, F. E. and Hoigne, J., J. *Chemosphere* **16**(4), 681–694 (1987).

100. Latch, D. E., Packer, J. L., Arnold, W. A., and McNeill, K. *Journal of Photochemistry and Photobiology a-Chemistry* **158**(1), 63–66 (2003).

101. Razavi, B., Ben Abdelmelek, S., Song, W., O'Shea, K. E., and Cooper, W. J. *Water Research* **45**(2), 625–631 (2011).

102. Zhou, W. and Moore, D. E. *International Journal of Pharmaceutics* **110**(1), 55–63 (1994).

103. Ryan, C. C., Tan, D. T., and Arnold, W. A. *Water Research* **45**(3), 1280–1286 (2011).

104. Buxton, G. V., Greenstock, C. L., Helman, W. P., and Ross, A. B. *Journal of Physical and Chemical Reference Data* **17**(2), 513–886 (1988).

105. Wols, B. A. and Hofman-Caris, C. H. M. *Water Research* **46**(9), 2815–2827 (2012).

106. Brezonik, P. L. and Fulkerson-Brekken, J. *Environmental Science & Technology* **32**(19), 3004–3010 (1998).

107. Lam, M. W. and Mabury, S. A. *Aquatic Sciences* **67**(2), 177–188 (2005).

108. Lam, M. W., Tantuco, K., and Mabury, S. A. *Environmental Science & Technology* **37**(5), 899–907 (2003).

109. Ji, Y., Zeng, C., Ferronato, C., Chovelon, J.-M., and Yang, X. *Chemosphere* **88**(5), 644–649 (2012).

110. Torniainen, K., Tammilehto, S., and Ulvi, V. *International Journal of Pharmaceutics* **132**(1-2), 53–61 (1996).

111. Sortino, S., De Guidi, G., Giuffrida, S., Monti, S., and Velardita, A. *Photochemistry and Photobiology* **67**(2), 167–173 (1998).

112. Fasani, E., Rampi, M., and Albini, A. *Journal of the Chemical Society, Perkin Transactions 2* (9), 1901–1907 (1999).

113. Sortino, S., Cosa, G., and Scaiano, J. C. *New Journal of Chemistry* **24**(3), 159–163 (2000).

114. Vione, D., Feitosa-Felizzola, J., Minero, C., and Chiron, S. *Water Research* **43**(7), 1959–1967 (2009).

115. Buser, H. R., Poiger, T., and Muller, M. D. *Environmental Science & Technology* **32**, 3449–3456 (1998).

116. Robinson, P. F., Liu, Q.-T., Riddle, A. M., and Murray-Smith, R. *Chemosphere* **66**(4), 757–766 (2007).

117. Tixier, C., Singer, H. P., Oellers, S., and Muller, S. R. *Environmental Science & Technology* **37**(6), 1061–1068 (2003).

118. Daneshvar, A., Svanfelt, J., Kronberg, L., and Weyhenmeyer, G. A. *Environmental Science and Pollution Research* **17**(4), 908–916 (2010).

119. Fono, L. J. and Sedlak, D. L. *Environmental Science & Technology* **39**(23), 9244–9252 (2005).

120. Reichenberger, S., Bach, M., Skitschak, A., and Frede, H. G. *Science of the Total Environment* **384**(1-3), 1–35 (2007).

121. Ashton, D., Hilton, M., and Thomas, K. V. *Science of the Total Environment* **333**(1-3), 167–184 (2004).

122. Metcalfe, C. D., Miao, X. S., Koenig, B. G., and Struger, J. *Environmental Toxicology and Chemistry* **22**(12), 2881–2889 (2003).

123. Giger, W., Schaffner, C., and Kohler, H. P. E. *Environmental Science & Technology* **40**(23), 7186–7192 (2006).

124. Tian, X., Roberts, P. J. W., and Daviero, G. J. *Journal of Hydraulic Engineering-ASCE* **130**(12), 1137–1146 (2004).

125. Sinton, L. W. and Ching, S. B. *Water, Air, & Soil Pollution* **35**(3), 347–356 (1987).

126. Vandenberg, J. A., Ryan, M. C., Nuell, D. D., and Chu, A. *Environmental Monitoring and Assessment* **107**(1), 45–57 (2005).

127. Benotti, M. J. and Brownawell, B. J. *Environmental Science & Technology* **41**(16), 5795–5802 (2007).

128. Carvalho, J. L. B., Roberts, P. J. W., and Roldao, J. *Journal of Hydraulic Engineering-ASCE* **128**(2), 151–160 (2002).

129. Chevre, N., Guignard, C., Rossi, L., Pfeifer, H. R., Bader, H. P., and Scheidegger, R. *Water Science and Technology* **63**(7), 1341–1348 (2011).

130. Pote, J., Goldscheider, N., Haller, L., Zopfi, J., Khajehnouri, F., and Wildi, W. *Environmental Monitoring and Assessment* **154**(1-4), 337–348 (2009).

131. Goldscheider, N., Haller, L., Pote, J., Wildi, W., and Zopfi, J. *Environmental Science & Technology* **41**(15), 5252–5258 (2007).

132. Ramos, P. A., Neves, M. V., and Pereira, F. L. *Continental Shelf Research* **27**(5), 583–593 (2007).

133. Bernard, M. and Arnold, C. Technical report, CIPEL, (2009).

134. Singer, H., Jaus, S., Hanke, I., Lück, A., Hollender, J., and Alder, A. C. *Environmental Pollution* **158**(10), 3054–3064 (2010).

135. Kasprzyk-Hordern, B., Dinsdale, R. M., and Guwy, A. J. *Water Research* **42**(13), 3498–3518 (2008).

136. Pote, J., Haller, L., Loizeau, J. L., Bravo, A. G., Sastre, V., and Wildi, W. *Bioresource Technology* **99**(15), 7122–7131 (2008).

137. Razmi, A., Barry, D., Bakhtyar, N., Le Dantec, N., Dastgheib, A., Lemmin, U., and Wuest, A. *Journal of Great Lakes Research* (submitted (2012)).

138. Tixier, C., Singer, H. P., Canonica, S., and Muller, S. R. *Environmental Science & Technology* **36**(16), 3482–3489 (2002).

139. Ort, C., Hollender, J., Schaerer, M., and Siegrist, H. *Environmental Science & Technology* **43**, 3214–3220 (2009).

140. Bonvin, F., Rutler, R., Chevre, N., Halder, J., and Kohn, T. *Environmental Science & Technology* **45**(11), 4702–4709 (2011).

141. Razmi, A.and Barry, D., Lemmin, U., Bakhtyar, R., Bonvin, F., and Kohn, T. *Aquatic Sciences* (to be submitted, 2012).

142. Lazzarotto, J., Nirel, P., and Rapin, F. Technical report, CIPEL, (2011).

143. Dodd, M. C., Kohler, H.-P. E., and Von Gunten, U. *Environmental Science & Technology* **43**(7), 2498–2504 (2009).

144. Andreozzi, R., Caprio, V., Insola, A., and Longo, G. *Journal of Chemical Technology and Biotechnology* **73**, 93–98 (1998).

145. Vel Leitner, N. K. and Roshani, B. *Water Research* **44**(6), 2058–2066 (2010).

146. Huber, M. M., Canonica, S., Park, G. Y., and Von Gunten, U. *Environmental Science & Technology* **37**(5), 1016–1024 (2003).

147. Razavi, B., Song, W., Cooper, W. J., Greaves, J., and Jeong, J. *Journal of Physical Chemistry A* **113**, 1287–1294 (2009).

148. Wammer, K. H., Korte, A. R., Lundeen, R. A., Sundberg, J. E., McNeill, K., and Arnold, W. A. *Water Research* **47**, 439–48 (2013).

149. Real, F. J., Benitez, F. J., Acero, J. L., Sagasti, J. J. P., and Casas, F. *Industrial & Engineering Chemistry Research* **48**(7), 3380–3388 (2009).

150. Chen, Y., Hu, C., Hu, X., and Qu, J. *Environmental Science & Technology* **43**(8), 2760–2765 (2009).

151. Kortenkamp, A., Backhaus, T., and Faust, M. Technical report, The School of Pharmacy University of London (ULSOP), (2009).

152. Tercier-Waeber, M.-L., Masson, M., and Loizeau, J. L. Technical report, Bulletin de l'ARPEA, (2012).

153. Lemmin, U. and Dadamo, N. *Annales Geophysicae-Atmospheres Hydrospheres and Space Sciences* **11**, 1207–1220 (1996).

154. Kolpin, D. W., Thurman, E. M., and Linhart, S. M. *Archives of Environmental Contamination and Toxicology* **35**(3), 385–390 (1998).

155. Kolpin, D. W., Furlong, E. T., Meyer, M. T., Thurman, E. M., Zaugg, S. D., Barber, L. B., and Buxton, H. T. *Environmental Science & Technology* **36**(6), 1202–1211 (2002).

156. Kagle, J., Porter, A. W., Murdoch, R. W., Rivera-Cancel, G., and Hay, A. G. In *Advances in Applied Mircobiology, Vol 67,* Laskin, A. I., editor, volume 67 of *Advances in Applied Microbiology*, 65–108. Elsevier Academic Press Inc, San Diego (2009).

157. Johnson, D. R., Czechowska, K., Chèvre, N., and Van Der Meer, J. R. *Environmental Microbiology* **11**(7), 1682–1691 (2009).

158. Sumpter, J. *Toxicology Letters* **82-3**, 737–742 (1995).

159. Hayes, T., Haston, K., Tsui, M., Hoang, A., Haeffele, C., and Vonk, A. *Nature* **419**(6910), 895–896 (2002).

160. Gebel, T., Lechtenberg-Auffarth, E., and Guhe, C. *Reproductive Toxicology* **28**(2), 188–195 (2009).

161. Edder, P., Ortelli, D., and Ramseier, S. Technical report, (2006).

162. Edder, P., Ortelli, D., Ramseier, S., and Chèvre, N. Technical report, (2007).

163. Edder, P., Ortelli, D., Klein, A., and Ramseier, S. Technical report, (2008).

164. Perez, S. and Barcelo, D. *Analytical Chemistry* **80**(21), 8135–8145 (2008).

165. Debska, J., Kot-Wasik, A., and Namiesnik, J. *Critical Reviews in Analytical Chemistry* **34**(1), 51–67 (2004).

166. Trovo, A. G., Nogueira, R. F. P., Aguera, A., Fernandez-Alba, A. R., Sirtori, C., and Malato, S. *Water Research* **43**(16), 3922–3931 (2009).

167. Radke, M., Lauwigi, C., Heinkele, G., Murdter, T. E., and Letzel, M. *Environmental Science & Technology* **43**(9), 3135–3141 (2009).

168. Bonvin, F., Omlin, J., Rutler, R., Schweizer, W. B., Alaimo, P., Strathmann, T., McNeill, K., and Kohn, T. *Environmental Science & Technology* (2013).

169. Noedler, K., Licha, T., Barbieri, M., and Perez, S. *Water Research* **46**(7), 2131–2139 (2012).

170. Boxall, A. B. A., Sinclair, C. J., Fenner, K., Kolpin, D., and Maud, S. J. *Environmental Science & Technology* **38**(19), 368A–375A (2004).

171. Backhaus, T., Altenburger, R., Arrhenius, A., Blanck, H., Faust, M., Finizio, A., Gramatica, P., Grote, M., Junghans, M., Meyer, W., Pavan, M., Porsbring, T., Scholze, M., Todeschini, R., Vighi, M., Walter, H., and Grimme, L. H. *Continental Shelf Research* **23**(17-19), 1757–1769 (2003).

172. Bellucci, G., Berti, G., Chiappe, C., Lippi, A., and Marioni, F. *Journal of Medicinal Chemistry* **30**(5), 768–773 (1987).

173. Miao, X.-S. and Metcalfe, C. D. *Analytical Chemistry* **75**(15), 3731–3738 (2003).

174. Stierlin, H., Faigle, J. W., Sallmann, A., Kung, W., Richter, W. J., Kriemler, H. P., Alt, K. O., and Winkler, T. *Xenobiotica* **9**(10), 601–610 (1979).

175. Vanderven, A., Vree, T. B., Kolmer, E., Koopmans, P. P., and Vandermeer, J. W. M. *British Journal of Clinical Pharmacology* **39**(6), 621–625 (1995).

176. Silva, E., Rajapakse, N., and Kortenkamp, A. *Environmental Science & Technology* **36**, 1751–1756 (2002).

177. Dahmane, E., Mercier, T., Zanolari, B., Cruchon, S., Guignard, N., Buclin, T., Leyvraz, S., and Zaman, K. Csajka, C. D. L. A. *Journal of Chromatography B* **878**, 3402–3414 (2010).

178. Miao, X.-S., Bishay, F., Chen, M., and Metcalfe, C. D. *Environmental Science & Technology* **38**(13), 3533–3541 (2004).

179. Garcia-Galan, M. J., Diaz-Cruz, M. S., and Barcelo, D. *Environment International* **37**(2), 462–473 (2011).

180. Hirsch, R., Ternes, T., Haberer, K., and Kratz, K.-L. *Science of the Total Environment* **225**(1–2), 109–118 (1999).

181. Gomez, M. J., Sirtori, C., Mezcua, M., Fernandez-Alba, A. R.ndez-Alba, A. R., and Aguera, A. *Water Research* **42**(10–11), 2698–2706 (2008).

182. Naisbitt, D. J., Hough, S. J., Gill, H. J., Pirmohamed, M., Kitteringham, N. R., and Park, B. K. *British Journal of Pharmacology* **126**(6), 1393–1407 (1999).

183. Spillane, W. J., Kelly, L. M., Feeney, B. G., Drew, M. G. B., and Hattotuwagama, C. K. *Arkivoc* , 297–309 (2003).

184. Leifer, A. *The kinetics of environmental aquatic photochemistry : theory and practice*. American Chemical Society, Washington, DC, (1988).

185. Bonvin, F., Chevre, N., Rutler, R., and Kohn, T. *Archives des Sciences* **65** (2012).

186. Fery-Forgues, S. and Lavabre, D. *Journal of Chemical Education* **76**(9), 1260 (1999).

187. Garcia-Galan, M. J., Diaz-Cruz, S., and Barcelo, D. *Water Research* **46**, 711–722 (2012).

188. Dopp, D. *Topics in Current Chemistry* (55), 49–85 (1975).

189. Vialaton, D. and Richard, C. *Aquatic Sciences* **64**(2), 207–215 (2002).

190. Tanikaga, R. *Bulletin of the Chemical Society of Japan* **42**(1), 210–& (1969).

191. Zelentsov, S. V. and Logunov, A. A. *High Energy Chemistry* **39**(4), 244–249 (2005).

192. Konieczka, P. and Namiesnik, J. *Journal of Chromatography A* **1217**(6), 882–891 (2010).

193. OekotoxZentrum. *Propositions for water quality standards in Switzerland* (2010).

194. Junghans, M., Kase, R., di Paolo, C., Eggen, R., Homazava, N., Ashauer, R., Fenner, K., Gälli, R., Häner, A., Chèvre, N., Perazzolo, C., and Gregorio, V. (2010).

195. Chevre, N. *Gaz Wasser Abwasser (GWA)* **87**(7), 529–539 (2007).

196. Fass. *Swedish database for pharmaceuticals* .

197. ANSES. *Base de donn sur les substances actives phytopharmaceutiques* .

198. Christensen, A. M., Markussen, B., Baun, A., and Halling-Sorensen, B. *Chemosphere* **77**(3), 351–358 (2009).

199. Kummerer, K., editor. *Pharmaceuticals in the environment: Sources, fate, effects and risks*. Springer-Verlag, Berlin Heidelberg New York, 1st edition, (2001).

200. Lambert, S. J., Thomas, K. V., and Davy, A. J. *Chemosphere* **63**(5), 734–743 (2006).

201. Arrhenius, A., Backhaus, T., Gronvall, F., Junghans, M., Scholze, M., and Blanck, H. *Archives of Environmental Contamination and Toxicology* **50**(3), 335–345 (2006).

202. Zhang, A. Q., Leung, K. M. Y., Kwok, K. W. H., Bao, V. W. W., and Lam, M. H. W. *Marine Pollution Bulletin* **57**(6-12), 575–586 (2008).

203. DeLorenzo, M. E. and Serrano, L. *Journal of Environmental Science and Health Part B-Pesticides Food Contaminants and Agricultural Wastes* **41**(8), 1349–1360 (2006).

204. Okamura, H., Aoyama, I., Liu, D., Maguire, R. J., Pacepavicius, G. J., and Lau, Y. L. *Water Research* **34**(14), 3523–3530 (2000).

205. Nystrm, B., Becker-Van Slooten, K., Brd, A., Grandjean, D., Druart, J.-C., and Leboulanger, C. *Water Research* **36**(8), 2020–2028 (2002).

206. Scarlett, A., Donkin, M. E., Fileman, T. W., and Donkin, P. *Marine Pollution Bulletin* **34**(8), 645–651 (1997).

207. Braithwaite, R. A. and Fletcher, R. L. *Journal of Experimental Marine Biology and Ecology* **322**(2), 111–121 (2005).

208. van Wezel, A. P. and van Vlaardingen, P. *Aquatic Toxicology* **66**(4), 427–444 (2004).

209. Larson, R. A. and Zepp, R. G. *Environmental Toxicology and Chemistry* **7**(4), 265–274 (1988).

210. Spillane, W. J., McGlinchey, G., and Benson, A. *Journal of Pharmaceutical Science* **72**, 852–856 (1983).

Florence Bonvin

✉ *florence.bonvin@gmail.com*
Rte du Sanetsch 73, 1950 Sion, Switzerland
16.12.1983 – Swiss citizen

Education

02.2009 – 02.2013 **PhD in Environmental Chemistry**, *Ecole Polytechnique Fédérale de Lausanne, Lausanne, Switzerland.*
Dissertation: "Spatio-temporal presence of micropollutants in Lake Geneva and susceptibility to direct and indirect photodegradation processes."

10.2006 – 07.2008 **Master in Environmental Science and Engineering**, *Ecole Polytechnique Fédérale de Lausanne (EPFL), Lausanne, Switzerland*, Minor in Environmental Biotechnology.
Master's Project at Stanford University, California, USA (with Prof. A.B Boehm). "Presence of pathogenic *E.coli* in coastal streams and relation to land use."

10.2003 – 07.2006 **Bachelor in Environmental Science and Engineering**, *Ecole Polytechnique Fédérale de Lausanne (EPFL), Lausanne, Switzerland.*
Exchange year abroad (ERASMUS), Universidad de Granada, Spain

09.1998 – 06.2003 **Baccalaureate math and physics section**.
- Gymnasium Spiritus Sanctus (German), Brig, Switzerland (09.2000 – 06.2003)
- Collège des Creusets (French), Sion, Switzerland (09.1998 – 06.2000)

1990 – 1997 **Elementary school**, *Kingston, ON, Canada (English).*

Skills

Languages French (mother tongue), English (bilingual), German (advanced writing skills, conversational proficiency), Spanish (intermediate oral and writing skills)

Computer Matlab, SimpleTreat, Aquasim, MS Office Suite, Latex, Web of Science, EndNote, PHREEQC, MODFLOW, basics of Arcview GIS

Laboratory Solid phase extraction (SPE), gas and liquid chromatography (GC, HPLC, UPLC), mass spectrometry (preparative MS, MS-MS, high-resolution MS), bacterial and viral purification and culture, RNA/DNA extraction, standard and quantitative PCR, field sampling of surface and waste waters.

Work Experience

Research Assistant Environmental Chemistry Laboratory
EPFL, Switzerland
08.2008-12.2008

Research Assistant Environmental Biotechnology Laboratory
EPFL, Switzerland
09.2007-12.2007

Intern Membratec SA (membrane separation processes)
Sierre, Switzerland
08.2006-09.2006

Personal Interests

- **Outdoor sports:** running, hiking, mountain biking, ski touring
- Cooking and baking

Publications

1. **Bonvin, F.**, Razmi, A.M., Barry, D.A. and Kohn, T. A coupled hydrodynamic-photolysis model to simulate the fate of micropollutants in Vidy Bay. *To be submitted to ES&T in March 2013.*
2. Razmi, A.M , Barry, D.A., Lemmin, U., Bakhtyar, R., **Bonvin, F.** and Kohn, T. Residence time in an open, wide and deep lacustrine embayment: Vidy Bay (Lake Geneva, Switzerland). *Submitted to Aquatic Sciences.*
3. Hörger, C., Akhtman, Y., Martelletti, L., Rutler, R., **Bonvin, F.** and Kohn, T. Spatial extent and ecotoxicological risk assessment of wastewater-derived micropollutant plume in Lake Geneva. *Submitted to Aquatic Sciences.*
4. **Bonvin, F.**, Omlin, J., Rutler, R., Schweizer, B., Alaimo, P.J., Strathmann, T.J., McNeill, K., Kohn, T. Direct photolysis of human metabolites of antibiotic sulfamethoxazole - evidence for abiotic back-transformation. *Environmental Science and Technology*, **2013**.
5. **Bonvin, F.**, Chèvre, N., Rutler, R., Kohn, T. Pharmaceuticals and their human metabolites in Lake Geneva: occurrence, fate and ecotoxicological relevance. *Archives des Sciences*, **2012**, 65.
6. **Bonvin, F.**, Rutler, R., Chèvre, N., Halder, N. and Kohn, T. Spatial and temporal presence of a wastewater-derived micropollutant plume in Lake Geneva. *Environmental Science and Technology*, **2011**, 45, 4702-4709.
7. Morasch, B., **Bonvin, F.**, Reiser, H., Grandjean, D. de Alencastro, L.F., Perazzolo, C., Chèvre, N. and Kohn, T. Occurrence and fate of micropollutants in the Vidy Bay of Lake Geneva, part II: Micropollutant removal between wastewater and raw drinking water. *Environmental Toxicology and Chemistry*, **2010**, 29, 1658-1668.

Conference presentations

8^{th} IWA Micropol & Ecohazard Conference
Zürich, Switzerland
June 16-18, 2013

Micropollutant dynamics in Vidy Bay - A coupled photolysis-hydrodynamic model to assess the spatial extent of ecotoxicological risk. *Bonvin, F., Razmi, A.M., Barry, D.A., and Kohn, T.* Oral presentation.

Gordon Research Conference on Environmental Sciences: Water
Plymouth, NH,USA
June 24-29, 2012

Can solar irradiation transform human metabolites of pharmaceuticals back to their parent compound? - Insights on the direct photolysis products and pathways of sulfamethoxazole. *Bonvin, F., Omlin, J., Strathmann, T., McNeill, K. and Kohn, T.* **Recipient of Best Poster award**

6^{th} SETAC World Congress
Berlin, Germany
May 20-24, 2012

Direct and indirect photolysis of human metabolites of antibiotic sulfamethoxazole. *Bonvin, F., Omlin, J., Rutler, R. and Kohn, T.* Poster presentation.

6^{th} SETAC World Congress
Berlin, Germany
May 20-24, 2012

Can solar irradiation transform human metabolites of pharmaceuticals back to their parent compound? - Insights on the direct photolysis products and pathways of Sulfamethoxazole. *Bonvin, F.,Rutler, R., Kohn, T. and McNeill, K.* Plenary talk.

International Conference on Chemistry in the Environment
Zürich, Switzerland
September 11-15, 2011

Micropollutant plume in Lake Geneva. *Hörger, C.C., Bonvin, F., Rutler, R. and Kohn, T.* Poster Presentation.

242^{nd} American Chemical Society National Meeting
Denver, USA
Aug. 28-1 Sept. 2011

Photodegradation kinetics of antibiotic sulfamethoxazole and four human metabolites. *Bonvin, F., Omlin, J., Rutler, R., Strathmann, T. and Kohn, T.* Poster Presentation.

21st SETAC European Meeting
Milan, Italy
May 15-19, 2011

Micropollutant plume in Lake Geneva. *Bonvin, F., Rutler, R, and Kohn, T.* Oral presentation.

TransCon2010 Conference
Monte Verità, Switzerland
September 12-17, 2010

Occurrence and photodegradation of pharmaceuticals and their metabolites in Lake Geneva. *Bonvin, F., Rutler, R., and Kohn, T.* Poster presentation.

Gordon Research Conference on Environmental Sciences: Water
Plymouth, NH,USA
June 20-25, 2010

Contribution of direct and indirect photolysis to the degradation of pharmaceuticals in lake water. *Bonvin, F., Rutler, R., Halder, J. and Kohn, T.* Poster presentation.

20th SETAC European Meeting
Seville, Spain
May 23-27, 2010

Photodegradation and fate of pharmaceuticals in the water column of a mid-sized lake. *Bonvin, F., Morasch, B., Reiser, H. and Kohn, T.* Poster presentation.

20th SETAC European Meeting
Seville, Spain
May 23-27, 2010

Input and fate of wastewater-derived micropollutants in the Vidy Bay of Lake Geneva: removal during wastewater treatment and upon passage through the bay into raw drinking water. *Kohn, T. Morasch, B., Bonvin, F., Grandjean, D. and de Alencastro, L.F.* Poster presentation.

6th IWA Micropol & Ecohazard Conference
San Francisco, USA
June 8-10, 2009

Occurrence and fate of micropollutants during their passage from a wastewater effluent through Lake Geneva into finished drinking water. *Kohn, T., Morasch, B., Bonvin, F., Grandjean, D., and de Alencastro, L.F.* Poster presentation.

References

Prof. Tamar Kohn
Ecole Polytechnique Fédérale de Lausanne, EPFL, Lausanne, Switzerland
tamar.kohn@epfl.ch

Prof. Kristopher McNeill
ETH Zürich, Zürich, Switzerland
kristopher.mcneill@env.ethz.ch

Prof. Timothy J. Strathmann
University of Illinois at Urbana-Champaign, IL, USA
strthmnn@illinois.edu